2015

DESIGN AND ANALYSIS OF INTEGRALLY- HEATED TOOLING FOR POLYMER COMPOSITES

Rzgar Abdalrahman

PHD

DESIGN AND ANALYSIS OF INTEGRALLY- HEATED TOOLING FOR POLYMER COMPOSITES

Abdalrahman, Rzgar

Award date:
2015

Awarding institution:
University of Plymouth

DESIGN AND ANALYSIS OF INTEGRALLY- HEATED TOOLING FOR POLYMER COMPOSITES

by

RZGAR MHAMMED ABDALRAHMAN

A thesis submitted to the University of Plymouth in partial fulfilment for the degree of PhD

DOCTOR OF PHILOSOPHY

School of Marine Sciences and Engineering

Faculty of Science and Engineering

October 2015

DESIGN AND ANALYSIS OF INTEGRALLY- HEATED TOOLING FOR POLYMER COMPOSITES

ABSTRACT

Tooling design is crucial for the production of cost-effective and durable composite products. As part of the current search for cost reduction (by reducing capital investment, energy use and cycle time), integrally-heated tooling is one of the technologies available for 'out-of-autoclave' processing of advanced thermoset polymer composites. Despite their advantages, integrally-heated tools can suffer from uneven distribution of temperature, variability in heat flow rate and inconsistency in heating/cooling time. This research, therefore, investigates a number of design variables such as shape and layout of heating channels in order to improve the heating performance of an integrally-heated tool. Design of Experiments (DoE) has been carried out using Taguchi's Orthogonal Array (OA) method to set several combinations of design parameters. Each of these design combinations has been evaluated through numerical simulation to investigate heating time and mould surface temperature variation. The simulation results suggest that the layout of the channels and their separation play a vital role in the heating performance. Signal-to-Noise (S/N) ratio and analysis of variance (ANOVA) have been applied to the results obtained to identify the optimal design combination of the integrally-heated tool. Statistical analysis reveals that the heating performance of an integrally-heated tool can be significantly improved when the channels' layout is parallel. The

shape of the channels has negligible effect and the distance between the channels should be determined based on the production requirement.

According to the predicted optimal design, a developed integrally water-heated tool is manufactured. The actual thermal properties of the constituent materials of the produced tool are also measured. Then a numerical model of the experimental tool model is simulated in ANSYS software, with setting the actual material properties and boundary condition to define the temperature uniformity and heating rate of the experimental tool. Comparison of the experimental and numerical results of the experimental tool confirmed the well assigning of the boundary conditions and material properties during simulation the heated tool. The experimental results also confirmed the predicted optimal design of the integrally heated tool. Finally, in order to define its thermomechanical behaviour under the effective (in service) thermal loads, a tool model is simulated. Numerical results presented that the produced extremes of thermal deformation, elastic strain, normal and plane shear stresses, under the effective thermal loading, are within the allowable elastic limits of the participated materials.

List of contents

List of figures

List of tables

List of symbols

Symbols		Discerptions	Units
A	:	Surface area of conduction or convection	m^2
A	:	Design parameter of channel layout	-
A_1	:	Surface area of the mould face	m^2
A_2	:	Surface area of the insulated bottom face	m^2
A_3	:	Surface area of the insulated side faces	m^2
A_c	:	Cross-sectional area of flow or channel.	m^2
A_f	:	Fibre Areal weight	g/m^3
A_H	:	Sectional area of the high dilatable strip material	m^2
A_L	:	Sectional area of the low dilatable strip material	m^2
A_m	:	Mould surface area	m^2
A_r	:	Values of the corresponding area weights	g/m^2
A_s	:	Wet peripheral convection area of the channel	m^2
A_t	:	Length of the square tool model.	m
b	:	Internal length of the rectangular channel profile.	m
B	:	Design Parameter of channel profile	-
Bi	:	Biot number	-
B_t	:	A dimension of the channel layout.	m
c	:	Internal width of the rectangular channel profile.	m
c_p	:	Specific heat capacity of fluid (water) or general	J/kg.K
c_{p_c}	:	Specific heat capacity of channel material	J/kg.K
c_{p_m}	:	Specific heat capacity of mould material	J/kg.K
c_{p_r}	:	Specific heat capacity of the reference	J/kg.K
c_{p_s}	:	Specific heat capacity of the sample	J/kg.K
c_{p_t}	:	Specific heat capacity of tool material	J/kg.K
C	:	Constant to be determined empirically	-
C	:	Design Parameter of channel separation	-
$C.I.$	:	Confidence Interval	-
C_t	:	A dimension of channel layout.	m
ξ	:	Coefficients calculated according to Biot number	rad
D_h	:	Hydraulic diameter of channel	m
D_i	:	Internal diameter of channel	m

D_o	:	External diameter of channel	m
D_t	:	A dimension of channel layout.	m
e	:	Repetition number	-
E	:	Modulus of Elasticity	Pa
E_{CF}	:	Modulus of elasticity of CFRP	Pa
E_H	:	Modulus of elasticity of high dilatable material	Pa
E_L	:	Modulus of elasticity of low dilatable materials	Pa
E_{in}	:	Rate of energy transferred in	W
E_{Loss}	:	Rate of energy lost	W
E_{out}	:	Rate of energy transferred out	W
E_g	:	Rate of Energy generated	W
E_{st}	:	Rate of Energy stored	W
f_A	:	Degree of freedom of parameter **A**	-
f_A	:	Average performance (factor effect) for parameter **A**	-
f_B	:	Degree of freedom of parameter **B**	-
f_C	:	Degree of freedom of parameter **C**	-
f_C	:	Average performance (factor effect) for parameter **C**	-
f_{max}	:	maximum average performance (factor effect) for each parameter	-
f_{min}	:	minimum average performance (factor effect) for each parameter	-
f_e	:	Degree of freedom of the error term	-
$\bar{f}_e$	:	Pure degree of freedom of the error term after pooling	-
f_f	:	Moody, Darcy or Fanning friction factor	-
f_P	:	Degree of freedom of each parameter	-
f_{P_j}	:	Average performance (or factor effect) of each parameter at each given level.	-
f_T	:	Total degrees of freedom of the test cases	-
F	:	Total force in the bimetallic strip	N
F_I	:	Inertia force	N
F_H	:	Interfacial force of high dilatable strip material	N
F_L	:	Interfacial force of low dilatable strip material	N
F_O	:	Fourier number	-
F_P	:	Variance ratio of each parameter	-
F_s	:	Shear force	N
F_{th}	:	Thermal force	N

$F(1, \bar{f}_e)$	:	Value of variance ratio at the DoFs of 1 and $\bar{f}_e$ (from F-Table)	-
g	:	Acceleration due to gravity	m/s^2
h	:	Heat transfer coefficient of fluid, or Thickness of the tool surface	W/m^2.K m
$\bar{h}$	:	Average heat transfer coefficient	W/m^2.K
h_a	:	Heat transfer coefficient of ambient or air	W/m^2.K
h_b	:	Heat transfer coefficient of bottom face	W/m^2.K
h_c	:	Heat transfer coefficient around horizontal cylinder	W/m^2.K
h_H	:	Thickness of high dilatable strip material	m
h_i	:	Total thickness of the bimetallic strip	m
h_L	:	Thickness of low dilatable strip material	m
h_s	:	Heat transfer coefficient of side face	W/m^2.K
h_t	:	Heat transfer coefficient of top face	W/m^2.K
H	:	Height of the mould and the tool surface together	m
H_t	:	Experimental heating time of the tool heated by hot inlet water	s
H_{t_C}	:	Experimental heating time of the tool heated from cold	s
$H_{t_{S1}}$	:	Numerically-calculated heating time of the first case	s
$H_{t_{S2}}$	:	Numerically-calculated heating time of the second case	s
i	:	Represents coordinate directions, Test case counter and Parallel branch channels counter	-
I_H	:	Moment of inertia of high dilatable strip material	kg.m^2
I_L	:	Moment of inertia of low dilatable strip material	kg.m^2
j	:	Level counter or Parallel channel counter	-
k	:	Thermal conductivity of fluid (water) or general	W/m.K
k_c	:	Thermal conductivity of channel material	W/m.K
k_g	:	Thermal conductivity of glass fibre (insulation)	W/m.K
k_m	:	Thermal conductivity of mould material	W/m.K
k_t	:	Thermal conductivity of tool material	W/m.K
k_w	:	Thermal conductivity of plywood material	W/m.K
l	:	Internal length of square channel	m
l_m	:	Distance between the channel wall and tool face	m
L	:	Length	m
L_c	:	Length of channel	m
L_o	:	Length of top or bottom faces	m
L_s	:	Length of side face	m

L_t	:	Length of the longitudinal part of the parallel channels	m
L_w	:	Thickness of the tube wall	m
L_{hel}	:	Length of helical channel	m
L_{par}	:	Length of parallel channel	m
L_{zig}	:	Length zigzag channel	m
ΔL_{th}	:	Thermal elongation	mm
$\dot{m}$	:	Mass flow rate	kg/min
m_o	:	Mass of object in air	g
$\bar{m}_o$	:	Mass of object in water	g
m_r	:	Mass of reference in air	g
m_s	:	Mass of sample in air	g
m_w	:	Mass of displaced water	g
M	:	Thermal mass of water $(\rho V c_p)$	J/K
M_H	:	Moment of high dilatable strip material	N.m
M_L	:	Moment of low dilatable strip material	N.m
M_o	:	Total moment	N.m
M_t	:	Thermal mass of the tool	J/K
n	:	Total number of the test cases in OA	-
n_l	:	Number of layers	-
N	:	Total number of the tests contains intended parameter at a given level	-
N_P	:	Total number of the levels of each parameter	-
Nu_D	:	Nusselt number of cylindrical channel	-
Nu_D	:	Nusselt number flat face	-
p	:	Pressure	Pa
p_m	:	Pressure applied to the mould surface	Pa
Δp	:	Pressure drop in the main inlet	Pa, ($kg/m.s^2$)
$\Delta p_1, .., \Delta p_4$	:	Pressure drops in the parallel branches	Pa, ($kg/m.s^2$)
P	:	Flat surface perimeter	m
P_c	:	Peripheral wet perimeter of the channel	m
P_{co}	:	Composite property	-
P_f	:	Fibre property	-
P_m	:	Matrix property	-
P_P	:	Percentage contribution of each parameter	-

Pr	:	Prandtl number $(c_p\mu/k)$	-
Q	:	Volumetric flow rate in the main inlet	m^3/min, (L/min)
$Q_1,.,Q_4$	:	Volumetric flow rate in the parallel branches	m^3/min, (L/min)
Q_f	:	Measured volumetric flow rate	m^3/min, (L/min)
q	:	Amount of heat transferred	W (J/s)
q_{conv}	:	Convected heat	W (J/s)
q_{cond}	:	Conductive heat	W (J/s)
r	:	Radius	m
r_b	:	Radius of channel bending	m
r_i	:	Internal radius	m
r_o	:	Outer radius	m
$\mathcal{R}$	:	Radius of curvature	m
R_1	:	Total thermal resistance of the mould and channel	K/W
R_2	:	Total thermal resistance of the model parts	K/W
R_c	:	Thermal resistance of channel material	K/W
R_g	:	Thermal resistance of glass fibre (insulation)	K/W
R_m	:	Thermal resistance of mould material	K/W
R_w	:	Thermal resistance of plywood	K/W
Ra_L	:	Rayleigh number	-
$\mathrm{Re_D}$	:	Reynold's number of channel flow $(\rho u D_h/\mu)$	-
$\mathrm{Re_L}$	:	Reynold's number of flat face flow	-
$\mathrm{R_i}$	:	Ratio of pipe length to its diameter	-
$\mathrm{R_j}$	:	Ratio of channel length to tool surface area	m^{-1}
S	:	Constant	-
S_c	:	Stiffness of the cracking ply	N/m
S_{P_j}	:	Sum of the test results containing each parameter at each given level	-
S_{re}	:	Stiffness of the remainder of the laminate (F/δ)	N/m
SS_T	:	Total sum of squared deviations of the test results	-
SS_P	:	Sum of squared deviations of each parameter	-
SS_e	:	Sum of squared deviations of the error term.	-
SS_A	:	Sum of squared deviation of parameter **A**	-
SS_B	:	Sum of squared deviation of parameter **B**	-
SS_C	:	Sum of squared deviation of parameter **C**	-
t	:	Time	s

$t_{1/2}$	:	Half rise time	s
t_c	:	Thickness of the cracking ply	m
t_l	:	Thickness of the laminate	m
t_{max}	:	Corresponding heating time to achieve $\boldsymbol{T_{max}}$	ºC
t_{min}	:	Corresponding heating time to achieve $\boldsymbol{T_{min}}$	ºC
t_{re}	:	Thickness of the of the remainder of the laminate	m
t_s	:	Thickness of the sample	m
T	:	Temperature	ºC
T_A	:	Absolute temperature	ºC
T_a	:	Fluid wall temperature	ºC
T_{a_t}	:	Time dependent fluid wall temperature	ºC
T_{ave}	:	Area-weighted average temperature	ºC
T_b	:	Mean bulk temperature of fluid	ºC
T_{b_i}	:	Water temperature at the inlet	ºC
T_{b_o}	:	Water temperature at the outlet	ºC
T_{f_a}	:	Air film temperature	ºC
T_{f_w}	:	Water film temperature	ºC
T_i	:	Internal tube face temperature	ºC
T_m	:	Final mould face temperature	ºC
T_{m_i}	:	Initial temperature of mould face	ºC
T_{m_m}	:	Mould mean temperature	ºC
T_{m_t}	:	Time dependent temperature of the mould face	ºC
T_{max}	:	Maximum temperature (higher than the target temperature)	ºC
T_{min}	:	Minimum temperature (lower than the target temperature)	ºC
T_o	:	External tube face temperature	ºC
T_r	:	Values of the temperatures for which an average is being calculated	ºC
T_s	:	Temperature of the surface	ºC
T_t	:	Target temperatures	ºC
T_{w_t}	:	Time dependent temperature of the plywood face	ºC
T_∞	:	Ambient temperature	ºC
∇T	:	Temperature variance per axial changes	ºC
u	:	Fluid velocity	m/s
$u_1 \ldots . u_4$	:	Fluid velocity in the parallel branches	m/s
u_x	:	Fluid velocity in x-coordinate direction	m/s

u_y	:	Fluid velocity in y-coordinate direction	m/s
u_z	:	Fluid velocity in z-coordinate direction	m/s
U	:	Water conductance	W/K
U_1	:	Mould surface conductance	W/K
U_2	:	Insulated surfaces conductance	W/K
V	:	Volume	m^3
V_c	:	Volume of channel	m^3
$\bar{V}_{co}$	:	Volume of composite mixture or laminate	m^3
V_e	:	Variance of the error term	-
$\bar{V}_e$	:	Pure variance of the error term after pooling	-
V_f	:	Fibre volume fraction	-
$\bar{V}_f$	:	Volume of fibre	m^3
$\bar{V}_h$	:	Volume of hardener	m^3
V_H	:	Volume of high dilatable materials	m^3
V_L	:	Volume of low dilatable materials	m^3
V_m	:	Volume of mould	m^3
$\bar{V}_{ma}$	:	Volume of matrix	m^3
V_o	:	Volume of object	m^3
V_P	:	Variance (or mean of the squared deviations) of each process parameter	-
V_r	:	Resin volume fraction	-
$\bar{V}_\mathrm{r}$	:	Volume of resin	m^3
V_t	:	Volume of tool	m^3
V_v	:	Volume of vessel (vessel capacity)	m^3
V_w	:	Volume of displaced water	m
w_H	:	Width of high dilatable strip material	m
w_L	:	Width of low dilatable strip material	m
$\bar{W}_\mathrm{co}$	:	Weight of composite mixture or laminate	m
W_f	:	Fibre weight fraction	-
$\bar{W}_f$	:	Weight of fibre	kg
W_g	:	Width of the bottom face of the glass fibre (insulation)	m
W_gs	:	Height of the side face of the glass fibre (insulation)	m
W_h	:	Weight fraction of hardener	-
$\bar{W}_h$	:	Weight of hardener	kg
W_m	:	Channel separation value	m

W_{ma}	:	Weight fraction of matrix	-
$\bar{W}_{\mathrm{ma}}$	:	Weight of matrix	kg
W_{r}	:	Weight fraction of resin	-
$\bar{W}_{\mathrm{r}}$	:	Weight of resin	kg
W_{w}	:	Width of the bottom face of the plywood	m
W_{ws}	:	Height of the side face of the plywood	m
WH_t	:	Water heating time (for hot connection)	H_t
WH_{t_C}	:	Water heating time (for cold connection)	H_{t_C}
x	:	Distance from the leading edge of channel	m
x_i	:	Values of the response variable or simulation results	-
x_{opt}	:	Equivalent value of $\boldsymbol{y_{opt}}$.	-
y	:	Thickness of the first inflation layer	m
y^+	:	Dimensionless parameter of y^+ Law	-
y_e	:	Deflection of the empty pan at the specified temperature	mm
y_i	:	Test results (S/N ratio value of x_i)	-
y_{opt}	:	Expected result of the optimal combination according to S/N ratio	-
y_{P_j}	:	Test results of each parameter at each given level	-
y_r	:	Deflection of the reference at the specified temperature	mm
y_s	:	Deflection of the sample at the specified temperature	mm
Y	:	Energy release rate	J,(W.s)
z	:	Axial length	m
α	:	Coefficient of thermal expansion (CTE)	$^oC^{-1}$
α_c	:	CTE of the cracking ply	$^oC^{-1}$
α_H	:	CTE of the high dilatable strip material	$^oC^{-1}$
α_L	:	CTE of the low dilatable strip material	$^oC^{-1}$
α_m	:	CTE of the material	$^oC^{-1}$
α_{re}	:	CTE of the remainder of the laminate	$^oC^{-1}$
α_r	:	CTE of the reference	$^oC^{-1}$
$\propto$	:	Thermal diffusivity	m^2/s
ρ	:	Density of fluid (water) or Density in general	Kg/m^3
ρ_c	:	Density of channel material	Kg/m^3
ρ_{co}	:	Density of composite mixture or laminate	Kg/m^3
ρ_f	:	Density of fibre	Kg/m^3

ρ_h	:	Density of hardener	Kg/m^3
ρ_m	:	Density of mould material	Kg/m^3
ρ_{ma}	:	Density of matrix	Kg/m^3
ρ_{o}	:	Density of object	Kg/m^3
ρ_{r}	:	Density of resin	Kg/m^3
ρ_t	:	Density of tool material	Kg/m^3
υ	:	Kinematic viscosity (μ/ρ)	m^2/s
ν	:	Poisons ratio	-
μ	:	Dynamic viscosity	N.m/s^2, kg/m.s
ϑ	:	Geometric fitting factor	-
ε_H	:	Strain in the high dilatable strip material	-
ε_L	:	Strain in the low dilatable strip material	-
ε_m	:	Apparent strain of the material	-
ε_r	:	Apparent strain of the reference	-
$\mathcal{E}_{th}$	:	Thermal strain	-
$\mathcal{E}_\theta$	:	Tangential strain	-
δ	:	Deflection	mm
δ_{max}	:	Maximum deflection	mm
$\sigma_{\mathrm{H}_{\mathrm{min}}}$	:	Minimum normal stress in high dilatable strip	Pa
$\sigma_{\mathrm{H}_{\mathrm{max}}}$	:	Maximum normal stress in high dilatable strip	Pa
σ_L	:	Longitudinal (x-axis) stress	Pa
$\sigma_{\mathrm{L}_{\mathrm{max}}}$	:	Maximum normal stress in low dilatable strip	Pa
$\sigma_{\mathrm{L}_{\mathrm{min}}}$	:	Minimum normal stress in low dilatable strip	Pa
σ_{max}	:	Maximum tensile stress	Pa
σ_θ	:	Tangential stress	Pa
σ_r	:	Radial stress	Pa
σ_{th}	:	Thermal stress	Pa
σ_z	:	Axial stress	Pa
τ_{xy}	:	Shear stress in xy-plane	Pa
τ_{max}	:	Maximum shear strength	Pa
$\theta(\Delta T_o)$	:	Temperature variance	^{o}C
$\theta_i(\Delta T_i)$	:	Initial temperature variance	^{o}C
η	:	Geometry factor (Ding et al., 2001)	-
∇	:	Gradient vector field of a scalar function	-

List of abbreviations

Symbols		Discerptions
AlN	:	Aluminium Nitried
Alepoxy	:	Aluminium and epoxy mixture
ASTM	:	American society for testing and materials
CFD	:	Computational fluid dynamic
CF	:	Carbon fibre
CFRP	:	Carbon fibre reinforced polymer
CJC	:	Cold-junction compensation
CMC	:	Ceramic matrix composite
Co4	:	Corner number four
CPU	:	Computer Processing unit
CTE	:	Coefficient of thermal expansion
1D	:	one dimensions
2D	:	Two dimensions
3D	:	Three dimensions
DAQ	:	Data acquisition
DGEBA	:	Diglycidyl Ether of Bisphenol A
DoF	:	Degree of freedom
DVB	:	Double vacuum bag
FDM	:	Finite differential method
FEM	:	Finite element method
FFE	:	Fractional factorial experiment
E-glass	:	Electrical resistance glass fibres
FOS	:	Factor of safety
FVM	:	Finite volume method
FV	:	Finite volume
GGI	:	General grid interface
GKN	:	Guest, Keen and Nettlefolds
GMC	:	Graphite matrix composite
HM	:	High modulus
HT	:	High tensile
HTM	:	High temperature moulding
IEC	:	International electrical commission
IM	:	Intermediate modulus
ISO	:	International standardization organisation
KWU	:	Kansas Wesleyan University
LB	:	Low is better
LFA	:	Laser flash analysis
LM	:	Low modulus
LTM	:	Low temperature moulding
M&S	:	Modelling and simulation

MMC	:	Metal matrix composite
MTM	:	Medium temperature moulding
MW	:	Microwave
NCF	:	Non crimp fabric
NRC-IAR	:	National research council Canada-institute for aerospace research
OA	:	Orthogonal array
OoA	:	Out of autoclave
PDE	:	Partial differential equation
PL-DSC	:	Plasma- differential scanning calorimetry
PMC	:	Polymer matrix composite
PVC	:	Polyvinyl chloride
RFI	:	Risen film infusion
ROM	:	Rule of mixture
RTM	:	Resin transfer moulding
SCRIMP	:	Seemann composite resin infusion moulding process
SEM	:	Scanning electron microscopy
S-glass	:	Stiffer/ Stroger version of E-glass fibres
SiO_2	:	Silicon dioxide
S/N	:	Signal to noise
SQRTM	:	Same quality resin transfer moulding
SST	:	Shear stress transport
SVB	:	Single vacuum bag
TCX^{TM}	:	ThermoCeramic
Tg	:	Glass transition temperature
UHM	:	Ultra-high modulus
USB-TC	:	Universal serial bus- Time counter
VBRI	:	Vacuum bagging resin infusion
VRTM	:	Vacuum assist resin transfer moulding
VTM	:	Variable temperature moulding

Acknowledgements

I want to express now my most sincere thanks to all who contributed to the development of this thesis during the last four years.

I dedicate this PhD work to my lovely wife Gulala for her unceasing encouragement, support and attention, my mother the most important person in my life and my sons Rawaz and Yad for providing a balance in my life, which made this PhD work easier.

I would like to express my appreciation for the support and guidance of the director of my studies, Professor Stephen Grove, School of Marine Science and Engineering at Plymouth University.

I would also like to gratefully acknowledge my three supervisors, Dr Jahir Rizvi, Lecturer in the School of Marine Science & Engineering at Plymouth University, and Adam Kyte, for their expert guidance, advice, support, and encouragement. They have generously provided me with everything I needed. Without their help this PhD work would never have been possible. I take this opportunity to express gratitude to all of the department faculty members, who directly or indirectly, have lent their hand in this PhD study, especially Dr Richard Cullen, Dr Robert Allen, Peter Mills and Terry Richards.

I have to express my gratitude to the Iraqi Government-Ministry of Higher Education and Scientific Research, which provided all the financial support for my stays in Plymouth and study expenses. Particular thanks are given to Polytechnic University of Slemani for their support.

Author's declaration

At no time during the registration for the degree of Doctor of Philosophy has the author has been registered for any other University award without prior agreement of the Graduate Committee.

This PhD study was financed with the aid of a scholarship from the Ministry of Higher Education and Scientific Research, Iraqi Government Research Council, and carried out in collaboration with Plymouth Marine Computer Laboratory.

Relevant scientific seminars and conferences were regularly attended, at which work was often presented; external institutions were visited for consultation purposes and several papers prepared for publication.

Publications (or presentation of other forms of creative and performing work): **Presentation and** Conferences Attended:

1) Conference paper (**Numerical Studies of Integrally-Heated Composite Tooling**). Presented in ECCM16, 22-26 June 2014 Seville, Spain.
2) Journal paper (**Numerical simulation and design optimization of an integrally-heated tool for composite manufacturing**). Submitted 29 April 2014 to journal of Materials and Design for publication, Accepted 10 July 2014 and Available online 1 August 2014.
3) Journal paper (**Numerical Simulation and Experimental Verification of Heating Performance of an Integrally Water-heated Tool**). Submitted 16 September 2015 to journal of Reinforced Plastics & Composites, Accepted 23 November 2015 and Available online 28 January 2016.

External Contacts: rzgarm03@ yahoo.com

Word count of main body of thesis: **42,250** *Signature*:
Date: 9/10/2015

Chapter 1

Introduction

1.1 Introduction

Composite materials are currently of interest due to their attractive characteristics. Polymer matrix composite (PMC) reinforced by carbon and glass is the most widely used composite category, because CFRP compared to aerospace aluminium and steel alloys can provide lower density and expansivity as well higher specific modulus (modulus/density), higher specific strength (strength/density) and chemical inertness, e.g. the specific strength of CFRP and aluminium (Al) are 1.62 $MPa.m^3/kg$ and 0.03 $MPa.m^3/kg$, respectively. Therefore carbon fibre reinforced polymer (CFRP) composites currently have become preferred materials in aerospace, automotive, defence, marine, sporting goods and infrastructure industries (Thomas, 2013). CFRP structures are often manufactured from prepreg (the pre-impregnated carbon fibre with suitable resin) and finds wide ranging applications due to its superiority in achieving the aforementioned properties in addition to high damage tolerance, high durability to the environment (e.g. temperature variance, humidity, vibration and fatigue), very low expansivity (low CTE), low void content and ease of repair, compared to the metals. Additionally prepregs facilitate the manufacturing of complex shapes with low cost and also they have potential for automation that reduces processing time and cost (SP Systems, 2001).

Although the thermoset epoxy resin used in most CFRP composites can provide well-bonded (three dimensional cross-linked) structures with excellent strength and hardness after curing, it has the problems of complexity and high cost processing (curing) in autoclaves, which restrict its application. Therefore researchers and manufacturers nowadays have been attempting to find

alternative methods to overcome these problems and produce composites without autoclave with the same quality (Gardiner, 2011; Payette et al., 2015).

Producing a successful composite component with the desired shape and characteristics depends on proper curing process in an appropriate mould. The curing process of advanced composites (prepregs) requires pressure and elevated temperature for a predetermined length of time (curing cycle time). Heating occurs according to a specified isotherm (ramp and dwells) and curing involves internal heat generation (exothermic heat) due to a complex reaction between the resin and hardener (Almeida, Neto & Nogueira, 1994; Hagstrand, 2005). The elevated temperature of curing initially reduces the resin viscosity that facilitates its flow before it gels and then initiates and maintains the chemical reaction in the resin that changes the molecular structure, while the applied pressure consolidates individual plies, compresses voids and squeezes the excess resin out of the composite material. Therefore uneven heating of the laminate during processing, as mentioned by Yan (2007), causes uneven cure, residual stress across the laminate and finally producing components with degraded quality. Consequently improvement of the heating performance of the composite tooling will be an effective factor in improving the quality and productivity (production time) of the composite components.

Although the autoclave produces components from prepreg with high quality, it cannot achieve the main requirements of production which are; low cost and high quantity and also producing large components (Johnston, 1997; Monaghan, Brogan & Oosthuizen, 1991). Many different alternative methods, techniques and materials have been created and developed as alternatives to autoclave to overcome its disadvantages in processing advanced composites.

Lots of the manufacturers are keenly pursuing out of the autoclave (OoA) processes that enable producing advanced composite components with the same quality as autoclaves. The tried and examined alternatives with their advantages and drawbacks are illustrated in Table 1-1

Table 1-1 Advantages and drawbacks of the OoA techniques

OoA technologies	Advantages	Drawback
OoA prepreg[1]	• Provides more flexibility in manufacturing. • Saving significant energy • Less requirement of expensive tooling	• Expensive raw material
SQRTM[2]	• Produces true net shape and highly unitized components with tight tolerance • High level of integration • High surface finish	• High tool cost • Injecting extra liquid resin is cost effective
Quickstep[3]	• Provides faster cure • Produces high quality components	• Size limitation
DVB[4]	• Enables cure of prepreg under VB	• Sealing difficulties
Integrally heated tools[5]	• Heating the composite parts more directly, during curing. • Enables fabricating large and complex shape components. • Consumes lower amounts of heat (energy), time and capital	• Low component quality compared to autoclave

1: (Gardiner, 2011), 2: (Black, 2011), 3: (Griffiths & Noble, 2004), 4: (Sherwin, 1999), 5: (Baril-Gosselin, 2013; Grove et al., 2005).

Attempts are continuing to improve or add more alternatives for the manufacturing of advanced composite products. Some researchers have been focused on developing integrally heated tools in which the heating element and the tool are combined in-mould or on-mould (Marsh, 2003). The direct contact between the tool and heating unit increases heating rate, decreases heating time and saves energy compared to the traditional methods (Arney et al., 2004; Raizenne, Hind & Poupore, 2006; Walczyk & Kuppers, 2012). The importance of integrally heated tooling is that the required heat, to process the curing

assembly, transfers directly from the heating source to the component through the mould and across its surface by conduction, making the heating process faster with lower energy loss compared to the traditional methods of ovens and autoclaves, in which the heat transfers by convection from the environment. Another benefit of the integrally heated tool is that the component is heated from one side, which enables the exothermic heat from curing reactions to transfer out from the other side, which prevents temperature overshoot and facilitates heating at a higher rate than in an autoclave. A number of integrally heated tools are already available commercially and are suitable for use in closed mould processes such as compression moulding, resin transfer moulding (RTM) and its variations, for example; vacuum assisted resin transfer moulding (VARTM) as well as Seemann Composite Resin Infusion Moulding Process (SCRIMP) (Mason, 2006; Mazumdar, 2001).

Various heating techniques are available to combine with the integrally heated tools (Mason, 2006). Despite some disadvantages, fluid circulation is considered as the most appropriate technique in the concept of integrally heated tools (Black, 2010b; Petrykowski & Fischer, 2012; PMC; Sloan, 2013). Fluid circulation is widely used in different industries because it can also be used for cooling as well assuming that the achieved temperature inside the cure assembly dose not exceeds the desired value at any point in the heating process. Many studies have been carried out for optimising the geometry of the mould and the channel as well as selecting the proper heating fluid and tool material (Black, 2011). Water and steam are the preferred heating fluids when the desired mould face temperature will be lower than 100ºC (Guilong et al., 2010; Wang, Zhao & Guan, 2011; Wang et al., 2011a; Wang et al., 2011b). Latest investigations show that the water heating technique, compared to oil

and electrical, is superior in providing better heating performance, in the self-heated tools, with lowest time and power consuming (Sloan, 2013).

Most of the published investigations were conducted in the fields of plastic injection and the thermoforming industries, which are completely different from the curing process of thermosetting composites. That is because the heat, in the curing process, must be provided uniformly in a specified time (ramp and dwell) to prevent problems of temperature lag or overshoot at the centre of the laminate. Therefore the fluid circulation technique has potential to achieve better control during the cure cycle because the temperature inside the cure assembly will not exceed the desired value at any time of the heating process and overheating (temperature overshoot) is prevented (Marsh, 2003).

Tool efficiency and performance also depend on its construction materials, which must be selected according to the working tool lifetime requirements, number of items to be produced (run length), complexity of product shape and possible savings in assembly costs. Metallic tools provide good durability and relatively high thermal conductivity, but the mismatch of thermal expansion between the tool and the composite part causes manufacturing defects and lack of accuracy in the geometries of the composite components (Lorincz, 2009; Morey, 2010). Despite its very low thermal expansion coefficient, which nearly matches that of composite, Invar (36% nickel-iron alloy) is also undesirable in industry due to the high weight of the tooling as well as the initial tooling investment and operation costs (Baril-Gosselin, 2013).

Carbon fibre reinforced polymer (CFRP) has the issues of low thermal conductivity and matrix cracking under thermal loading, as mentioned by Campbell (2004), after repeated cycles of heating that restricts its application as

a tooling material, but it can be considered as the most appropriate material for building composite tooling because of its good structural performance, low coefficient of thermal expansion (3.5 x 10^{-6} m/m K^{-1} or less), low weight and easy configuration. Particulate composites, such as Alepoxy (aluminium particles and epoxy) that is frequently applied in the rapid tooling technologies, are used in this PhD research due to its low cost, higher thermal conductivity (compared to CFRP) and ability of embedding the channels in the mould.

Integrally-heated tools, which are heated straightway without the need to heat the surrounding environment, possess the potential to be an alternative to autoclave. Therefore a water-heated tool, made of composite, is considered as an effort to obtain the effective design factors and optimised design that can improve the heating performance of the tool and define suitable material combination that facilitates the tool construction and provides acceptable strength (to resist the applied moulding pressure), thermal conductivity as well as tool lifecycle under the effect of thermal loads. The proposed tool will be suitable for moulding composites of low temperature matrixes (LTM) with cure temperatures ranging between 30ºC to 80ºC, e.g. the LTM10, LTM12 and LTM45 types that are manufactured by Cytec (2014).

Three design factors (channel cross section, channel alignment and channel separation) are selected due the expectation of their significant effect on the tool heating performance and lack of consideration in previous studies. Then nine design combinations are defined using Taghuchi's orthogonal array (OA). The ANSYS software, after verification its performance analytically, is applied to simulate the transient heat transfer in the proposed nine test cases and analyse the heating performance of the integrally water-heated. The statistical approach

of S/N ratio has been applied to allow the control of the numerical response variables. Based on ANOVA the effect of each design parameter on the response strategies (heating time per unit mass and temperature variation) are determined and the optimal tool design is predicted.

An experimental is built, after some amendments in the predicted optimal tool design that facilitate tool manufacturing and increase the tool surface area and thus monitoring the tool surface temperature becomes easier and clearer. The heating performance of the experimental tool is analysed practically and experimentally to verify the numerical conclusions and confirm the predicted optimal tool design. Also ANSYS transient structural, after analytical verification, is applied to simulate a model of the experimental tool and to define the static thermomechanical characteristics of deformation, stresses and strain in the tool (under the effective thermal loads) that presents the tool durability during heating. The actual material properties and boundary conditions are defined practically and set during the simulations to achieve more reliable results.

1.2 Motivation and Objective

This PhD research is performed as a result of:

- The disadvantages of the autoclave method in manufacturing advanced composite components, requiring alternatives to overcome its problems.
- The demands of cost reduction, energy efficiency and production time in the composite manufacturing sector, which has increased and spread widely in the last two decades.
- The problem of thermal expansion mismatch between metallic tools and composite components.

- The recent development of producing large composite products in one-piece that needs larger tools and cannot be processed traditionally or may be very expensive as mentioned by Jiang et al. (2002).

Integrally-heated tools have the potential to be an alternative to autoclave because of supplying heat directly to the tool without need to heat the surrounding environment, but still require improvement to produce components with autoclave quality. Consequently this PhD work aims to investigate the heating performance of an integrally water-heated tool, made of composite, numerically under the effect of different factors in order to design and construct a successful optimal tool for processing advanced composites of LTM prepregs in various manufacturing sectors, which can be accomplished by fulfilling the following research objectives:

- Identifying the effective design factors that influence the heating performance of proposed tool.
- Determining an optimised design that can improve the heating performance of the integrally heated tool and maintain its strength.
- Identifying a suitable material combination that can facilitate the tool construction, while providing acceptable mechanical strength, tool life and thermal conductivity.
- Estimating the tool structural behaviour and durability under the effect of thermal loads due to temperature variation.

Achievement of these objectives will serve to provide answers for each of the following guiding research questions:

- What are the most effective design factors on the heating performance of the tool, which have not been considered previously?

- What material combination can offer suitable thermal conductivity and durability to the effective thermal loads?
- What is the most appropriate methodology for investigating the heating performance and thermomechanical behaviour of the heated tool?
- How can the suitability of numerical study for the heated tool be verified?

1.3 Structure of the study

Chapter One provides an introduction to the research topic, the study's structure, and the guiding research questions. It explains the significance of the research, and its motivations.

Chapter Two systematically reviews the existing literature relating to composite materials and their properties, manufacturing of composites and curing, tooling design for composites, OoA tooling technologies, Integrally heated tools and heating technologies, thermal cycling and its effects, heat transfer equations, modelling, simulation and verification. Accordingly the achieved results and concluded theoretical and practical relations of literature, related to the concepts of this PhD research, are presented and illustrated as basics of analysis, calculations and comparisons, performed during this PhD research.

Chapter Three presents comparison between analytical and numerical analysis of a proposed simple tool model in order to verify the suitability of the ANSYS CFX software in simulating and well assigning of the boundary conditions and material properties during simulating the heat transfer throughout the proposed tool models. The chapter also includes comparison between the 2D and 3D simulation methodologies, selection the optimised time step size and proper

number of the meshing elements that ensures lower computation time with reliable results.

Chapter Four defines the selection of the proposed design parameters and design combinations according to Taghuchi's OA that provides a minimum number of experiments necessary to study in an economical way, numerical simulation of the proposed designs of the heated tool (selected tool test case models), the response variables of heating time per unit mass and temperature variance for evaluating the heating performance of each tool model as well as application the S/N ratio to control the response variables and reduce the variability about the response. Finally illustrates the application of ANOVA in analysing the effect of each design parameter on the heating performance of the heated tool and predicting the optimal design of the water heated tool.

Chapter Five illustrates construction of the experimental tool according to the predicted optimal design, simulation a model of the optimal tool after modifications, testing the experimental tool through a test rig for verifying the simulation results and confirming the predicted optimal tool design. The chapter also explains the measurement methods of the physical and thermal properties (density, volume fraction, thermal diffusivity, specific heat and thermal conductivity) of the tool material to set during simulation as well as a sections defines the calibration and error estimation of the applied apparatuses (thermal camera, thermocouples and flowmeter) to obtain actual practical measure-ments.

Chapter Six illustrates effect of the actual thermal loads (repeated temperature), numerically, on the heterogeneous composite structure of the experimental tool that has anisotropic properties and defines the generated thermal deformations,

stresses and strains through the tool due to temperature variation and mismatch between the CTEs of the tool materials. Simple models of bimetallic strips and single tube are analysed analytically to compare with that simulated numerically by ANSYS transient structural to verify the well assigning of the boundary condition and material properties during simulating the experimental tool structure under the effective thermal loads. The chapter also introduces the measurement method of the CTEs and the mechanical properties of the tool materials as well as the boundary conditions to set during simulation.

Finally, **Chapter Seven** gives a general conclusion of the study's findings, leading to some recommendation for future work.

Chapter 2
Literature Review

2.1 Composite materials

Composites are a combination of two basic constituents, called reinforcement and matrix, which are differ in their physical form and chemical composition and are insoluble in each other. The fibre content improves the mechanical properties such as strength and stiffness, whereas the resin matrix holds the fibre together, transfers mechanical loads through the fibres to the rest of the structure and protects fibres from mechanical (impact, abrasion and corrosion) and environmental damages as well as rough handling. The main categories of composites according to the matrix type are shown in Figure 2-1 (Mazumdar, 2001; Singh, Sarita & Sonal, 2014). Recently polymer is the most widely used matrix because it makes ideal lightweight materials with desirable mechanical properties that can processed easily (Harris, 2001).

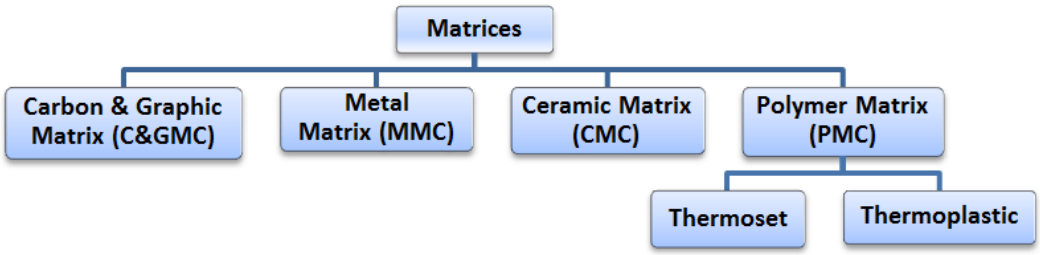

Figure2-1 Classification of matrices.

According to the effect of heat on their properties, polymers can be classified into thermoplastic and thermoset. Upon the application of heat to the mixture of thermoset resins with hardener or catalyst, it undergoes a non-reversible chemical reaction to produce hard, infusible products (Bandyopadhyay & Odegard, 2012; Pigford, Ashraf & Miron, 1983). The cured thermosets will not become liquid again by heat, but their mechanical properties will change

significantly above certain temperature known as Glass Transition Temperature (T_g) and this change is reversible on cooling back below T_g. The most common chemical families of thermoset resin in PMC construction are polyester, vinyl ester, phenolic and epoxy. However epoxy resin has the problems of high cost and processing difficulty due to the requirement of heat for curing, it can provide well-bonding three dimensional cross-linking structures with excellent strength and hardness after curing (Harris, 2001). Epoxy resin can be processed healthier because its cure mechanism does not forms a volatile by-product (Mazumdar, 2001).

2.2 Composite properties

Composites have adjustable and tailored properties because they are not only functions of their components, but also depend on their distribution (laminate stacking sequence), interaction (fibre volume fraction), and processing (cure cycle). Therefore the composite systems can be described by specifying the reinforcement shape, size and distribution (Daniel & Ishai, 2006), as illustrated in Figure 2-2.

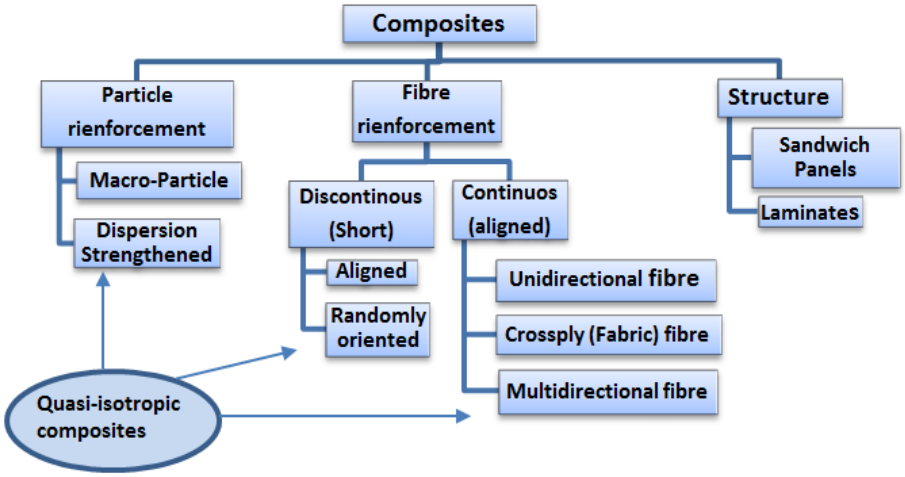

Figure2-2 Composites type (Daniel & Ishai, 2006).

Properties of composites (especially the fibre reinforced), unlike metals, are heterogeneous because they vary from point to point (moving from matrix to fibre) and anisotropic because they change when orientation is changed. Therefore composite properties (e.g., strength, stiffness and thermal conductivity) along the reinforcement direction are much greater than they are in transverse direction. Micro-mechanics deals with the mechanical properties of the constituents and their interaction, whereas macro-mechanics is concerned with the mechanical characteristics of the produced composite structure without direct regarding for the constituents and their interaction. Compared to traditional isotropic materials, there is a complicated relationship between the affected loads and deformation in anisotropic composites that can lead to unexpected behaviours. For example, temperature variation produces uniform expansion or contraction in all directions of isotropic materials, whereas it is non-uniform in composites and causes distortion.

2.3 Carbon fibre reinforced polymer (CFRP) and prepregs

Nowadays different types of fibre materials are available for manufacturing composite components. The most common reinforcing fibres and some conventional bulk materials are illustrated in Figure 2-3, for comparison, according to their tensile strength versus modulus of elasticity. Carbon fibres enable manufacturing of very strong and stiff structures with low density, low thermal expansivity, chemical inertness, specific modulus (modulus/density) and specific strength (strength/density).

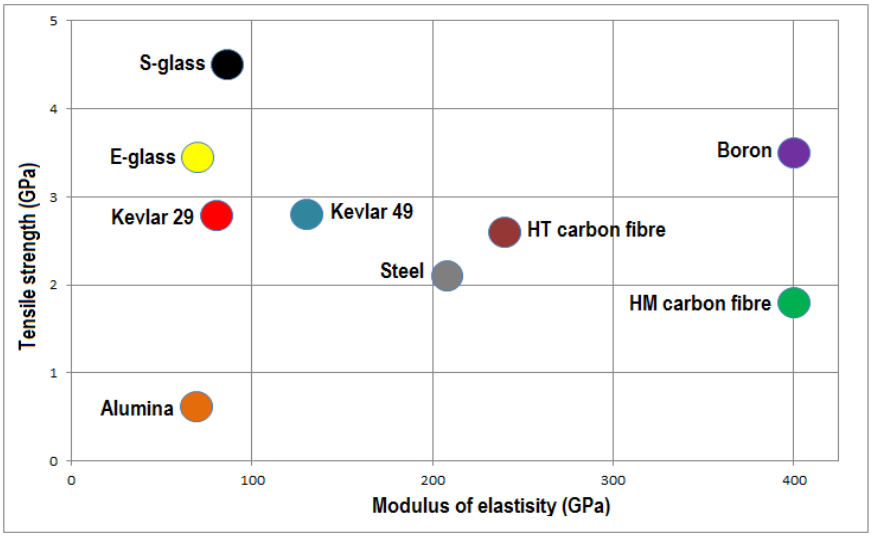

Figure 2-3 Tensile and Modulus properties of composite and conventional metals (Mansfield, 2015; Mazumdar, 2001).

Figure 2-4 illustrates the main types of carbon fibres according to their elasticity and strength. The fibre properties are dominant in the resin fibre mixtures; therefore carbon fibre reinforced polymers (CFRP) are the most prevalent product forms of composites that find wide range of applications.

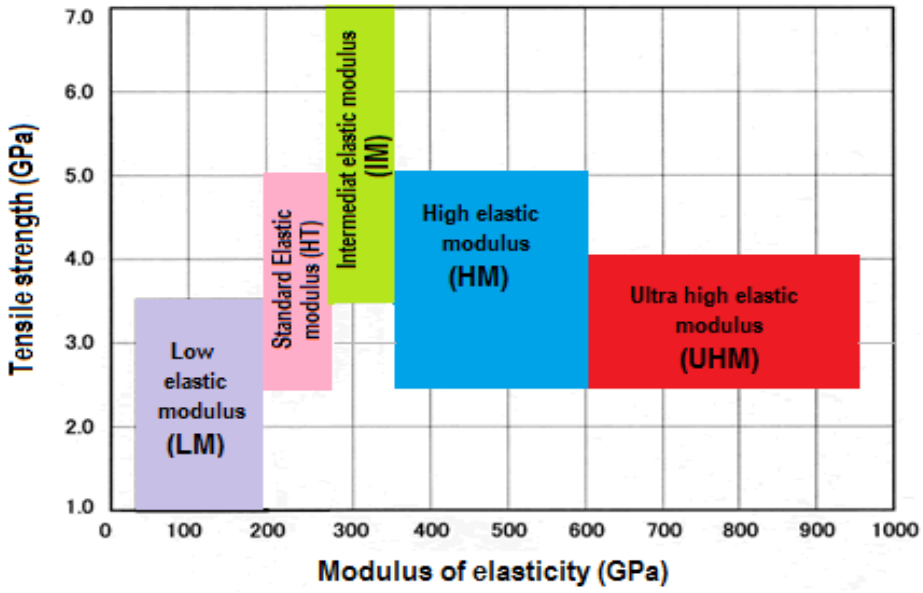

Figure 2-4 Carbon fibre types by mechanical properties(JCFA, 2014; Kopeliovich, 2012)

The polymer matrix in CFRP combination can be retained in a partially cured condition over prolonged period of time and produces a premixed advanced compound known as prepreg (Thomas, 2013). The generic name of “prepregs” belongs to its manufacturing that is processed from high performance fibres pre-impregnated with suitable resin matrix by means of heat and pressure. Prepreg contains some tack or stickiness to allow it to adhere to itself during lay-up operation.

Hot melt technology is the most preferred manufacturing methods of epoxy-based prepregs because it produces less harmful waste compared to the solvent impregnation method. In this method the prepreg is produced by sandwiching and squeezing, simultaneously, the reinforcement between layers of melted resin, Figure 2-5. The dry reinforcement of prepreg may be unidirectional, stitched or woven cloth.

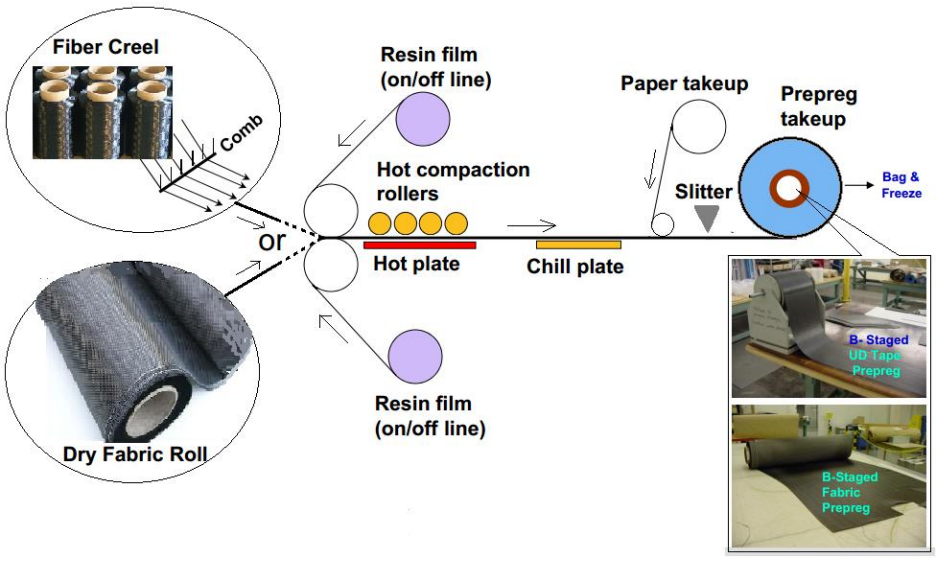

Figure 2-5 Hot melt process of prepreg manufacturing method (Burton et al., 2011).

Thermoset prepregs have limited shelf life, therefore they must be stored in a cool and dry place in order to minimize further cross-linking, increase out-time

and prevent them from aging (Mazumdar, 2001). The pre-catalysed resin system of prepregs requires heating to a prescribed temperature with high-pressure to activate curing reaction and consolidation (Campbell, 2004).

According to the curing temperature of the matrix, prepregs can be classified into low (LTM)(30°C-80°C), medium (MTM)(80°C-120°C), variable (VTM)(65°C-125°C) and high (HTM)(>180°C) temperatures (Bashford, 2007). The prepreg components are manufactured by vacuum bagging method as explained in Figure 2-6. In this process the wet laid-up laminate of prepregs is sealed by a plastic film onto the tool and the air under the bag is extracted by a vacuum pump, up to one atmosphere of pressure, in order to consolidate the laminate. Then the tool is heated indirectly in autoclave or directly if the tool is integrally heated type.

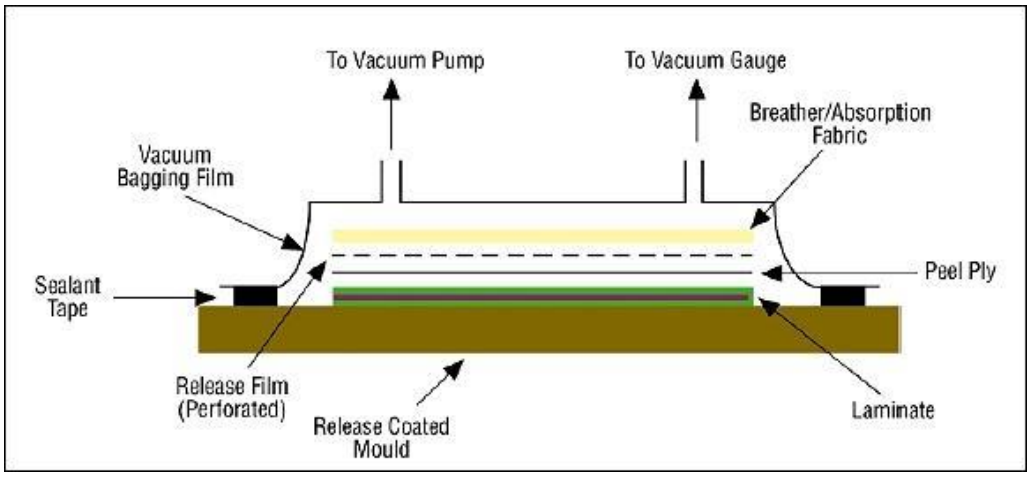

Figure 2-6 Vacuum bagging process for processing prepregs (Cripps, 1998)

2.4 Tooling design for composites

Tooling or tools, the moulds on which composite components are formed, are basis of composite manufacturing. They are not only the means providing reproducible shape and geometry to the mixture of reinforcement and matrix,

but also the mean by which consolidation is achieved and heat is transferred into the composite mixture for curing. Cost and complexity of the composite tools are defined by the performance requirements of the produced composite part and its desired number (ACG-Staff, 2014). Also Arney et al. (2004) deduced that design of the mould tool is the key factor in achieving successful, effective and efficient composite components.

Mazumdar (2001) and Rudd et al. (1997) indicated to the most important factors that must be considered during designing and construction of composite tools, which are; manufacturing time, size, shape, operating pressure and temperature, CTE, strength, durability, stiffness and surface finish of the desired tool. Additionally they deduced that previous considerations must be regarded with the required properties of the desired component; to be produced by the tool, such as the cost, quality and quantity, cure cycle time and temperature, size, shape, CTE and surface finish. Morena (1990) and (2007) as well as Murphy (1994) concluded that selecting a proper tooling material, heating technique and positioning of the heating unit in the tool are the main factors that guarantee obtaining the following properties of the heated tool:

- High heating performances of temperature uniformity and fast heating rate.
- Durability and high lifecycle
- Low manufacturing cost.
- Manufacturability or ease of construction.
- Good thermal conductivity.
- Low weight.
- High thermal stability or low CTE.

Almost all the materials, which can be used in composite tool construction, provide unique capabilities and drawbacks and accordingly composite tooling can be classified into hard tooling and soft tooling(Raizenne, Hind & Poupore, 2006). Hard tooling is relatively heavy and expensive, but potentially superior in its results when they are applied in manufacturing high-performance parts because they are made from the robust materials of ceramic and metals that can withstand higher repeated heating cycle, wear and tear as in addition to maintain good surface finish and dimensional accuracy. Therefore hard tooling is suitable for mass production without becoming damaged (ACG-Staff, 2014; LeggeroForte, 2014). Soft tooling is made up of composites that can be produced with less cost, but they provide low thermal (heating cycle), wear and tear resistances. Therefore this type of tooling is more suited to prototypes than mass production. The appreciated advantage of the soft tools, over the hard tools, is their low thermal expansivity that is often closer to the CTE of the component materials and eliminates the problem of CTE mismatch (ACG-Staff, 2014; ACG-Staff, 2015). Also, compared to hard tooling, soft tooling can provide greater facility through faster fabrication time, complex tool shapes and lower investment cost.

The previous review deduced that of selection the proper tooling material needs balancing between many factors providing that gives the desire properties of low shrinkage, high stiffness and low cost. Sometimes several composite tools can be manufactured for less than the cost of a single hard tool thus making somewhat larger volumes affordable because the final manufacturing cost of the composite tools is lower than that of a hard tool. Typically composite tools, compared to the hard tools, provide more facility for manufacturing large size tools due to their low density and light weight.

2.5 Tooling materials

Tool material can offer most of the required characteristics of the tool providing that it is selected properly between the normal choices of the tool materials that include steel, aluminium, electroform nickel, wet laminated composites, prepregs, monolithic graphite, ceramic and wood (Murphy, 1994; Rosato, 2004; Scott Bader Company, 2005). Figure 2-7 illustrates comparison of the thermal mass between different tooling materials of composites and metals.

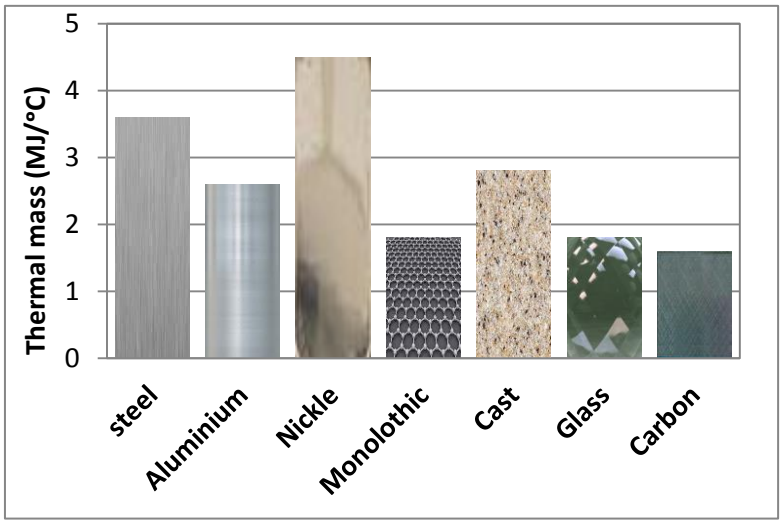

Figure 2-7 Thermal masses of different tooling materials (Bishop, 1992)

Metallic too ls provide high durability, high tool life and relatively high thermal conductivity, but the issues of their high CTE, thermal mass and density make them undesirable as tooling material in composite industry (ACG-Staff, 2015; Parker et al., 1981; Schwarz, Krahn & Hartwig, 1991). That is because the mismatch between CTEs of the tool and the composite part produces thermal stresses, lack of accuracy, distortion (e.g. spring back) and damages in the produced part (Baril-Gosselin, 2013; Sloan, 2011). Invar 36 has a good CTE which nearly matches that of CFRP, but slowly lose its place in industry due to the issues of tooling weight, operation and initial investment costs (Mazumdar,

2001). Another issue of invar tooling is long cure cycles due to the high density and thermal mass (volumetric heat capacity) that makes the tooling absorb most of the heat (Callister, 2002).

Although composites, especially CFRP, as applied by Grove et al. (2005) for constructing a proposed integrally heated tool, have potential to overcome the problems of the hard tools due to its low density, thermal mass and CTE, their application is still restricted because of its low lifecycle, thermal conductivity and low resistance to matrix cracking under the effect of repeated thermal loading (Campbell, 2004). On the other hand each of Lucas & Danford (2009) and Khairul & Anghelescu (2009) investigated the manufacturability, tool cost, and durability performances of carbon foam as tooling material and they deduced that the residual stresses in the part and the tooling can be reduced due the low CTE and modulus of the carbon foam, but the mechanical strength of the foam must be considered during the tooling design.

In order investigate the effect of tooling materials on the durability and lifecycle time of composite tooling, Morena (2007) quoted the lower lifecycle values of some composite and metallic tools from reports of various industries, as listed in Table 2-1. Results show that the metallic tools are more durable (higher lifecycle) and the lifecycle of composite tooling depends heavily on the manufacturing method because there is a big difference between the quoted values of prepreg and wet lay up toolings.

CFRP composites are the most appropriate tooling materials, Although, compared to the hard tools, they have low wear resistance and matrix micro-cracking that occurs due to thermal fatigue and humidity, especially during intermittent operating (Campbell, 2004; Zimmer et al., 2012). Because

composite properties can be adjusted and tailored, different studies were conducted to improve the wear and fatigue resistance of the CFRP tools, for example Ji *et al.* (2005) applied nano-dopants (e.g. nano-SiC and Nickel-coat) to the surface layer of a CFRP mould and achieved improvement in the tool wear resistance. On the other hand Nair *et al.* (2001) improved micro-cracking of carbon fibre by using matrix possesses higher temperature endurance and humidity resistance.

Table 2-1 A fabricated mould, tool and fixture life (fabricated in autoclave at 85-100 psi) (Morena, 2007).

Mould type				**Autoclave cycles** at 170°C (before repair)	
Material	Fabrication method			Tool	Bonding fixture
Steel	Sheet, Cast or Machined			700	1000
Aluminium	Sheet, Cast or Machined			300	500
Composites	***temperature***	***Lay-up***	***Process***		
Epoxy, Glass, Carbon fibre reinforced	Room	Wet	Vacuum Bagged	30	50
	Room/High	Wet		50	80
	High	Wet		60	90
	High	Prepreg Wet surface coat		100	150
	High	Prepreg Film surface coat		200	300

Another key problem of composite tools is their low thermal conductivity, especially through thickness, due to the poor conductor resin that acts as an insulation material (Han & Chung, 2011; Han et al., 2008). The thermal conductivity of carbon fibre is investigated by Hind & Robitaille (2010) and they concluded that the values of in-plane and through thickness thermal conductivities of cross-ply laminates with fibre volume fractions between 0.55 and 0.62 are 2.6 - 3.9 W/m.K and 0.45 - 0.74 W/m.K, respectively. The through-thickness thermal conductivity of carbon fibre composites can significantly be enhanced by; using three-dimensional weaving fabrics, filler incorporation as

well as curing pressure, which provides higher volume fraction (Schuster et al., 2008; Schuster et al., 2009). Adding filling materials can improve thermal conductivity of composites, as deduced by Milella *et al.* (2014). Accordingly Gallagher (2012) applied a heterogeneously structured resin with conductive silver filler of 9% weight fraction and obtained highest thermal conductivity in excess of 5 W/m.K.

Regarding the particulate composites Konzelmann et al.(2008) studied the influence of silica glass (SiO_2) and aluminium nitride (AlN) as a filling material in the thermal conductivity and electrical properties of epoxy resin, as a result they advised application of AlN in constructing the moulds that need heat transfer. Akatsuka and Takezawa (2003) concluded that thermal conductivity of isotropic resins can be increased approximately 1.5 to 5 times by adding certain kinds of ceramic powder as filler. Papanicolaou *et al.* (2012) studied the mechanical properties of aluminium-epoxy particulate composites and concluded that the bending modulus increases continuously with fibre volume fraction, however the flexural strength decreases due to agglomerations. Senthilkumar et al. (2012) also investigated the mechanical and thermal properties of particulate epoxy resin-aluminium (Alepoxy) composite with various volume fractions, which are frequently applied in rapid tooling technologies, and concluded that the mixture with 0.5 fibre volume fraction provides 4.67 W/m.K thermal conductivity, while Tomlinson and Stapley (1977) concluded 1.35 W/m.K and the variation may return to the difference of resin type, fibre particle size, measurement methods applied. Zhou and Yu (2010) concluded that the thermal conductivity of aluminium/epoxy resin composites is influenced by the size, concentration and surface modification of the particles e.g. composites of 2 μm particles with 0.48 volume fraction has thermal conductivity of 1.25 W/m.K while that of 40 μm has

1.16 W/m.K. Also they deduced that uniform dispersion of the particles eliminates agglomerate and decreases air voids.

Some researchers studied application of bonded dissimilar materials, e.g. metal faced composite, as tool material to solve the key problems of through thickness conductivity (Baril-Gosselin, 2013; Morgan, 2014; Raizenne, Hind & Poupore, 2006). Different attempts were carried out by NRC-IAR to develop the heating performance of an integrally PMC tool by lining a copper sheet at its back surface (Lynn et al., 2010; Raizenne, Hind & Li, 2005). Their results show that the tool thermal conductivity in the directions of in-plane and through thickness is increased by 1.3 W/m.K and 0.3 W/m.K, respectively. The main issue of this type of tools is obtaining intimate contact and preventing it from delamination, erosion, melting and thermal degradation.

2.6 Curing process

Curing is the toughening or hardening of the composite materials and cross-linking of polymer chains, after exposing the composite mixture to elevated temperatures and pressures simultaneously. Curing process occurs through a predetermined length of time and cure cycle refers to the magnitudes and durations (historic) of the temperature and pressure applied during the curing process (Loos & Springer, 1983). The pressure is applied to compact and consolidate the cure assembly during processing, remove the excess resin and entrapped voids inside the laminate and finally to obtain a cured component with good quality (high volume fraction and strength as well as low void content) (Yan, 2007). The cure process of thermoset composites requires external heating and involves two nested stages of impregnation and gelation (Shigue et

al., 2004). During the impregnation stage the resin melts and its viscosity drops to a lower amount that facilitates the resin flow under the applied pressure to impregnate the fibre. The gelation stage starts with initiation of the resin reaction initiates and cross-linking, through which the resin viscosity increases slowly until the resin gels and flow ceases. The cure reaction, during the gelation stage, generates internal heat (resin exotherm) (Loos & Springer, 1983). Garschke et al. (2012) concluded that further heating of the resin, while the cross linking is still low enough, results in another drop in viscosity.

Slow heat transfer through the cure assembly, especially the large thickness laminates, due to its low thermal conductivity produces higher temperature gradients in the cured composites that may produce components with mechanical and thermal properties below the expected (McGee, 1982). Sometimes high temperature overshoot at the centre areas of the laminate resulting in material degradation (Yan, 2007). On this account the cure of thermoset resin in a cylindrical mould heated by air is investigated by Kosar et al. (2005) and concluded that temperature gradients developed within the resin with the highest temperature in the centre due to the internal heat of cure reaction, low thermal conductivity and moderate heat capacity of the resin.

The cure cycle has a significant effect on the ultimate thermal and mechanical properties of the produced component and efficiency of composite processing is a function of performing the cure cycle with the following major considerations (Loos & Springer, 1983; McGee, 1982; Plesu et al., 1994):

- The temperature inside the resin must not exceed (overshoot) the present maximum value of curing temperature, at any time during cure.

- All the excess resin must be squeezed out from every ply of the composite at the end of the process.
- Uniform cure must be achieved completely.
- The entrapped voids must be removed out to produce components with the lowest possible void content.
- The curing process must be achieved in the shortest amount of time.

Ding et al. (2001) mentioned that heat transfer in the curing assembly (composite laminate) is complex and involves conduction, convection by resin flow, exothermic heat of cure reaction as well as phase change due to resin polymerisation. Numerous models have been developed based on that of Loose and Springer (1983) to simulate and analyse the curing process of thermoset composites during manufacturing (Skordos et al., 1997). The models are an incremental transient finite difference method that accounts for both thermal and chemical interactions, involving simultaneous mechanisms of resin flow, heat transfer, consolidation, void content, residual stress and heat generation (Skordos & Partridge, 1999). Modelling of cure assembly is performed to define the spatial transient distributions of the temperature and degree of the cure across the laminate thickness, therefore successful modelling requires extensive knowledge of material properties and processing characteristics (consolidation pressure and curing cycle temperature) of the cure assembly (Yan, 2007).

Previous inferences show that curing processes involves a complex heat transfer and the mould temperature must be enough for curing (decomposition of the initiator) without causing high temperature gradient and overheating, in the resin, that produce parts with mechanical and thermal properties below their specification. This reality should be taken into account for improving any

process of curing outside autoclave, successfully. Although rapid curing reduces initial resin viscosity and improves resin flow properties thereby increases production, sometimes it may cause dry spots in the produced components due to the low impregnation time therefore care must be taken for defining appropriate curing cycle (ramp rate and dwell time) to prevent the curing problems of dry spots and resin richness.

2.7 Autoclave curing

Autoclave is still widely used in advanced industries, such as; high performance automotive and aerospace because it produces high-quality composite components (Davies et al., 2007; Herring & Fox, 2011; Johnston, 1997; Slesinger N., 2009). Autoclave is a combination of versatile equipment and typically consists of pressure vessel, a control system, electrical heating system, gas generation system and vacuum system (Monaghan, Brogan & Oosthuizen, 1991). The heat convection coefficient inside the autoclaves pressurised at 7atm (7.1 bar) ranges between 80-180 $W/m^2.K$ and generally the effectiveness of heat transfer of the pressurised air inside the autoclaves varies significantly with location due to uneven gas circulation (Johnston, 1997; Slesinger N., 2009). The operating environment of this traditional method, high pressure and temperature, facilitate the removal and dissolution (disappearance) of the voids present in the part (Almeida, Neto & Nogueira, 1994; Hagstrand, 2005). Autoclaves can provide high consolidation pressure that enables fibre volume fraction typically above 60% in laminates of advanced composites and improves the mechanical properties of the products (Bashford, 2007; Hexcel, 1998; Stringer, 1989).

Although autoclave technique lends considerable versatility to the composite manufacturing process and produces components with high-quality, it needs high-capital and operating costs despite the problems of size limitation (Johnston, 1997; Monaghan, Brogan & Oosthuizen, 1991; Slesinger N., 2009). Additionally, in autoclave the heat-up rates cannot be more than 1- 4°C because the resin exothermic could not be run away quickly in the autoclave environments (Ciriscioli & Springer, 1990; Strong, 2008). Tool heating in autoclave is achieved by forced convention from heating air or gas, typically at 120 - 180°C, but low thermal capacity of air restricts the insertion rate of heat into the mass of the composite material and the tooling (Li et al., 2008).

Accordingly the heating process in autoclave will be time consuming and costly ($1000 to $3000 per an autoclave run, especially for the large moulds) depending on curing time and chamber size (Gardiner, 2008). Plesu et al. (1994) deduced that the resin temperature, in autoclave curing, may rise up to 100°C above the mould temperature and Ciriscioli & Springer (1990) and Strong (2008) mentioned that to avoid a resin exotherm 'run away' in the autoclave environment, the heating rate in autoclave should not be more than 1-4°C. Uneven gas circulation in the autoclave produces non-uniform heat transfer to the laminate that causes curing gradient and internal stresses (Walczyk & Kuppers, 2012). As a result of the mentioned disadvantages of autoclave, efforts have been raised in the innovation of new alternatives in materials, processes and techniques which achieve the autoclave curing quality without autoclave in shorter time and lower cost.

2.8 Out of Autoclave (OoA) technologies

Different materials, methods and approaches are developed and improved to manufacture the advanced composites without autoclave, but with the same quality. Generally they are called as the Out of Autoclave (OoA) technologies or methods that can overcome the problems of high operation costs, energy losses and long curing time of the traditional methods.

2.8.1 Oven curing method

In order to reduce the typical cost of autoclave in acquisition and maintenance, the manufacturers and researchers tried to use oven as an alternative method for producing polymer matrix composites. This method retains vacuum bagging to consolidate prepreg under a pressure of one atmosphere, but uses the oven for curing (Hsiao, 2013; Ridgard, 2009). The absence of external pressure in the traditional method of oven curing typically results in lower fibre volume fraction and greater porosity content (Davies *et al.*, 2007; Hayes, Gilbert & Seferis, 2000). Johnston (1997) concluded that removing the external pressure in autoclave curing reduces the convection coefficient of environment from 180 to 80 $W/m^2.K$, which affects curing time and also may cause its inconsistency. For example, curing of a CFRP reinforced panel of 400 x 400 x 4 mm size, with a ramp of 2 $^{\circ}C$/min, takes about 7 hours and a production cost of £164 in autoclave, while it takes about 5 hours with 6% cost reduction in oven (Witik et al., 2011). Also Tong et al. (2011) concluded that an L-shape composite component of 305 x 102 x 8 mm requires 2.5 hours for curing in autoclave and costs about £70, but it takes about 10 hours in oven with £48 cost. Also Progoulakis (2004) concluded that oven is a cost effective processing method.

Another method of oven curing for manufacturing PMCs reinforced with glass or carbon fibre is microwave (MW) oven curing. Despite the problems of energy distribution, arcing, tool design and ultimately part quality and consistency, this method still has not taken off in industry and academia, as mentioned by Kwak et al. (2015), however MW can save 80% of energy, 40% of cycle time and their associated costs, compared to autoclave, as evaluated by GKN aerospace (Sloan, 2011).

2.8.2 Out of autoclave (OoA) prepreg

Manufacturers, nowadays, produced a new type of prepreg known as out of autoclave prepreg that enables manufacturing of high quality components more quickly and efficiently outside autoclave. This product is designed to be processed in ovens, which can also be cured on the heated tools to provide a cost effective processing solution, compared to autoclave, for manufacturing aerospace components (Kwak *et al.*, 2015). That is because OoA prepregs have the advantages of providing more flexibility in manufacturing, saving significant energy, less requirements for expensive tooling. They are available in a ranges of different low viscosity resins, fibres, thinners and additives, e.g. fillers and initiators(CPA, 2006; TenCate, 2013). The OoA prepregs resins are suited with vacuum processing only and can be cured at temperature ranging from 70°C to 120°C (Gardiner, 2011; Hayes et al., 2014). This type of prepregs are specially designed and partially impregnated to create a porous medium that can be evacuated, to remove the entrapped air during the lay-up, before the resin becomes liquid and infused the fibre (Repecka & Boyd, 2002). Regarding the properties Dang et al. (2011) concluded that the produced

components of OoA prepreg systems, with same volume fraction of 0.59, are mechanically comparable to that of autoclave.

2.8.3 Same quality resin transfer mould (SQRTM) process

The dry carbon fibre, in the resin transfer moulding (RTM), is consolidated between the upper and down parts of a closed heated mould, combined with heated press or as stand-alone unit, and then catalysed resin with low viscosity is injected into the mould. The resin is pumped under a pressure lower than 500kPa (5 bar) for displacing the air at the edges, until the mould is filled (Cripps, Searle & Summerscales, 2000; Kruckenberg & Paton, 1998; Potter, 1997).

However the OoA process of RTM is considered as the most appropriate alternative to autoclave and produces liquid epoxy carbon components with the same quality of autoclave, it cannot be used in manufacturing of prepreg (Rudd *et al.*, 1997). Recently some designers and manufacturers fabricated prepregs by RTM method in a new process called SQRTM that can overcome the issues of qualification and produce sub-preforms that cannot be made with dry fabric easily due to lack of tack (Thuis, 1999). In SQRTM process, the dry preform is replaced by toughened prepreg, which is laid up on the surface of the lower part of robust, sealed and matched metallic heated mould. Then a small amount resin, of the same used in the prepreg, is injected into the closed mould under a positive pressure of approximately 100 psi (6.89 bar) (Black, 2010a). The resin is injected just to maintain a uniform hydrostatic pressure in the mould that prevents void formation and eliminate the problem of dry spots and not to impregnate the prepreg. SQRTM can produce true net shape and highly

unitized components with tight tolerance, high level of integration and high surface finish (Vries, 2002). This new technique, if compared to autoclave, can produce complex structures in a single cure cycle (shorter by 2 hours) and lower curing cost by 20%. Although the method offers autoclave quality, eliminates the vacuum bagging and assembly steps with associated costs, the high tool cost and injecting extra liquid resin are still problems (Roover, 2011).

2.8.4 Quickstep technology

Quickstep is an OoA process developed by Quickstep technology in Australia, patented by Graham (2000), in which a heat exchange liquid such as glycol is applied instead of air in autoclave. In this method the uncured prepreg is laid up on the tool face and vacuum bagged then they inserted together between tool impermeable bladders containing heat transfer liquid at 1 to 4 psi (0.07- 0.28 bar) operating pressures on parts (Arney *et al.*, 2004). Compared to autoclave and oven processing, Quickstep can cure faster because the heating medium provides higher convection coefficients and also it is close proximity from the part during processing (Herring & Fox, 2011).

Bond et al. (2005) and Davies et al.(2007) concluded that, compared to autoclave, Quickstep can reduce cure cycle time by 50% and 43%, respectively, because Quickstep can perform heating with faster rate. Also Garschke *et al* (2012) deduced that cure cycle in Quickstep enhances flow properties and saves at least 27% of curing time and reduces the laminate porosity to 4% under the pressures of vacuum bag plus Quickstep chamber of - 97 kPa (-14 psi) and 10 kPa (1.45 psi), respectively. On the other hand Griffiths & Noble (2004) mentioned that this process can be used for melding process (joining or

welding the composite parts) by insulating specific areas of the components to be cured partially in those area and fully cured in others and finally two components could be joined together, from the places of partial curing, in another cycle without the cost of adhesive. Zhang, Guo & Fox (2009) and Coenen et al. (2005) concluded that the mechanical, physical and chemical properties of the carbon epoxy laminates, produced by Quickstep, are in the range or superior to the autoclave.

Arguably Quickstep technology can be considered as an alternative to the autoclave processing because it can perform fast curing with higher heating rates up to 15°C/min, compared to autoclave (Garschke *et al.*, 2012). Although Quickstep can produce components with autoclave quality, low tooling cost and curing cycle time (Walczyk & Kuppers, 2012), it is still has the problem of size limitation and cannot be used to produce large parts because larger parts require a larger heating chamber.

2.8.5 Double vacuum bagging technology

The traditional single vacuum-bag (SVB) is often ineffective in moulding prepreg composite because the resin matrix contains by-products or solvent that produces volatile during processing and SVB assembly hinders their escape (Hou & Jensen, 2004). Therefore the Naval Air Warfare Centre, Warminster, PA proposed a new, workable and low cost out-of-autoclave double vacuum bag (DVB) processing technique for the management of volatiles (Sherwin, 1999). In this procedure, as shown in Figure 2-8, the laminates of prepreg composite are laid up between a caul and tool face and enclosed by two vacuum bags (inner and outer bags) and sealed around the edges onto the tool face.

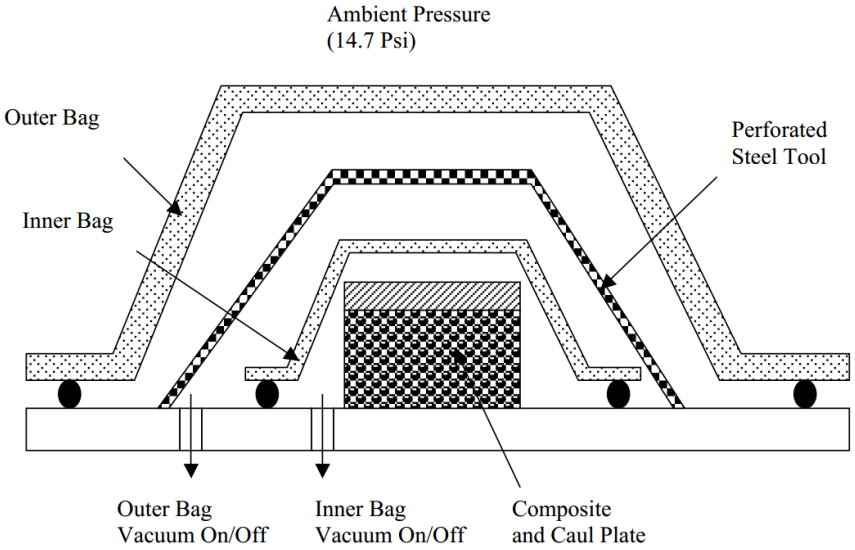

Figure 2-8 Double vacuum bag (DVB) process (Hou & Jensen, 2004)

Before assembling the outer bag, a perforated tool that can withstand the atmospheric pressure of 14.7 psi is installed outside the perimeter of the Inner bag. The two vacuum ports (located on the tool face inside the bag) are connected separately to two vacuum pumps. Then the DVB assembly is placed in an oven to cure, then the inside pressures of the outer and inner bags are set to full vacuum of 14 psi (30” Hg) and 13.8 psi (28” Hg), respectively. During the B-stage of curing (low temperature ramp-and-hold period), the outer bag is collapsed onto the stiff perforated tool due to the outside atmospheric pressure, but the inner bag is ballooned and presses against the perforated stiff tool because of the vacuum differential between the two bags. The produced curing volatiles will be free to escape in this method, while the composite lay-up in the DVB is vacuumed, because the lay-up is not compacted via the inner bag by the atmospheric pressure and remains loose.

Hou & Jensen (2004) mentioned that this procedure can easily be implemented without the outer bag and perforated tool in any vacuum heating chamber

(vacuum oven, vacuum press or autoclave), because the chamber wall serves as the outer bag. Also they stated that DVB process, which was pursued at the NASA Langley Research Centre, is applicable to other important composite fabrication processes, such as resin film infusion (RFI), resin transfer moulding (RTM) and vacuum assisted resin transfer moulding (VARTM). Sherwin (1999) applied DVB to repair CFRP laminates outside autoclave. Despite the feasibility of the technique for curing laminates that cannot be cured conventionally under vacuum bag, the process has the disadvantages of sealing difficulties, especially for the flat parts.

2.8.6 Integrally heated tools

Integrally heated tool is the innovative alternative of the conventional methods of composite fabrication that can offer the following abilities for composite manufacturing (Arney *et al.*, 2004; Raizenne, Hind & Poupore, 2006; Walczyk & Kuppers, 2012).

- Heating the composite parts more directly, during curing.
- Fabricating the large and complex shape components.
- Consuming lower amounts of heat (energy), time and capital, compared to the traditional methods.

This conductive technology can be used in all processes of vacuum bagging resin infusion (VBRI) and resin transfer moulding (RTM). Comparing to the traditional methods, integrally heated tools can save more energy and reduce approximately 40% of the curing time by increasing heating rate up to 5°C/min, as concluded by Baril-Gosselin (2013) and Raizenne *et al*. (2006). That is because the heating source, in the integrally heated tools, is directly attaches

tool (may be connected to the tool externally or embedded according to installation facility) and eliminates the need for heating the surrounding environment (Black, 2011). Payette et al. (2015) evaluated the curing performance and energy efficiency of a ThermoCeramic (TCX^{TM}) heated tool (flat aluminium plate with a novel TCX^{TM} heating technology) in terms of laminate quality and energy consumption and found that the tool, compared to oven cure, produce laminates with oven quality and saves 66% of the energy required for standard curing of OoA prepreg in an oven.

Marsh (2003) and Mason (2006) reported that integrally heated tools nowadays are widely used in different industries, such as, wind energy, aerospace, surface transport. For example Brandes (2008) explained that the developers optimised a cost effective resin infusion heated tool to produce lining sets for the VIP aircraft of Lufthansa, due to the considerable required expenditure for the production of large scale prepreg components in autoclave. Progoulakis (2004) concluded that the integrally heated tool, compared to oven an autoclave, can cure the identical prepreg laminate faster by 20% with a ramp rate higher by 50%. Also he prepared cost data (Table 2-2), for comparison of an integrally heated tool with the autoclave and oven for manufacturing a 12 m long composite C beam by resin film infusion, and concluded that the heated tool reduced the estimated power requirements, operating cost, equipment procurement costs, except that of the procurement. Furthermore he deduced that integrally heated tool offers a 15% reduction in manufacturing risk of potential damage to tooling equipment and components because it does not require a frequent move in and out of autoclave and oven.

Table 2-2 Cost data and performance comparison of processing options (Progoulakis, 2004)

Cost Data	unit	Processing Methods		
		Heated tool	Autoclave	oven
Estimated power requirements	kW	30	720	150
Operating cost	£/h	3	10	7.5
Procurement costs	£	15,000	475,000	85,000
Pre-production requirements costs		72,000	66,600	66,600
Production requirements costs		2,165,000	2,625,000	2,150,000

2.8.7 Heating technologies

Different categories of heating technique are available nowadays; each has its advantages and drawbacks (Astrom, 1997). According to the applied heating source, they can be classified into three categories. The first is known as the radiation method such as, flame, laser, infrared, microwave, induction and radio frequency (Chen et al., 2005; Ó Brádaigh et al., 2011). Second type is the electrical heating element that has different techniques with typically different heating performance and its most available categories are heater mats, resistive heaters, heating fabrics (Arney *et al.*, 2004; Progoulakis, 2004). The third technique is fluid circulation in which different fluids, such as, gas, water, oil, steam are applied as heating medium to flow in pockets or through channels to heat the tool. This technique, especially water and oil, can also be utilized for cooling (Astrom, 1997; Black, 2011).

2.8.7.1 Electrical heating technology

Most of the electrical heating units are available in different sizes that could serve a wide range of processes and applications (Arney *et al.*, 2004; Progoulakis, 2004). Black (2011) and Marsh (2003) clarified that on-mould

application of resistive heating elements is more preferable than in-mould due to the ease of installation, operation and maintenance.

PM solutions explored a digital controlled heating technique that has a thickness less than 2mm (PPM Solution Ltd., 2014). Grove *et al.*(2005) applied electric-resistive heating element in an integrally heated tool made of CFRP of a resin film infusion RFI process. The tool is applied in producing CFRP laminates with thicknesses up to 11mm. Then the heating performance (e.g., through thickness and in-plane temperature distribution) of the heated tool is defined and physical properties (e.g. thickness, curing degree, fibre volume fraction (V_f) and void content) of the produced laminates are evaluated. Finally they compared the results with that of oven and autoclave cure and concluded that the integrally heated tool with electric-resistive heating is better in saving energy and operation costs as illustrated in Table 2-3.

Table 2-3 Cost data and performance comparison of processing options (Grove *et al.*, 2005; Progoulakis, 2004)

Cost Data	unit	Comparison of processing options	
		Heated tool vs autoclave	Heated tool vs oven
Estimated power requirements	kW	96% less power	80% less power
Operating cost	£/h	70% cost saving	60% cost saving
Procurement cost	£	97% cost saving	82% cost saving
Production requirements costs		17.5% more expensive	0.7% more expensive
Pre-production requirements costs		14.5% more expensive	
Risk level	-	15% reduced risk	

Also Liu and Lam (1997), as cited by Ding, Chiu and Liu (1999), investigated the performance of an RTM tool assembly, heated in-situ by an electric–strip heater, and compared with that of oven and autoclave. Results show that the integrally heated tool with attached electric heaters provides heating much faster, but temperature distribution over the tool face was not uniform as in oven and autoclave. The heating unit in this method have the advantages of being sufficiently pliable to bond to the back of variety mould shapes, occupying a

small space on the tool during installing, it offers fast curing and has ability of local heating with different heat flux (Black, 2011; Marsh, 2003). Recently Tiberghien (2015) used heating pouches, made of high temperature rubber or silicon with embedded Tibgrid or Thermostretch flexible layer (a flexible electro-heating grid integrated in a woven yarn), that facilitates the layup of functional circuits on complex or deformable shapes and does not take up space during use and storage, but the technique has three principal constraints of fatigue strength, dielectric and heat exchange within the specific framework of composite materials.

Bromley (2015) investigated integrally-heated tooling for the cure of resin infused CFRP composites and provided recommendations for the team into the next phase of their research of the technology (heated tool) and its applications comparing the type of components that could be produced by heated tools and the energy intensity required. Induction heating is another heating technology, which heats the metallic tool through the joule losses from induced eddy current flows in the tool in response to an applied alternating magnetic field (Bromley, 2015; France & Alanta, 2009; Sloan, 2014). Kaden (2015) deduced that this technique can provide heating rates of up to 65ºC/min and temperatures over 300 ºC.

A recent technique, as reported by Gardiner (2015), is the PowerFilm that can generate up to 10 KW/m^2 of heat from electricity efficiently and it is a thin layer of 100 micron CF insulated with a polymer and incorporating copper contacts. Athanasopoulus *et al.* (2013) investigated application of carbon fibres as heating element in an open lightweight composite mould, due to the ability of CFs to conduct electric current. They concluded a thermal gradient at the edges

of heated area with strict limits of ± 2.6°C for temperature deviation over the tool face.

Regarding the disadvantages of the method, each of Sloan (2013) Petrykowski & Fischer (2012) and Black (2010b) deduced that electrical heating methods, comparing to the other heating methods of oil and pressurised water, have the problems of large energy consumption, cannot provide cooling, are inconsistent in temperature distribution and in operation the required temperature may be exceeded depends on control strategy.

2.8.7.2 Fluid- circulation heating method

Fluid circulation method heats the mould by circulating a hot fluid in a pocket connected directly to the tool or a channel embedded in the tool (Yao, Chen & Kim, 2008). The main advantage and disadvantages of fluid circulation method, comparing to electrical heating techniques (such as, the resistive heaters of PPM solution), are listed in Table 2-4. Despite its drawbacks, fluid circulation technique is still widely used in composite industry, plastic injection moulding and thermoforming processes due to its preferred advantages (Marsh, 2003).

Various fluids (e.g. oil, water and steam) are available to apply as a heating medium in this technique and temperature spectrum of water and oil can be increased up to 227°C and 349°C, respectively, by pressurisation that increases their boiling points (Petrykowski, 2012; Petrykowski & Fischer, 2012). Accordingly different studies are conducted to compare between these and other heating techniques (e.g. electric cartridge, electric resistive, and oven and infrared induction) in achieving the following performance variables (Black, 2010b; Petrykowski & Fischer, 2012; PMC; Sloan, 2013).

- Temperature range or the maximum temperature could be achieved by the method.
- Cooling ability.
- Temperature gradient, which means temperature uniformity over the tool surface.
- Ramp rate or heating speed.
- Energy consumption, which is defined by the amount of energy required to heat the tool to a specific temperature.

Table 2-4 Advantages and disadvantages of fluid circulation heating technique (Marsh, 2003)

Advantages	**Disadvantages**
1. Low cost and efficient heating medium. 2. Low power required for heating while the fluid medium has low viscosity 3. Low power required for pumping, while the fluid medium has high thermal capacity. 4. The method can also be used for cooling. 5. The achieved temperature never exceeds required tool surface temperature. 6. Heating medium defines maximum temperature.	1. Need for pipework which may be expensive to install. 2. Additional weight of pipes and fluid medium. 3. Leaking may occur. 4. Repairing the embedded pipes can be challenging.

As listed in Table 2-5, it was concluded that fluid circulation, especially Pressurised water, can provide inherent energy saving, precise temperature control and fast ramp rates for heating and cooling, while oil is very slow to build temperature, consuming large amounts of energy and it is not suitable for clean

room processing. So water is superior in achieving the desired temperature uniformly over the mould face with the lowest cost, time and consumed energy.

Various studies have been conducted for developing the heating ability of fluid circulation method and accordingly different improvements are achieved and techniques are created. For example, Boyce and Prybyla (2010) utilized a LLC K-Factor carbon nanotube-based heating system to the interior of a composite tool that is covered by a single-ply of prepreg and subsequent surface coats. The technique provides more efficient heated tool with advantages of ease of fabrication, simple construction, rapid heating-up and cool-down and high temperature uniformity. Unfortunately the method is expensive and requires external attachments of plumbing, pumping unit and control system.

Table 2-5 Comparison between the heating performances of different heating techniques (Petrykowski, 2012)

Heating Method	Comparison variables				
	Temperature range	Cooling	Tool temperature gradient	Ramp rates	Energy consumption
	°C				
Electric Cartridge	371	non	11	high	high
Embedded Resistive	371	non	11	high	high
IR/Induction	371	non	11	high	high
Ovens	260	limited	3.9-5.6	low	high
Oil (pressurised)	349	Yes	2.2	medium	medium
Steam (pressurised)	149	Yes	2.8	high	medium
Water (Pressurised)	227	Yes	1	high	low

Surface Generation formed a new multi-channel system, called Functional Specification (PtFS) process, depending on the principles of fluid-circulation heating method (Surface Generation, 2011). The system is a special tool consisting of multi regions, typically 32, connected to a multi-channel control system. This heating system allows the manufacturers to dynamically control temperatures of each mould area and process stage to the exact heating and

cooling level requirements in real time. It is applicable in a range of industry sectors, e.g. aerospace and automotive.

Tube circulation is the commonest example of the fluid circulation heating method. Therefore thermal response of the oil-heated tool under the influence of different flow rates were investigated numerically and verified experimentally by Ding, Chiu and Liu (1999) as well as Ding et al. (2001). Results showed that temperature of the integrally oil-heated tools could be controlled by controlling the flow rates of the oil. Furthermore they deduced that higher flow rates, that make turbulent flow, will heat the tool faster. Then they developed an analytical model for defining the heat transfer process in the oil-heated tools.

On the other hand, for optimizing the performance of rapid heat cycle mould (RHCM) , in the field of plastic injection manufacturing, Guilong et al. (2010) and Wang et al. (2011b) studied numerically the effect of channel geometries, heating medium and tool material on the tool heating efficiency and temperature uniformity along the tool face. They concluded that an appropriate reduction in the both distances between the centres of the adjacent channels as well as the tool face and the channel centre can improve the thermal efficiency of the heated tool. Also they deduced that the importance of thermal conductivity and thermal capacity of the tool and channel materials in improving temperature uniformity and heating time of the tool. Finally their results indicated that the achieved tool temperature by water and steam heating cannot exceed 90°C and 100°C, respectively, while oil-heating can attain up to 180°C. According to the results of previous studies Wang et al. (2010),(2011a) and Wang Y. et al (2011c) constructed the optimised mould design to verify, experimentally, the

numerical results, thereby confirming the effectiveness of the optimised tool design in heating and cooling.

Yoo (2008) quoted that accurate heating performance on the heated mould surfaces ensures reasonable part quality and production cycle time in all processes of thermoforming, plastic injection moulding and moulding curing of fibre reinforced polymer composites. Conformal heating and cooling channels are designed and formed to follow the tool surface and to conform to the shape of the parts as much as possible. Therefore many researchers and designers have studied conformal channels as an approach to provide enhanced thermal control over the manufacturing process (Walczyk & Yoo, 2009; Xu, Sachs & Allen, 2001; Yoo & Walczyk, 2007). During an optimisation study for the design of the conformal cooling channels in plastic injection moulding, Dimla *et al.* (2005) concluded that conformal channels, compared to the straight channels, can heat and cool the tool faster. Although research has been conducted to improve the moulds of thermoplastic and thermoset injection moulding processes, their achievements can be considered in improving the tooling for manufacturing advanced composites.

2.9 Thermal cycling

Thermal cycling is the process of repeatedly cycling a material, typically between two temperature extremes at relatively sufficient dwell time and rates of change (ramp rate). It involves two main stages of heating and cooling that redistributes the internal energy in the system or the heated body (Ashby, 2011; Hancox, 1998). The heating cycle, contrary to the cooling cycle, produces a relative change in the linear dimensions called expansion because heating

increases both the vibration and separation energies of the material atoms, especially the solid materials (Stone, 2014). Therefore each material has a special characteristic of expansion known as thermal expansivity or coefficient of thermal expansion (CTE).

Thermal response or behaviour of the heated or cooled materials throughout thermal cycling is understood as “thermal effect” or “effect of heat on materials” that depends on the thermal properties of the material such as thermal conductivity, specific heat and CTE (Bokstein, Mendelev & Srolovitz, 2014; Martinez, 2014; Speyer, 1994). Thermal effect is sometime advantageous as in thermometers, while it is generally an undesired phenomenon because the temperature variation not only degrades mechanical behaviour of the materials, but also modifies all the material properties, that may affect the performance of the system or destroy its geometry and structure completely (Crompton, 2013; Jones, 2000).

2.9.1 Thermal stress

Thermoelastic deformation occurs when any material changes in temperature due to the expansion or contraction resulted in the structure (Brown, 2011; Martinez, 2014). Thermal deformation will be stress-free in unrestrained isotropic materials, if the temperature variation is uniform all over the body, and amounts of thermal elongation and strain, in each direction, could be defined as follows (Askeland et al., 2011; Rogin, 2010).

$$\Delta L_{th} = \alpha L \, \Delta T \qquad (2\text{- }1)$$

$$\mathcal{E}_{th} = \frac{\Delta L_{th}}{L} = \alpha \Delta T \qquad (2\text{- }2)$$

Generally thermoelastic stress will occur in constrained anisotropic materials under the effect of non-uniform temperature variation. If the attained thermal stress exceeds the elastic limit, irreversible thermoplastic deformation occurs. Amounts of the effective thermoelastic stress and load, in each direction, are calculated respectively by the following equations (Martinez, 2014; Rogin, 2010).

$$\sigma_{th} = E\mathcal{E}_{th} = E\alpha\Delta T \qquad (2\text{- }3)$$

$$F_{th} = \sigma_{th}A = E\alpha A\Delta T \qquad (2\text{- }4)$$

Boley & Weiner (Bruno & Weiner, 2011) and Chen & Nelson (1979) presented that the lower dilatable material, during heating the bonded materials, constrains the expansion of the higher and becomes under a tension load, while the later becomes under compression, cooling reverses the situation completely. Therefore the expansivity mismatch between the bonded materials, e.g. bi-material strips and composites, causes internal thermal stresses and thus thermal deformation or bending. The amount of misfit displacement and strain in the longitudinal direction of bi-material strips can be calculated as follows.

$$\Delta L = L(\alpha_H - \alpha_L)\Delta T \qquad (2\text{- }5)$$

Based on an elementary beam theory Timoshenko (1925) obtained a model defines the longitudinal normal stresses occurring in the thermostat strips (bimetallic strips), as shown in Figure 2-9, during operation (under thermal loading). The shear force and the moment acting at the interface of a bi-material strip, In Timoshenko's model, can be converted to an equivalent force and moment system on the centroid axis of each layer, as illustrated in Appendix A.

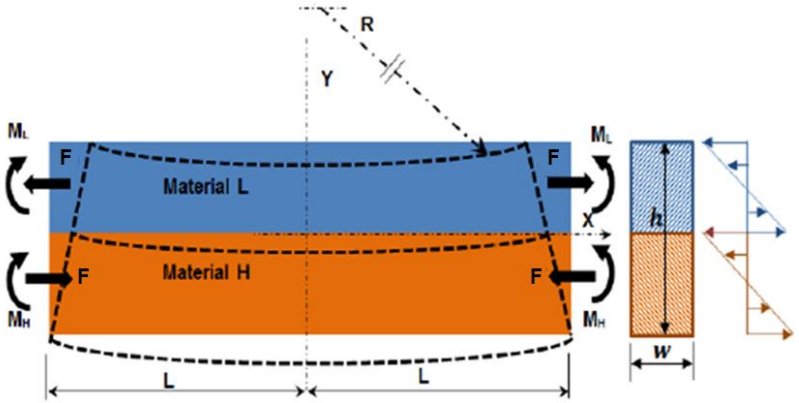

Figure 2-9 Bimetallic strip

Fo-van (1983) concluded that the maximum shearing and normal stresses, at the contact surface of the strips, are concentrated at the ends along a length almost equals the strip thickness. In a report about bending of the bonded layers due to thermal stress, Abawi (2004) addressed the problem of bonded materials with two considerations of movement and no slip at the interface between the strips. Additionally during an investigation Mahrenholtz & Johnson (1962) included the elastic-plastic behaviour of the bonded materials to the Timoshenko's elastic analysis model to ascertain the residual stresses and deformations present after the thermostat has been cooled.

Many researchers applied numerical methods to analyse bimaterial structures with different geometries and material properties. For example, with considering the longitudinal and transverse interfacial compliances, Suhair (1989) suggested a somewhat complicated analytical model for evaluating the interfacial stresses that satisfy the boundary conditions for the interfacial shearing and normal stresses in the thermostat strips. Eischen et al. (1990) compared the performance of Suhair's model with two others, in predicting the interfacial normal and shear stresses in bimaterial strips subjected to thermal

loading, and concluded that extreme care must be taken in calculation of stresses near the free edge of bimaterial strips.

In the case of the bi-material plates while uniformly heated, as considered by Timoshenko (1925), the plate takes almost spherical form because an equal and constant curvature occurs along the both in-plane directions of the plate. Furthermore he proposed that the same equation of curvature of bi-material strip can be used for calculating the radius of curvature of the bi-material plate, but values of the plate modulus of elasticity must be divided by $(1-v)$ where v is Poisson's ratio (Suhir, 1989; Timoshenko, 1925).

Composite materials are combinations of different materials, so it can be predicted that they act as the bonded materials when they are exposed to internal thermal stresses. Accordingly Tanigawa *et al.* (1991) obtained an analytical model to analyse the thermal deformation and stresses of a rectangular laminated composite plate under partial heating that cannot be predicted in isothermal problems due to its complicated thermomechanical behaviour and characteristic. Also, in order to calculate the compressive or tensile stresses generated in the resin matrix, under the effect of thermal loads, Hancox (1998) presented the following approximation.

$$\sigma_L = \frac{(\alpha_H - \alpha_L)\Delta T E_L \mathrm{V}_H}{\mathrm{V}_L\left[\frac{E_L}{E_H} - 1\right] + 1} \qquad (2\text{- }6)$$

Tubes are used widely in many industrial applications for holding or transporting materials, e.g. liquids or gases, and similar to the other mechanical elements they are also subjected to thermal stresses and deformations under the effect of cyclic thermal loads. Timoshenko proposed an analytic model for single tubes with different wall thickness (e.g., "thick", "thin" and "very thin"), Appendix B,

under the effect of thermal load. The model can be used to calculate the steady state thermal stress, strain and deformation, with the following assumptions (Timoshenko, 1925; Timoshenko, 1956; Timoshenko & Goodier, 1951).

- Gradient distribution of temperature across the tube wall thickness (radial axis).
- Axisymmetric temperature distribution.
- Constant axial temperature distribution.
- Free tube expansion.

Distribution of thermal stresses, near the free ends of the tube, is more complicated due to local irregularities. The tube edge stresses are produced by thermal forces equal and opposite to those illustrated in Figure 2-10a that can be reduced to bending moments as shown in Figure 2-10b (Irfan & Chapman, 2009; Timoshenko & Goodier, 1951).

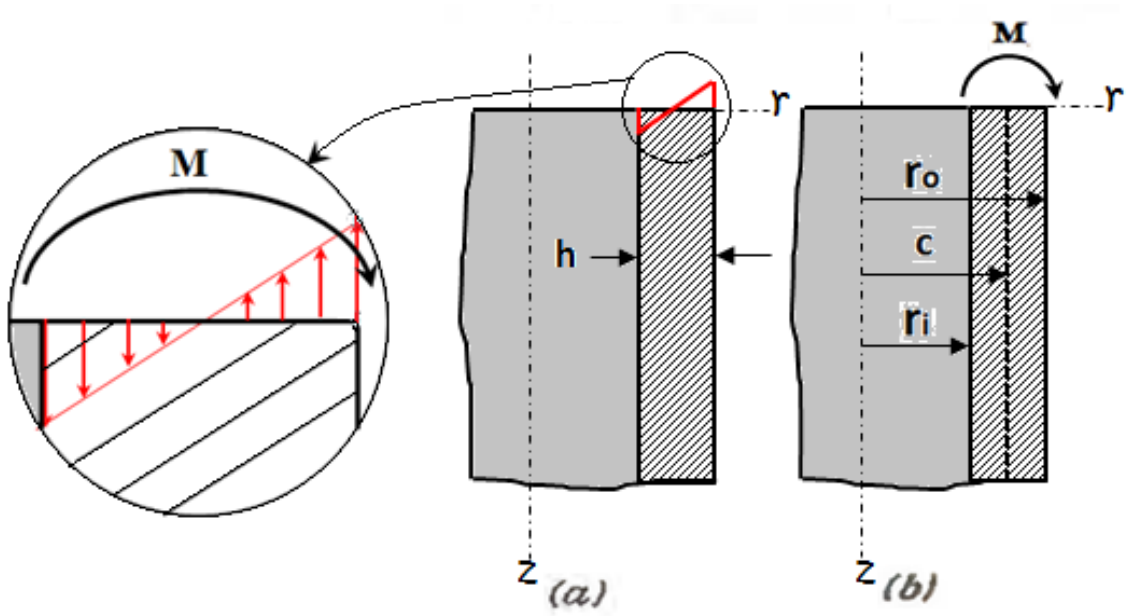

Figure 2-10 Thermal force and bending moment distribution over the tube edge (Timoshenko & Goodier, 1951)

2.9.2 Thermal failure of materials

While temperature variation affects the composite properties of strength, modulus, CTE, volume fraction and Tg, different types of failure are expected to occur under the effect of cyclic thermal loads, for example:

- Thermoplastic deformation, when the generated thermal stress exceeds the elastic limits of the material (Carden, 1963; Herakovich & Hyer, 1986).
- Thermal shock, when the material subjected to a fast rate heating that causes non-uniform expansion or contraction of the entire material structure, as in quenching process (Hancox, 1998).
- Thermal creep, which is a time dependent elongation under the influence of certain high applied load and temperature and it could be dangerous while in service (Goertzen & Kessler, 2006).
- Thermal fatigue, when the material works under a repeated fluctuation of thermoelastic stress (Carden, 1963; Herakovich & Hyer, 1986).

Thermal failure may damage the heated system structure directly (e.g. thermal deformation and thermal shock) or gradually by an incremental obstruction to the system performances until it fails completely (e.g. fatigue and creep failure). The significant variables that influence thermal fatigue are the thermal stress, fluctuating time, temperature range and its rate of change (Carden, 1963; Zung-fang, 1986).

Composite materials show complicated and characteristic thermomechanical behaviour throughout thermal cycling, because they consist of two or more different materials with different thermal properties (Hancox, 1998; Kamiya,

1979). The most expected thermal damages in composites are (Han & Hahn, 1989; Park & McManus, 1996):

- Transverse microcracks in the laminate matrix when its tensile strength is exceeded.
- Delamination of the plies due to exceeding interlaminar shear strength.
- Fibre failure due to the buckling of fibres.

Different studies concluded that cracks ran through the resin, interface regions and sometime the fibres are cracked as well (Cohen, Hyer & Tompkins, 1984; Tompkins & Williams, 1984). Generated microcracks in resin alter unfavourably gas permeability, fatigue life, mechanical and thermal properties of the composite (Adams, Bowles & Herakovich, 1986; Eselun, Wolfe & Neubert, 1979; Herakovich & Hyer, 1986; Zhang et al., 2013). During an investigation Zhang et al. (2012) evaluated microcrack distribution and mass change in different carbon/epoxy braided composites under cyclic thermal loading between - 55ºC and 120ºC and results show that strength and stiffness followed an inverse relation to crack density. Roberts et al. (Roberts et al., 2003) reported that braided and triaxial fibre orientation composites show higher resistance to crack initiation and propagation.

During investigation of the effect of repeated thermal heating Cohen *et al.* (1984) noted that the cracks accumulated in a limited number of heating cycles and remained constant, then increase with the increase of working cycles. This illustrates that cracks do not grow consistently, but hinges during a limited number of loading cycles due to the changes that happen to the material properties, which extends the lifecycle. Harris (2003) deduced that the dry composites (free of moisture) would not crack normally under thermal cycling

below the cure temperature. In their research article about thermal cracking Park & McManus (1996) mentioned that “when a new crack forms some of thermal strain energy stored in the laminate due to thermal load will be released” and accordingly they presented a general analysis method to predict energy release rate matrix cracks in composite laminate geometry.

$$Y = \frac{t_{re} t_c S_{re} S_c (\alpha_c - \alpha_{re})^2 \Delta T^2}{2\vartheta (t_{re} S_{re} + t_c S_c)} \qquad (2\text{- }7)$$

The suffixes c and r present the cracking ply group and the rest of the laminate, respectively, as shown in Figure 2-11. Regarding delamination and its effects in the heated tools, Progoulakis (2004) indicated that expansivity mismatch between the incompatible materials in the tool structure can result in disbonding of the heater and delamination of the composites that demolish the structural and heating performances of the tooling. Adams *et al.* (1986) concluded that delamination grows from transverse cracks, while microcracks avoid resin rich area in the resin matrix composites. For example Shahidi (2000) observed significant delamination in composite integrally heated tools, by each of steam and hot air, after a few short cycles, while both Herakovich & Hyer (1986) and Ramanujam et al. (2008) found delamination in the extensive damage of epoxy resin due to thermal loading.

Previous conclusions of literature show that temperature fluctuation produces different damages in the composite structure and thermal cracking is the most expected damage that causes direct or gradual failure to the system. Therefore calculating the fatigue life data, which requires long term test, of composite tools that work under thermal cyclic loads must be considered to predict the intended service life through which the designed tool retains its durability and structural integrity.

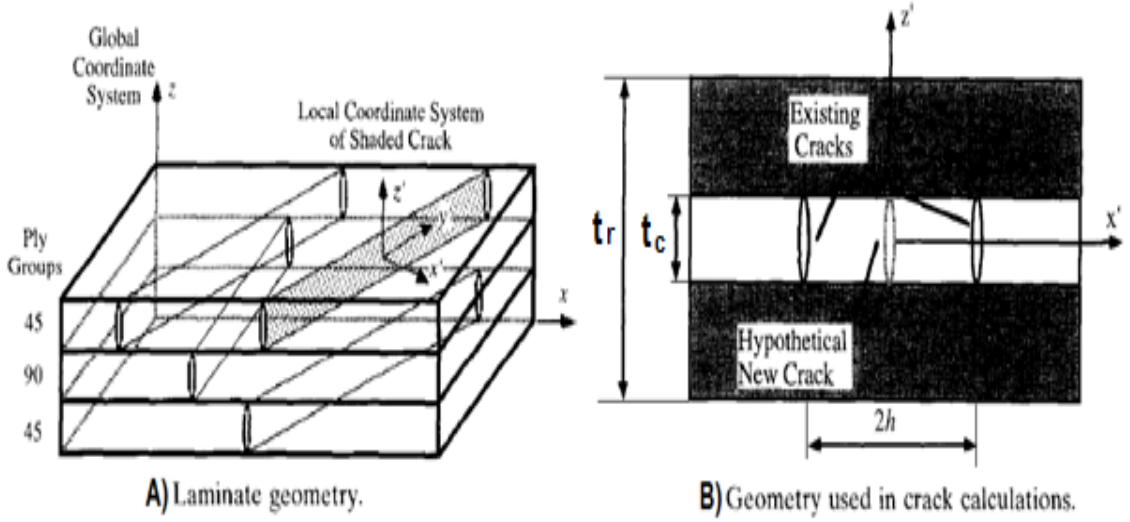

Figure 2-11 Figure Geometry used in crack calculation (Park & McManus, 1996)

2.9.3 Durability and tool lifecycle

Durability or tool life of composite tooling refers to number of production cycles (parts can be produced by the tool) and it is the most important issue of the composite manufacturing that affects productivity (number and quality of the produced parts) and the capital expenditure. Tool life, as illustrated in both Morena (2007) and (1990), may be affected during storage and handling, therefore they suggested for maintaining the tool surface integrity.

Generally composite tool life, under either thermal or mechanical loading or their combination, is a function of fatigue crack initiation mechanism depends on matrix reinforcement and loading detail, which is also called fatigue life (Carlson & Kardomateas, 1996 ; Figiel & Kamiński, 2003). Conclusions from literature, Section 2.9.2, show that thermal cycling may affect the heating performance of heated tools before the extensive damage of its structure, because the generated delamination and cracks, under the reversible thermal loading, create

gaps through the tool parts and their interfaces (e.g. the channel and the mould) that hinder the heat transfer through the tool.

Concluding generalised fatigue data, as safe life data strategies, for composites is not easy, because of availability wide variety reinforced-matrix combinations and their tailorable properties. Therefore various researches have been conducted in the concept of fatigue life of composites. During operation an oil or water heated tool (made of vinylester) in VARTM processing at temperature below 100°C Williams and Bland (2003), as cited in Progoulakis (2004), observed a lifecycle of 2×10^3 - 6×10^3 cycles and also deduced that tool lifecycle decreases with the increase of working temperature. Also during their research Lafarie-Frenot et al. (2006) observed that both the tensile strength and the lifecycle are influenced by matrix cracking.

Particulate composites, compared to the continuous type, have lower fatigue resistance because the weak matrix, especially at the fibre/resin interface that has lower glass transition temperature (Tg), must sustain most of the fluctuating loads (Harris, 2003; Noda & Rubingh, 1992). Kawai et al.(2001) investigated the off-axis fatigue behaviour of unidirectional CFRP laminates (prepreg) with different matrices at 100°C, which was below the curing temperature of 130°C and under the T_g temperature. They deduced that the off-axis fatigue strength of the laminate is matrix dependent and a 2mm thick laminate, T800H/epoxy (2500EP) with 0.64 volume fraction, fails after 10^3 cycles of a fluctuating stress rang equals about 20 MPa or after 10^6 cycles of a repeated strain range of 2.57×10^{-3} (0.19 of the laminate fracture or ultimate strain of 1.35×10^{-2}). Also Abdullah et al. (2012) concluded that the fracture limit of neat DGEBA epoxy is 10^3 cycles under a repeated stress level of 18MPa at ambient temperature. On

the other hand Senthilkumar et al. (2012) extracted that the Alepoxy composite with 0.5 fibre volume fraction fails or fractures after 5384 cycles of a fluctuating load equals 375 MPa (moment of 5 N.m) at the ambient temperature. the post cure and thermal cycling, as deduced by Montoya (2003), shift Tg of to higher temperature region and allows the user to adjust the polymers Tg.

2.10 Heat transfer equations

The desired curing heat, over the surface of integrally fluid heated tools, is provided by convection from the fluid and then conduction throughout the channel and tool. Convection is a mode of heat transfer associated with fluid flow and occurs due to the random motion of molecules (diffusion) in addition to the bulk or macroscopic motion of the fluid. The random molecular motion contributes near the internal channel surface where the fluid velocity is low, especially at the interface between the solid face and the fluid at which velocity is zero, while the bulk fluid motion contribution originates from the fact that the boundary layer grows as the flow progresses in the flow direction (Bell & Mueller, 1984; Cengel & Boles, 2002; Gebhart, 1971). Consequently the terms of convection and advection are applied to define the cumulative transport by each of molecular motion and bulk fluid motion, respectively (Janna, 2000; Kays & Crawford, 1993).

The general form of energy conservation or balance equation states that the amount of heat enters a domain plus that is generated equals the stored heat in the domain plus that transfers out as follows (Holman, 2002):

$$E_{in} + E_g = E_{st} + E_{out} \qquad (2\text{- }8)$$

The fluid flow, in the channels of fluid circulation heating technique, has an enclosed nature as shown in Figure 2-12. When a pumped fluid flows in tube at a constant mass flow rate a forced convection heat transfer occurs and the amount of the energy convected, due to the bulk fluid motion, can be calculated according to the following thermal energy equation of steady-flow (Holman, 2002):

$$E_{in} = q_{conv} = \dot{m}\, c_p\left(T_{b_i} - T_{b_o}\right) \qquad (2\text{- }9)$$

When $\dot{m} = \rho u A_c$

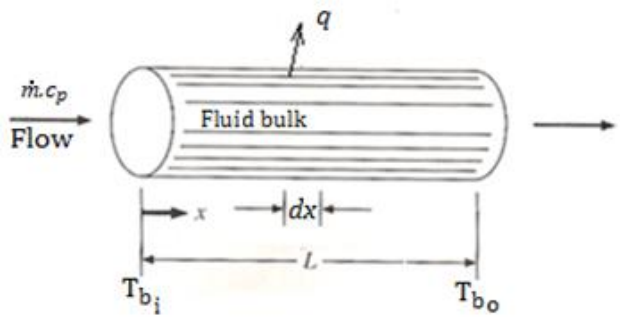

Figure 2-12 Fluid element flow in a tube (Holman, 2002)

While the physical mechanism of convection at the tube wall is a conduction process, Newton's Law of cooling with an appropriate heat transfer coefficient can be used to define the total convected heat at the tube wall as follows (Holman, 2002).

$$E_{in} = q_{conv} = hA_s(T_b - T_a) \qquad (2\text{- }10)$$

Both previous equations are combined, by considering the energy balance at the interface of the fluid and tube, to obtain the following relation that could be applied for finding the value of heat transfer coefficient (Holman, 2002):

$$\dot{m}c_p\left(T_{b_i} - T_{b_o}\right) = hA_s(T_b - T_a) \qquad (2\text{- }11)$$

When $T_b = \frac{(T_{b_i} + T_{b_o})}{2}$ (2- 12)

Conduction is another method of heat transfer occurring inside the solid tool and channel materials. The amount of the heat conducted through a 3D element of materials, Figure 2-13 is expressed by Fourier's law as follows (Holman, 2002).

$$q_{cond} = -kA\frac{dT}{di} = -kA\nabla T \qquad (2\text{- }13)$$

The tool face, in this PhD research, is considered to be opened to ambient temperature in order to represent the worst possible scenario for heat loss (Petrykowski, 2012). The tool surface is also considered without any curing assembly due to the complexity of heat transfer in the process, as illustrated in Section 2.6 and on this account, the concept of tool heating (energy conservation or balance equation) in this PhD research does not include exothermic reactions of curing process and energy generation will be zero.

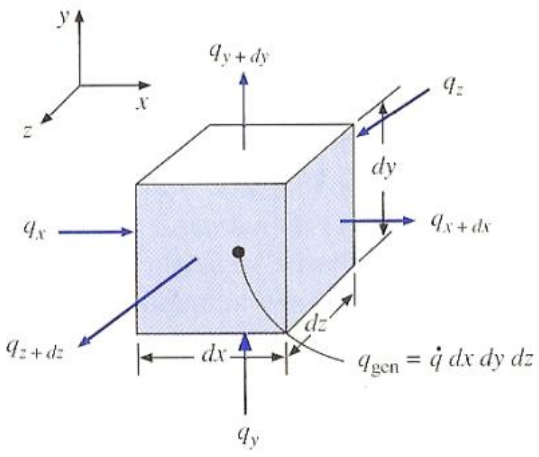

Figure 2-13 Three dimensional heat-flows through a solid element with Cartesian coordinates (Holman, 2002)

Energy rate storage in the tool (mould and channel) depends on the thermal mass that governs the heating rate of the tool face and however thermal mass

be lower, the tool could be heated (heating rate) is faster (Morena, 2007). Amount of energy rate storage could be defined according to the following relation (Holman, 2002).

$$E_{st} = M_t \frac{dT}{dt} = \rho_t \mathrm{V}_t c_{p_t} \frac{dT}{dt} \qquad (2\text{- }14)$$

While the tool face, in this PhD research, is opened to the environment and not insulated, it transfers the tool heat out to ambient due to temperature difference and depending on the heat transfer coefficient of the surrounding. The amount of heat transferred out from the surface can be defined by Equation 2-10.

$$E_{out} = q_{cond} \qquad (2\text{- }15a)$$

Rate of energy loss can be calculated by applying the following balance of energy at the tool face:

$$h_a A_m (T_m - T_\infty) = -kA\nabla T \qquad (2\text{-}15b)$$

Also according to the lumped-heat capacity analyses (Holman, 2002).

$$E_{out} = -E_{st} \qquad (2\text{-}16a)$$

$$h_a A_m (T_m - T_\infty) = -\rho_t \mathrm{V}_t c_{p_t} \frac{dT}{dt} \qquad (2\text{-}16b)$$

2.11 Prediction of transient heat transfer

Transient heat transfer is the temperature variation of a heated domain due to changes in location and time until the establishment of steady state. Generally the unsteady physical state of the heated body, during heating, is the result of variation of the internal energy, material properties and surrounding boundary condition. So analysis of transient heat transfer must be adjusted to match the unsteady situation of the domain to achieve actual outputs (Holman, 2002).

Different analytical models have been obtained for analysing transient heat transfer in many cases of geometries and boundary conditions. Incropera et al. (2013) presented an analytical model to predict transient response of long cylinders, while the pipe wall is assumed as a plane wall.

$$\frac{T_{b_o}-T_\infty}{T_{b_i}-T_\infty} = Ce^{\left(-\xi_1^2 Fo\right)} \qquad (2\text{- }17)$$

The coefficients C and ξ_1 are evaluated from tables according to the value of Biot number. The model is appropriate for the hollow cylinders with the following condition; otherwise the error will be large. So the cylinder must have:

- High length/radius ratio. $(L/r_o) \geq 10$
- Fourier number. $(Fo = \propto t/L_w^2) > 0.2$
- Situations with Biot numbers $(Bi = hL_w/k) < 0.1$, which mean the solution not valid at short times.

Yoo and Walczyk (2007) investigated the sealing issues of heating and cooling channels of injection moulds and based on the energy balance at the channel interface (Equation 2-15b) that involves conduction and convections they developed the following analytical model to analyse transient heat transfer of conformal channel heating.

$$T_{m_t} = \frac{g_3}{g_2} + \left(T_{m_i} - \frac{g_3}{g_2}\right) e^{-(g_2/g_1)t} \qquad (2\text{- }18)$$

When $g_1 = \rho_m 2 l_m W_m c_{p_m}$,

$$g_2 = \frac{h\pi D_i}{2}\left(\frac{h_a l_m}{k_m} + 1\right) + 2h_a W_m$$

And $$g_3 = \frac{h\pi D_i T_b}{2} + \left(\frac{h_a l_m h\pi D_i}{2k_m} + 2h_a W_m\right) T_\infty$$

The model contains some aspects regarding application:

- Calculation of thermal resistance of the mould.
- The internal radius of the channel is applied instead of hydraulic diameter that is defined as follows.

$$D_h = \frac{4A_c}{P_C} \qquad (2\text{- }19)$$

- Instead of the whole mould thickness, only the distance between the channel and mould face, as shown in Figure 2-14, is applied in defining the mould volume per unit length as follows.

$$V_m = 2l_m W_m \qquad (2\text{- }20)$$

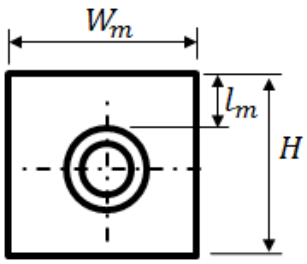

Figure 2-14 Mould section.

Ding et al. (1999) and (2001) investigated the effect of flow rate on the thermal response of an oil-heated tool numerically and after experimental verification of the results, they derived the following analytical model for transient heat transfer in the fluid circulated heated tools.

$$T_{m_t} = T_{b_i} - \left[T_{b_i} - T_{m_i}\right] e^{-\psi t/\eta} \qquad (2\text{- }21)$$

Where $\psi = \frac{\pi D_h^2 \rho\, c_p}{4 \mathrm{V}_t \rho_t c_{p_t}} \left(1 - e^{-\beta L_c}\right) u$ *and* $\beta = \frac{4h}{u \rho D_h\, c_p}$

The model was based on consideration of equal temperature over the tool mould, adiabatic tool face (no heat loss over the tool face) and applying energy

balance at the interface between the flowing fluid and the channel depending on the analyses of lumped-heat capacity (amounts of energy convected by the bulk fluid motion or mass flow rate) and tool thermal mass (Equation 2-16b).

2.12 General aspects of internal flow:

When a fluid flows in a tube and the fluid contacts the internal surface of the tube, a boundary layer develops due the viscous forces with the flow progress (increase of x), as illustrated in Figure 2-15. Both the fluid velocity and fluid temperature has a special boundary layer profile that explains their gradients between the internal surface and centre of the tube. When the flow becomes fully developed, the velocity or temperature profile remains constant and no longer changes as the flow progress.

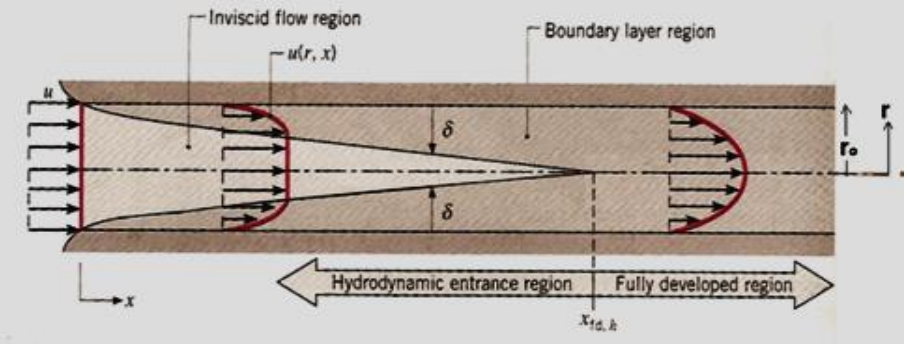

Figure 2-15 Fluid flow boundary layer in tubes (Incropera & DeWitt, 1996)

The distance between the inlet of tube and the position at which the flow becomes fully developed is known as hydrodynamic length (Daugherty, Franzini & Finnemore, 1989; Douglas, Gasiorek & Swaffield, 1995). Regarding the single-phase flow in the curved circular tubes Prusa and Yao (1982), as cited in Naphon and Wongwises (2006), investigated the effect curvature ratio of the flow path (radius of the tube bend/internal radius of the tube) on fully developed heat transfer and concluded that a secondary flow is generated in the curved

tube, which drastically reduces the mass flow rate and the total heat transfer rate due to higher curved tube and overheating conditions. Depending on the flow rate, the flow regime may be laminar, transient or turbulent. The flow profile of a layer in the fully developed region is parabolic for laminar flow, but it is somewhat blunter for turbulent (Incropera & DeWitt, 1996).

Different dimensionless parameters, in the concept of internal flow, are predicted to facilitate the calculation and definition of the fluid flow and the heat transfer characteristics:

- Reynolds number represents the ratio of the inertia force to the viscous or shear forces per unit mass as follows (Incropera & DeWitt, 1996):

$$Re_D = \frac{F_I}{F_s} = \frac{\rho u D_h}{\mu} = \frac{u D_h}{\upsilon} \qquad \text{(2- 22)}$$

  The value of this parameter defines the fluid flow regime and fluid flow boundary layer as follows (Bell & Mueller, 1984).

  When $Re_D \leq 2{,}300$ Flow is *Laminar,*

  $2300 \leq Re_D \leq 4{,}000$ Flow is transitional

  And $Re_D > 4{,}000$ Flow is fully turbulent.

- Prandtl number equals the ratio of the fluid viscosity to its thermal diffusivity, as follows.

$$Pr = \frac{\upsilon}{\propto} = \frac{\mu/\rho}{k/\rho c_p} = \frac{c_p \mu}{k} \qquad \text{(2- 23)}$$

- Nusselt number provides the ratio of total conductive heat to the convective heat between the flowing fluid and the tube surface. This dimensionless parameter can be used in determining the value of heat transfer coefficient of the flowing fluid and it can be calculated as follows (Cengel & Boles, 2002).

$$Nu_D = \frac{hD_h}{k} \qquad (2\text{- }24)$$

The Nusselt parameter is related to the exponential function of Reynolds and Prandtl numbers as follows.

$$Nu_D = CRe_D^m Pr^n \qquad (2\text{- }25)$$

The previous equation illustrates dependence of convection heat transfer of a flowing fluid on the value of Reynolds number, Prandtl number and the expected products of their exponential functions. Analytic approach of calculating heat transfer coefficient may not coincide with the practical solutions to all flow situations because each particular geometry and flow condition has its own empirical correlation. For example, forced heat convection occurs when the fluid, unlike natural flow, is pumped into the tube. Therefore many correlations were developed to estimate the heat transfer coefficient in different situations. The most correct and correlated relation, as shown in Figure 2-16, for the forced turbulent flow in a smooth tube was developed by Dittus and Boelter (1930) as cited in Holman (2002)

$$Nu_D = 0.023\, R_{e_D}^{0.8} Pr^n \qquad (2\text{- }26)$$

When $n = \begin{cases} 0.4 & for\ heating\ of\ the\ fluid \\ 0.3 & for\ cooling\ the\ fluid \end{cases}$

The equation is valid for the forced tube flow with following conditions (Ding, Chiu & Liu, 1999; Incropera *et al.*, 2013):

- Prandtl numbers $160 \geq Pr \geq 0.6$
- Reynolds number $Re_D \geq 10{,}000$
- Length to diameter ratio $L_c/D_h \geq 10$
-

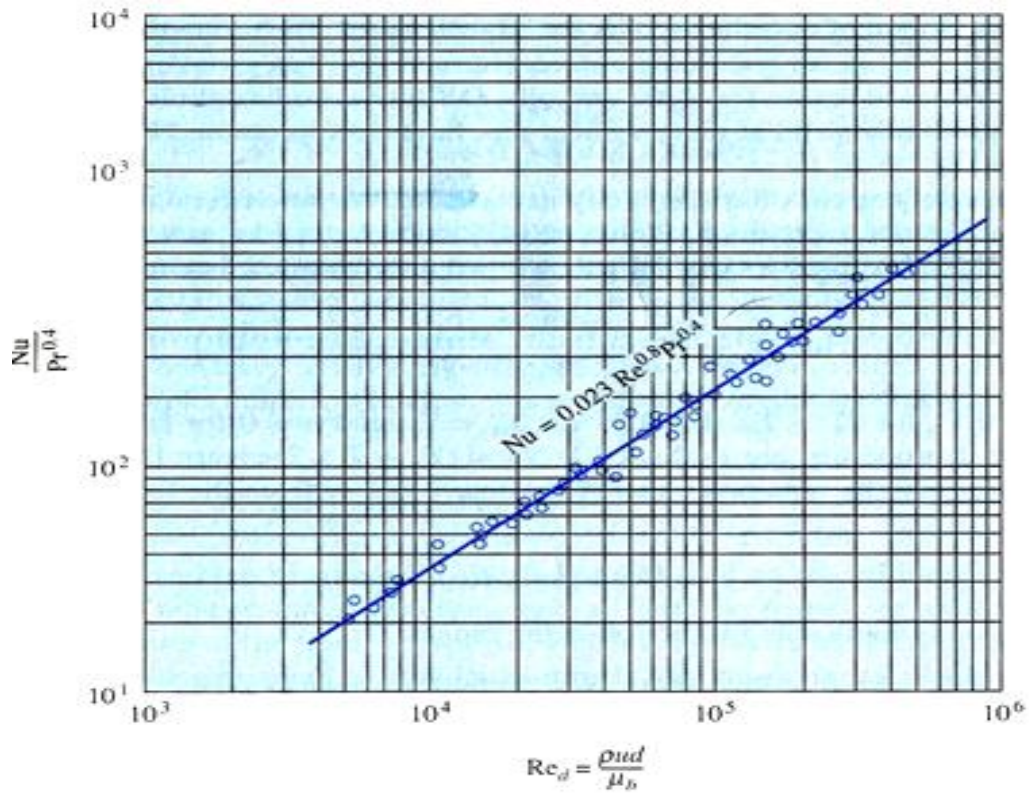

Figure 2-16 Typical data correlation for forced convection in smooth tube, turbulent flow within ±25% (Holman, 2002).

The appropriate fluid properties are evaluated at the mean bulk temperature, Equation 2-12, of water that can be defined as follows (Holman, 2002; Incropera *et al.*, 2013). The hydraulic diameter is commonly used when dealing with non-circular pipes and can be calculated by the generic Equation 2-19 (Kays & Crawford, 1993). Nusselt and Reynolds numbers are calculated according to hydraulic diameter and yields satisfactory relations for fluid friction and heat transfer in many practical problems (Holman, 2002). Therefore the cross section form of the flow channel affects the magnitude of the pressure gradient, boundary layer profile of the fluid velocity and the hydrodynamic entrance region (the distance between the tubes inlet to the position at which fully developed condition is first encountered).

2.13 Natural heat transfer coefficient

Heat transfer, in the free or natural (at atmospheric pressure) flow fluids, is generated by natural convection due to density variation and temperature gradients. For example the fluid near a hot surface receives heat becomes less dense and rises up, then cooler (or higher density) fluid moves to replace it. This makes a continuous natural motion in the fluid boundary layer at some distance from the leading edge of the surface, as shown in Figure 2-17a & b. So, the natural or free convection, through the free fluid boundary layer, is the result of the driving force of buoyancy that occurs due to the density decrement and gravity force.

The flow regime in the boundary layer of free flow fluid, as shown in Figure 2-17c, is not restricted to laminar and may change to turbulent due to hydrodynamic instabilities. This transition, of flow regime, correlates with Rayleigh number (free or natural convection number) that is based on characteristic length of the geometry (Incropera *et al.*, 2013). Rayleigh number is a dimensionless parameter defined as the ratio of buoyancy and viscosity forces multiplied by the ratio of momentum and thermal diffusivities, as in the following relation (Incropera *et al.*, 2013).

$$Ra_L = \left(\frac{g\alpha(T_a - T_\infty)L^3}{\upsilon^2}.Pr\right) = \frac{g\alpha(T_a - T_\infty)L^3}{\upsilon\propto} \qquad (2\text{-}27)$$

When $\alpha = \frac{1}{T_A}$ for ideal gases

Fluid properties are evaluated at the film temperature as follows (Incropera & DeWitt, 1996; Yoo & Walczyk, 2007).

$$T_{fa} = \frac{T_{m_m} + T_\infty}{2} \qquad (2\text{- }28)$$

Where $T_{m_m} = \frac{T_m + T_{m_i}}{2}$

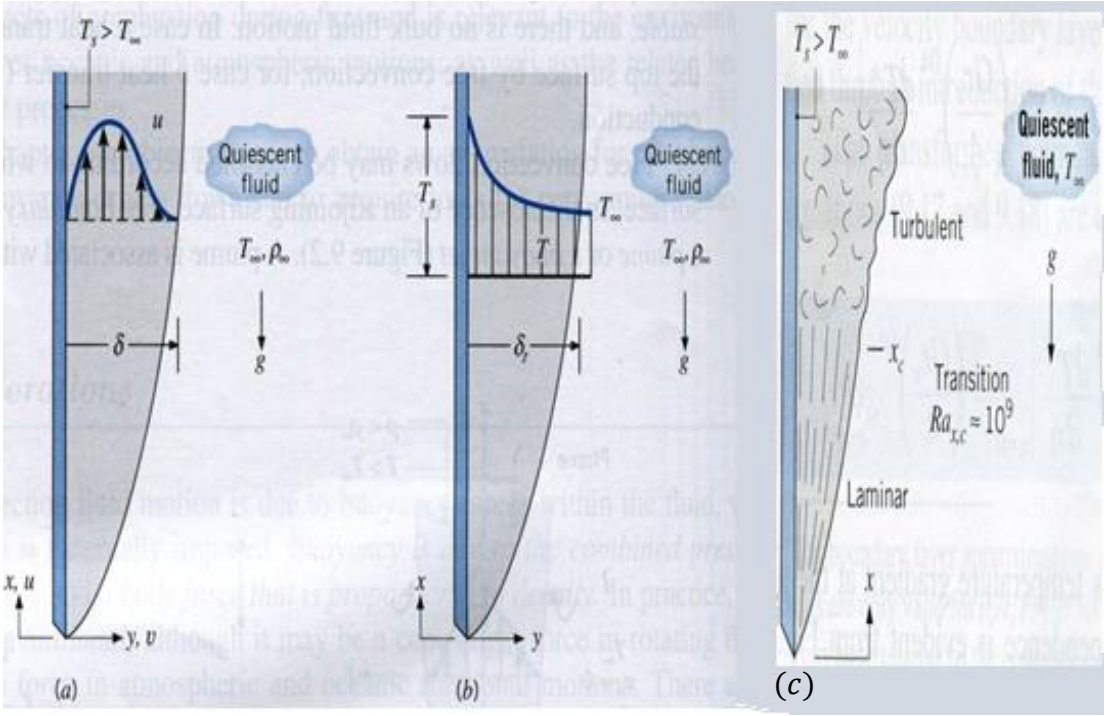

Figure 2-17 Boundary layers of free convection on a heated vertical plate. (a) Velocity boundary layer. (b) Thermal boundary layer. (c) Change of flow regime (Incropera *et al.*, 2013)

Incropera et al. (2013) summarised an empirical correlation suitable for determining the heat transfer coefficient in many engineering calculations.

$$Nu_L = \frac{hL}{k} = C\ Ra_L^n \qquad (2\text{- }29)$$

Typically n equals 1/4 and 1/3 for laminar and turbulent flows, respectively. Accordingly different simplified expressions are derived for finding heat transfer coefficient of free flow air convection on different hot surfaces e.g., vertical, horizontal, upward and downward plates as well as horizontal cylinders, as illustrated in Appendix C (Holman, 2002). The effective length that indicates better agreement with experimental results, as mentioned by Goldstein *et al.*

(1973), is the height for the vertical surface, but for the horizontal surface equals the area to perimeter ratio as follows.

$$L_o = \frac{A}{P} \qquad (2\text{- }30)$$

The simplified equations could be extended to the flows at higher or lower pressure by multiplying by the following factors.

$\left(\frac{p}{101.32}\right)^{1/2}$ For laminar flow and $\left(\frac{p}{101.32}\right)^{2/3}$ for turbulent flow

Heat transfer coefficient of forced air convection ranges between 10 to 200 W/m^2.K cannot be determined easily (Kreith & Black, 1980). Cunningham *et al.* (1997) presented that value of forced air convection coefficient, in most cases, is below 60 W/m^2.K, while Liu and Lam cited in Ding *et al.* (2001) concluded that the value of 20 W/m^2.K agreed well with the experimental results of forced-air-convection in autoclave. Also Johnston (1997) and Slesinger (2009) deduced that heat transfer of pressurised air inside autoclaves at 7atm ranges between 80-180 W/m^2.K, which varies significantly with location due to uneven gas circulation.

2.14 Modelling and Simulation (M&S)

Modelling and simulation are two different activities, which respectively imitate the system itself and its operation, but are mutually dependent and cannot be conducted individually. Therefore the terms of modelling and simulation are used as synonyms in defining the procedures (FrontlineSolvers, 2014). Simulation is widely used in analysing the behaviour of existing or proposed systems e.g. business activity, new product, manufacturing line or plant

expansion…etc. The simulation experiments are usually performed on a model of the real system instead of the system itself. Compared to the experimental tests, simulation tests can be achieved faster, cheaper and safer. Also it can provide information about how a system behaves or how the variables affect the system performance. Additionally sometimes the complexity of the process will not be easy to handle experimentally, e.g. the heat transfer processes in the curved and helical coiled tubes as mentioned by Naphon & Wongwises (2006). Successful simulation must be conducted as follows (Carson, 2005; Law, 2003; Maria, 1997).

- Define the system problem that needs solution, after understanding the system and its performance.
- Define the input variables or the decision variables that may affect the system problem and can be controlled by the program.
- Define the values and constraints of the variables that can be controlled.
- Define the desired response variables as a result of the simulation.
- Define the real system data and information, that remain constant, to input into the simulation.
- Develop a model for the real system to be studied.
- Validate the model by comparing its performance with that of the real system.
- Select simulation software to run the model.
- Optimise the model by simulation tests to find the best possible solution to the problem.
- Implement the optimised (best) results of simulation to the actual system.

Computer modelling and analysis methods have become an everyday tool in the modern product design due to the following advantages:

- Facilitates analysis, predicting and innovation the design and behaviour of the proposed or existing assemblies.
- Eliminates requirement for prototypes, physical tests and reduces development time scales and their prohibitive costs.
- Motivates simulation, optimizing and innovation of the engineering designs.
- Solves the problems of intractable scale of size, complexity and security issues and lack of prototypes.

The powerful program of ANSYS is a multi-purpose analysis tool and capable of simulating problems in wide variety of engineering disciplines correctly and efficiently, after considering the problem type, time dependence, nonlinearity as well as modelling idealisations and simplifications (Lawrence, 2011; Madenci & Guven, 2015). The program was developed by Swanson Analysis Systems, at beginning in the early eighties, and is now used to perform advanced coupled-physics numerical simulations to solve complex engineering problems. ANSYS software now covers a wide range of engineering fields, such as, structural mechanics, fluid dynamics, heat transfer, electrical, magnetism, piezoelectricity and etc. (Müller, 2002). A typical ANSYS analysis has three distinct steps of modelling, pre-processing (apply loads and obtain solution) and post-processing (review results).

ANSYS fluid flow CFX has ability of simulation and modelling of 2D and 3D transient diffusion, heat transfer and forced convection combined with fluid flow and achieves effective and accurate numerical analysis. Also ANSYS static structural can be applied in analysing the effect of thermal loads in 3D structures and predicting the resulted thermal deformation, strains and stresses (ANSYS, 2009).

Meshing is one of the main steps of numerical analysis in which the domain to be analysed is divided into a number of small regions and its quality or sensitivity can be checked by the program itself (Morton, 1996). The governing or partial differential equations (PDE) that describe the mathematical model of the physical reliabilities (actual system) can be solved by various numerical solution methods of finite differential (FDM), finite element (FEM) and finite volume (FVM). Both the FEM and FVM being applied for computational fluid dynamics (CFD), but the latter is increasingly used in recent years due to special advantages in its formulation (Peir´o & Sherwin, 2005).

The domain in FVM is divided into boxes with finite volume (FV) that refers to the volume surrounding each node point. Nodal connectivity is not mandatory in FVM, but face connectivity is important because FV solution converts volume integrals to surface integrals, using the divergence theorem (Davis, 2008; Versteeg & Malalasekera, 2007). The numerical solution of FVM is powerful on coarser and non-uniform grids or when the mesh moves and provides accurate results with lower computation time (Fallah et al., 2000). FVM is rigorous in mass and energy conservation due to its dependence on integration to accord a more fundamental interpretation of mass or energy flux between interfaces (Grossmann, Roos & Stynes, 2007).

The centre of each region in FV, as shown in Figure 2-18, is assigned as a reference point to the entire region, which is called nodal point or node. Each region is described by nodal network, grid or mesh. Hence the nodal points are designed by a numbering scheme according to the dimensional system, for instance, x, y and z their locations are designated by m, n and c indices respectively.

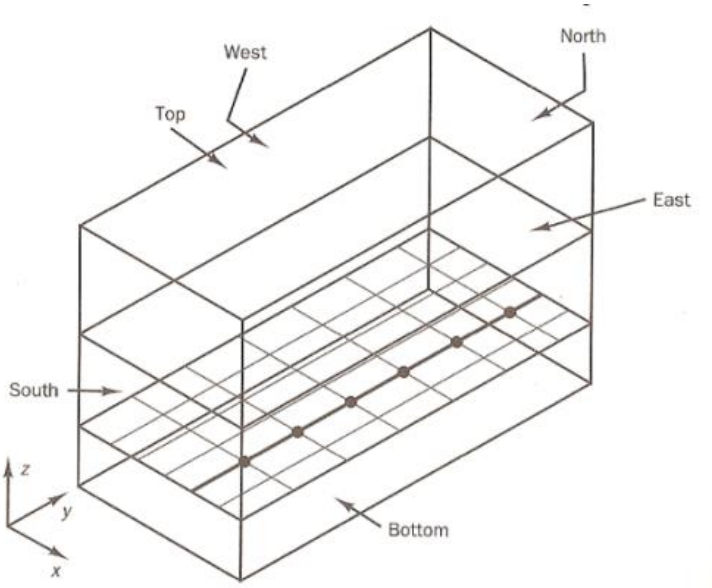

Figure 2-18 Grid generation (meshing) (Versteeg & Malalasekera, 2007)

Through computer M&S, a mathematical model of the real system, expressed by formulas and programming statements, is applied to relate between the inputs and outputs. Nowadays almost all phenomena in science and engineering are described in terms of partial differential equations (PDE), which are called conservation or governing equations (Nikishkov, 2004; Reddy, 2005). The numerical methods obtain approximate solutions by reducing the PDEs to simultaneous linear algebraic equations that can be solved numerically as mentioned by Stolarski *et al.* (2006). For example the governing equation of un-steady heat conduction, in one dimensional control volume as illustrated in Figure 2-19, is expressed by Versteeg & Malalasekera (2007):

$$\rho c_p \frac{\partial T}{\partial t} = \frac{\partial}{\partial x}\left(k \frac{\partial T}{\partial x}\right) + S \qquad (2\text{- }31)$$

Where S is a constant

Time step, in the simulation process, must be selected carefully according to the selected mesh size and the material properties. According to the time

marching procedure, the computer starts with a given initial temperature to solve the equation after selecting a time step then the next solution assigns current solution to an initial state and the procedure is repeated.

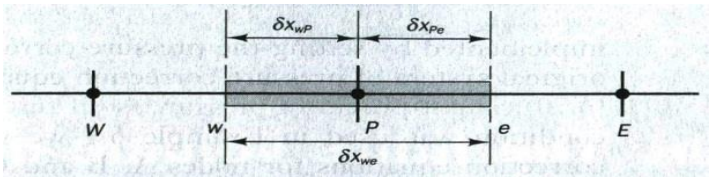

Figure 2-19 One dimensional control volume (Versteeg & Malalasekera, 2007).

Time step must be suitable with the natural increment of the procedure. For instance in transient calculation, as in this PhD research, the time step size should be the smaller of the convection and thermal diffusion timescales. The value of the convection time scale is obtained as follows, assuming a ratio of pipe length to its diameter.

$$\text{Convective time scale} = \frac{R_i D_h}{u} \qquad (2\text{- }32)$$

If the flow is turbulent, the thermal time scale is

$$\text{Thermal diffusion time scale } = \frac{D_h^2}{100(k/\rho c_p)} \qquad (2\text{- }33)$$

2.15 Verification and validation

The scientific problems and equations can be solved analytically, experimentally and numerically. Selecting the appropriate technique is function of the complexity and cost of the solution. Due to the improvements in computational systems (e.g. cost reduction and speed increases), nowadays, the numerical software is extensively used in solving complex problems with nonlinear

behaviours that are impossible to solve analytically or has expensive experimental solution (Jauregui & Silva, 2011). If a numerical method is applied, it is necessary to validate its approximate results to assign the real boundary conditions during simulation (Pace, 2004; Sargent, 2013). Many methods available to affirm that the result of a numerical solution is fully consistent with the reality (Oberkampf, Trucano & Hirsch, 2004). For example comparing the numerical results to that of a valid analytic model or experimentally after setting the actual boundary and internal (material properties) conditions during the simulation method (Archambeault & Connor, 2008; MITRE, 2014).

2.16 Summery

The literature reviewed in this chapter shows that:

- Composite materials, compared to metals, have lower thermal conductivity, but can provide lower density and CTE.
- Water, compared to other fluids, is suitable for clean room processing and superior in achieving the desired temperature uniformly over the mould face with lower cost, time and consumed energy.
- Simulation methods solve the complex governing equations by iteration and provide approximate results; therefore verification is necessary to define the errors involved and ensure the boundary conditions and material properties.
- The traditional method of autoclave curing has various disadvantages of cost, time and energy consumption. Integrally heated tools, especially fluid-heated, have the potential to overcome most of these problems.

- Although heated tool can cure advanced composites outside the autoclave faster, cheaper and overcome the problem of size limitation, the quality of the produced or the cured parts are still below that produced in the autoclave.
- Many researchers and designers have studied the effect of tool material, flow rate, heating medium, tool geometry, and channel separation, but this research has been mainly for metallic tools in the field of plastic injection manufacturing.
- No comprehensive investigations to study the effect of channel profile, channel layout and channel separation on the performance of integrally fluid circulation heated tools made of composites has been made.

Chapter 3
Thermal Analysis and Verification

3.1 Introduction

Scientific problems can be presented by the analytic, experimental or numerical techniques and selecting the proper method depends on the complexity of the problem and its solution cost. For instance the experimental method cannot be performed every time due to the constraints of cost, time and complexity, while analytic or closed form solutions are impossible or time consuming in the cases of nonlinear and complex problems. Most systems possess complex functionality due to the complexity of their geometry, boundary and loading conditions that are difficult to analyse. The integrally water heated tool in this PhD study combines the fluid flow, heat conduction and convection as well as geometry factors. Furthermore the governing equations of the complex systems or problems are functions of several parameters and they have non-linear characteristics that require advanced functional analysis. Therefore numerical solver will be the only choice, especially when the case is:

- A complicated equation has more than just one solution.
- A special type, called “data fitting” (“solving the equation system with more equations than there are unknowns”, and when the fitted data are uncertain), that need to switch to solve a different problem, closely related to the original system of equation.

Since the late seventies, when the first ANSYS seminar was held at KWU in Berlin and then large number of simulations in the design process was performed, the numerical methods that can be performed quickly by computers changed everything in research (Müller, 2002). Nowadays numerical software is used extensively to solve many complex problems with nonlinear behaviours that are impossible to solve analytically or has expensive experimental solution.

Numerical methods solve phenomena (e.g. flow) that are described partially or integrally by differential equations cannot be solved analytically and illustrate the effect of parameters in graphs and tables. On the other hand, numerical methods give approximate (not exact) solutions because they calculate the required answers by iteration and performing thousands of repetitive calculations that losses some of accuracy and gives the final results with some error. For obtaining good approximated results under certain circumstances, the selected numerical approach must have the following characteristics (Arnold, 2015; Iaccarino, 2009):

- Stability, which means that the generated numerical errors should be minimised during solution of the discretized equations.
- Convergence that means the numerical solution should approach the exact solution of the PDE and converge to it, when the mesh size tends to zero.
- Consistency, this means that the discretization of a PDE should become exact as the truncation error should vanish, when the mesh size tends to zero.
- Conservative means the underlying conservation laws should be respected at the discrete level, e.g. artificial sources and sinks are to be avoided).
- Boundedness that means that some quantities, like density, temperature, concentration…etc., should remain positive and free of spurious wiggles.

When a numerical method is applied, the approximate results must be validated to assign the real boundary condition during simulation. The analytic method, or closed solution, is the simplification of reality that works only for

simple models and illustrates the effect of parameters in a restricted way and cannot solve all problems, however it gives an exact solution and its results are straight forward in understanding the behaviour, mechanism or physics of the systems under any circumstances (effect of parameters). Accordingly the analytic method provides a good insight in phenomena under question and can be applied in validating or verifying the numerical method analytically.

While this PhD study aims to investigate the heating performance of an integrally water-heated tool numerically, in this chapter a simplified tool model is designed initially and its heating performance is analysed numerically (by ANSYS CFX software) and analytically. This is to validate the suitability of the numerical approach in terms of assigning the correct material properties and boundary conditions. Two different analytic models that calculate the one dimensional (1D) transient heat transfer between water and the proposed model surface are applied for further validation. The response variables are considered to be the transient surface temperature and the required heating time (or heating rate) to reach the steady state. The simulation is performed with lower running time and PC memory size by selecting;

- The maximum mesh size (element number) with acceptable mesh quality and time step size that gives accurate results.
- The two dimensions (2D) method, compared to three dimensions (3D), for simulation.
- The average method facility, compared to the expression, for setting the nonlinear properties of water during simulation.

3.2 Simplified square tool model

A simplified model of a square tool is proposed according to those published by each of Ding *et al.*(2001), Yoo & Walczyk (2007) and (2009). The model, as

shown in Figure 3-1, is an aluminium mould in which a copper tube is embedded as a heating channel and hot water flows through it. Two cases are also proposed for the model, which are defined as “insulated” and “non-insulated”, during this PhD study. All the model faces, except the top, of the first case are considered to be insulated by a thick layer of glass fibre heled in a box of hardwood, while they remain not insulted in the second case.

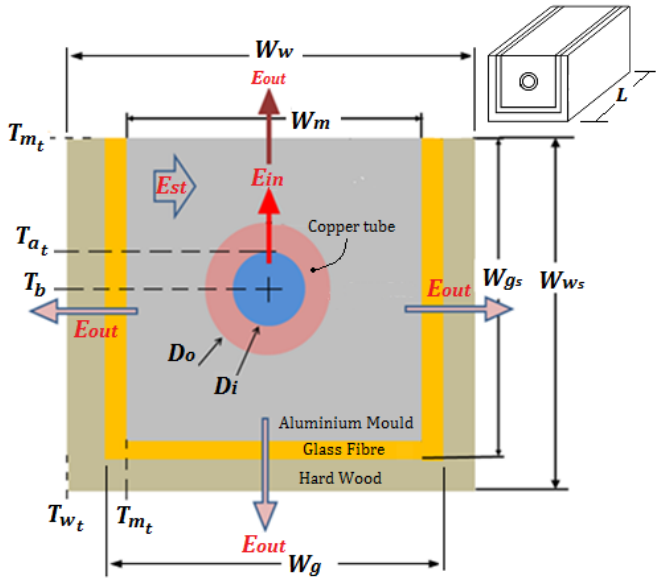

Figure 3-1 Cross section of the simplified tool model geometry (see Table 3-1)

The top surface is considered to be open to ambient in both cases, but the side and the bottom faces are assumed to be non-adiabatic in the insulated case and adiabatic in the non-insulated case. Table 3-1 illustrates the main dimensions of the proposed model.

Table 3-1 Dimensions of the square and cylindrical models (see Figure3-1)

Dimensions of the model	Symbol	Unit	Amount
Channel length	L_c	m	1
Internal channel diameter	D_i & D_h		0.008
External channel diameter	D_o		0.01
Mould Width	W_m		0.09
Glass fibre insulation width	W_g		0.104
Wood ply width	W_w		0.13
Glass fibre insulation side width	W_{g_s}		0.097
Wood ply side width	W_{w_s}		0.11

3.3 Boundary conditions

The fluid velocity is assumed to be 1 m/s to produce fully turbulent flow in the smooth copper channel that heats the mould faster as concluded by Ding *et al.* (1999). The proposed temperatures of the model and its boundaries are presented in Table 3-2.

Table 3-2 Proposed boundary temperatures

Temperature type	Symbol	Value	
		℃	K
Ambient, mould Initial &Water outlet	$T_\infty, T_{m_i} \& T_{b_o}$	25	298
Water inlet & mould final	T_{b_i}, T_m	90	363

3.4 Material properties

The thermal properties of the model materials, as illustrated in Table 3-3, are collected from literature and assumed to be constant because of their relatively small variation with temperature (Davis, 2001; Incropera *et al.*, 2013).

Table 3-3 Thermal properties of the model materials (Davis, 2001; Incropera *et al.*, 2013).

Properties (at 25℃)	Units	Materials			
		Aluminium	Copper	Glass Fibre	Plywood
k	*W/m.K*	237	401	0.046	0.12
ρ	*kg/m^3*	2702	8933	16	545
c_p	*J/kg.K*	903	385	835	1215
$\propto = k/\rho c_p$	*m^2/s*	**97.1x10^{-6}**	**117 x10^{-6}**	**3.44 x10^{-6}**	**0.18 x10^{-6}**

A perfect contact is assumed between the adjacent solid materials, therefore no heat transfer resistance is assumed at their interfaces. According to basic properties of water (Appendix D), the values of both the dimensionless parameters of Reynolds and Prandtl numbers are calculated by the Equations 2-22 and 2-23, respectively. While the water bulk temperature is 57.5°C according to Equation 2-12 and the corresponding Reynold's number is higher

than 10^4, the calculated heat transfer coefficient of water equals 6848 W/m^2.K according to the following equation.

$$h = 0.023\, Re_D^{0.8} Pr^{0.4} \frac{k}{D_h} \qquad (3\text{- }1)$$

The basic properties of water, e.g. thermal conductivity, dynamic viscosity, specific heat capacity and density, as shown in Figure 3-2 and Figure 3-3, change widely with temperature.

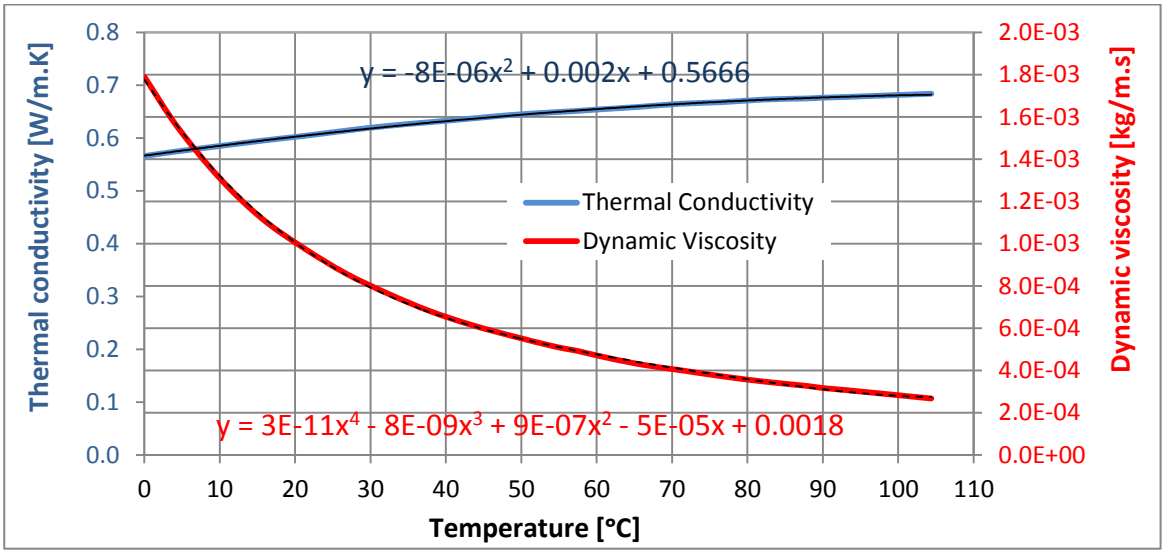

Figure 3-2 Effect of temperature change on the thermal conductivity and dynamic viscosity of water

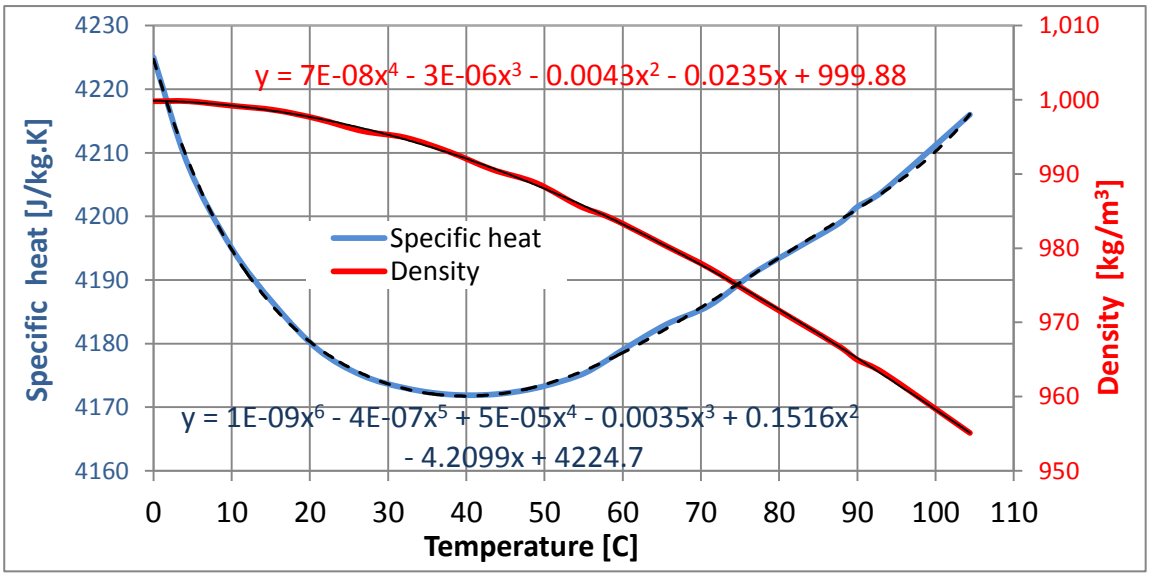

Figure 3-3 Effect of temperature change on the specific heat and density of water

Accordingly the Prandtl number (Figure 3-4), opposite to the heat transfer coefficient and Reynolds number (Figure 3-5), changes reversely with temperature. The polynomial fit is applied to define the equation of each property (property behaviour with temperature change) that is utilized during simulation.

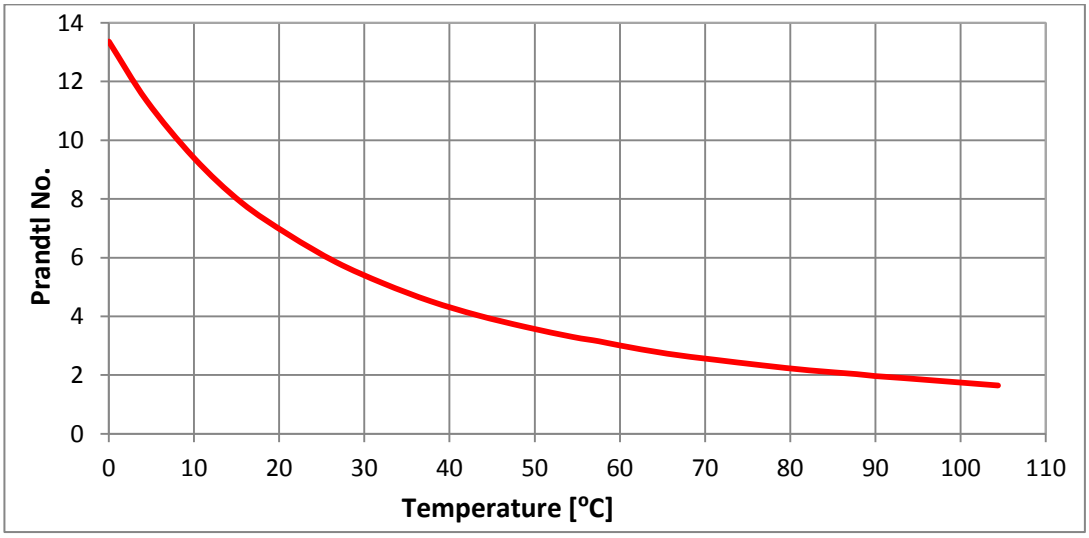

Figure 3-4 Effect of temperature variance on Prandtl No. of water. u =1m/s

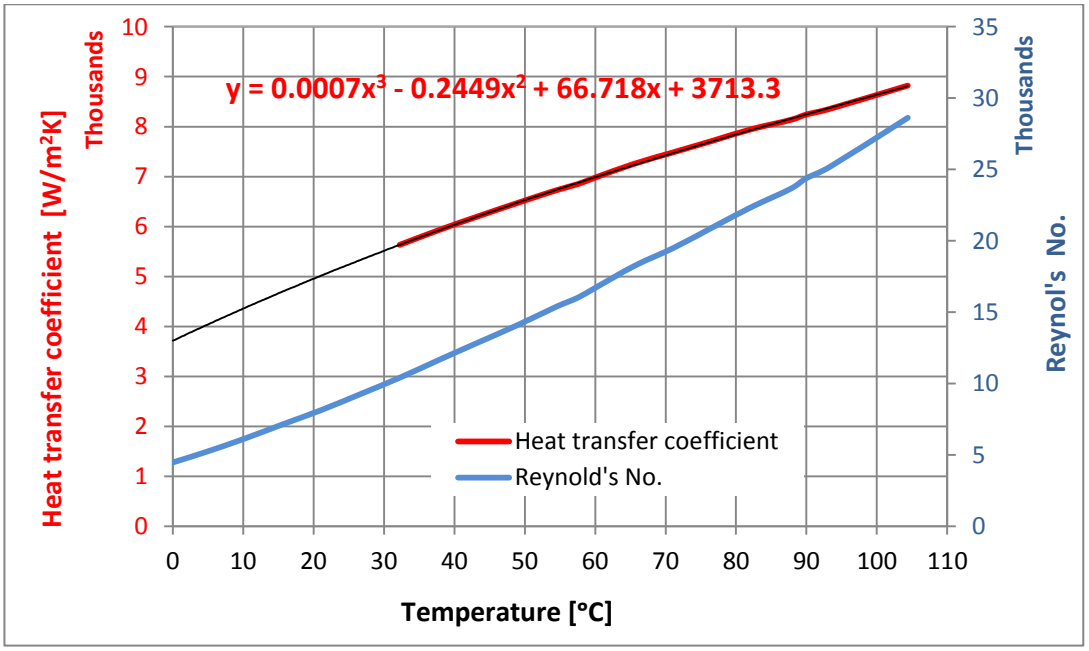

Figure 3-5 Effect of temperature variance on both the Reynold's number and heat transfer coefficient of water, when u = 1 m/s and D_h= 0.008 mm.

The air film temperature of 41°C is calculated by Equation 2-28, after defining the temperatures of ambient and corresponding mould mean that equals 57.5°C. Consequently the required air properties, as listed in Table 3-4, are defined from that presented by Holman (2002).

Table 3-4 Properties of air at 41°C and atmospheric pressure (Holman, 2002).

Density	Specific Heat	Thermal Conductivity	Expansion Coefficient	Thermal Diffusivity	Kinematic viscosity	Prandtl No.	Rayleigh No.
ρ	c_p	k	α	$\propto$	υ	Pr	Ra_L
kg/m^3	*J/kg.K*	*W/m. K*	*1/K*	*m^2/s*	*m^2/s*	-	-
1.127	1005	2.7x10^{-2}	3.2x10^{-3}	2.4x10^{-2}	1.7x10^{-5}	7x10^{-4}	5x10^6

The boundary condition of the air surrounding the external faces of the square model is assumed to be free convection. The value of its Rayleigh number that calculated by Equation 2-27 is higher than 10^4, so the following equations are selected from Appendix C for calculating the values of heat transfer coefficient at different faces of the model, as listed in Table 3-5.

Top surface $$h_t = 1.32\left(\frac{T_{m_m}-T_\infty}{L_o}\right)^{0.25} \quad (3\text{-}2)$$

Bottom surface $$h_b = 0.59\left(\frac{T_{m_m}-T_\infty}{L_o}\right)^{0.25} \quad (3\text{-}3)$$

Side surfaces $$h_s = 1.42\left(\frac{T_{m_m}-T_\infty}{L_s}\right)^{0.25} \quad (3\text{-}4)$$

As illustrated in Section 2.13, the effective length for the vertical surface is its height, but for the horizontal surface is calculated by Equation 2-30.

Table 3-5 Heat transfer coefficient over the external surfaces of the tool

Model Surface	Symbol	Length	Heat Transfer Coefficient
		m	*W/m^{2}K*
Top	h_t	41 X 10^{-3}	6.4
bottom	h_b	58 X 10^{-3}	2.6
Side	h_s	11 X 10^{-2}	5.4

3.5 Numerical simulation

The CFX code of ANSYS software is the FVM used to foresee the conjugate heat transfer and fluid flow in the proposed simplified square model by 2D and 3D simulations. Typical ANSYS analysis has three distinct steps of building the model, obtaining the solution (after applying loads and boundary conditions) and reviewing the results.

3.5.1 Model geometry

The geometry of the proposed model shown in Figure 3-6 is created in ANSYS workbench according to the proposed dimensions.

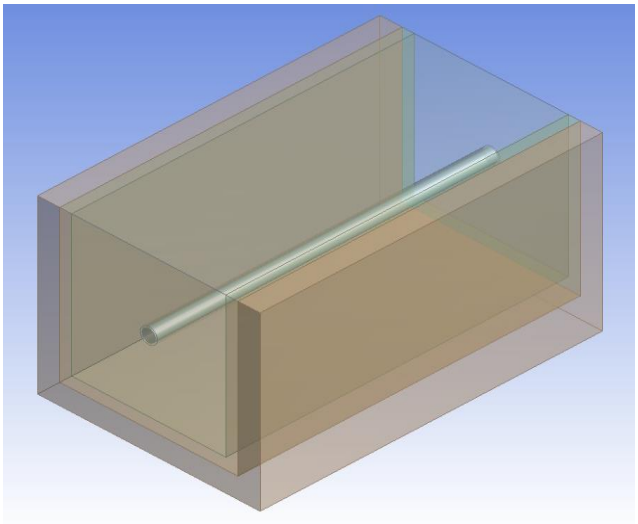

Figure 3-6 Geometry of the square model in ANSYS workbench (for dimensions see Figure 3-1)

3.5.2 Meshing

The meshing process divides the model geometry into a high number of small elements as shown in Figure 3-7. Inflation method is selected for meshing near the solid wall region of the water domain in order to create fine mesh and

ensure accurate simulation of the flow field. That is because the fluid near the solid wall, compared to the flow regions further from the wall, slows down by friction and becomes stationary.

The distance between the stationary and the free flowing fluid is very small, therefore this steep velocity gradient boundary layer region needs lots of elements (Marriott & Jayaratne, 2010). The y-plus (y^+) law, in CFD, describes thickness of the first inflation layer as follows (ANSYS, 2009).

$$y = \frac{y^+ \mu \, Re_L^{0.4}}{0.1703 \, \rho u} \qquad (3\text{- }5)$$

For $Re_L < 10^9$ and $Re_L = \frac{\rho u L_c}{\mu}$

y^+ is a dimensionless parameter that determines how coarse or fine the mesh should be in a particular flow and the most desirable value of y^+ is 1 for the eddy-viscosity model of shear stress transport (SST) (Gerasimov, 2006). The incremental ratio for the remaining layers must be between 1.1 and 1.4. Then the number of inflation layers can be calculated from the wall spacing distance (thickness of the first inflation layer) and the incremental ratio, provided that the total thickness of all layers together does not exceed the height of the neighbour grid in the domain or the mesh size.

While each part of the model is meshed separately, the general grid Interface (GGI) method is set at the interfaces for mesh connection because it facilitates the connection of the surfaces where the grids do not match and permits non-matching of node location (ANSYS, 2009).

Although the accuracy improves as the mesh size approaches zero, the element numbers, CPU memory requirements and computation time for solution and post processing the results increase as well, especially for nonlinear and transient analysis that have typical multiple-iteration runs. Consequently

acceptable solution accuracy and much faster running time are function of a good mesh that provides complete convergence between the elements of the dissimilar parts and has a minimum number of elements. The proper largest grid size, which obtains lower number of element and computation time with acceptable results, is defined as follows.

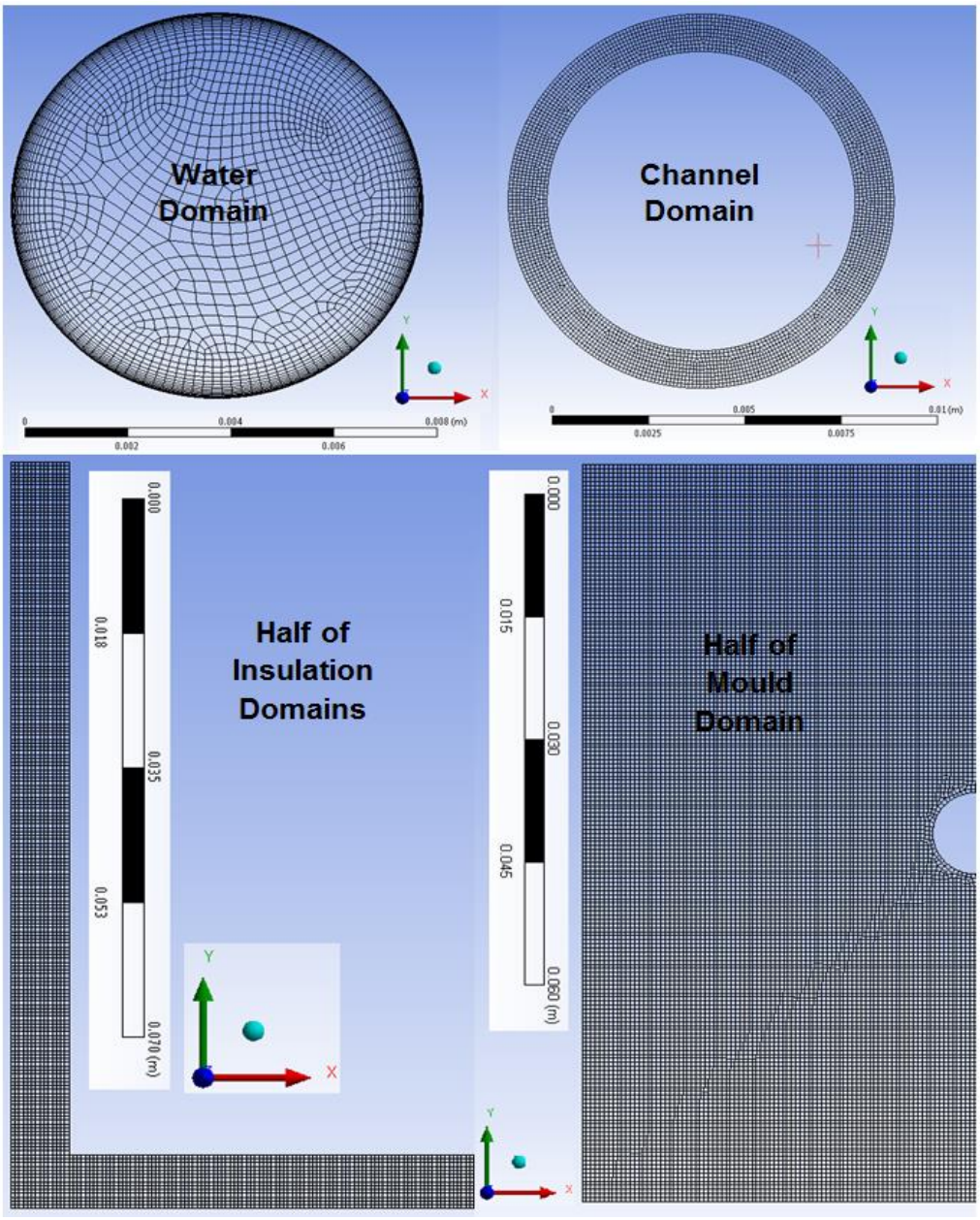

Figure 3-7 Meshing the model domains

- Various preliminary tests are achieved with random mesh sizes (or element numbers) to define the approximate extremes that could be run

and results concluded 559,225 and 126,221elements as the highest and lowest limits, respectively.

- Five cases of the proposed model, as shown in Figure 3-8, are meshed with different element numbers within the limits defined initially and the cases are simulated with the same time step of 0.1s.
- Mesh quality is evaluated through the available mesh metric function of the software and obtained that orthogonal quality of the cells are close to 1, cell skewness values are below 0.9, while the sudden and large changes in cell aspect ratios is avoided to achieve best aspect ratios.
- The heating curve of a specified point on the surface of each case, from the simulation result, is defined and plotted together in Figure 3-8.
- Accordingly the proper element numbers of 250,624 and related mesh size, which can give acceptable results and reduce 68% of running time, is selected.

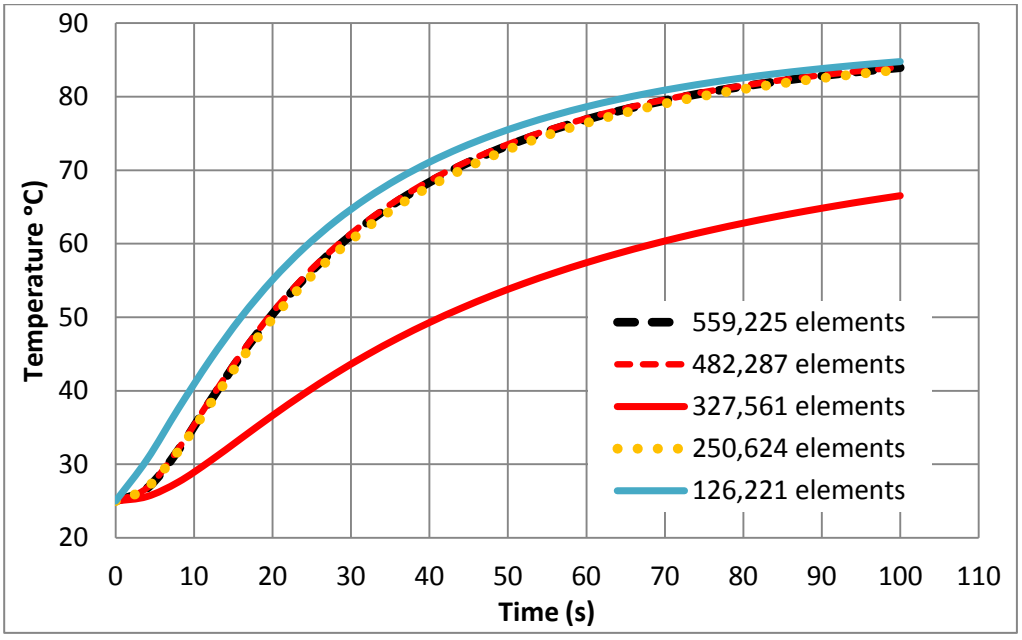

Figure 3-8 Heating curve of the model face with different element number, time step is 0.1 s.

3.5.3 Time step (time scale)

Time step is a basic factor that can affects the running speed and the outputs accuracy of the simulation process. The time step size of transient calculation should be the smaller of the convection and thermal diffusion timescales (ANSYS, 2009). Therefore the convection time scale of 0.1s is obtained by Equation 2-32, after assuming the ratio of 10^2 for the pipe length to diameter. Also the thermal time scale of 4.5 s is defined according to Equation 2-33 for turbulent flow. Consequently the smaller time scale of 0.1 s is selected. Hence various tests were conducted with different time step sizes up to 2 s, as shown in Figure 3-9, which concluded that 1 s can achieve the same results of 0.1s and reduce 72% of the computation time.

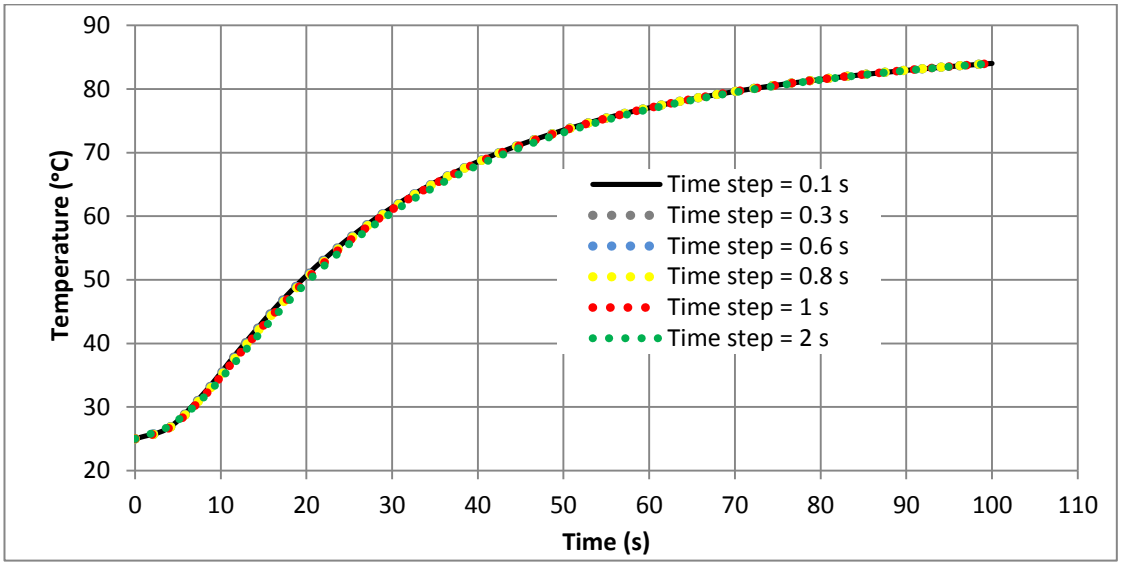

Figure 3-9 Heating curve of the model face with different Time step sizes and constant grid sizes

3.5.4 Boundary condition

The proposed material properties and boundary conditions (temperature, fluid velocity and heat transfer coefficients) are applied to the domains and their boundaries (inlet, outlet and interfaces) according to their availability and

simulation type (2D and 3D). Generally the heat transfer coefficients of air, as listed in Table 3-5, are applied to the corresponding non-adiabatic surfaces of the model.

3.5.4.1 Boundary condition in 3D simulation

The 3D simulation contains water domain that has inlet and outlet boundaries. Properties of water are set through two facilities provided in ANSYS CFX software. The first is achieved by setting the expressions that describe the property behaviours of water with temperature change (Figures 3-2 and 3-3), while the second sets the average value of each property, calculated at the bulk temperature of water, as listed and highlighted in Appendix D.

The axial fluid velocity in the z-direction of inlet boundary is set to 1 m/s and the others are set to zero because the flow is enclosed. The shear stress transport (SST) model is selected for solving the heat transfer model within the water bulk because SST can compromise between both the k-ε and k- ω models in the turbulent free stream and the laminar flow close to the wall (Menter et al., 2003).

Value of the turbulence intensity (the average of the velocity at the same location over the same time period) is set to 5% at the inlet boundary because the flow in water domain is fully turbulent (Re > 4000). Medium-turbulence case is also considered during setting because the flow inside the tube is not so complex and turbulent velocity fluctuations at a particular location are not very high (Li et al., 1994).

A pressure drop of 0.05 bars is calculated for the flow in channel domain by the following expressions (Incropera *et al.*, 2013).

$$\Delta p = \frac{\rho u^2 L_c}{2D_h(0.79\,ln\,Re_D - 1.64)^2} \qquad (3\text{- }6)$$

Accordingly the amount of pressure at outlet boundary is set to 4.45 bars, while the pressure of the available pump, that pumps water into the channel at the inlet boundary, equals 4.5 bars.

3.5.4.2 Boundary condition in 2D simulation

The water domain does not exist in 2D simulation. Therefore the wet peripheral area of the channel (tube interface), which contacts the flowing water at a constant temperature of 90°C, is set instead as a convection boundary and the water heat transfer coefficient, at the calculated water bulk temperature (Appendix D), is applied.

3.6 Analytic models

Simplified analytic or closed form solutions can provide the behaviour of the model, so it can be considered as a perfect base for verifying the simulation results and assigning the applied boundary conditions. Based on literature, two analytical models are utilised for calculating the one dimensional (1D) heat transfer in the proposed tool model to compare with that obtained numerically by ANSYS CFX.

3.6.1 Analytic model 1

This model is an amended version of that concluded by Yoo and Walczyk (2007) that contains some aspects regarding application, as illustrated in Section 2.11. The amendments are performed to make the model, in this PhD

study, most effective in obtaining more accurate and real results. Appendix E illustrates the derivation details of the revised version with performing the following modifications.

- The total mould volume is defined according to Equation E-13.
- The hydraulic diameter (Equation 2-19) is applied instead of the internal radius of the channel.
- The thermal resistance of the model parts (channel, mould and insulation layers of glass fibre and plywood) are calculated by applying the conduction shape factors (cases 6 and 11 of Appendix F) in Equations E-15, 16 and, 20, 21, respectively.
- The thermal resistance of the non-insulated top face is considered as a quarter of the total mould resistance, therefore the total resistance is multiplied by 4 in Equation E-14, while resistance of the other three insulated faces are considered as three quarters of the total resistance, so the total resistance is multiplied by 4/3 in Equation E-19.
- The final mathematical model for defining the transient temperature, at mould surface, is Equations E-33.
- A new expression is defined for determining the transient temperature at the external insulated surfaces as follows:

$$T_{w_t} = MT_{m_t} + M_1 T_\infty \qquad (3\text{- }7)$$

While M and M_1 are ratios of heat transfer resistances of the model domains.

3.6.2 Analytic model 2

This model, as illustrated in Section 2.11, is derived by Ding *et al.* (2001) and can be used for describing transient heat transfer with turbulent flow.

3.7 Discussion

Table 3-6 lists the details of the eight tests that are conducted numerically and analytically for describing the transient temperature over the surfaces (top, side and bottom) of the proposed model. The both versions of the first analytical method (basic and revised), as mentioned in Section 3.6.1, are applied for comparison.

Table 3-6 Summery of the numerical and analytical tests

Boundary condition		Insulated *& no-Adiabatic*		non-Insulated *& Adiabatic*	
Water properties definition		Expression	Average	Average	
Test cases	**3D-**Numerical	Test 1	Test 2	-	-
	2D-Numerical	-	Test 3	-	Test 6
	Analytical-**1**	-	Test 4 (revised)	Test 5 (basic)	Test 7 (revised)
	Analytical-**2**	-	-	-	Test 8

Figure 3-10 illustrates results of the 2D and 3D simulations of transient heat transfer at each of the top, side and bottom faces of the insulated non-adiabatic (i.e. transfer of temperature is not constant) model with the both methods of expression and average for defining the water properties.

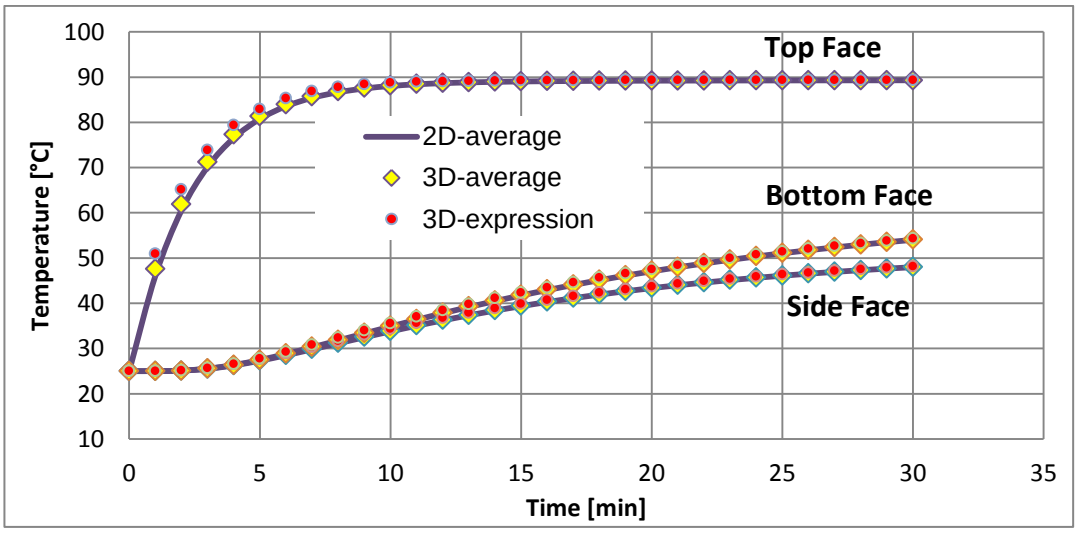

Figure 3-10 Numerical heating curves of all model faces, different definition of water properties, insulated non-adiabatic (tests number 1, 2 and 3)

The numerical outputs of heating rate for the first three test cases (testes number 1, 2 and 3) are 7.2, 7.1 and 7°C/min, respectively. The maximum difference of 2.7%, between the heating rates, indicates that the results are well agreed, but their computation times are 5.49, 3.10 and 0.57 hours, respectively, therefore the last case (2D simulation method with average water properties) is considered the appropriate method because it obtains the same result (transient temperatures over the top, side and bottom faces) in a shorter computation time. The 2D numerical method and both the first (before and after revision) and the second analytical models (tests number 5, 6, 7 and 8) are applied in defining the transient heat transfer over the top face of the model and results are plotted together in Figure 3-11.

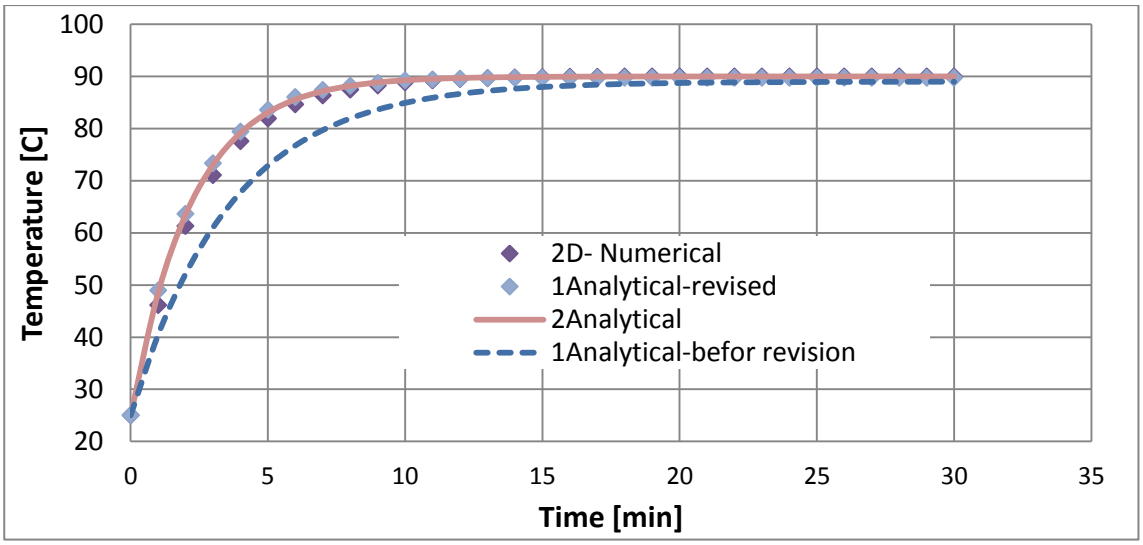

Figure 3-11 Analytical and numerical heating curves of the top face, non-insulated adiabatic model (tests number 5, 6, 7 and 8)

The calculated heating rates, according to achieved results, are 4.6, 7, 7.2 and 7.2°C/min, respectively. The maximum difference of 2.7%, between the heating rates, presents the well agreement between the numerical and analytical calculations except that of the first analytic before modification (test 5) due to aspects illustrated previously in section 2.11. This illustrates that the revised

version of the first analytic method, compared to the basic, is more accurate in predicting the model behaviour under the proposed boundary conditions. Figure 3-12 illustrates heating curves of the side and bottom faces of the insulated non-adiabatic case obtained by each of the 2D simulation and the first revised analysis methods (tests number 3 and 4).

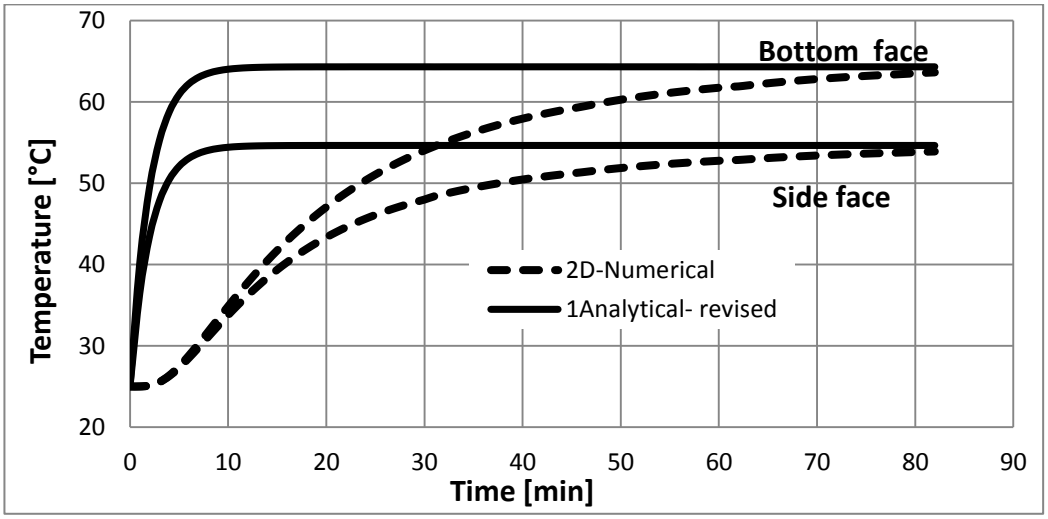

Figure 3-12 Analytical and numerical heating curves of the side and bottom faces, insulated non-adiabatic model (tests number 3 and4)

It shows that the final steady state temperature at the insulated surfaces of both the analytic and numerical methods are the same, however the insulated surfaces in the analytic methods, compared to the numerical, are heated more rapidly. That is because the analytic method combines the parallel or series thermal resistances of the model parts, as illustrated in Appendix E, and treats them as an element during calculation. So it can be concluded that the analytic method, opposite to simulation, ignores the effect of material difference during calculation because the numerical method splits the model into thousands of very fine elements, as shown in Figure 3-7, and the software can calculates simultaneous spatial and time temperature of the model. Therefore the numerical results present the most accurate and actual heating behaviour of the insulated surfaces.

3.8 Conclusion

Numerical analysis, especially ANSYS software, can perform advanced engineering analysis quickly, safely and practically by variety of contact algorithms, time based loading feature and nonlinear material models. Depending on iteration, simulation method provides approximate results of the complex governing equations that describe the nonlinear behaviour of the systems and have more than one variable. Therefore numerical results require validation of assigning of the real boundary conditions during simulation. A simplified representative tool model, in the current chapter, is proposed and analysed numerically using ANSYS CFX software to define the transient heating behaviour at the model top and side surfaces. Then two analytical models are applied to analyse the model and to verify the numerical results analytically. The well agreed analytical and numerical results proved that:

- The modified version of the first analytic method predicts the most actual results.
- 2D simulation, compared to 3D simulation, provides the desired results accurately in a lower computation time.
- The analytic results confirm the good performance of ANSYS simulation in assigning the proposed boundary conditions and predicting the real characteristic behaviours of the proposed model

Chapter 4
Design Analysis and Optimisation

4.1 Introduction

Almost the entire chapter is published in an article in the journal of Materials and Design, available online since 1 August 2014 and also a conference paper presented in ECCM16, 22-26 June 2014. All types of fibre-reinforced composite products require accurate and robust tooling because the performance of the tool determines the integrity of the manufactured part. Tooling not only provides a reproducible geometry, it also provides consolidation which influences the mechanical and physical properties of the product and helps the transfer of heat into the polymer matrix. Throughout the last two decades, composite manufacturers have given high priority to cost reduction and increased energy efficiency in composite manufacturing (Gibbons et al., 2009). In advanced composites, this requires alternatives to autoclave processing of prepregs (Athanasopoulos *et al.*, 2013; Grove *et al.*, 2005; Plesu *et al.*, 1994). Also the increasing demands of producing increasingly large composite products as a single piece cannot be fulfilled using traditional manufacturing methods as larger tools are required (Jiang, Zhang & Wang, 2002). A variety of technologies known as 'Out of Autoclave' (OoA) processes includes novel approaches to heating of tooling, liquid composite moulding (e.g. resin infusion) and prepregs which can produce satisfactory fibre content without autoclave pressure (Coenen *et al.*, 2005; Gardiner, 2011; Roover, 2011; Sherwin, 1999; Zhang, Guo & Fox, 2009).

In integrally-heated tools, the heating element and the tool are combined in-mould or on-mould (Marsh, 2003). This approach transfers the required heat through the mould and across its surface to cure the composite faster than traditional methods. A number of such heated tools are commercially available

and are suitable for closed mould processes such as compression moulding, resin transfer mould (RTM) and its variations (Mason, 2006; Mazumdar, 2001).

However, there have been few systematic studies of heated tooling for thermoset composites. This PhD study has been carried out with the aim of improving the heating performance of integrally water-heated composite tooling, suitable for moulding a variety of composites with low temperature moulding (LTM) liquid resin or prepregs. Three design factors are selected and nine design combinations have been identified according to Taghuchi's orthogonal array. Numerical simulation of transient heat transfer has been carried out for each of the proposed nine designs of the integrally-heated tool. Then the statistical approach of S/N ratio has been applied to allow the control of the response variables and identify their optimal parametric combination. Analysis of variance has been applied to investigate the effect of design parameters on the response strategies of heating time per unit mass and on the maximum temperature variation over the tool surface, to identify the most critical performance parameters.

4.2 Basic principles

Various variables are considered for improving the heating performance of integrally-heated tools as shown in the Fishbone diagram of Figure 4-1. In this PhD study three parameters channel distance, channel profile and channel layout are chosen as design factors. The factors have not been considered in previous studies and are expected to be significant in obtaining optimal design of a tool that can achieve most uniform temperature at the minimum heating time. The desired operating temperature of the mould has been chosen as 90^{o}C, as a typical processing temperature of a low temperature moulding (LTM)

prepreg (ACG-Staff, 2007; Gardiner, 2011). In order to compare heating times between different designs, an arbitrary target temperature of 81^{o}C has been used, to avoid uncertainties as the operating temperature is approached asymptotically.

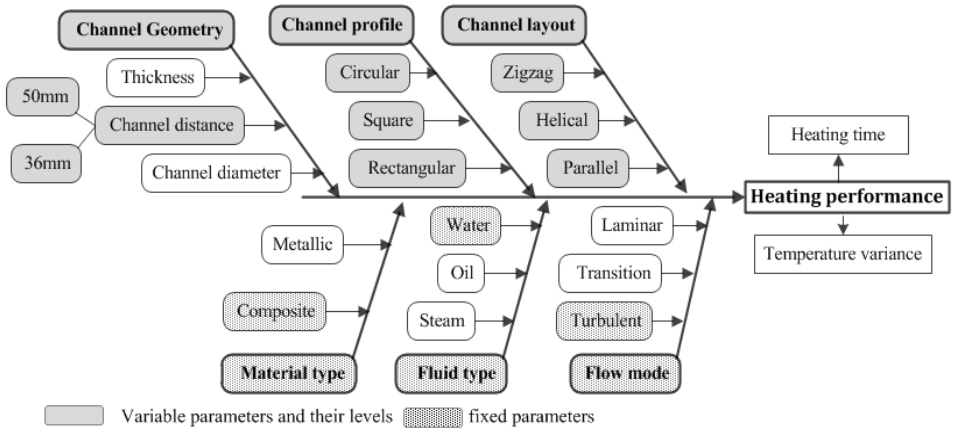

Figure 4-1 Fishbone diagram of the effective factors

Different designs are proposed for the model tool which comprises five parts: tool face, mould, channel, insulation and back face, using a variety of different materials, Figure 4-2. The tool face made from a square composite laminate of carbon fibre reinforced polymer (CFRP), due to its reasonable thermal conductivity, low coefficients of thermal expansion (CTE) and high strength (Campbell, 2004).

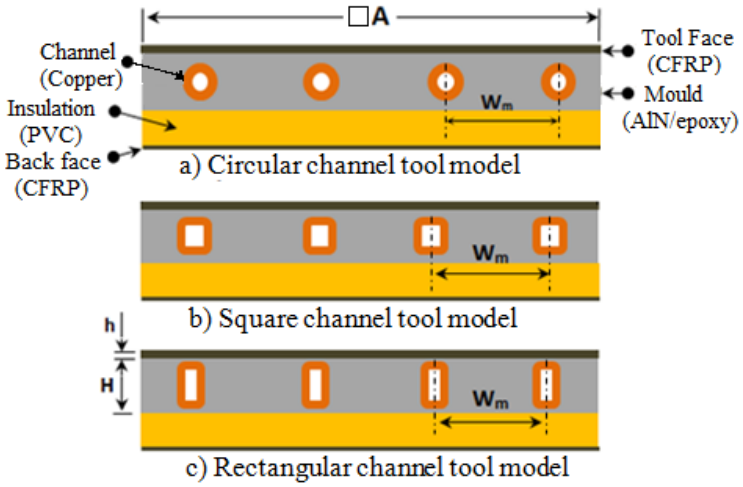

Figure 4- 2 Architecture of the experimental test tool

The copper channel is embedded in the mould, under the tool face, in a mixture of aluminium nitride (AlN) and epoxy resin, which has a good heat conductivity (Konzelmann *et al.*, 2008). The mould is backed with an insulation material, e.g. PVC foam and a skin of CFRP laminate for strengthening and protecting the foam. Table 4-1 illustrates the main thermal and mechanical properties of the materials used.

Table 4-1 Properties of the proposed tool materials

Properties		Units	Materials					
			Water[1] @ 90°C	**Copper**[2]	**PVC foam**[3]	**CFRP**[4] 0°/90°		**AlN/ epoxy**[5]
Thermal	V_f	%	-	-	-	50		68.5
	μ	$Kg/m.s$	3.1×10^{-4}	-	-	-		-
	k	$W/m.K$	0.677	401	0.04	4.09 In-plane	0.64 out-plane	7
	∝	m^2/s	1.7×10^{-7}	1166×10^{-7}	1.6×10^{-7}	23.8×10^{-7}	3.7×10^{-7}	41×10^{-7}
	ρ	kg/m^3	964.95	8933	160	1600		1956
	$\mathbf{c_p}$	$J/kg.K$	4201.5	385	1600	1075.5		875
Mechanical	σ_{max}	GPa	-	0.455	0.0051	0.600		0.320
	τ_{max}	GPa	-	0.230	0.0026	0.090		0.0614
	E	GPa	-	117	0.17	70		7.89
	G	GPa	-	44	0.066	5		2.93
	υ	-	-	0.3	0.3	0.1		0.24

1.(Holman, 2002), 2. (Davis, 2001), 3.(MatWeb, 2014), 4. (Athanasopoulos *et al.*, 2013; Khairul & Anghelescu, 2009; Performance Composites Ltd) and 5. (Konzelmann *et al.*, 2008; Nagai & Lai, 1997; Xu & Chung, 2000; Zhu et al., 2013)

4.3 Limitations of current tool

Certain structural design constraints were imposed on the tool model; these were:

4.3.1 Tool strength

The thickness of the tool face and the combined height of the tool surface and the mould (Figure 4-3) must be as small as possible to provide lowest heat transfer resistance, while large enough to provide sufficient tool strength to resist the applied moulding pressure.

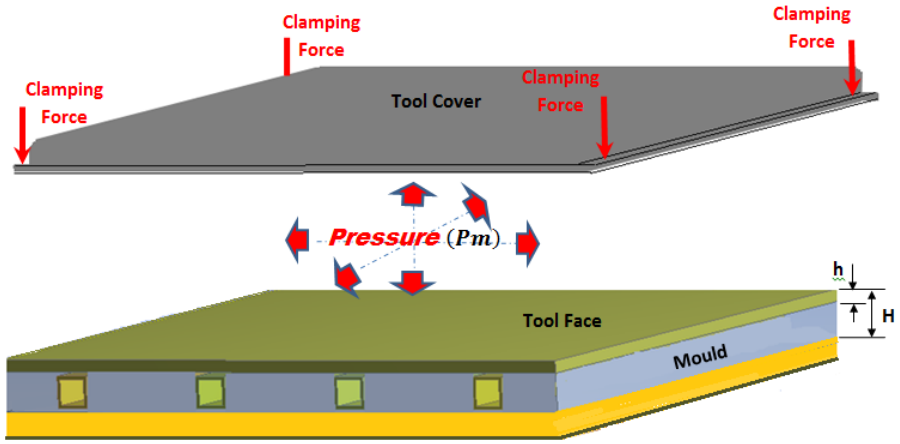

Figure 4-3 Isometric of the proposed tool when used in RTM

A worst case scenario was considered by assuming the use of the tool in RTM with an internal pressure of 14 bar (1.4×10^6 N/m^2) (Lacovara, 1995; Lawrence et al., 2006), due to resin injection and fibre consolidation or clamping pressures. Also the square channel profile of 8 mm width is assumed (Figure 4-4), which provides half the strength of a circular channel profile (Xu, Sachs & Allen, 2001).

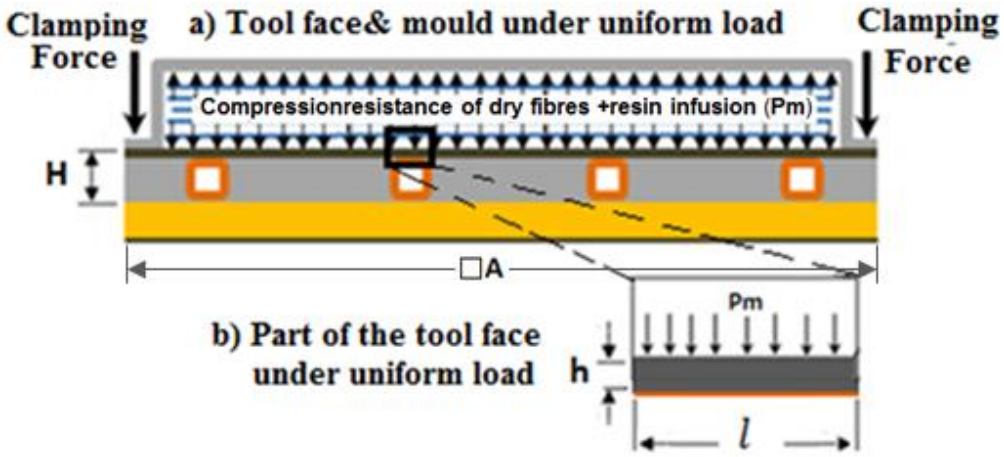

Figure 4-4 Section of the proposed tool model used in RTM process

The minimum value of H was determined from the following expressions (Roark & Raymond, 1989) for bending stress and deflection respectively:

$$\sigma_{max} = \frac{0.308\, p_m A^2}{H^2} \qquad (4\text{-}1)$$

$$\delta_{max} = \frac{0.014 p_m A^4}{EH^3} \qquad (4\text{- }2)$$

A trivial deflection of 0.3 mm was determined for *H* = 16mm, and the magnitude of tensile stress remains well below its allowable value. To ensure acceptable tool face strength, h was predicted from the following equations (Rao, 1991; Xu, Sachs & Allen, 2001).

$$\sigma_{max} = \frac{p_m l^2}{4h^2} \qquad (4\text{- }3)$$

$$\tau_{max} = \frac{0.75 p_m l}{h} \qquad (4\text{- }4)$$

$$\delta_{max} = \frac{p_m l^2}{h^2}\left(\frac{l^2}{32 E_{CF} h^2} + \frac{0.15}{G_{CF}}\right) \qquad (4\text{- }5)$$

Assuming an initial value of 0.5 mm for h, an extremely small deflection of 2.1×10^{-2} mm was calculated and the magnitude of shear and tensile stresses remain below their allowable values. Hence it was concluded that selecting any value $H \geq 16$ mm and $h \geq 0.5$ mm will guarantee mechanical safety for the proposed tool as well as an accurate dimensions for the moulded composite products.

4.3.2 Pressure drop

The pressure drop of a fluid flowing in a channel is a function of: channel length, hydraulic diameter and fluid mass flow rate (Holman, 2002; Incropera *et al.*, 2013). Therefore, given values for each of the aforementioned variables, channel design must ensure that the total pressure drop does not exceed the available pump pressure. The amount of pressure drop, for the fully developed flow, can be determined by the following expression (Incropera *et al.*, 2013).

$$\Delta p = f_f \frac{\dot{m}}{2D_h} L_c = f_f \frac{\rho u^2}{2D_h} L_c \qquad (4\text{- }6)$$

The proposed flow regime in this PhD study is turbulent in a smooth tube, so the value of f_f is given by

$$f_f = (0.79 \ln Re_D - 1.64)^{-2} \qquad (4\text{- }7)$$

4.4 Proposed design

The design of the model tools in this PhD study is proposed by changing the levels of the following variables and relevant geometries, while the other contributing factors remain constant. These variables have not generally been considered in previous investigations, yet are expected to be important in improving the heating performance of the proposed tool. The first parameter is channel profile- three forms (circular, square and rectangular), with a fixed cross section area are considered. Each profile gives a different hydraulic diameter, Equation 2-19, as well as wet peripheral convection area of the channel, according to the following expression (Holman, 2002):

$$A_s = P_c L_c \qquad (4\text{- }8)$$

Both D_h and A_s have significant effects on pressure drop, mass flow rate, flow regime and hence heat transfer coefficient of the fluid and the amount of the heat energy entering the mould. The second parameter is channel layout which is selected with the aim of reducing heat losses from the mould and the path of heat conduction. For embedding the channel in the mould, three economic and easy to manufacture layouts are proposed: zigzag, helical and parallel, as shown in Figure 4-5. The different channel layouts are selected to investigate the effect of flow path on the tool heating performance and to define the conformal path that can achieve reasonable heating time and uniform temperature distribution over the tool surface.

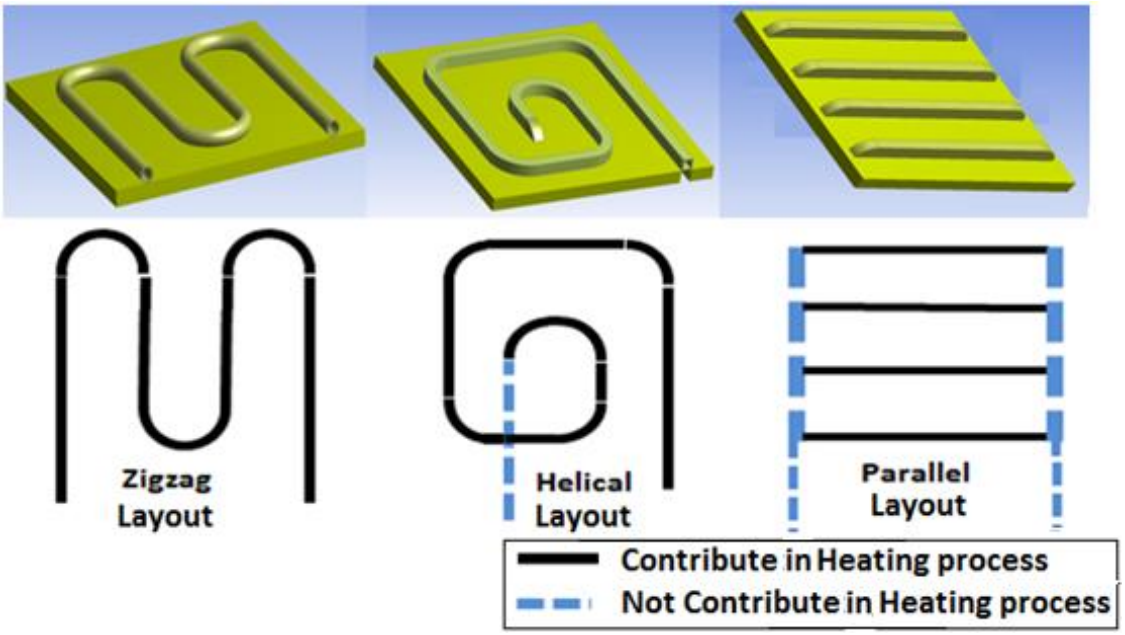

Figure 4-5 Forms of channel layout in the tool models

The third parameter is the channel separation which represents the distance between the centres of two adjacent turns of the aligned channel (Figure 4-2). This factor is selected to assist in defining the conformal distance that can achieve a reasonable tool heating performance. Figure 4-6 illustrates the relation between the values of channel separation and the corresponding ratios between the unified channel length and the tool surface area (Appendix G).

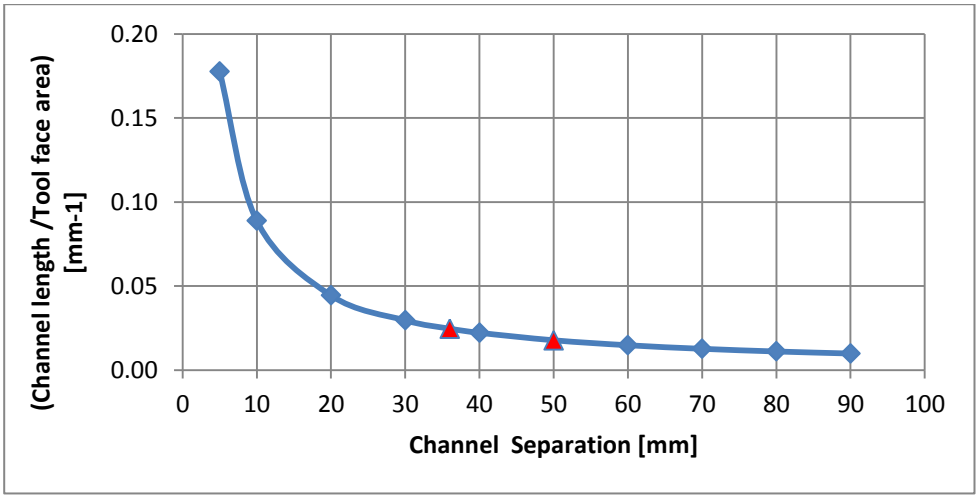

Figure 4-6 Effect of channel separation on the ratio of channel length/tool surface area

Due to the expected low thermal conductivity of the composite tool materials, CFRP and AlN/epoxy, two levels are proposed for this factor. An appropriate value for the first level is 50 mm because the value of R_j for the higher separations becomes approximately stable. The second level is proposed as 36 mm, because it was employed in the design of a high conductive aluminium tool by Ding *et al.* (1999) and (2001) and also values of R_j increase rapidly when the channel separation becomes lower, as shown in Figure 4-6, and that will be undesirable for economic reasons.

4.5 Design of experiments

4.5.1 Taguchi's method:

Taguchi's orthogonal array provides a minimum number of experiments necessary to study the influence of any desired factor on the quality characteristics in an economical way, while the signal-to-noise (S/N) ratio can be used to analyse the resulting data, to control the response and reduce the variability about the response (Gopalsamy, Mondal & Ghosh, 2009; Rao & Padmanabhan, 2012; Roy, 1990; Roy, 2001). Analysis of variance (ANOVA) is performed on the S/N ratios of the response variables to define the statistically significant design parameters and then predict their optimum combination (Ross, 1989).

4.5.2 Setting the factors and goals:

As mentioned previously, we are examining the effect of three factors in improving the heating performance of the water-heated tool. The tool face must be heated to the target temperature in a minimum heating time and with minimum temperature difference across the tool face. The variables and their

levels are illustrated in Table 4-2; the third parameter has two levels, while the others have three.

Table 4- 2 Design parameters and their levels

Test cases	Parameters and Levels			Results	
	A	**B**	**C**	**Heating Time/unit mass**	**Temperature Variations**
1	Z	C	1	$x1$	S1
2	Z	S	2	$x2$	S2
3	Z	R	1	$x3$	S3
4	H	C	2	$x4$	S4
5	H	S	1	$x5$	S5
6	H	R	2	$x6$	S6
7	P	C	2	$x7$	S7
8	P	S	1	$x8$	S8
9	P	R	1	$x9$	S9

4.5.3 Setting the design points

The selection of the correct orthogonal array from the Taguchi's family of fractional factorial experiment (FFE) matrices depends on the number of the parameters and their levels (Chen et al., 1996; Roy, 1990; Roy, 2001). In this PhD study are not equal, the highest number of levels (3) is applied, so the appropriate orthogonal array will be *L9* which means that nine test models or cases must be designed at different parameter combinations. The *L9* OA includes 3 levels for each factor as shown in Table 4-3, but the third parameter has only two levels. So, the proper strategy is used to fill in the entries for **C**3 with 36 or 50 in a random and balanced way (Fraley et al., 2006).

Table 4-3 Test case plan using $L9$ OA

Symbol	Parameters	Units	Levels		
			1	**2**	**3**
A	Channel layout	-	Zigzag (Z)	Helical (H)	Parallel (P)
B	Channel Profile	-	Circular (C)	Square (S)	Rectangular (R)
C	Channel Distance	mm	50	36	-

4.5.4 Dimensions of the proposed design points

All the dimensions of the tool models (Figure 4-7a) are calculated according to the proposed value of channel separation and the details are illustrated in Appendix A. The channel profiles have an equal cross section area and their internal dimensions, as illustrated in Figure 4-7b, are constant in all the nine test models.

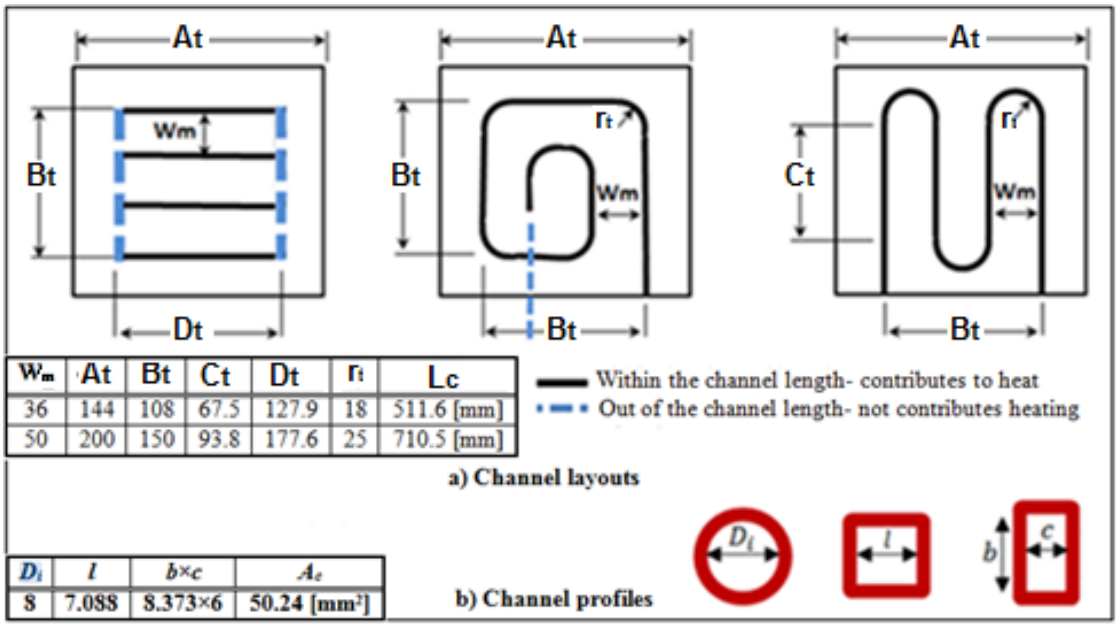

Wm	At	Bt	Ct	Dt	rt	Lc
36	144	108	67.5	127.9	18	511.6 [mm]
50	200	150	93.8	177.6	25	710.5 [mm]

D_i	l	$b \times c$	A_c
8	7.088	8.373×6	50.24 [mm²]

Figure 4-7 Geometries and dimensions of the proposed tool models.

The thickness of tool face, channel, mould, insulation and back face, are 4 mm, 1 mm, 12 mm, 10 mm and 2 mm respectively, and they were kept constant in the design of all the nine models to maintain an equal percentage volume, thereby the thermal mass, contribution to each part and in the total tool volume (or thermal mass). The mismatch between the volume contribution percentages of some parts, as appears in Figure 4-8, returns to the difference of the channel profile and layout.

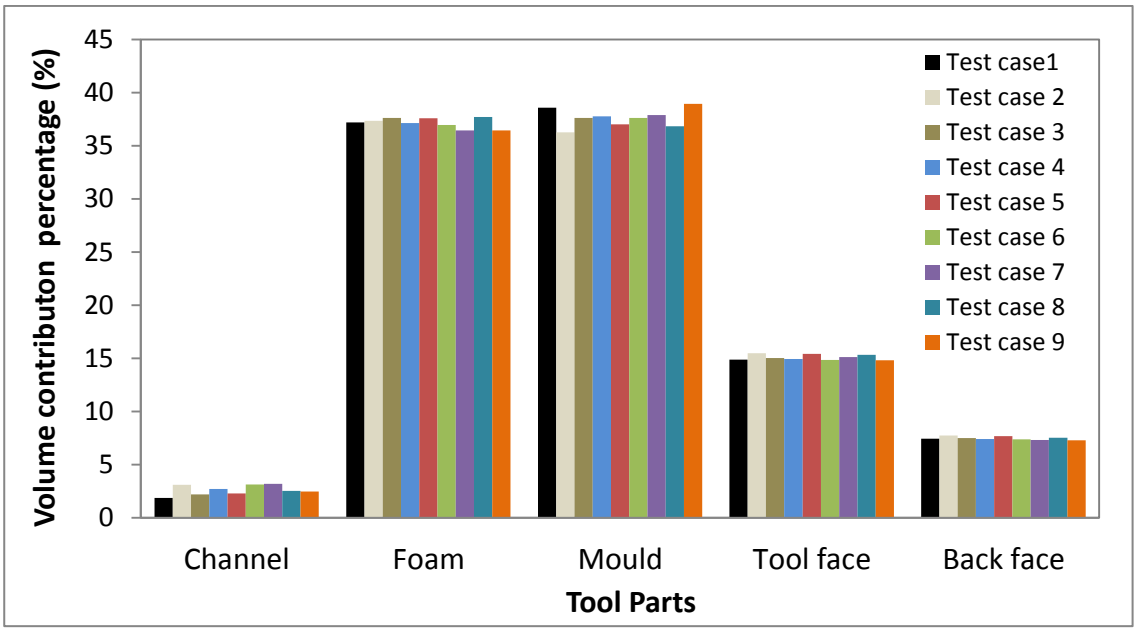

Figure 4-8 Volume contribution percentages of the tool models parts in each test case

4.6 Numerical simulation

4.6.1 Simulation methodology

ANSYS-CFX (ANSYS, 2009) software was used to simulate the heating performance through 3D conjugate heat transfer. In this PhD study, the inner surface of the heating channels is set as a convection boundary, in contact with the circulating water (maintained at 90°C). The heating-up period and temperature uniformity over the tool surface are considered as the response variables of the simulations. The governing equations for transient heat convection and diffusion through the tool are:

$$\frac{\partial^2 T}{\partial x^2}+\frac{\partial^2 T}{\partial y^2}+\frac{\partial^2 T}{\partial z^2}=\frac{\rho c_p}{k}\left(\frac{\partial T}{\partial t}+u_x\frac{\partial T}{\partial x}+u_y\frac{\partial T}{\partial y}+u_z\frac{\partial T}{\partial z}\right) \qquad (4\text{- }9)$$

$$\frac{\partial^2 T}{\partial x^2}+\frac{\partial^2 T}{\partial y^2}+\frac{\partial^2 T}{\partial z^2}=\frac{\rho_t c_{p_t}}{k_t}\left(\frac{\partial T}{\partial t}\right) \qquad (4\text{- }10)$$

4.6.2 Model geometry

The full geometry of the test models with zigzag and helical layouts (Figs. 4-9a and b) were created within the design module of ANSYS Workbench; for the parallel layout, a half model using symmetry was used (Figure 4-9c).

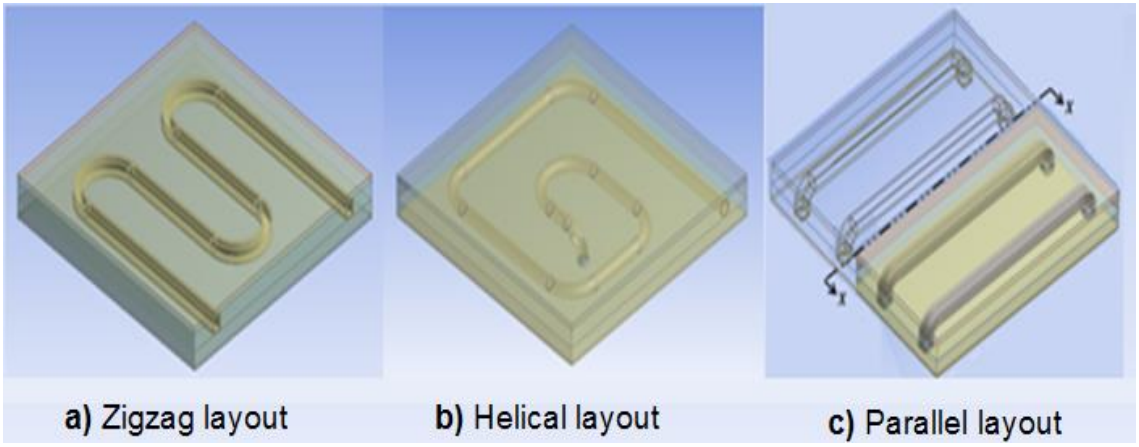

Figure 4-9 Geometries of different tool models within ANSYS Workbench

4.6.3 Applied boundary conditions

A water velocity of 2 m/s was used to ensure turbulent flow (Re_D ≥10,000) in all the cases. The heating medium was be water at 90^{o}C, while the initial temperature of all tool parts and ambient is assumed to be 25^{o}C.

4.6.4 Calculating the heat transfer coefficients

A forced convection boundary was specified at the interface between the water and the channel, with the heat transfer coefficient calculated by equation 3-1. While Pr is constant (equal to 1.97) in all the test cases, the value of heat transfer coefficient depends on the values of hydraulic diameter, fluid velocity and Reynolds number as shown in Table 4-4. The fluid velocity in each of the

four parallel branches of the parallel model is calculated from the total volumetric flow rate according to the equation of head loss equality and continuity (Appendix H) as follows (Munson, 2010):

$$\Delta p_1 = \Delta p_2 = \Delta p_3 = \Delta p_4 \qquad (4\text{- }11)$$

$$Q = Q_1 + Q_2 + Q_3 + Q_4 \qquad (4\text{- }12)$$

Table 4-4 Heat transfer coefficient at the interface between water and the channel according to the channel profile and layout

Channel		***u***	***D_h***	***Re***	***h* @ 90°C**
Profiles	Layouts	m/s	m	-	W/m^2.K
Circular	Zigzag & Helical	2	8.00×10^{-3}	48,781	14,352
	Parallel (4 branches)	2/4=0.5		12,195	4,734
Square	Zigzag & Helical	2	7.09×10^{-3}	43,232	14,703
	Parallel (4 branches)	2/4=0.5		10,808	4,850
Rectangular	Zigzag & Helical	2	6.99×10^{-3}	42,622	14,745
	Parallel (4 branches)	2/4=0.5		10,656	4,864

Heat transfer coefficients for convection from the external surfaces of the models were calculated assuming values of 25°C and 57.5°C for the ambient and mould mean temperatures, respectively. Three different values are found for the air heat transfer coefficient at the top, bottom and side surfaces of the tool models (Table 4-5) according to Equations 3-2 to 3-4.

Table 4-5 Heat transfer coefficients over the external surfaces of the tool models according to their lengths

A	***h_t***	***h_b***	***h_s***
mm	W/m^2.K		
144	7.24	6.67	8.3
200	3.23	2.98	8.3

4.6.5 Mesh generation:

In mesh generation, the models were divided into a high number of very small elements. The channel and the remainder of the tool were meshed separately

(Figure 4-10). With the two domains having different mesh densities, the connection of the interfaces is set to 'general grid interface' (GGI) to facilitate connection of the mismatched grids and node locations at the contact interfaces (ANSYS, 2009).

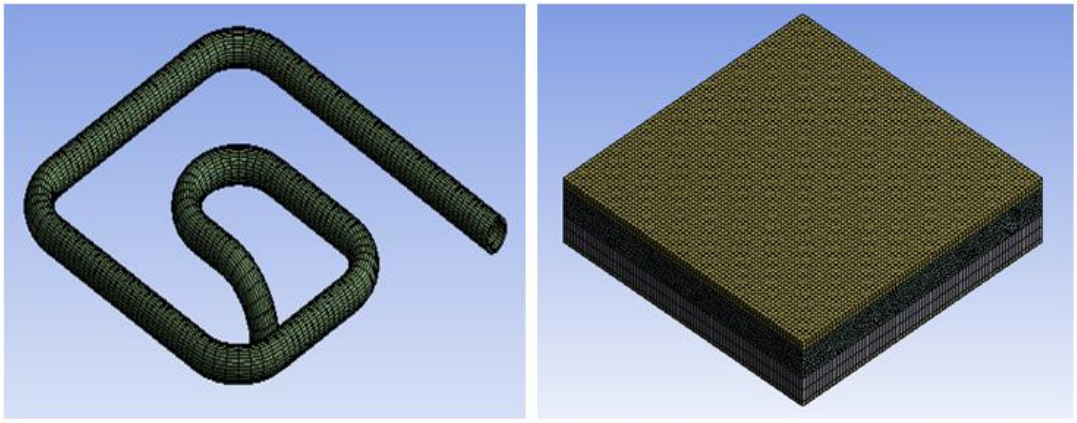

a: Channel **b:** Tool face, Mould, Insulation & Tool back

Figure 4-10 Tool model parts according to the mesh size

In order to reduce the number of elements and the simulation run time, tests were carried out (aforementioned in Section 3.5.2) on the largest and most complex model (the circular section helical layout with 50 mm channel separation) to find the largest mesh size that could give acceptable results. Eventually, each of the nine test cases was modelled with between 1.1×10^5 and 4.7×10^5 elements.

4.6.6 Time step (time scale)

The time step is another basic factor that affects running speed and the output results of simulation. For transient calculation, the time step size should be the smaller of the convection and thermal diffusion timescales. The convection time scale, assuming a pipe length: diameter ratio of 70 is given by Equation 2-32. The thermal time scale was determined for turbulent flow by Equation 2-33. So the calculated thermal time scale will be 0.3 s which is the smaller of the

convection and thermal diffusion timescale. Hence various tests were conducted (aforementioned in Section 3.5.3) with different time step sizes, larger than that calculated, leading to the conclusion that a value of 1s could achieve the same results as 0.3s with a shorter run time.

4.7 Simulation results

Each simulation run represents one experiment in the orthogonal array as shown in Table 4-2. Two strategies are defined for the response variables in terms of heating time per unit mass and temperature variation across the tool face.

4.7.1 Heating time per unit mass

For each run, the calculated transient temperatures of the four coolest points at the corners of the tool surface are measured and plotted (Figure 4-11).

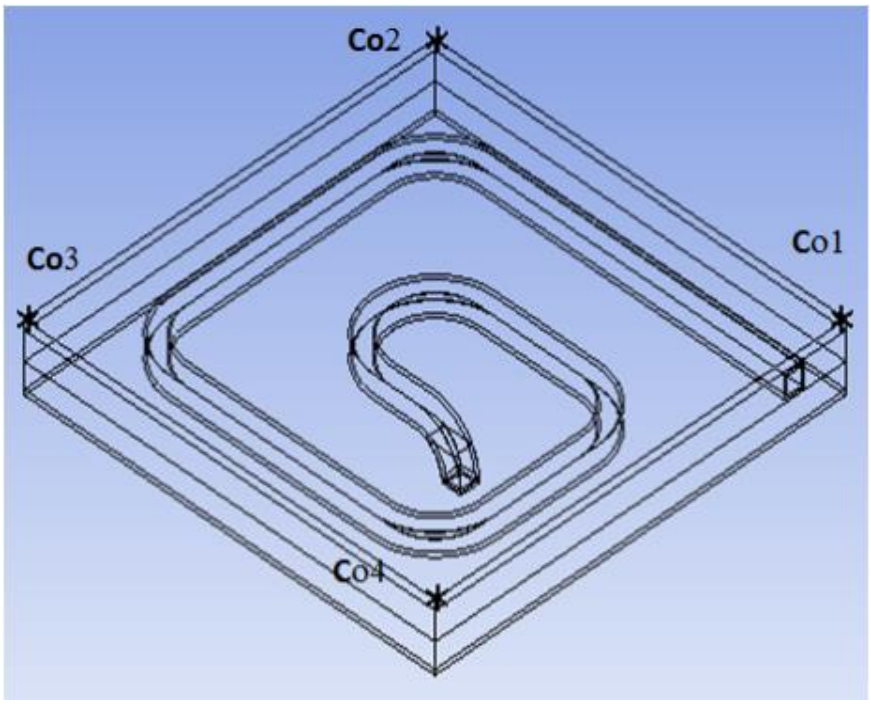

Figure 4-11 Corner points on the heated surface of a tool model

Then the lowest of these four is selected to define the required heating time to achieve the desired target temperature. For example, in test case 4 (helical layout, circular channel with 36 mm separation), the slowest heated corner is Co4 (Figure 4-12). From the results Table for this corner, two nearest temperatures (higher and lower) to the target temperature are defined, and the desired heating time is calculated, by interpolation, according to:

$$H_t = \frac{(t_{max} - t_{min})}{(T_{max} - T_{min})}(T_t - T_{min}) + t_{min} \qquad (4\text{-}13)$$

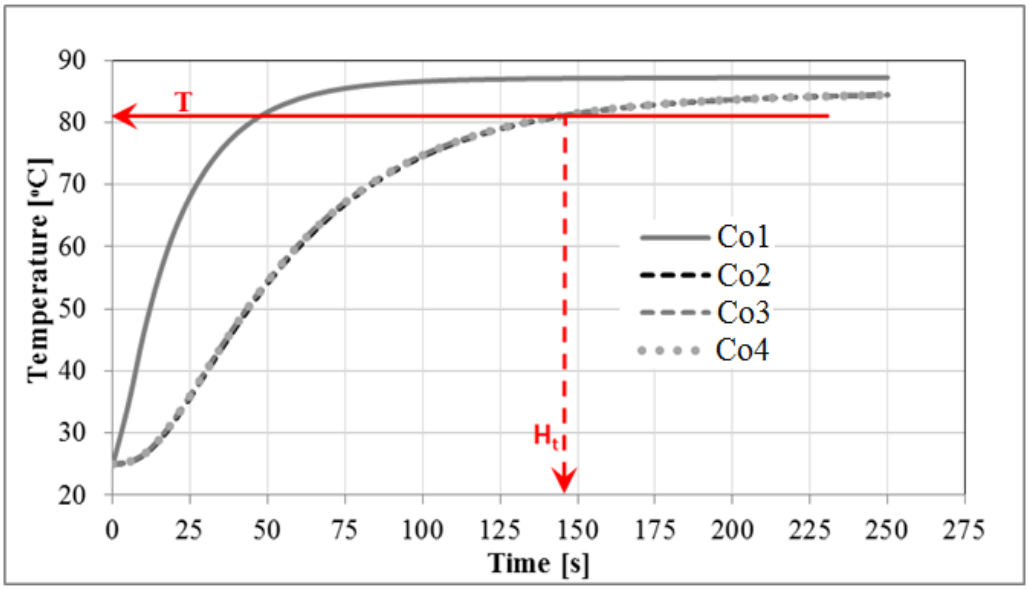

Figure 4-12 Heating curves of the surface corners of the tool model with a helical alignment, square channel and 36mm separation

So H_t will be the heating time to raise the temperature of all the tool surface to the target temperature, but this value is not a valid response variable due to the difference between the volumes of the three models. Therefore the heating time was divided by the total weight of the proposed tool to define a ratio of heating time per unit mass, as listed in Table 4-6. The proportions by volume of the tool parts in all the cases are similar.

4.7.2 Surface temperature variation

This response variable, as listed in Table 4-6, is defined as the difference between the area-weighted average temperature of the tool surface and the target temperature, with the former deduced directly from post-processing results of each test case at the specified heating time. Using T_{ave} in calculating this quality characteristic neglects the effect of the difference between the surface areas of the test cases, so the area-weighted average temperature is used (Phatak, 2012):

$$T_{ave} = \frac{\sum_{r=1}^{n}(T_r A_r)}{\sum_{r=1}^{n}(A_r)} \qquad (4\text{- }14)$$

Figure 4-13 illustrates the simulation results of temperature distribution over the surface of each test case, at the corresponding H_t. The test case results are divided into two gropes according to the values of channel separation and tool length: the first grope (left column of Figure 4-13) includes the cases 1, 3, 5, 8 and 9 with channel separation of 50 mm and tool length of 200 mm, while the second grope (right column of Figure 4-13 cases 2, 4, 6 and 7) has channel separation 36 mm and tool length of 144 mm.

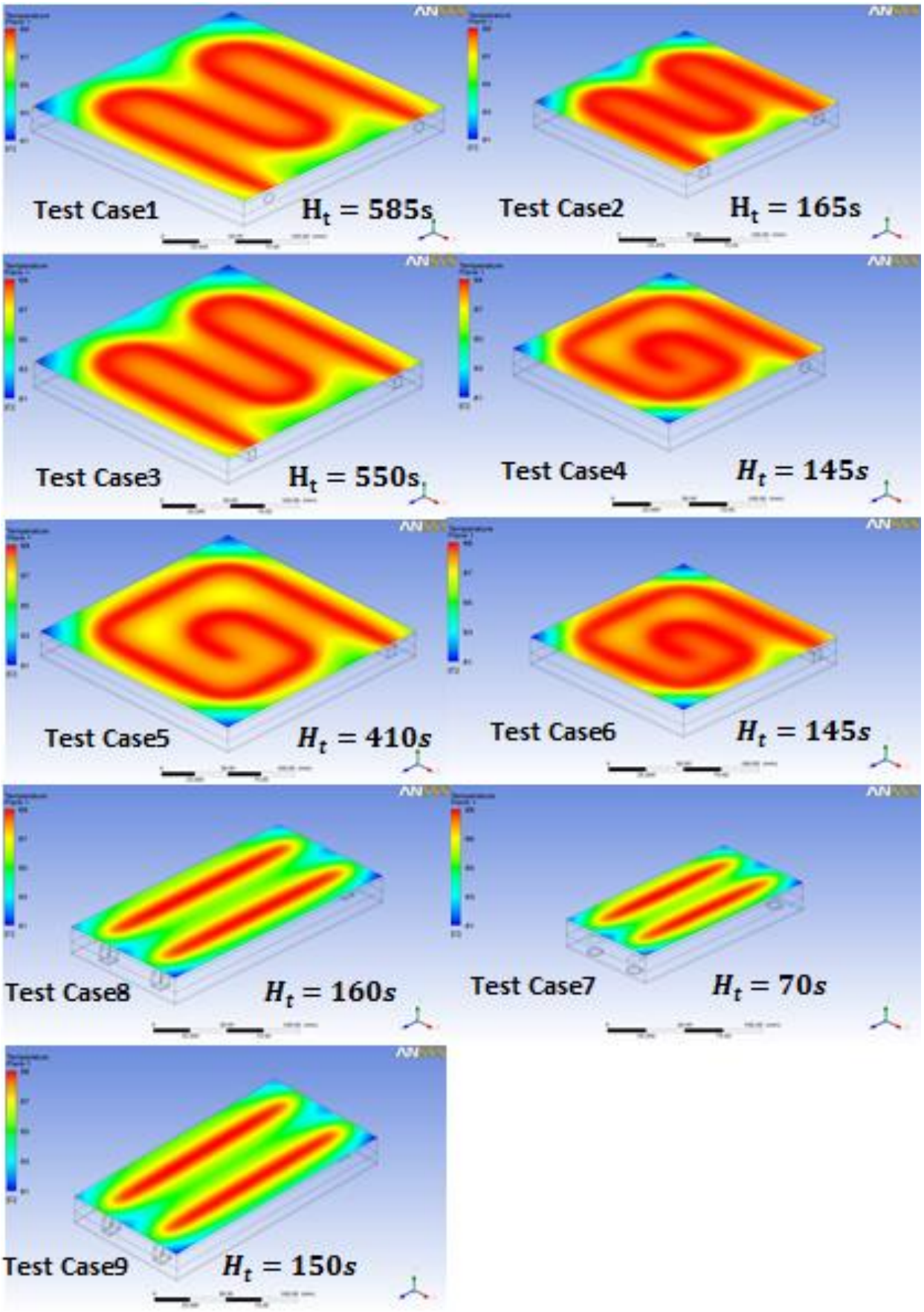

Figure 4-13 Temperature distribution over the surface for each test case after heating for the corresponding (H_t)

4.8 Design optimisation

4.8.1 S/N ratio

The heating time per unit mass and surface temperature variation were considered as the response variables with the concept of "lower-is-better" (LB). The S/N ratio, for an LB characteristic (in decibels) is given by (Chen *et al.*, 1996):

$$S/N_{LB} = -10\,Log\left(\frac{1}{e}\sum_{i=1}^{e} x_i^2\right) \qquad (4\text{- }15)$$

In this PhD study $\boldsymbol{e}$ (number of repetitions) is 1. The corresponding S/N ratio values of the response variables (the test results) are shown in Table 4-6.

Table 4-6 Response variables and their S/N ratios

Test Cases	A	B	C	Heating time /unit mass		Temperature Variation	
				Response variable	S/N ratio	Response variable	S/N ratio
				[min/kg]	dB	[°C]	dB
1	1	1	1	6.8	-16.7	6.9	-16.8
2	1	2	2	3.8	-11.6	7.0	-16.9
3	1	3	1	5.9	-15.4	6.7	-16.5
4	2	1	2	3.2	-10.0	7.2	-17.1
5	2	2	1	5.0	-14.0	6.8	-16.6
6	2	3	2	3.0	-9.7	7.2	-17.1
7	3	1	2	1.5	-3.5	5.2	-14.3
8	3	2	1	2.0	-6.0	5.0	-14.0
9	3	3	1	1.6	-4.0	4.7	-13.4

The average performance (Appendix I) for the S/N ratio values of each factor at each level is summarised in Table 4-7 (for the response variable of heating time per unit mass) and Table 4-8 (for the response variable of temperature variance).

Table 4-7 Average performance of S/N values of each level for heating time per unit mass

Levels	**A**	**B**	**C**
1	-14.6	-10.06	-11.2
2	-11.2	-10.52	-8.7
3	-4.5	-9.70	
(f_{max}-f_{min})	-10.1	-0.8	-2.5

Table 4-8 Average performance of S/N values of each level for temperature variance

Levels	**A**	**B**	**C**
1	-16.7	-16.07	-15.4
2	-16.9	-15.84	-16.4
3	-13.9	-15.67	
(f_{max}-f_{min})	-2.8	-0.4	-1.0

The optimum combination of the design factors, according to the results of heating time per unit mass in Figure 4-14, can be identified as: channel alignment (factor **A**)-Parallel (level 3), channel profile (factor **B**)- Rectangle (level 3) and channel distance (factor **C**)-36 mm (level 2).

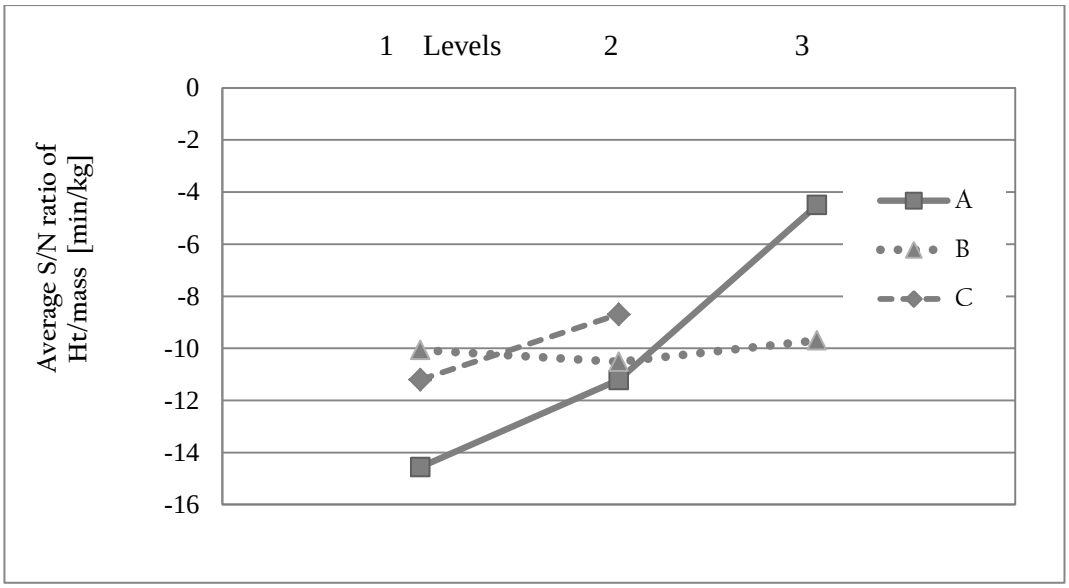

Figure 4-14 Main factor effects of average S/N for heating time per unit mass

Also the optimum combinations of design factors, according to the results of temperature variance along the tool face (Figure 4-15), can be identified as:

channel alignment (factor **A**) - Parallel (level 3), channel profile (factor **B**) - rectangle (level 3) and channel distance (factor **C**) - 50 mm (level 1).

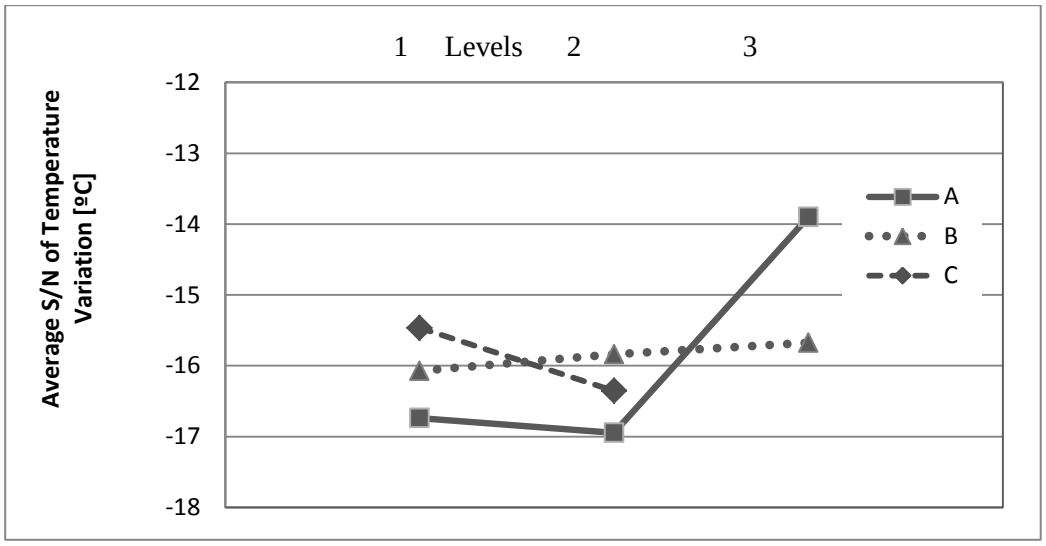

Figure 4-15 Main factor effects of average S/N for surface temperature variance

The results show that the channel profile has little effect on the heated tool performance, because the difference between the maximum and the minimum values of its main effects (f_{max}-f_{min}) is small. The square and rectangular profiles are only marginally better than circular, in terms of heating time and temperature difference, because they have lower D_h, higher A_s and h_w values than the circular profile (Table 4-4).

The high effectiveness of the parallel alignment can be explained by the fact that this method offers a straight flow with a constant boundary layer, lower head loss along the flow path and almost equal pressure drop between the parallel branches. It can be seen from Figure 4-13 that the heat transfer around the channel bends, in all the test cases, is lower than that in the straight sections.

4.8.2 ANOVA

ANOVA assists in analysing the response variables, finding the significant design parameters and predicting of optimal design parameters (Grove, Popham & Miles, 2006; Rao & Padmanabhan, 2012). The 90% confidence interval (Appendix I) was found to be 5.462. This illustrates that the parameters **A** and **C** are affecting the heating performance of the heated tool significantly, because their variance ratios (F_A and F_C) are higher than 5.465. The parameter **B** was pooled due to its low significance (F_B<5.465) to give a new error variance, sum of square, variance ratio (Roy, 1990). The calculated values of DoF, sum of squares, variance, variance ratio and percentage contribution (Appendix I) of each factor are listed in Table 4-9 (for the response variable of heating time per unit mass) and Table 4-10 (for temperature variance). Accordingly, the contribution percentage shows that channel layout and channel distance have the maximum effects of (84.3% and 9.7%) and (81.1% and 11.2%) on the tool quality characteristic, respectively.

Table 4-9 ANOVA results for the heating time per unit mass

Parameter	Design Parameters	Degree of Freedom	Sum of Squares	Variance	Variance Ratio	Percentage Contribution
		f	SS	V	F	P
A	Channel Layout	2	157.1	78.8	389.6	84.3
B	Channel Profile	2	1.011	0.505	0.157	Pooled
C	Channel Distance	1	18.0	18.2	90.3	9.7
Error		5	1.01	0.202	1.0	6.0
Total		8	186.4	-	-	100.0

Table 4-10 ANOVA Results for the temperature variation

Parameter	Design Parameters	Degree of Freedom	Sum of Squares	Variance	Variance Ratio	Percentage Contribution
		f	SS	*V*	*F*	*P*
A	Channel Layout	2	14.6	7.3	153.5	81.1
B	Channel Profile	2	0.24	0.12	0.36	Pooled
C	Channel Distance	1	2.0	2.1	43.0	11.2
Error		5	0.24	0.05	1.00	7.7
Total		8	18.0	-	-	100.0

4.8.3 Determining optimal design

Based on Taguchi's design method, the significant parameters are used to set the optimal conditions and the insignificant factors are set at economic levels. The expected results of combination the optimal design parameters and levels can be predicted by utilising their factor effects (f_A , f_C) (Appendix I). Therefore, the expected optimal result value is -3.1, (According to the optimal combination of **$A_3B_3C_2$** for the response variable of heating time per unit mass), while it is -13.5 (According to the optimal combination of **$A_3B_3C_1$** for the response variable of temperature variation) and their equivalent values are 1.4 min/kg and 4.7^{o}C, respectively (Appendix I).

The 95% confidence intervals are ±0.77 (for heating time per unit mass) and ±0.4 (for temperature variance). Achieving two different optimal conditions means that whenever the tool heating is faster, the temperature variation will be higher, because the temperature variation is defined as the difference between T_{ave} and T_t over the tool face and the area average temperature changes inversely with H_t, as shown in Figure 4-16. The quantity of stored heat during the heating time (H_t), is:

$$E_{st} = E_{in} - E_{loss} \qquad (4\text{-}16)$$

Where values of E_{in} and E_{loss} were obtained directly from the transient numerical results.

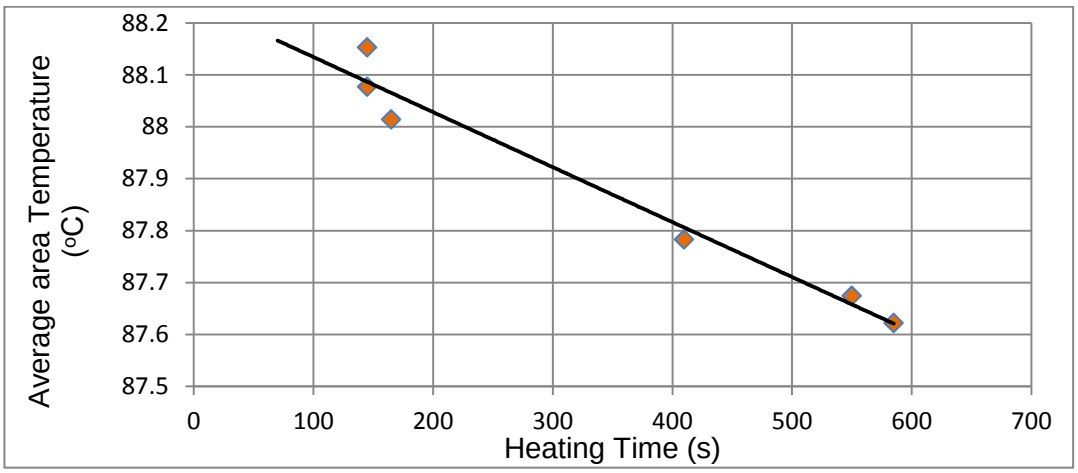

Figure 4-16 Area average temperature versus the corresponding heating time for the test cases

This shows that, at low H_t, there is insufficient time for heat to transfer to the surroundings or accumulate in the tool. So the amount of stored heat in the tool increases as the heating time decreases, as shown in Figure 4-17. Also at low times, heat is concentrated in positions near the channel, as is clear in Figure 4-13.

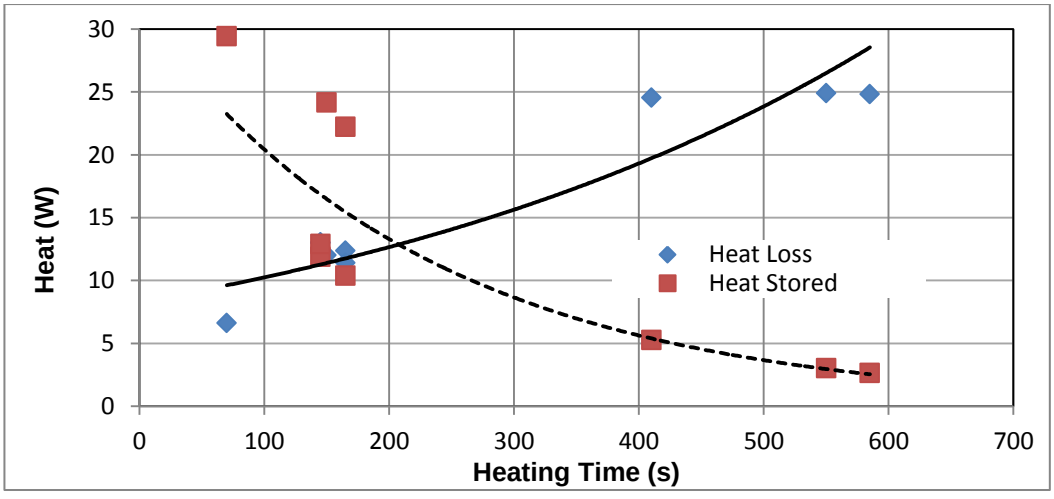

Figure 4-17 The effect of heating time on the amounts of stored and lost heat in the test tools

Results indicate that the effect of channel separation on the efficiency of the composite tool is different from results reported previously (Guilong *et al.*, 2010; Wang, Zhao & Guan, 2011) in studies of thermoplastic injection moulding, where reducing this design factor reduced the tool heating time. However, this PhD work was performed on relatively high thermal conductivity metallic tooling. In our work, the temperature uniformity is not improved by reducing the heating channel separation, as heat transfer is significantly slower through the low thermal diffusivity composite tool.

4.9 Conclusion

The heating performance of three alternative designs of an integrally- heated composite tool was studied by numerical analysis. By applying Taguchi methodology to the results from nine numerical experiments, the effect of different design parameters have been investigated, and preliminary conclusions can be drawn with regard to optimisation within the range of variables considered. It was shown that the channel cross-section has very little influence on heating efficiency, and consequently there is no reason to propose an alternative to the widely used and readily available circular piping systems. The most crucial parameter is the geometrical layout of heating pipes within the tool. Of the three geometries studied here, the parallel layout proved to be the most efficient, in terms of achieving the desired characteristics of surface temperature uniformity and minimum heating time. The third design parameter was the effect of heating channel separation; it was found that the relatively low

thermal conductivity of composite materials leads to different conclusions regarding optimum channel spacing compared to previous studies on metallic tooling for injection moulding. This preliminary study has demonstrated the usefulness of numerical experiments in understanding the heating performance of composite tooling.

Chapter 5

Experimental water-heated tool

5.1 Introduction

Most of the entire chapter is published in an article in the journal of Reinforced Plastics & Composites, available online since 29 January 2016. Recently, different approaches have been developed to overcome the problems of the traditional methods of composite manufacturing e.g. high operation costs, energy losses and long curing time. These disadvantages are particularly associated with the use of autoclaves. One of the technologies that can produce composite components without an autoclave is the integrally heated-tool, and is widely used in different industries, such as, wind energy, aerospace, surface transport (Marsh, 2003; Mason, 2006). This is because integrally heated-tools enable fabrication of large components with complex shapes and can overcome the size limitation problem of ovens and autoclaves and their significant consumption of heat energy, time and capital (Arney *et al.*, 2004; Raizenne, Hind & Poupore, 2006; Walczyk & Kuppers, 2012).

The heating unit in the integrally heated-tools directly attaches to the tool and eliminates the need for heating the surrounding environment, hence increasing the heating rate and saving energy (Baril-Gosselin, 2013; Raizenne, Hind & Poupore, 2006). According to the installation, the heating unit may be attached to the tool externally or embedded (Black, 2011). Heating is achieved by circulating a hot fluid in pockets connected directly to the tool or in a channel embedded in it (Yao, Chen & Kim, 2008). This method is widely used in the composite industry, and in plastic injection moulding and thermoforming processes due to its advantages compared to electrical heating techniques (Marsh, 2003). The most preferred heating medium is water because it is a low

cost and efficient heating medium, requiring minimum power for heating and pumping due to its low viscosity and high thermal capacity, and the achieved temperature never exceeds required tool surface temperature (Marsh, 2003). Water can also be used for cooling.

Various studies have been compared the heating performance of different heating fluids, e.g. oil, water, steam, pressurised water as well as other heating techniques such as electric cartridge, electric resistive, oven and infrared induction (Black, 2010b; Petrykowski & Fischer, 2012; PMC; Sloan, 2013). Results have shown that water is superior in achieving the desired temperature over the mould face uniformly with the lowest cost, time and consumed energy. Most of the tool's physical, thermal and mechanical characteristics depend on the tool material (Murphy, 1994; Rosato, 2004; Scott Bader Company, 2005). Composite materials, compared to metals, can offer the advantages of low manufacturing cost and time as well as low coefficients of thermal expansion (CTE). The key problem of composite tools is their low thermal conductivity, especially through-thickness; this is mainly due to the polymer matrix, the conductivity of which could be improved by adding filling materials (Milella *et al.*, 2014).

In order to improve the heating performance of an integrally water heated tool, the effect of a number of design variables, e.g. shape, layout and separation of heating channels, were investigated numerically in Chapter 4 based on the following assumptions:

- The bulk temperature of water entering the tool was assumed to be constant at its maximum possible temperature of 90^{o}C, which results in a constant thermal boundary condition at the model inlet. This boundary

condition could be achieved practically in industry with established adequate resources as mentioned by Ding et al.(2001).

- A free air convection boundary condition was assumed to the top, bottom and side surfaces of the tool model.

In the current chapter an experimental tool is built according to the predicted optimal design (Chapter 4), after some minor amendments to the channel separation and number of the parallel channels to increase the tool surface area and facilitate the tool manufacturing and temperature measurement. Tooling materials of carbon fibre reinforced epoxy (CFRP) laminate and Alepoxy (aluminium powder/epoxy composite) are selected according to their availability and cost for constructing the tool face and the mould, respectively. The tool is manufactured with an integrated method that can provide good contact between the tool parts and eliminate the problems of production (e.g. void content, resin richness, residual strain and low volume fraction) as much as possible. The tool materials are tested practically to calculate their diffusivity, specific heat and conductivity. The produced optimal tool (after amendment) is simulated in ANSYS software to explore its heating performance with regard to heating time and surface temperature uniformity. Finally the produced tool is tested experimentally defining its practical heating performance and verifying the numerical results. Calibrated measurement apparatus (thermal camera, thermocouples and a flowmeter) are used during the experiments. Results show good agreement between the numerical and experimental results, confirming the suitability of numerical simulation in predicting the optimal designs of integrally heated tool and appropriate assignment of the boundary conditions.

5.2 Design of the experimental heated-tool

The experimental tool was based on the predicted optimal combination of $\mathbf{A_3B_3C_2}$ for the response variable of heating time per unit mass, as established in Section 4.8.3. The following minor amendments were made:

- The channel separation was increased by 4 mm to facilitate the channel connection during manufacturing.
- Circular instead of rectangular channels were selected as they are readily available. This was found to have very little influence on heating efficiency.
- Number of parallel channels was increased to 8 in order to increase the tool surface area that facilitates monitoring the tool surface temperature and the ability to mould composite laminates, if required.

The width of the optimal experimental tool is a function of the channel separation (40 mm) and accordingly the effective heated zone of the CFRP tool face is considered to be a rectangle of 320 x 500 mm that locates directly over the mould. The main transverse pipes remain outside the mould to eliminate their effect in heating the tool face, which is achieved only by the parallel branches. The back and side faces of the tool as well as the exposed parts of the piping system are insulated completely by PVC foam in a wooden box, as illustrated in Figure 5-1.

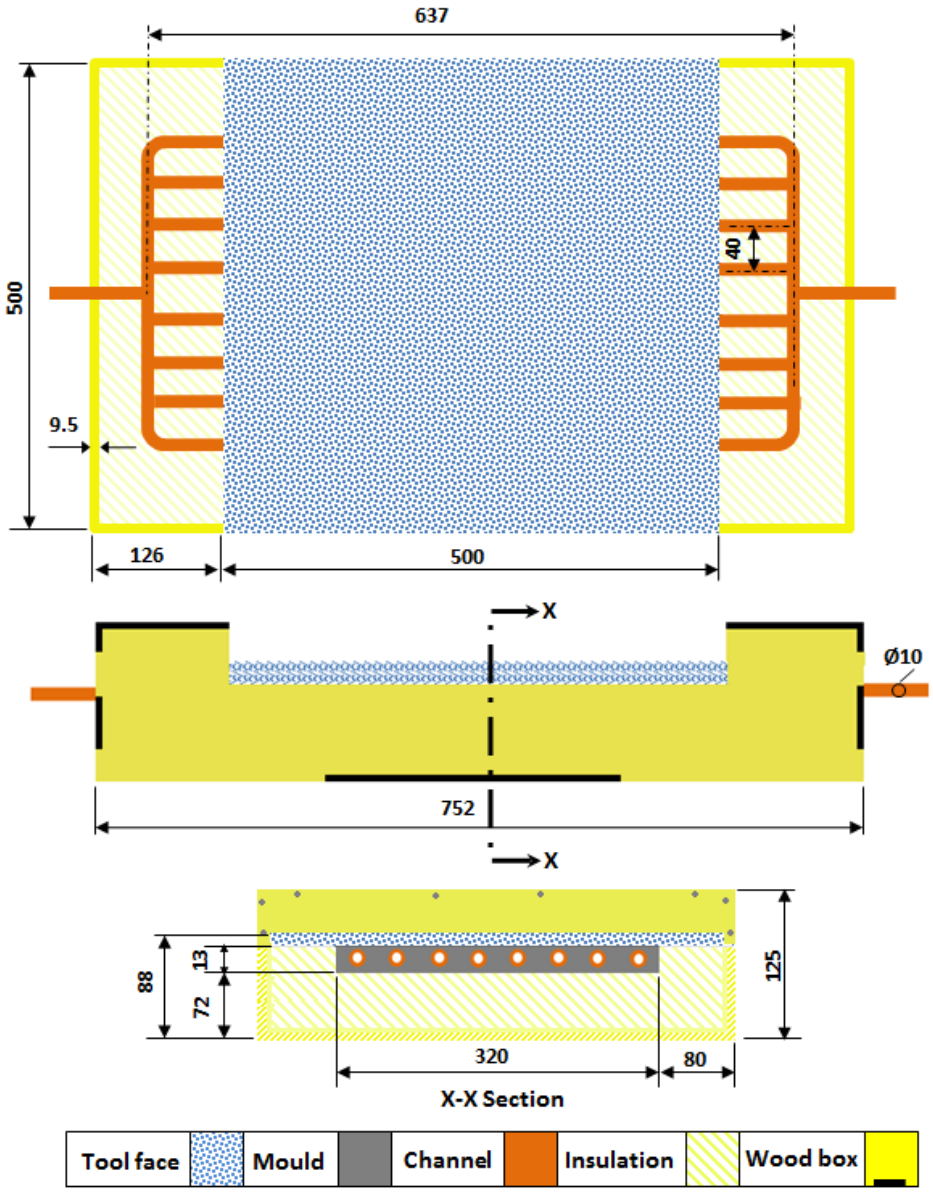

Figure 5-1 Dimensions (mm) of the optimal experimental tool

5.3 Tool building

The tool consists three main parts; two of them (the tool face and the channel or piping system) are initially combined temporarily in a special fixture that facilitates in situ casting of the third part (the mould). Two composite combinations of CFRP laminate and Alepoxy mixture are selected for the tool construction due to their availability and cost.

5.3.1 Piping system (Channels)

Copper pipes of 10 mm outside diameter and 0.7 mm thickness are used due to their availability, ease of forming and compatibility with the inlet and outlet of the heating unit. The eight parallel branches are joined by soldering to the main transverse outlet and inlet, using T and elbow joints as shown in Figure 5-2.

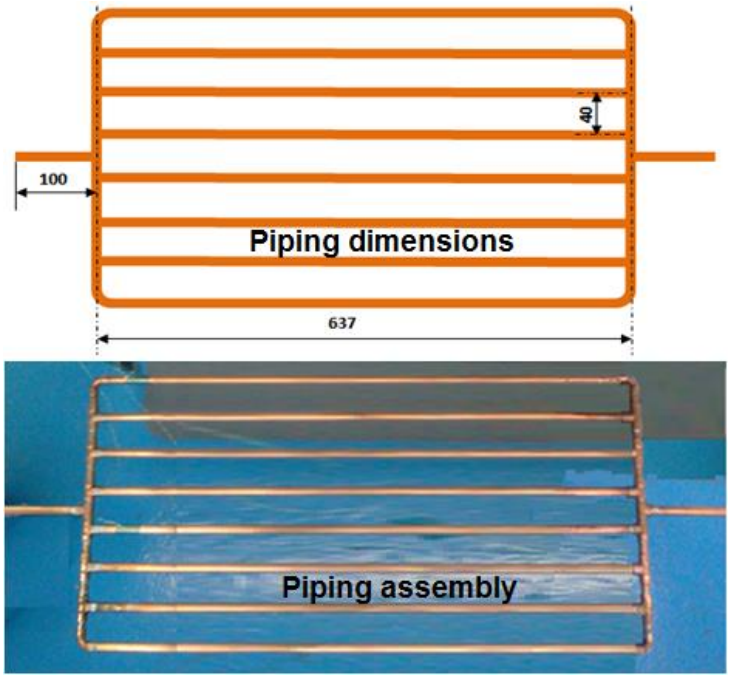

Figure 5-2 The piping system dimensions (mm)

The actual average flow rate, at the main inlet, was measured by a calibrated flowmeter at 75°C to be 15.68 l/min (4.5 m/s). Then the flow rate and fluid velocity in each parallel branch, as listed in Table 5-1, is calculated from the total average flow rate according to equations of continuity and pressure drop equality, as illustrated in Section 4.6.4 and Appendix H. The length of 637mm ensures more equal flow rate and flow profiles in the parallel branches; the maximum difference between the flow rates is 0.3 l/min and the flow rate in each channel creates turbulent flow with Reynolds number higher than 10^4.

Table 5-1 Flow rates, fluid velocities and Reynolds' numbers in the channel branches of the experimental tool

Channel No.		Outer Channels			Inner Channels	Main Inlet
		1 & **8**	**2** & **7**	**3** & **6**	**4** & **5**	
Flow rate	l/min	2.12	2.00	1.90	1.82	15.68
Fluid velocity	m/s	0.52	0.55	0.57	0.61	4.5
Reynolds No.	-	13,634	14,421	14,945	15,994	117,989

5.3.2 Tool face

The tool face is made of CFRP, chosen for its low CTE and thermal inertia, high strength and wear resistance. The reinforcement is non crimp fabric (NCF) triaxial carbon (0, ±45) of 660 g/m^2 areal-weight from Sigmatex Industries (Sigmatex, 2014), is laid up in a multi-axial lay-up configuration that will be helpful in obtaining higher volume fraction and thereby achieving the possible higher through-thickness thermal conductivity. The fibre cloth is stich-bonded layers fabric with polyester yarn in the warp direction and each layer consists three lamina of parallel fibres laid in three different orientations to produce two cloth types of 45, 0, -45 and -45, 0, 45, while the 0 orientation is along the weft. The matrix is the two component, injection and infusion, epoxy system SR8100 with SD8824 standard hardener from Sicomin Composites (Sicomin-Composites, 2013). Appendix J illustrates the manufacturing details of the CFRP laminate, as shown in Figures 5-3 and 5-4. The produced laminate thickness is 3.1 mm, which can provide the desired strength with lower thermal resistance, as aforementioned Section 4.3.1. Finally the edges of the CFRP laminate are trimmed to obtain a square plate of side 500 mm.

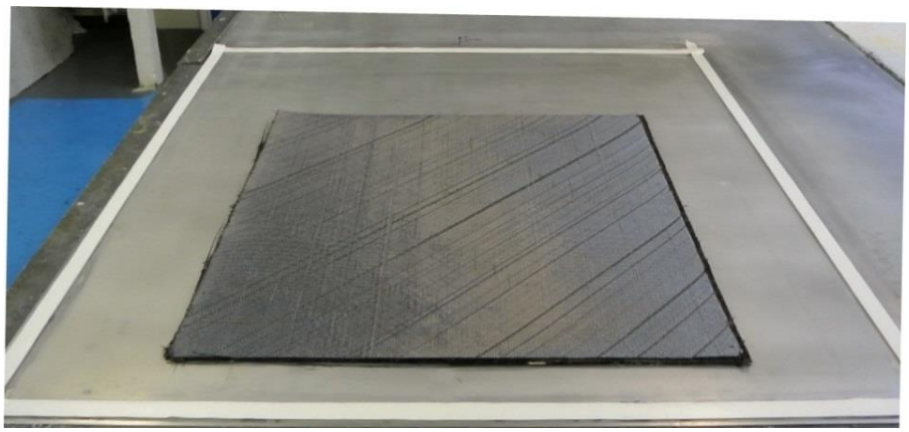

Figure 5-3 Stacking triaxial carbon fibre cloth layers.

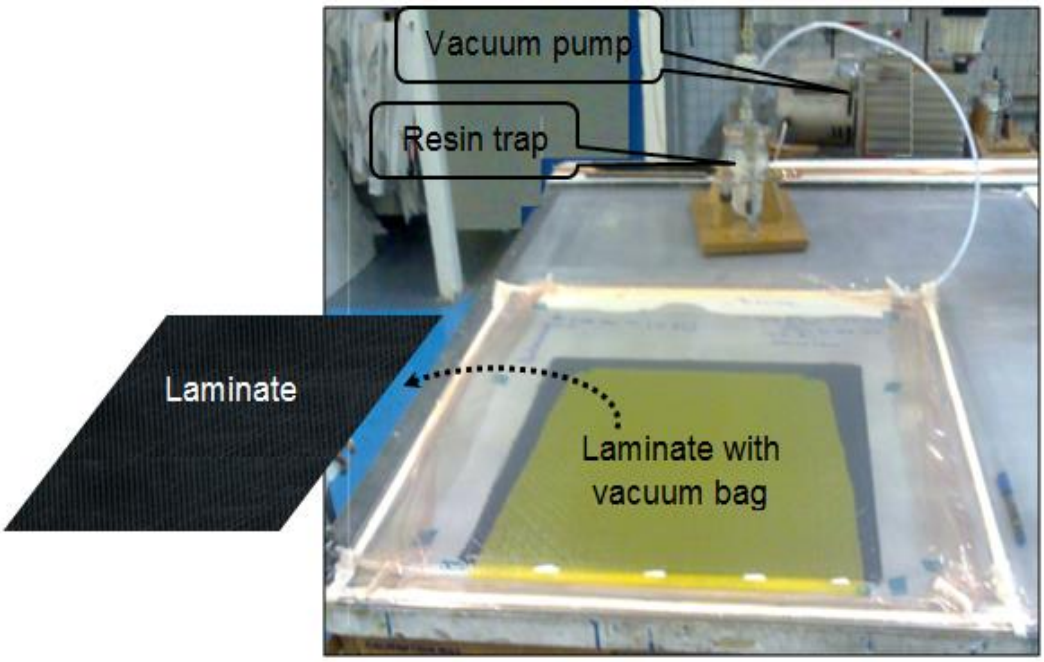

Figure 5-4 Vacuum bag resin infusion process and produced laminate.

5.3.3 Mould

Alepoxy particulate composite is used in manufacturing the mould, using 250 µm Aluminium particles (East Coast, 2013), while the epoxy system is SR8500 with ultra-slow hardener of SD8601(Sicomin-Composites, 2013). This mixture is selected because it is low cost, facilitates embedding the channel, provides a coherent joint with the tool face laminate that attains a strong mould with an

expected through-thickness thermal conductivity higher than CFRP. The main physical properties of the Alepoxy constituents are listed in Table 5-2.

Table 5-2 Density and mixing weight of the Alepoxy composite contents (Sicomin-Composites, 2013)

Alepoxy mixture contents		**Density** @ 20°C	**Mixing ratio**	
		gm/cm^3	$\bar{W}_h\ /\bar{W}_r$	$\bar{V}_h\ /\bar{V}_r$
Al particle	f	2.7	-	-
Resin (Epoxy)	r	1.176	0.35	0.425
Hardener	h	0.95		

A number of Alepoxy specimens with different volume fractions were prepared and tested for their castability (pouring into a die cavity with the desired shape) and obtaining the highest volume fraction that can be cast easily. That is because higher volume fraction provides higher thermal conductivity (Konzelmann *et al.*, 2008; Tomlinson & Stapley, 1977; Zhu *et al.*, 2013). Table 5-3 lists the proposed volume fractions and contribution weights of constituents (fibre, resin and hardener) of the Alepoxy specimens, which are calculated in Appendix K. The specimens are prepared in special cylindrical plastic cups with 40 mm diameter and 30 mm height. Results show that the mixture of 0.48 volume fraction is the most appropriate for casting the desired mould and its density is 1920 kg/m^3 according to Equation K-19.

Table 5-3 Proposed volume fractions and calculated weights of the Alepoxy mixture specimens and their constituents in the castability testing

Total specimen volume	**Particle volume fraction**	**Weights of the constituents**			**Total weight**
		Particle	Resin	Hardener	
$\bar{V}_{co}$	V_f	$\bar{W}_f$	$\bar{W}_r$	$\bar{W}_h$	$\bar{W}_{co}$
cm^3		gm			
2320	0.6	3758.4	765.8	268.0	4792.3
	0.5	3132.0	957.3	335.1	4424.4
	0.48	3006.7	995.6	348.5	4350.8
	0.45	2818.8	1053.0	368.6	4240.4
	0.4	2505.6	1148.8	402.1	4056.4

5.3.4 Tool fixture

The fixture, as illustrated in Figure 5-5, is a custom wooden box that is made especially to combine the tool face and the piping system together, temporarily, during manufacturing and facilitate the mould casting. This arrangement acts as fixture for both the pipe system and the CFRP plate and offers a cavity for casting the Alepoxy (Aluminium particles and epoxy) mixture, on the back face of the CFRP laminate, to form the mould

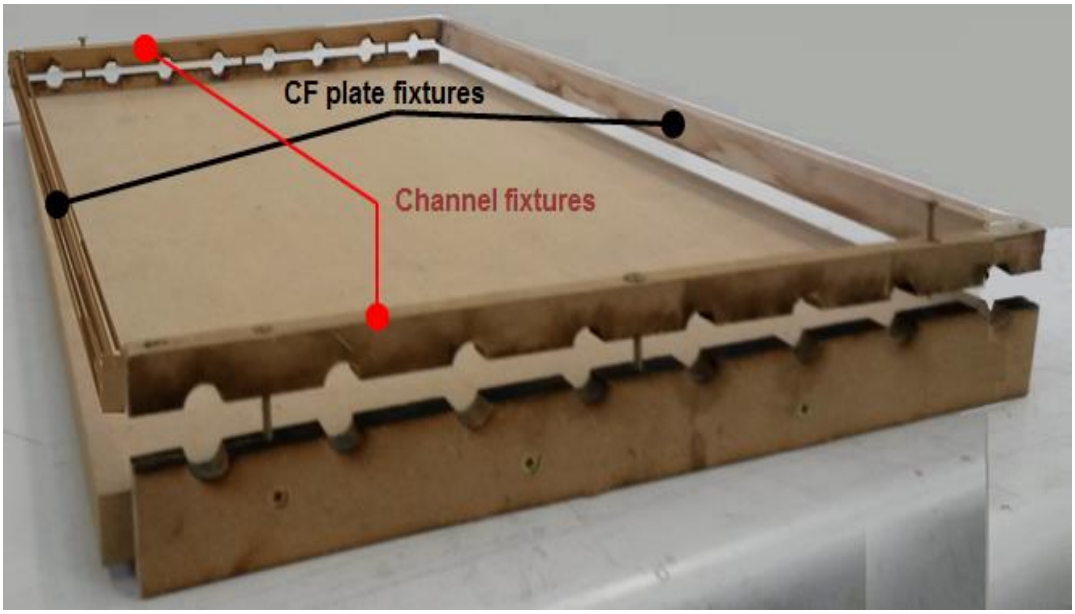

Figure 5-5 Wooden fixture configuration

5.3.5 Mould casting

Initially the tool parts of tool face and channels are combined in the fixture and then 30 K-type thermocouples (more details in Section 5.5.2), as shown in Figure 5-6, are distributed at the interfaces between the mould, tool face and the channel as well as the mould back face to enable monitoring the temperature change at these locations when desired.

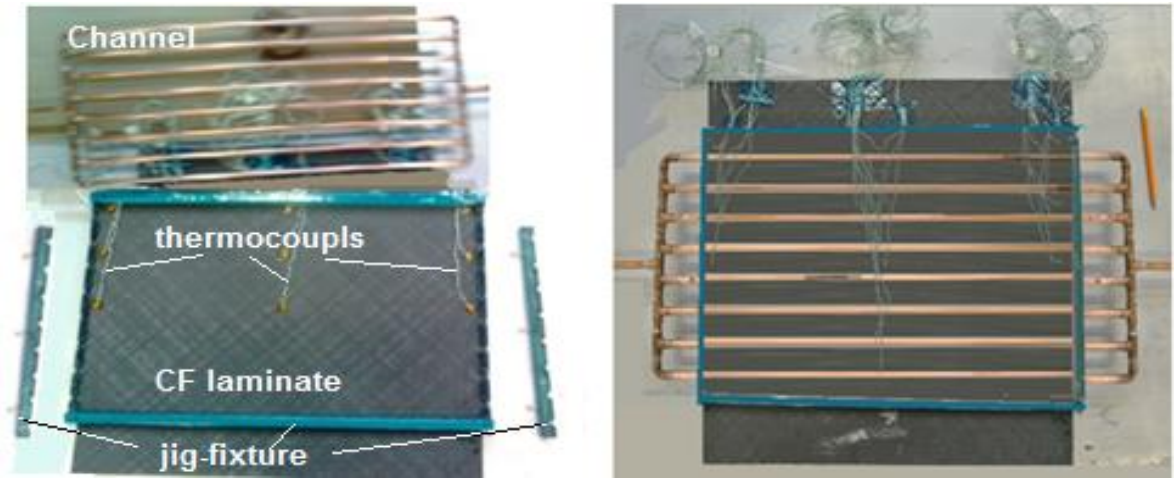

Figure 5-6 Combining the tool parts in the fixture with placing the thermocouples

The desired weights of the constituents of Alepoxy mixture are defined, as illustrated in Appendix K, according to the selected fibre volume fraction of 0.48, and the mould volume that equals the fixture cavity of 500 x 360 x 13 mm, as shown in Figure 5-7. Consequently the mixture is prepared and cast into the fixture cavity to form the mould that integrates with the channel and joins to the tool face permanently.

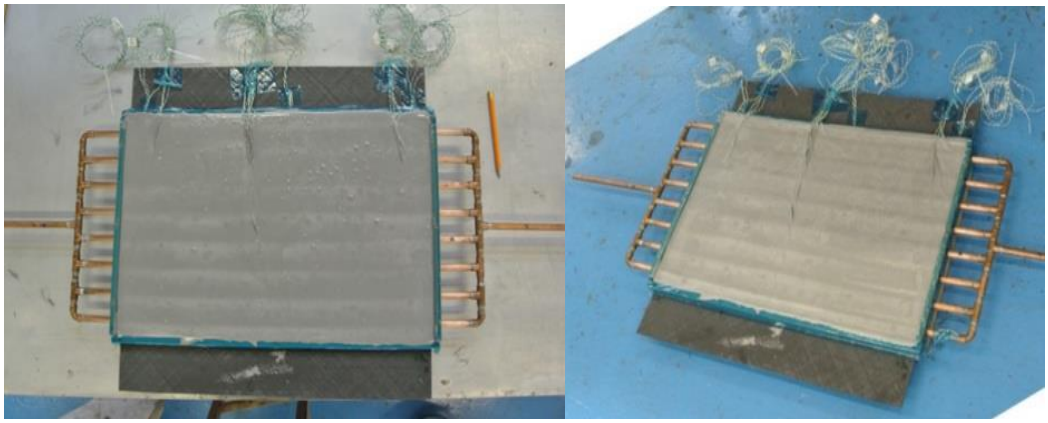

a) After casting process. b) After curing process.

Figure 5-7 Experimental tool

The mixture is cured under a high pressure of 100 psi at 25°C for 12 hours to reduce the void content and post cured, in an oven, at 80°C for about 8 hrs with

a ramp rate of 3 °C/min. Finally the wooden fixture is opened to extract the final tool as shown in Figure 5-8.

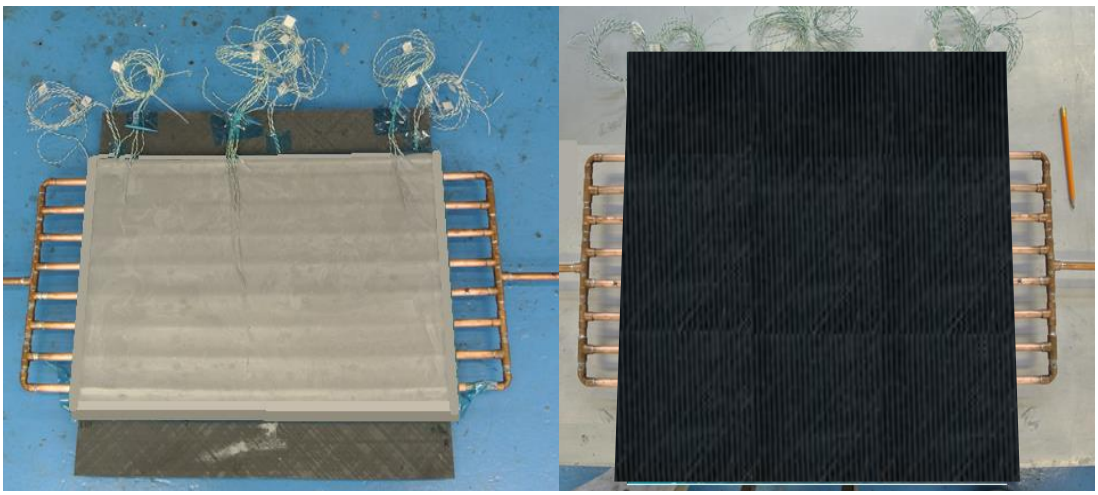

a. The tool from back b. The tool from top

Figure 5-8 The produced experimental tool after extracting from the tool fixture

In order to prevent heat loss from the experimental tool, during application, it is placed in a wooden box (Figure 5-9) padded with a thick layer of PVC foam to insulate the tool side and back faces in addition to the exposed parts of the piping, and then the box is closed tightly. The minimum thickness of insulation is 72 mm. Figure 5-10 illustrates the assembly detail of the produced experimental tool.

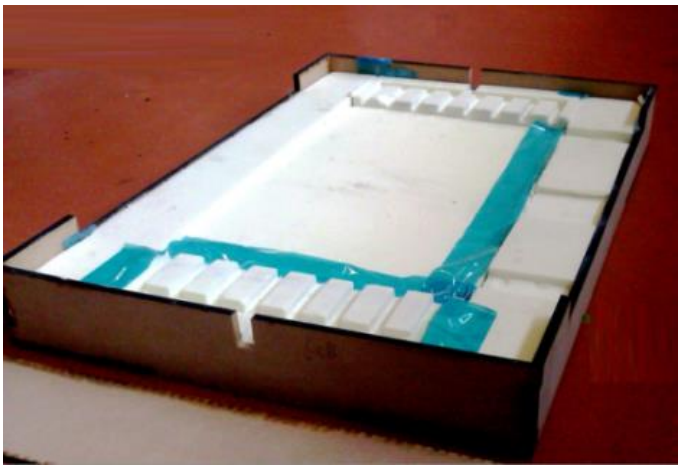

Figure 5-9 The wooden box padded with PVC insulation

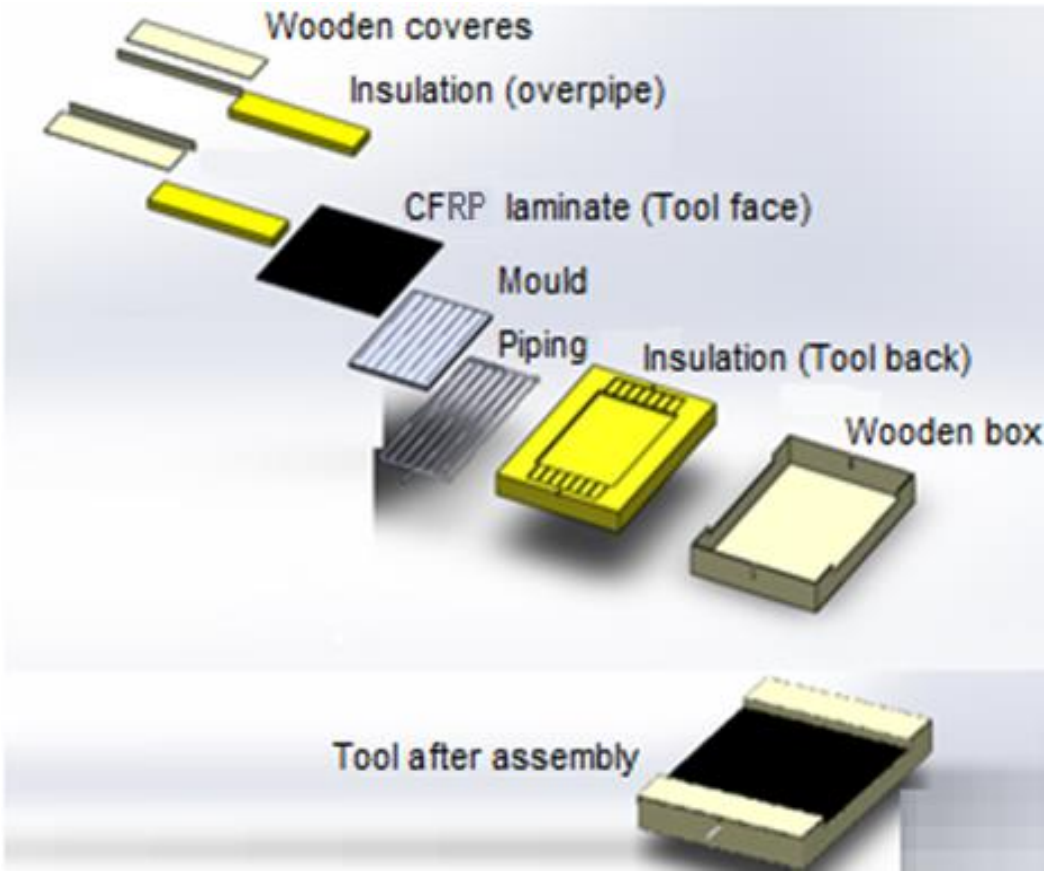

Figure 5-10 The assembly sequence of the experimental tool parts

5.3.6 Volume and weight contributions of the tool parts

The volume, weight and their contribution fractions of each part of the experimental tool (tool face, mould, channel and insulation) and their totals are listed in Table 5-4, while Figure 5-11 shows the relative volume and weight contribution fraction of each tool part.

Table 5-4 Volume, weight and their contribution of the tool parts

Tool parts	Material	Density	Volume	Volume contribution	Weight	Weight contribution
		kg/m^3	m^3	%	kg	%
Channel	Cu	8933	8.2E-05	0.7	0.73	11.60
Foam	PVC	160	9.1E-03	79.7	1.46	23.18
Mould	Alepoxy	1183.5	1.8E-03	15.4	3.39	53.78
tool face	CFRP	1492	4.8E-04	4.2	0.72	11.44
Total		-	1.1E-02	100	6.30	100

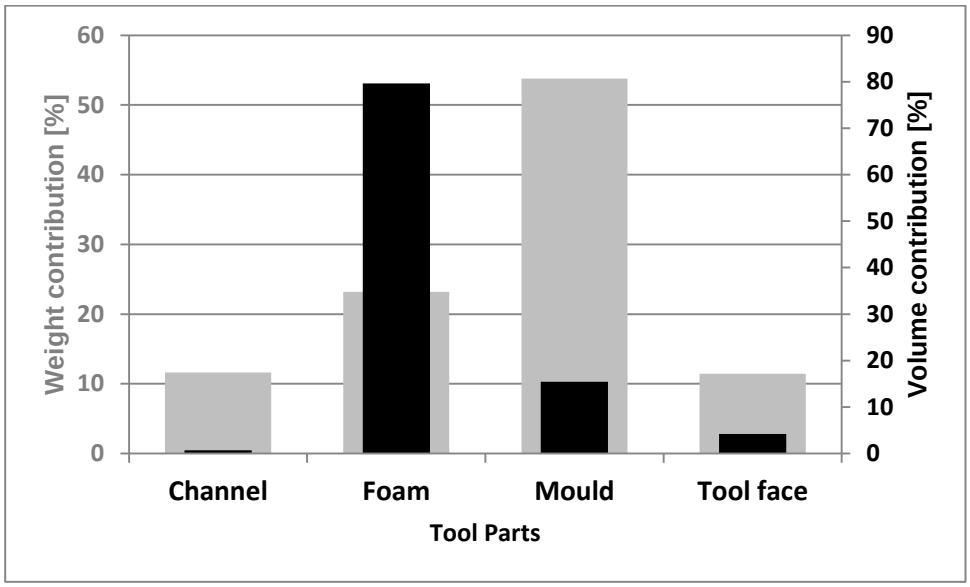

Figure 5-11 Volume and weight contribution fractions of the experimental tool parts

5.4 Measurement of the material properties

Setting the real properties of the materials, during simulation, is one of the basics of reliable comparison between the numerical and experimental results. Therefore thermal properties of the composite materials, applied in the experimental tool, are measured with different advanced and calibrated methods and apparatus.

5.4.1 Volume and weight fractions of CFRP laminate

The digestion method is applied to calculate the actual fibre weight in the samples of the produced CFRP laminate according to the GKN document LTI/CHEM/037 (2003) and British standard BS 7658 (1995). The digestion test of the CFRP laminate, in this PhD study, is achieved as follows (Griepink & Tolg, 1989).

- Three small pieces (test samples) were cut with random sizes from the CFRP laminate and then weighed.
- Each test sample is placed in a beaker containing 50 ml of concentrated nitric acid that removes the cured matrix without affecting the fibre.
- The beaker is heated up to the boiling point of the solution and remains for about 60-90 min, and then cooled down.
- The digested mixture is filtered through sintered glass crucible using a Buchner filtration flask and pump.
- The beaker is washed thoroughly with distilled water and the process is repeated with acetone. Then the remaining fibres are weighed and recorded as shown in Table 5-5.

Table 5-5 The digestion results of the CFRP laminate

Sample No	Sample Weight		Fibre Weight Fraction	Density		Fibre Volume Fraction
	Before Digestion	After Digestion		ρ_f	ρ_{ma}	
	g		W_f	g/cm^3		V_f
1	1.583	1.009	0.64	1.799	1.158	0.53
2	1.535	0.997	0.65			0.54
3	1.669	1.049	0.63			0.52
Average	1.596	1.018	0.64			0.53

Both the fibre weight and volume fractions, in each sample, are determined from the densities of fibre and matrix as well as the obtained weights (before and after digestion) of the sample, as follows (Grove, 2014; Kochetov et al., 2009).

$$W_f = \sum_{i=1}^{n} \left(\frac{\bar{W}_f}{\bar{W}_{co}}\right)_i \times 100 \qquad (5\text{- }1)$$

$$V_f = \frac{W_f}{W_f + (1 - W_f)\frac{\rho_f}{\rho_{ma}}} \qquad (5\text{- }2)$$

Finally the fibre weight and volume fraction of the produced CF is defined by the average of that of the specimens.

5.4.2 Concentration of Al particles through the mould thickness

The particles in a viscous liquid settle down due to gravity as mentioned by Murisic et al. (2013). This phenomenon also occurs during the cure of particulate composites (e.g. Alepoxy) and causes uneven distribution of the particles through the mould thickness that may affect its properties, especially the thermal conductivity. Therefore the concentration of the aluminium particles, across the thickness of a specimen of the mould material, is inspected by Scanning Electron Microscopy (SEM) that uses electron beam to view the sample structure instead the light in the normal microscopes (Stadtländer, 2007). The inspection is performed as follows.

- A cylindrical specimen, of 40 mm diameter and 15 mm height (Figure 5-12), is prepared simultaneously during the mould casting (Section 5.3.5) to attain similar properties of the produced mould.
- The specimen is cut axially to expose a through thickness plane. A low-speed diamond saw is used for cutting to minimise structural damage.
- The surface of the through thickness plane is polished and then carbon coated in order to prevent from charging and thereby obtaining clear images during the SEM scanning. The prepared specimen is placed in the special cabinet of the SEM for scanning and capturing images. Imaging covers the top, bottom and middle zones of the sample surface, as shown in Figure 5-12. At least five sequential images are captured from each zone in the horizontal direction. The bottom zone is the bottom of the specimen and also represents the upper face of the mould that contacts the tool surface.
- Finally the imageJ software is applied to determine area fraction of the particles in each zone from their images.

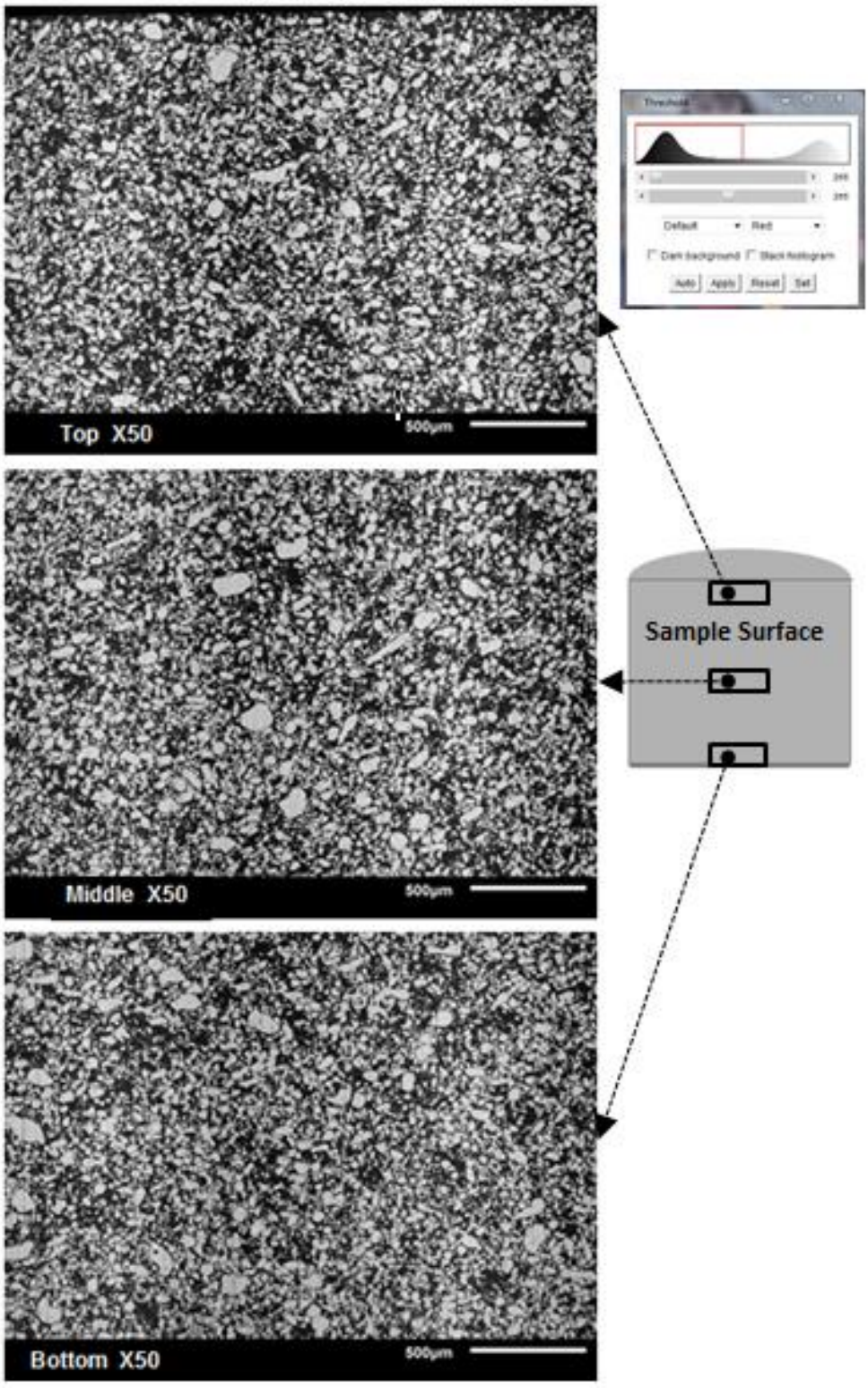

Figure 5-12 Aluminium particle concentration in the Al epoxy mixture, magnification is X50

The inspection results indicated that the area fraction, of the particles, changes slightly through the mould thickness from 47% at the mould bottom to 49.5% at the top, which means that the maximum difference of aluminium particle

distribution across the mould thickness does not exceed ±2.5%. This small difference does not have significant effect on the mould out-of-plane thermal conductivity. Consequently properties of the Alepoxy mould are assumed to be isotropic in this PhD study.

5.4.3 Density measurement of the composite materials

Density of the composite materials is a function of fibre volume fraction and densities of the constituents, which can be calculated according to the role of mixture (ROM), as explained in Appendix K. It can also be measured via water displacement (buoyancy) method according to ASTM D792-13 (2013), which is based on the Archimedes' principle, which proved that volume of a submerged material equals the volume of the displaced water (Derringh, Halliday & Resnick, 1988). The both methods are applied in this PhD study to obtain the most reliable densities of the applied materials. Practically the buoyancy method is performed as follows.

- Five small samples (pieces with arbitrary sizes and geometries) are prepared for each composite material.
- The mass of each sample is measured in air and then in water by a precision analytical weighing balance of Avery Berkel model WA205.
- Density of each sample is determined by Archimedes' law of buoyancy with assuming the water density of 1 g/cm^3 at room temperature (20^{o}C).

$$m_o - \bar{m}_o = m_w \qquad \text{(Archimedes Law)} \qquad (5\text{- }3)$$

$$V_w\rho = V_o\rho = \left(\frac{m_o}{\rho_o}\right)\rho \qquad (5\text{- }4)$$

$$\therefore\ \rho_o = \frac{m_o}{m_o - \bar{m}_o} \qquad (5\text{- }5)$$

The calculated and measured values of densities of the applied composites are listed in Table 5-6, which are well each other.

Table 5-6 Measured and calculated density values of the composites used

Composite type	Mass		Density	
	In air	In water	measured	calculated
	g		*g/cm^3*	
CFRP	6.95159	2.29264	1.49	1.50
Al epoxy	8.48824	4.06191	1.92	1.87

5.4.4 Thermal diffusivity

Thermal diffusivity defines the speed of heat propagation through materials and different techniques are available to measure its value (Gallagher, 2012). Thermal diffusivities of the tool materials is measured by laser flash method, using Nanoflash-xenon apparatus, type 1 x LFA 447 (Netzsch), which was calibrated according to the ASTM E-1461-01(2013). The test was performed at the mechanical engineering laboratories at the University of Portsmouth, UK as follows.

- Four standard square samples, of 12.7 mm length and 2.5 to 2.9 mm thickness, are prepared for each material. Therefore the in-plane diffusivity of the CFRP laminate was difficult to measure because the laminate thickness is too small for preparing the required specimens.
- Each specimen is coated initially with graphite spray to reduce the radiation effects on the test results.
- Thickness of each specimen is measured exactly prior to the testing.
- The four specimens are placed separately into the machine sample holders.

- The controlling software of the machine is activated to achieve the tests automatically at temperatures of 25°C, 50°C, 75°C and 100°C and to repeat each test three times.

In this method Pyroceram is used as a reference material to calibrate the device prior to each test and the machine achieves the testing as follows:

- A laser pulse of short duration, compared to the transient time through the sample, heats the front face of the square specimens.
- The temperature rise, on the specimen rear face, is measured by an infrared detector and recorded to plot the signal versus time.
- The half rise time ($t_{1/2}$), which equals the required time to heat the back face of the specimen to 50% of its maximum temperature, is taken from the plotted signal versus time.
- Finally, as mentioned by Nunes dos Santos *et al.* (2005), the thermal diffusivity is calculated by the following formula.

$$\propto = \frac{0.139\, t_s^2}{t_{1/2}} \qquad (5\text{- }6)$$

The measured diffusivities and their average for each material sample at each temperature are listed in Table 5-7.

Table 5-7 Diffusivity of the applied composites

Material	**Temperature (°C)**	**Diffusivity (**mm^2/s**)**				
		Sample1	Sample 2	Sample3	average	mean
CFRP (in-plane)	25	0.335	0.439	0.416	**0.397**	**0.4215**
	50	0.477	0.458	0.439	**0.458**	
	75	0.447	0.442	0.406	**0.432**	
	100	0.422	0.390	0.385	**0.399**	
Al/epoxy (isotropic)	25	0.889	0.892	0.885	**0.889**	**0.8073**
	50	0.863	0.865	0.862	**0.863**	
	75	0.799	0.795	0.794	**0.796**	
	100	0.680	0.685	0.678	**0.681**	
Pyroceram	25	1.984	1.994	1.984	**1.987**	**1.8328**
	50	1.890	1.906	1.872	**1.889**	
	75	1.785	1.777	1.774	**1.779**	
	100	1.670	1.678	1.680	**1.676**	

5.4.5 Specific heat capacity

Specific heat is the amount of heat required to change the temperature of unit mass of a material by one degree. Thermoanalytical technique of Differential Scanning Calorimetry (DSC), as mentioned by Cassel et al. (2012), is used to measure the specific heat according to ASTM E2716 – 09 (2014). In this PhD study a PL-DSC apparatus, calibrated by Thorn Calibration Service, is applied. As shown in Figure 5-13, it has two sample holders that are mounted symmetrically inside an enclosure held normally at room temperature (Kaiser et al., 2014).

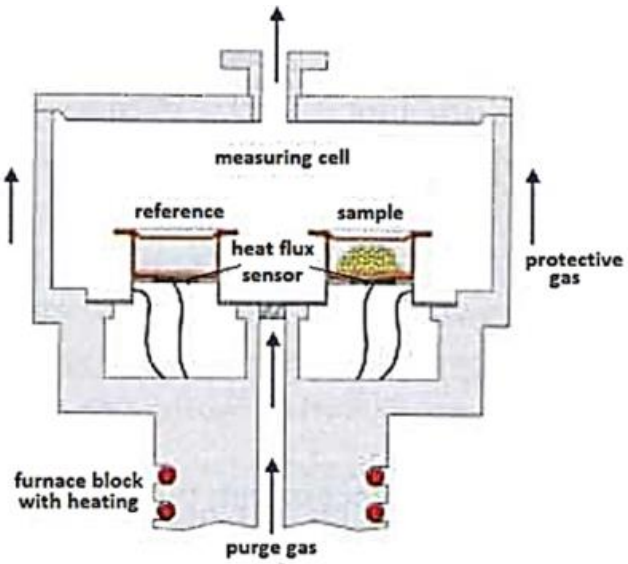

Figure 5-13 Schematic of a heat flux DSC cell (Kaiser *et al.*, 2014)

The device contains two (primary and secondary) temperature control systems. The first is a platinum resistance thermometer controls the average temperature of the sample holders, while the second measures the temperature difference between the sample holders and adjusts the difference to zero by controlling the total heating power. The heating elements are embedded in the sample holders and the differential power is measured and recorded.

Measuring of the specific heat by DSC is based on the difference between the amounts of the heat flows into each of the material sample and the reference or standard material (sapphire), which are derived as function of temperature or time (Tavman et al., 2011; Young & Whitaker, 1973). The procedure of heat capacity test is achieved as follows.

- Five small circular specimens, as shown in Figure 5-14, are prepared for each material with sizes suitable to seal into the sample pan.

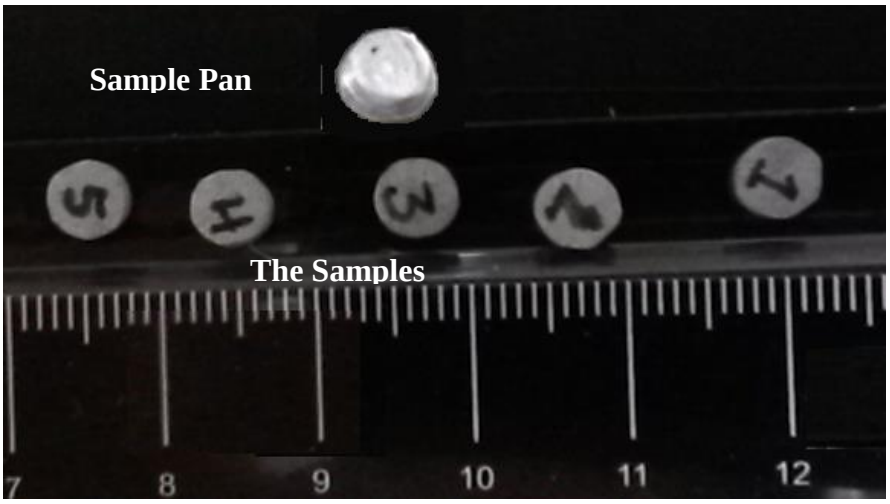

Figure 5-14 The Alepoxy samples for specific heat test.

- The test specimens and the reference material are weighed with a precise balance prior to each test and set into the machine software.

- An isothermal condition, Figure 5-15, is used for the test runs, which starts from Initial baseline temperature, equilibrate for 2 min isothermally at 35^{o}C, scan dynamically at 5^{o}C/min over the temperature range from 35 to 70^{o}C and then equilibrate isothermally at 70^{o}C for 2min.

- An initial run is performed, to obtain the thermogram of the reference material, by placing the sample pan containing the sapphire in the sample holder and an empty pan in the reference holder (O'neili, 1966;

Young & Whitaker, 1973). Knowing that the sapphire is 60.066 mg weight and has a specific heat capacity of 0.8188 J/g.ºC (J/g.K).

- The second run is carried out with no sample present in both the sample and the reference holders to establish a baseline, which indicates isothermally the differential losses of the two sample holders at the initial temperature (Cassel *et al.*, 2012; Exstar, 1981).
- The final runs are performed to the material samples separately by placing the sample in the sample pan and the empty pan in the reference holder.

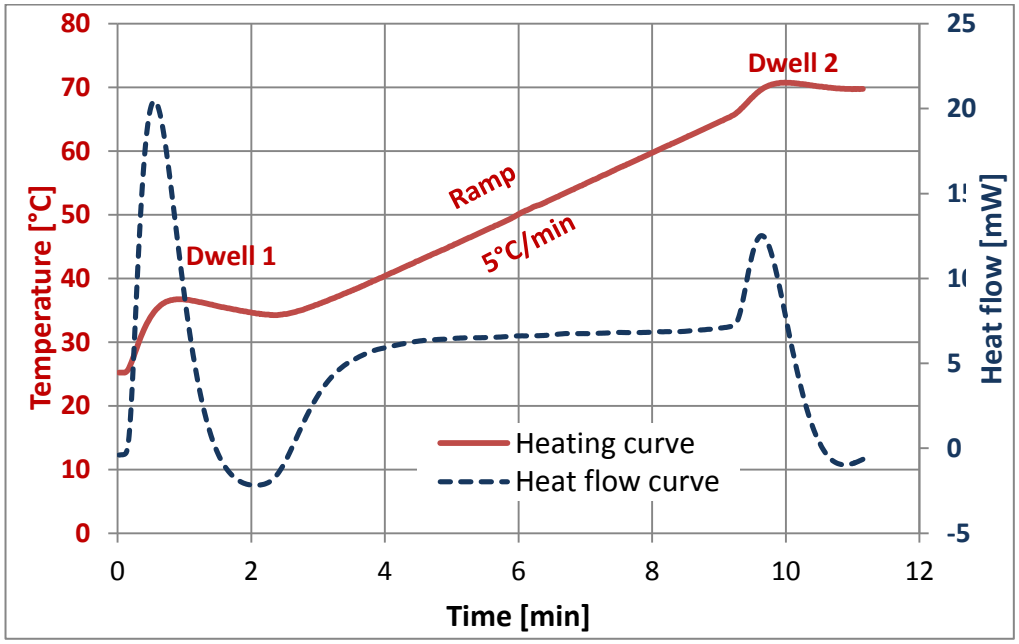

Figure 5-15 Heating and heat flow curves of an Alepoxy specimen during specific heat test by DSC device.

Figure 5-16 illustrates the superimposed plots of the three thermograms for calculating diffusivity of one of the Alepoxy samples. The abscissa of the thermograms represents temperature, while the ordinate represents both the rate of heat absorption by the material (on the left) and the deflection amount of the thermograms (on the right).

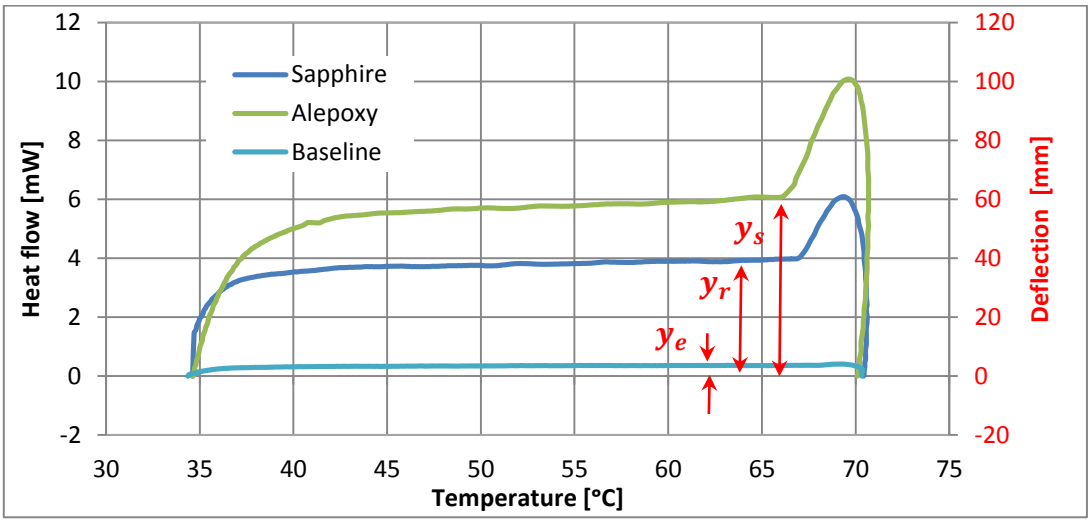

Figure 5-16 Thermograms of specific heat testing for an Alepoxy sample.

After calculating the amounts of thermogram deflections of the empty pan, sapphire, and the material specimens, as listed in Table 5-8, the specific heat of the material samples can be calculated as follows (O'neili, 1966; Young & Whitaker, 1973).

$$c_{p_s} = \frac{\mathrm{m_r}(y_s - y_e)}{\mathrm{m_s}(y_r - y_e)} c_{p_r} \qquad (5\text{-}7)$$

Table 5-8 Specific heats of the composite materials.

Sample No.	Pan	Sapphire			Alepoxy			CFRP		
	y_e	y_r	m_r	c_{p_r}	y_s	m_s	c_{p_s}	y_s	m_s	c_{p_s}
	mm	mm	g	J/g.°C	mm	g	J/g.°C	mm	g	J/g.°C
1	4.0	39.3	0.06	0.819	60.5	0.08	1.0370	55.6	0.07	0.9886
2					61.7	0.09	0.8858	49.8	0.07	0.9554
3					61.9	0.09	0.8842	50.7	0.07	0.9478
4					61.6	0.09	0.9524	52.1	0.07	0.938.9
5					60.9	0.08	0.9603	54.2	0.07	0.9991
Average					61.3	0.09	0.9402	52.5	0.07	0.9662

Figure 5-17 illustrates slow increment of specific heat versus temperature rising for an Alepoxy sample. Accordingly the average of specific heat of the Alepoxy specimen, between the both dwell temperature of 35°C and 65°C, is 0.9556 J/g.°C that agree well with the analytically calculated value (Table 5-8).

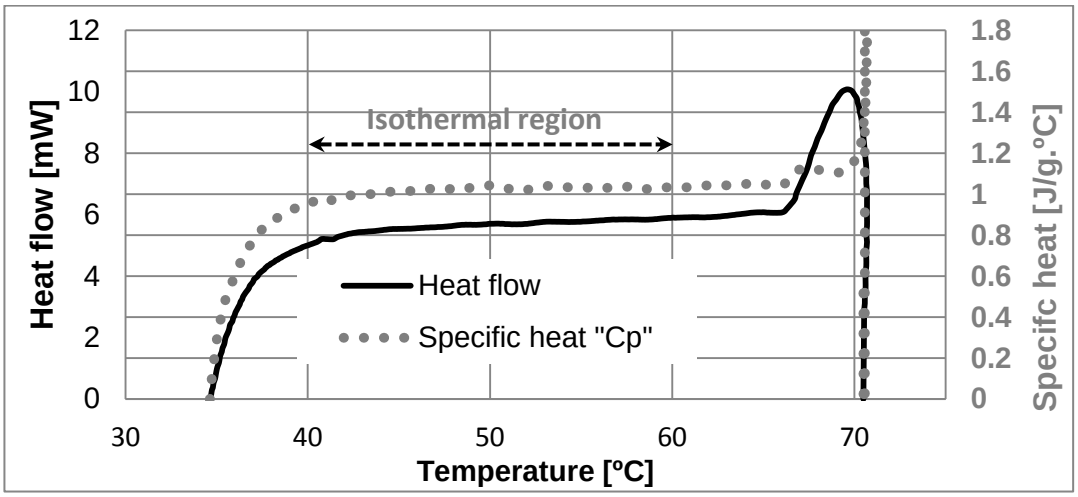

Figure 5-17 Heat flow rate and specific heat of an Alepoxy specimen versus temperature

5.4.6 Thermal Conductivity

The thermal conduction coefficient represents the heat transferability of materials. Various possible experimental methods are available for calculating thermal conductivity, which are classified into two categories of steady-state and transient methods. In this PhD study, thermal conductivities of the isotropic Alepoxy mixture and the CFRP laminate (out-plane) are calculated, after measuring their density, thermal diffusivity and specific heat, as listed in Tables 5-9 and 5-10, respectively, using the following equation (Joven et al., 2012; Kaiser *et al.*, 2014).

$$k = \propto \rho c_p \qquad (5\text{- }8)$$

Results show that the thermal conductivity of Alepoxy mixture is about 1.5 W/m.K and out-plane thermal conductivity of the CFRP laminate is 0.6 W/m.K. The in-plane diffusivity of the laminate is not easy to measure, as illustrated in Section 5.4.4, therefore the in-plane thermal conductivity of the laminate was determined by ROM depending on the calculated out-of-plane thermal

conductivity and that of the fibre reinforcement (21.6 W/m.K) was taken from literature (MatWeb, 2014).

Table 5-9 Isotropic thermal properties of the Alepoxy mixture

Sample No	$\propto_{\mathbf{Alepoxy}}$	$\rho_{\mathbf{Alepoxy}}$	$c_{p_{\mathbf{Alepoxy}}}$	$k_{\mathbf{Alepoxy}}$
	m^2/s	kg/m^3	J/kg.°C	W/m.°C
1	8.1×10^{-7}	1917	1037.0	1.6
2			885.8	1.4
3			884.2	1.4
4			952.4	1.5
5			960.3	1.5
Average			**943.9**	**1.5**

Table 5-10 Orthotropic thermal properties of the CFRP laminate

Sample No	$\propto_{\mathbf{CFRP}}$		$\rho_{\mathbf{CFRP}}$	$c_{p_{\mathbf{CFRP}}}$	$k_{\mathbf{CFRP}}$	
	m^2/s		kg/m^3	J/kg.°C	W/m.°C	
	out-plane	In-plane	All directions		out-plane	In-plane
1	4.2×10^{-7}	-	1500	988.6	0.62	**3.00**
2				955.4	0.60	
3				947.8	0.60	
4				938.9	0.59	
5				999.1	0.63	
Average				**966.0**	**0.60**	

5.5 Measuring apparatuses

Different apparatuses, e.g. thermal camera, thermocouples and flowmeter, are utilised for measuring the desired temperature and flow rate during application of the experimental tool.

5.5.1 Emissivity of the CFRP laminate for thermal camera

Measurement of temperature by the thermal camera depends on the emitted infra-red radiation, therefore the most important parameter is emissivity, which represents the ability of the object to absorb, transmit and emit infrared energy, compared to that of a perfect black body at the same temperature (Neuer, 1992; Orlove, 2012). Emissivity ranges from that of shiny mirror to that of black body and equals 0 and 1, respectively. When a higher value than the actual

emissivity is set in the thermal camera, the output temperature will be lower than the target and vice versa (Transcat, 2014), therefore the actual emissivity of the tested object must be set in the camera to obtain actual surface temperature. Li & Strider (2009) concluded that the effective emissivity value of a high-temperature CFRP composite surface depends on fibre-matrix emissivity, fibre volume fraction, ratio of protrusion length (fibres protruding out from composite matrix) to fibre radius and the perpendicular or the parallel edge fibre orientation. Also they found that the carbon-carbon composite with a volume fraction of 0.30 has an emissivity equals 0.8.

The reference method, as described in ISO 18434-1, is applied in this PhD study to determine the emissivity of the CFRP surface of the experimental tool. The method is suitable for objects with temperatures up to 260°C and based on applying a reference black material of known emissivity to determine that of the desired material (T&PI, 2014). The emissivity test procedure is achieved as follows.

- A rectangular area of 80 x 140 mm^2 at the centre of the tool face (Figure 5-18) is covered by the black PVC tape (Wilko BS3924) as the reference surface, which has an emissivity of 0.95.
- After adjusting the thermal camera over the tool face, the test location (Figure 5-19) is covered to shield the camera from the effects of surrounding radiation and the external lights as much as possible.
- The tool surface (Figure 5-20) is heated up to 75°C (because the tape suitability is limited to 80°C).
- Temperature of the tool surface is measured at the taped location by the thermal camera and then the tape is removed.

Figure 5-18 Black tape on the tool face as a reference for measuring emissivity.

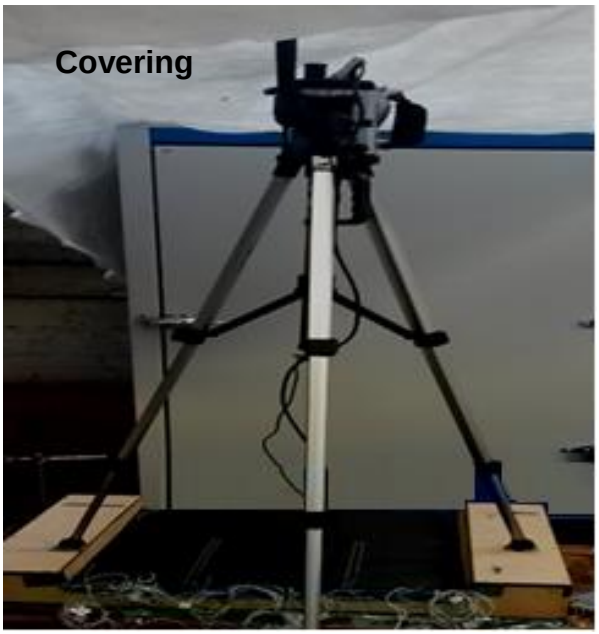

Figure 5-19 Covering the test location during the emissivity measuring test.

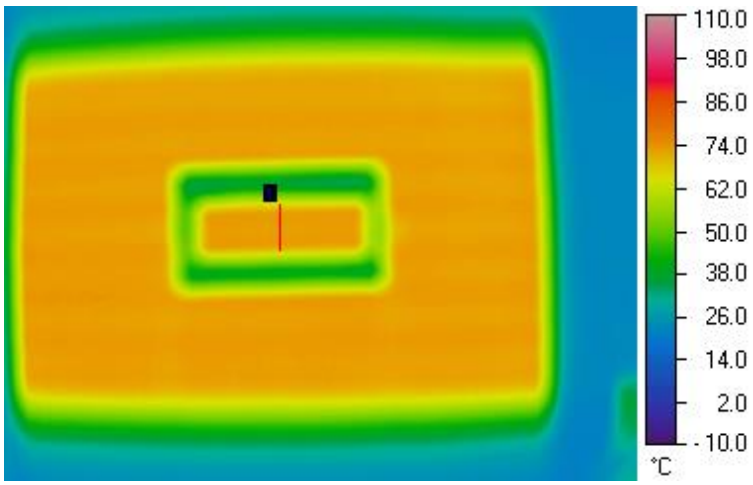

Figure 5-20 Thermal image of the tool surface at steady state temperature.

- Temperature of the tool face (without tape) is measured repeatedly by the thermal camera at different emissivity values ranging from 0.8 to 1.
- The distribution of temperature along the measured surface (the plotted red line in Figure 5-20) is calculated for each test case by the MicroSpec software and plotted in Figure 5-21.

Accordingly the most appropriate value of the tool face (CFRP laminate) emissivity of 0.94 is calculated by which the maximum uncertainty in temperature measurement with the thermal camera will be about 0.2°C.

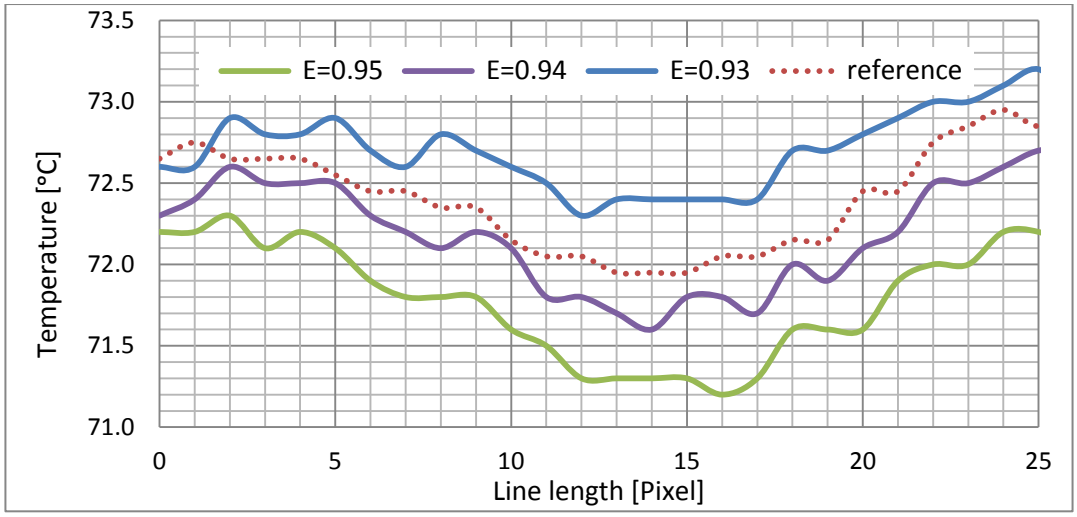

Figure 5-21 Temperature distribution along a specified line over the tool face, with and without tape

5.5.2 Error estimation test for the thermocouples

Thermocouples consist two dissimilar metallic wires, Figure 5-22, that are welded at one end separated with insulated leads and temperature measurement at the other (Huber, 2013). Thermocouples generally have a very low temperature to voltage sensitivity, therefore any temperature difference between their hot and cold junctions generates electrical voltage in the loop due to the Seebeck effect (Maxim-Integrated, 2007). Typically the output signals of thermocouple are in the millivolt range. In the most common configuration of

thermocouples a third intermediate metal and two additional junctions are introduce into the loop (Figure 5-22), as long as these additional junctions are remain at the same temperature the intermediate metal has no effect on the output voltage (Maxim-Integrated, 2007).

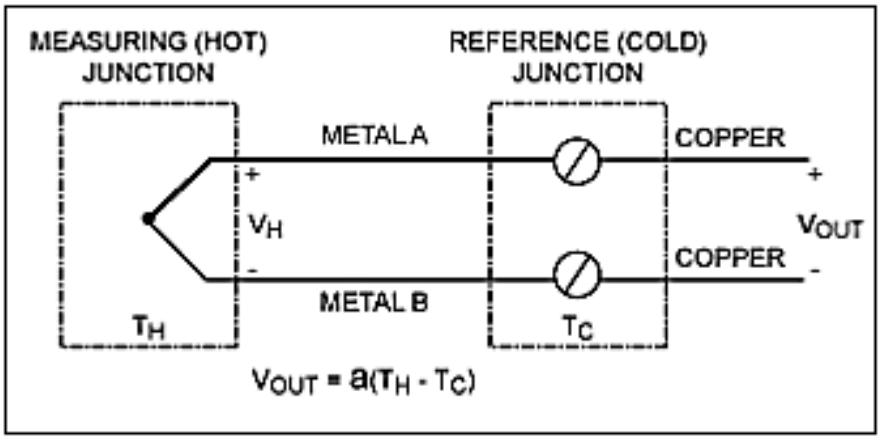

Figure 5-22 Thermocouple configuration (Huber, 2013).

The flexible K type thermocouples, made by Labfacility, are applied for measuring the surface and the interface temperatures of the tool. Each has a copper disc of 6.5 mm diameter and 0.3 mm thick welded to the hot junction. The measurement rang of the thermocouples is from 0°C to 200°C with a tolerance of ±2.5°C according to IEC 584-2 specification (formerly BS4937:1983).

Different sources of errors may affect the accuracy of thermocouples, such as noise, offset and gain errors, cold-junction compensation (CJC) accuracy and thermocouple errors (NI, 2011). So they must be taken into account and careful attention must be paid during temperature measurement. The thermocouples are tested experimentally to estimate the accuracy compared to the thermal camera and oven (Huber, 2013).

5.5.2.1 Oven method for error estimation test

This method compares the measurements of two thermocouples with that of an oven. One of the thermocouples is connected to a sample of CFRP laminate and the other is left free in the oven as shown in Figure 5-23.

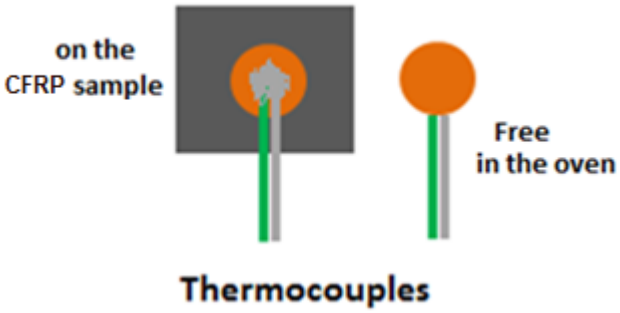

Figure 5-23 The thermocouples during the oven error estimation test

The oven temperature controller is set to heat the oven from ambient temperature to 90°C with a ramp of 1°C/min with two dwells of 5 min and 20 min at 30°C and 90°C, respectively. The measured transient temperature by the oven and each of the free and connected thermocouples, during the heating cycle, are plotted in Figure 5-24. Results show that the thermocouples are reading 2°C lower than the oven, but it is still within the specified tolerance of ±2.5°C.

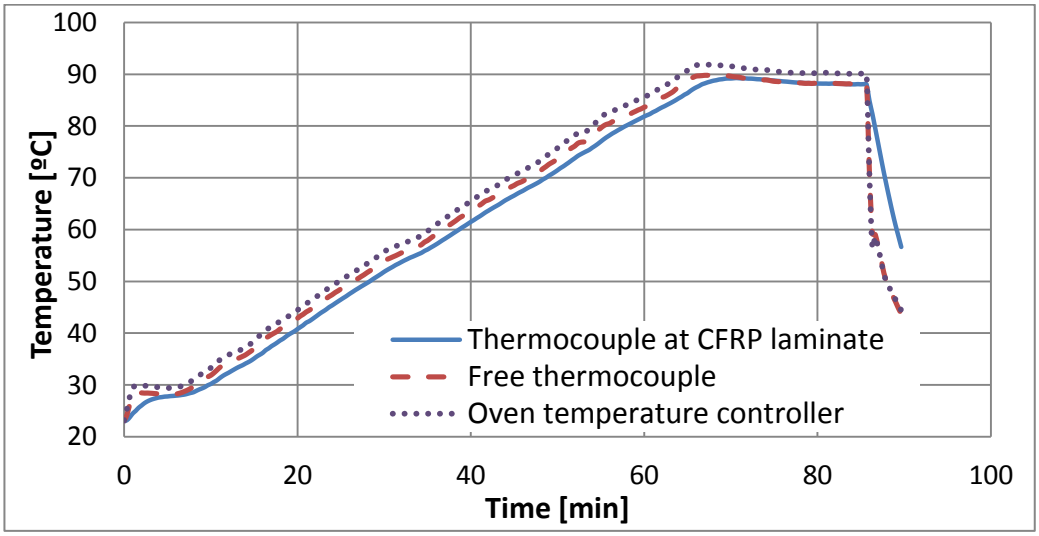

Figure 5-24 Heating curve of the oven with a ramp of 1 °C/min

5.5.2.2 Infrared camera method for error estimation test

In this method the tool surface temperature, as shown in Figure 5-18, is measured simultaneously by four K type thermocouples, connected to the tool face, and the thermal camera adjusted to emissivity of 0.94. results show that measurements of the thermocouples compared to that of the camera, Figure 5-25, are lower by about 2.4°C , but still within their specified tolerance.

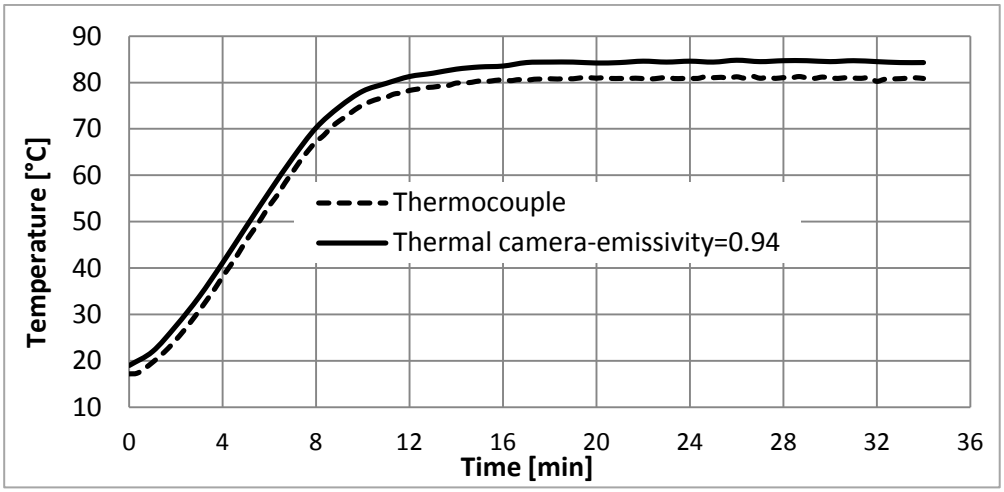

Figure 5-25 Heating curve of the centre of tool face measured by thermocouple and thermal camera.

5.5.3 Calibration of the flowmeter

The piping system in experimental tool contains many reasons of flow restriction (e.g., pipe surface, pipe length, water blocks, tubing bends, and fittings) that drop pressure and decrease the flow rate provided by the pump, as shown in Figure 5-26 (Vesilind, Perirce & Weiner, 1994). Therefore the flow rate is measured prior to the experiments to ensure from the actual value that generates turbulent flow. In this PhD study a liquid vortex OVAL Eggs Delta flowmeter (model FLM21-10PCW from Icenta) is used for measuring the flow

rate at the main inlet of the experimental tool. The flowmeter is calibrated gravimetrically as follows (Baker, 2000; Satterfield, 2013).

- The flowmeter is connected to a mains water tap that facilitates controlling the amount of flow rate through the flowmeter.
- After fixing the flow rate by the tap and flowmeter, the time to fill a vessel of 21.8 litre volume completely is measured by a stop watch and recorded.
- Previous test is repeated five times with different flow rates and three iterations for each test.

The average time of filling the vessel, proposed (measured by the flowmeter) and calculated volumetric flow rates of each test are listed in Table 5-11, while the flow rate is calculated according to the following relation.

$$Q_f = \frac{V_v}{\Delta t} \qquad (5\text{- }9)$$

Table 5-11 Calibration results of the flowmeter, vessel volume = 21.8 litres

Test number		1	2	3	4	5
Flowmeter measurement	l/min	3.365	6.03	8	8.54	10.73
Vessel filling time	min	6.78	3.58	2.68	2.52	1.98
Calculated volumetric flow rate	l/min	3.21	6.08	8.12	8.66	10.99

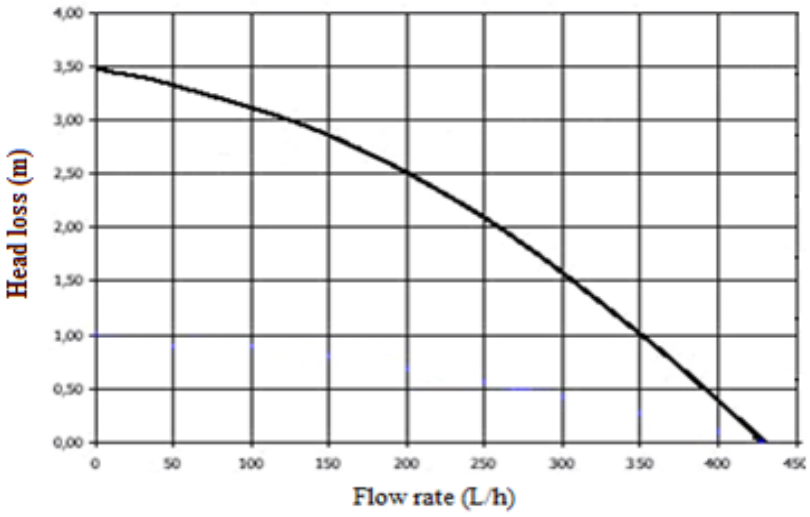

Figure 5-26 Typical pump curve (Vesilind, Perirce & Weiner, 1994)

Amounts of the flow rates measured by the flowmeter, during calibration, are plotted versus those calculated, as shown in Figure 5-27, that confirms the high accuracy of the flowmeter.

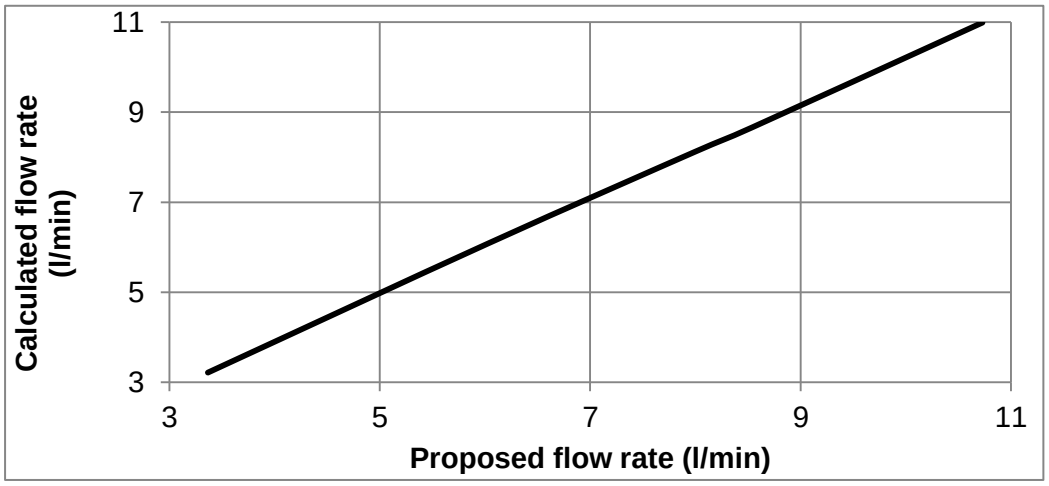

Figure 5-27 The flowmeter calibration test results.

5.6 Numerical simulation of the experimental tool

Due to the modifications achieved in the predicted optimal design (Section 5.2), a model of the experimental tool is simulated to investigate the performance of heating time and temperature uniformity over the tool face. A target temperature of 81ºC is considered to avoid uncertainties as the operating temperature is approached asymptotically. Actual boundary conditions and material properties are set during simulation to obtain most actual results (ANSYS, 2009). The governing equations of transient heat convection and diffusion are presented in Section 4.5.1.

5.6.1 Tool modelling

Using symmetry, a quarter of the experimental tool geometry, as illustrated in Figure 5-28, is modelled in ANSYS workbench. The model parts are divided into

3.1 x 10^5 tiny elements. The mesh quality was evaluated, through the available metric function of the software, and indicated that the orthogonal quality of the cells are close to 1, the cell skewness values are below 0.9, while the sudden and large changes was avoided in cells to achieve best aspect ratios.

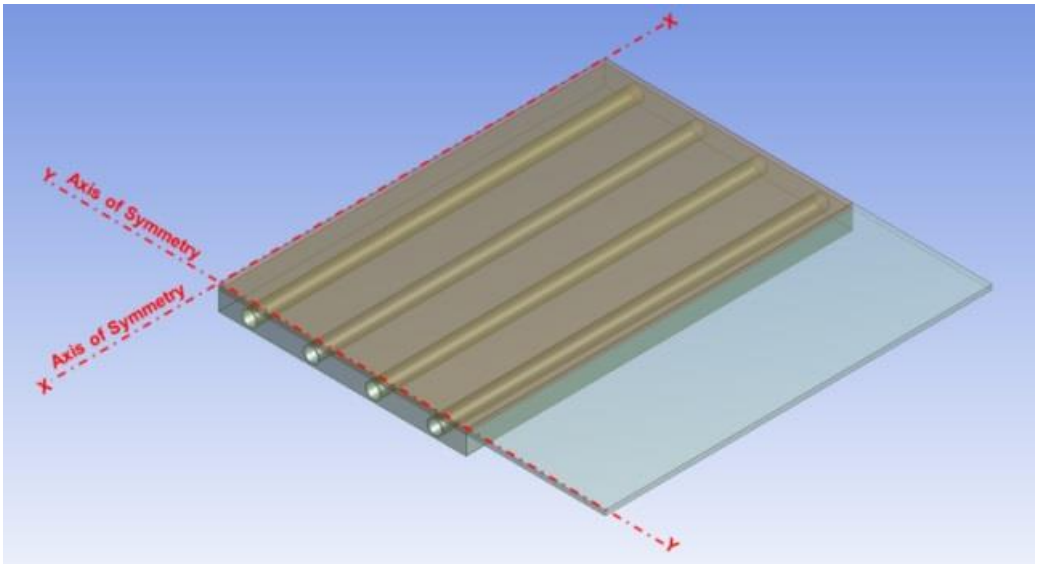

Figure 5-28 Geometry of the simulated part of the tool

The actual thermal properties of the tool materials (Table 5-12) are set. The inner surfaces of the channel branches are set as convection boundary, in contact with the circulating water at 90°C. This temperature assumption could be provided well practically for the industrial sites with established adequate resources (Ding *et al.*, 2001).

Table 5-12 Thermal properties of the experimental tool materials

Material	Direction	ρ	c_p	$\propto$	k
		Kg/m^3	J/kg.°C	m^2/s	W/m.°C
CFRP	In-plane	1500	966.0	-	3
	Out-plane			4.2X10^{-7}	0.6
Alepoxy	Isotropic	1917	943.9	8.1X10^{-7}	1.5
Copper	Isotropic	8933	385	1166X10^{-7}	401

According to the amounts of fluid velocity in each channel (Table 5-1) and properties of water at 90ºC (Appendix D), the Reynolds number in all channels

is higher than 10^4, therefore the heat transfer coefficient can be calculated (Table 5-13) according to the empirical Equation 3-1. The difference of heat transfer coefficients between the channels backs to the fluid velocity variance that affects the Reynold number.

Table 5-13 Heat transfer coefficient in the parallel channels, water properties at 90°C

Channel No.	u	Re_D	h
	m/s	-	(W/m^2.K)
1 (Outer channel)	0.52	13634	4815
2	0.55	14421	5036
3	0.57	14945	5182
4 (Inner channel)	0.61	15994	5471

Free air convection is assumed at the tool face, but other faces are assumed to be adiabatic; in practice they are insulated with 72 mm of PVC foam with ambient temperature 17°C, the mean mould and the air film temperatures are 53.5°C and 35°C, respectively, according to Equation 2-28. So the properties of air, as listed in Table 5-14, are taken from Holman (2002). Since the Rayleigh number (according to Equation 2-27) is between than 104 and 10^9, the heat transfer coefficient into air, at the tool surface, is 5.7 W/m^2.K according to Equation 3-2. As illustrated in Section 4.6.6 the proper value of 1s is ultimately defined as time step size.

Table 5-14 Air properties at atmospheric pressure and air film temperature of 35°C (Holman, 2002)

Density	Specific Heat	Thermal Conductivity	Expansion Coefficient	Thermal Diffusivity	Kinematic viscosity	Prandtl No.	Rayleigh No.
ρ	c_p	k	α	$\propto$	υ	Pr	Ra_L
kg/m^3	*kJ/kg.K*	*W/m. K*	*1/K*	*m^2/s*	*m^2/s*	-	-
1.147	1.005	2.68 x 10^{-2}	3.26 x 10^{-3}	2.26 x 10^{-2}	1.65 x 10^{-5}	7.1 x 10^{-4}	7.59 x 10^5

5.6.2 Simulation results (case1)

The numerical-calculated temperature at the 'slowest' corner and the centre of the heated area at the tool face are plotted in Figure 5-29 for comparison. Accordingly the 'heating time' (the time to reach a target temperature of 81°C) of 10.3 min is calculated.

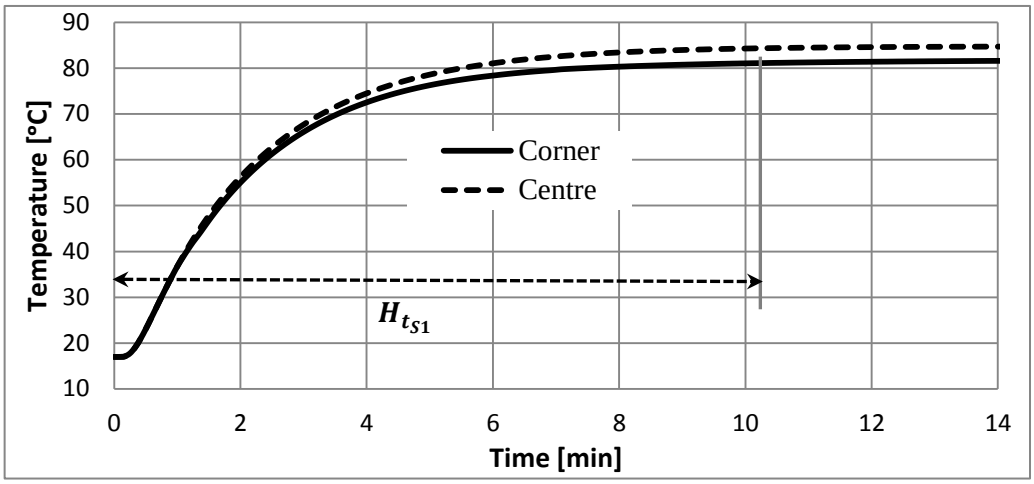

Figure 5-29 Numerical heating curves of points at the centre and slowest corner at the tool model face.

Figures 5-30 and 5-31 show temperature distribution over the whole (heated and extended) part of model tool surface and the heated part only, after the defined heating time, indicating that the maximum temperature over the tool face is 86.2°C.

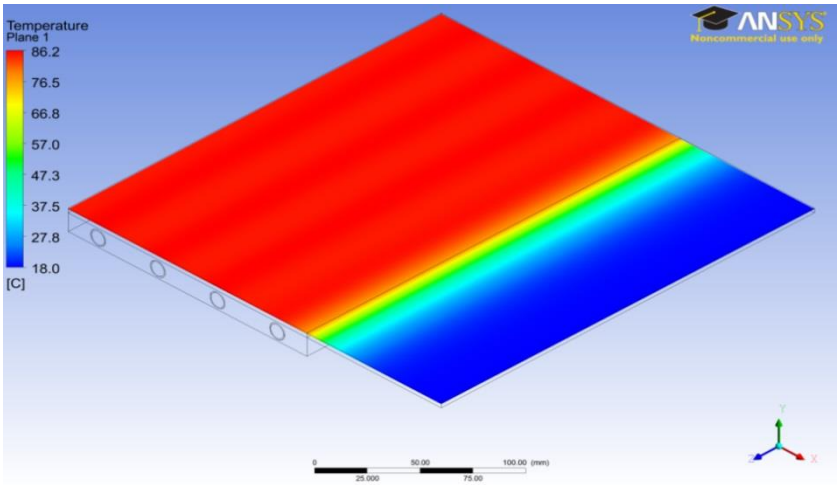

Figure 5-30 Numerical thermal image of the tool model surface (case 1), H_t =10.3 min

Figure 5-31 also shows temperature decreasing zone near the edges of the heated part that starts from the slowest heated point reached 81°C.

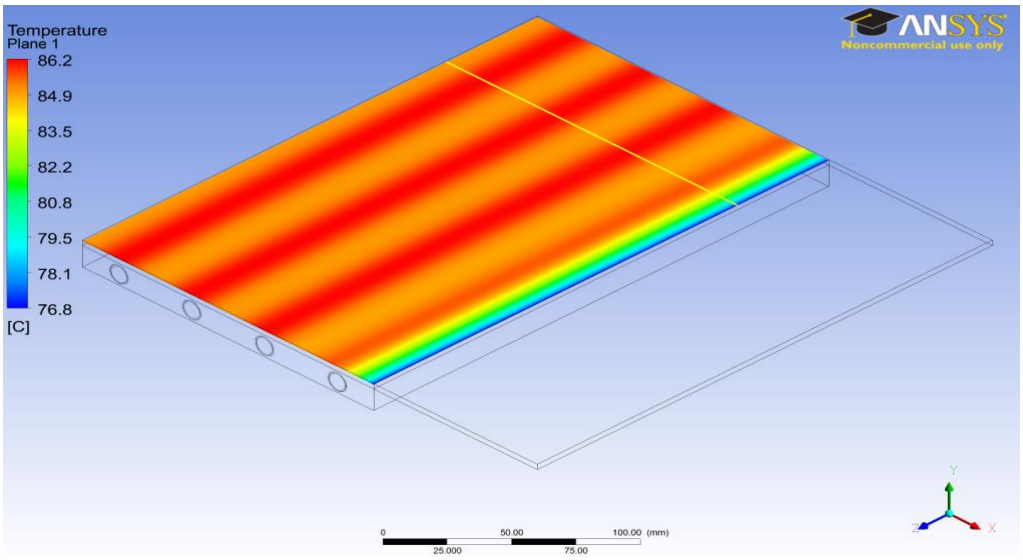

Figure 5-31 Numerical thermal image of the heated part of tool model surface (case 1), H_t = 10.3 min

Temperature distribution along the width of the heated part of the tool model face (the yellow line in Figure 5-31) is plotted in Figure 5-32.

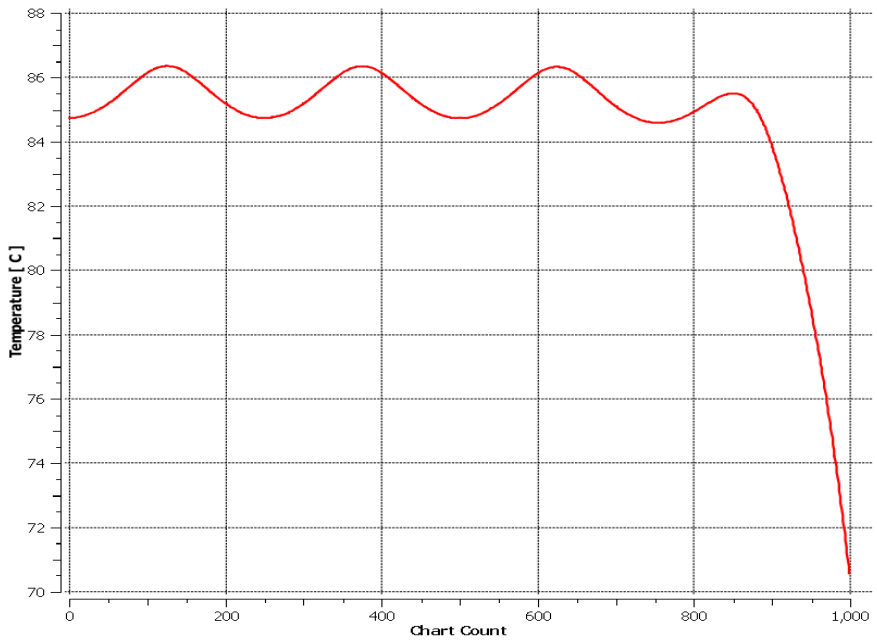

Figure 5-32 Temperature distribution along the half width of the heated part of the tool model surface (case 1), H_t =10.3 min

According to the numerical results of case1, following points could be concluded for comparison with the experimental results:

- Maximum temperature over the tool face is 86.2°C.
- Heating time per unit mass is 1.6 min/kg are according to the heating time and the total mass of experimental tool is 6.3 kg (Table 5-4).
- The average area temperature at the heated part area is 84.6°C and accordingly the temperature variance equals 3.6 °C.
- Width of the thermal gradient zone, from each edge, is about 12 mm.
- Temperature variance along the temperature decreasing zone is about 11°C.
- Temperature of a point over the outer channel is lower than the others by about 1°C.
- The temperature difference between the points over the channels, except the outer, and their middles is about 1.6°C.

5.7 Experimental work

5.7.1 Test rig construction

The experimental test rig (Figure 5-33) consists of the tool connected to a heating unit that has a temperature controller TT-188, type B-0558 produced by Switzerland Tool-Temp Company. The unit is designed to heat water up to 90°C with capacities of 3kW, 6kW and 9kW. It contains a 6 litre filling tank and a centrifugal pump that can provide maximum flow rate of 75 l/min at 4.5 bar pressure. The test rig also includes a flowmeter (Section 5.5.3) to measure the total actual flow rate at the main tool inlet, which is connected temporarily due to its temperature limitation (up to 80°C).

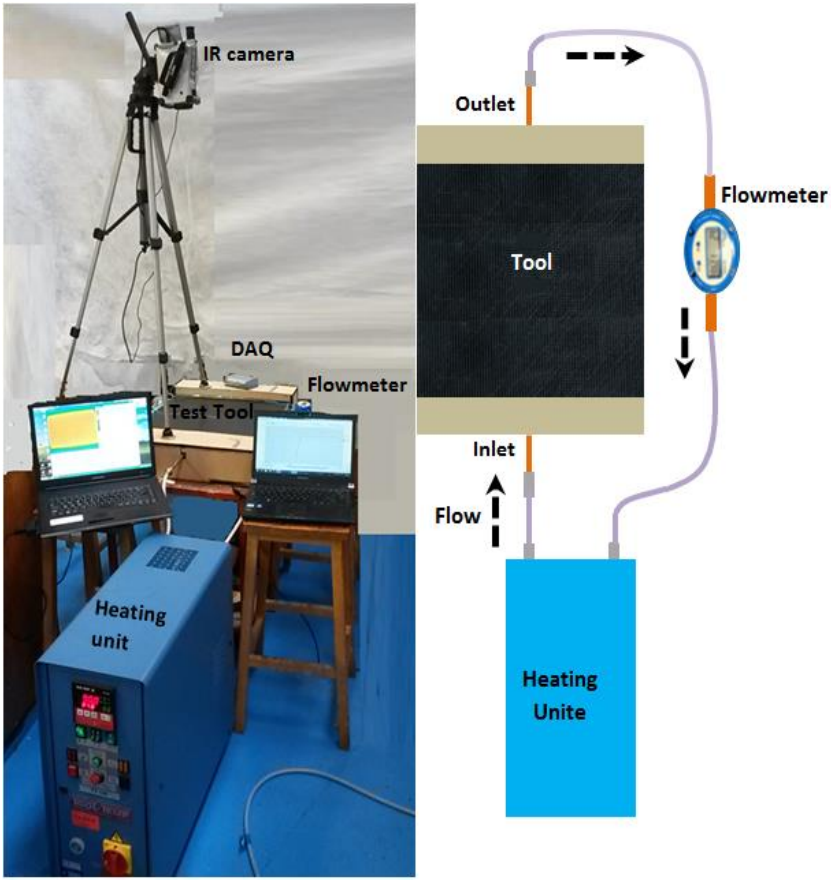

Figure 5-33 Test rig construction

The basic three parts of the test rig are connected temporarily by plastic tubes of 10 mm outside diameter. A USB-TC data acquisition (DAQ) system with eight Input channels is applied to record thermocouple outputs. As well as the permanent embedded thermocouples at the interfaces (Section 5.3.5); some others are joined temporarily to the inlet, outlet and the tool surface centre and corners. An Infrared camera is installed vertically over the tool face to monitor and measure the temperature of the tool surface through thermal images capture.

5.7.2 Experimental test

Initial tests found that the cold water, during tool heating, needs about 10 min to reach 90°C from the ambient (initial) temperature of 17°C, as shown in Figure 5-34. Also the slowest corner on the tool face reaches the target temperature of

81°C, after about 18 min. Therefore the subsequent experiments were performed by pumping hot water, at 90°C, into the tool channel as assumed in the numerical analysis (Section 5.6.1).

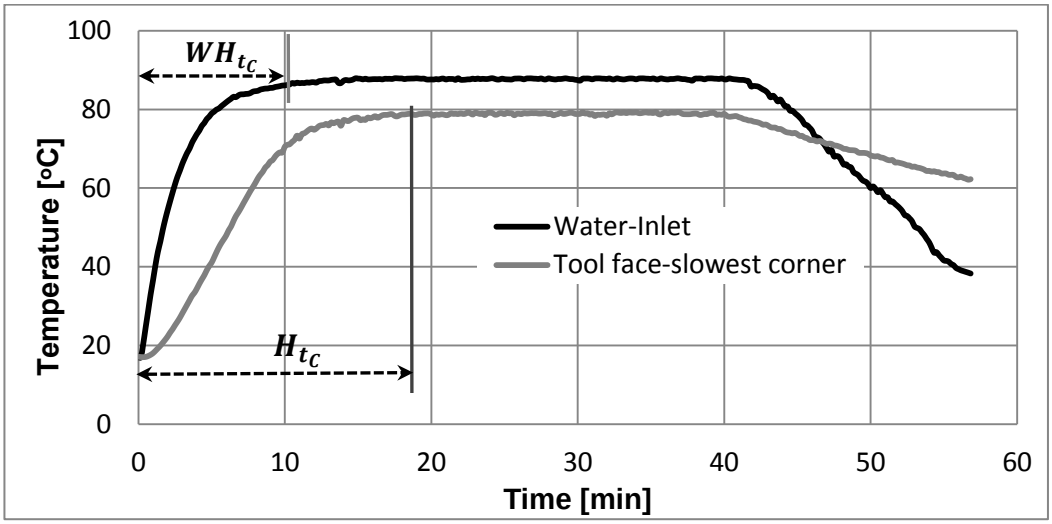

Figure 5-34 Heating curve of points at the inlet and slowest corner of the tool face, the water is cold initially.

As shown in Figure 5-35, hot water also requires 2.8 min to reach 90°C due to the delay in connecting the heating unit with the tool and also refilling the heating unit with extra water to replace the spilled during connection.

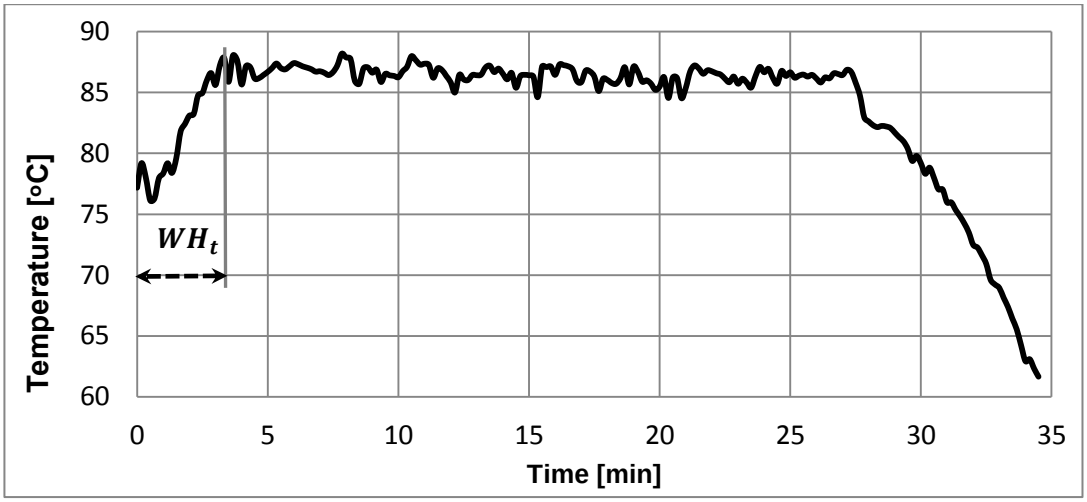

Figure 5-35 Heating curve of a point at the tool inlet, the water is hot initially.

Figure 5-36 presents temperature-time curves of points at the centre and the slowest corner of tool surface measured by the thermocouples and the thermal

camera. The temperature measured by the thermocouples is lower than that by thermal camera due to the systematic error mentioned in Section 5.5.2. It is concluded that the heating time (time required for the slowest corner to reach the target temperature) with hot water is 12.8 min; the actual value is 10 min if the delay time of 2.8 min as the water heated up to 90ºC is deducted.

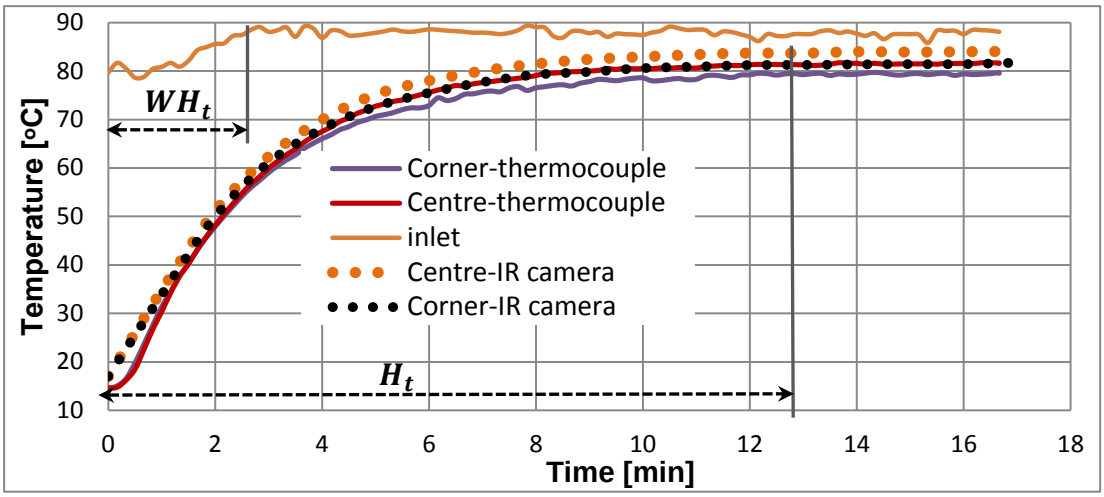

Figure 5-36 Experimental heating curve of points at the centre and corners of the tool face, the water is hot initially.

The image of the experimental tool face captured by the thermal camera with emissivity of 0.94, after 10 min heating, is illustrated in Figure 5-37. The black rectangular area is used by the camera's MicroSpec software to calculate area-weighted average temperature.

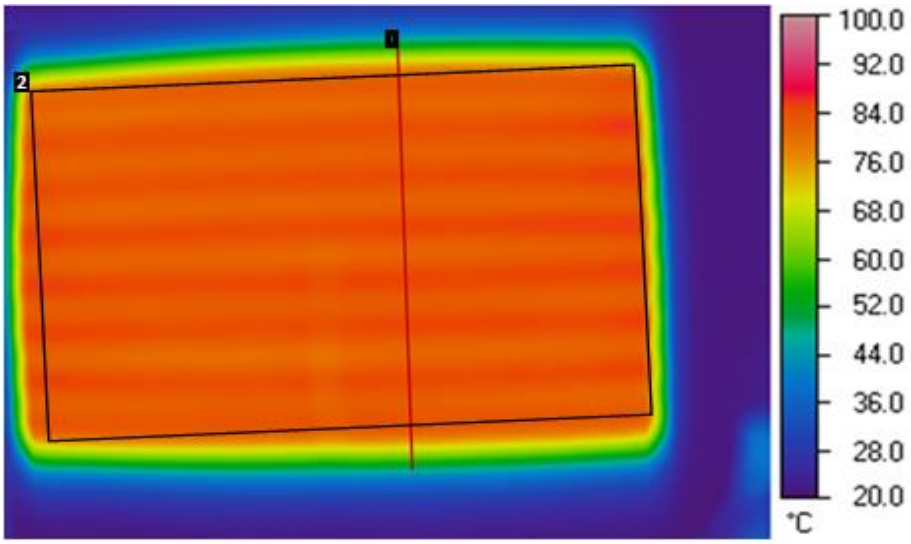

Figure 5-37 Experimental thermal image of the tool face, H_t = 10 min, emissivity = 0.94

Temperature distributions along the width of the tool face (the red line in Figure 5-37), are defined by the MicroSpec software at different times of heating and plotted in Figure 5-38.

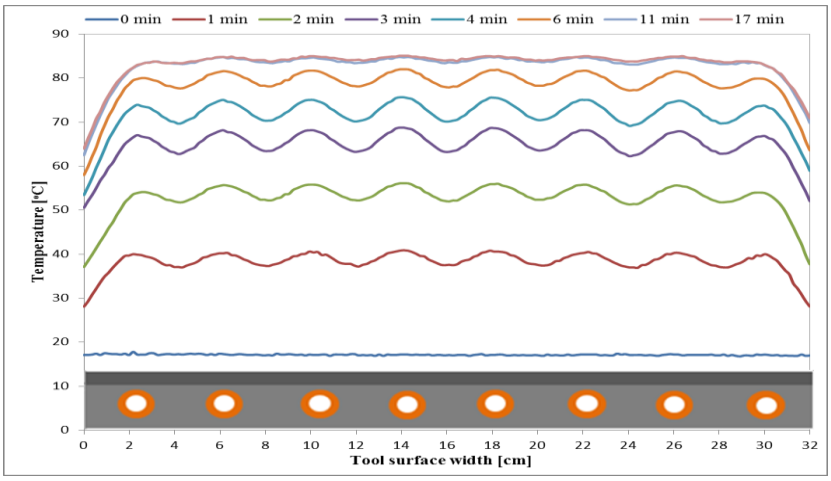

Figure 5-38 Experimental distribution of temperature along the width of the tool surface at different times of heating.

Accordingly the temperature difference between the points over the channels and their middles is about 4°C during the initial stages of heating and reduces to about 1.6°C at the steady state. A temperature decrease can be seen at the both edges of the heated area. Figure 5-39 is plotted by the MicroSpec software and illustrates the temperature distribution along the half width of the experimental tool. The relation is re-plotted in Figure 5-40 versus tool width for further illustration.

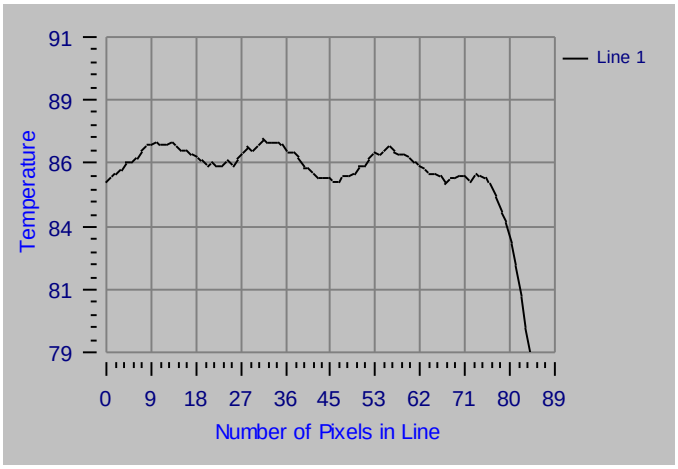

Figure 5-39 Experimental distribution of temperature along a half width of the tool face, H_t = 10 min, plotted by the MicroSpec software

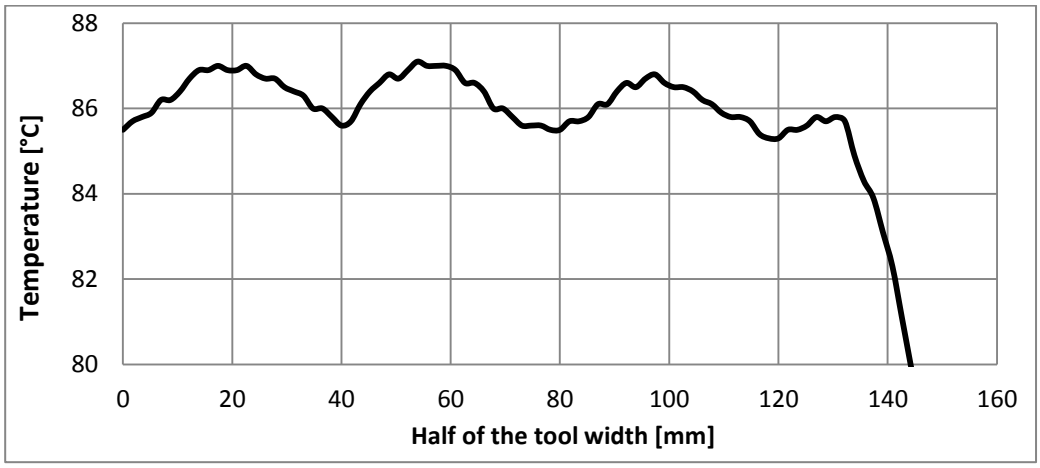

Figure 5-40 Experimental temperature distribution along a half width of the tool face, H_t = 10 min

The following points are drawn from the experimental results to compare with that of the simulation:

- Maximum temperature over the tool face is 87°C.
- Heating time per unit mass is 1.59 min/kg are according to the heating time and the total mass of experimental tool is 6.3 kg (Table 5-4).
- The average area temperature at the heated part area is 84.9°C and accordingly the temperature variance equals 3.9 °C.
- Width of the temperature decreasing zone, from the edges, is about 17 mm.
- Temperature variance along the thermal gradient zone is about 16°C.
- Temperature of a point over the outer channel is lower than the others by about 1.3°C.
    - The temperature difference between points directly over the channels, except the outer, and their middles is about 1.7°C.

5.7.3 Experimental verification

In order to facilitate their comparison, the numerical and experimental results are plotted or listed together as follows:

- The numerical and practical thermal images of the experimental tool face are shown together in Figure 5-41 and show that the temperature distributions resulted largely similar.

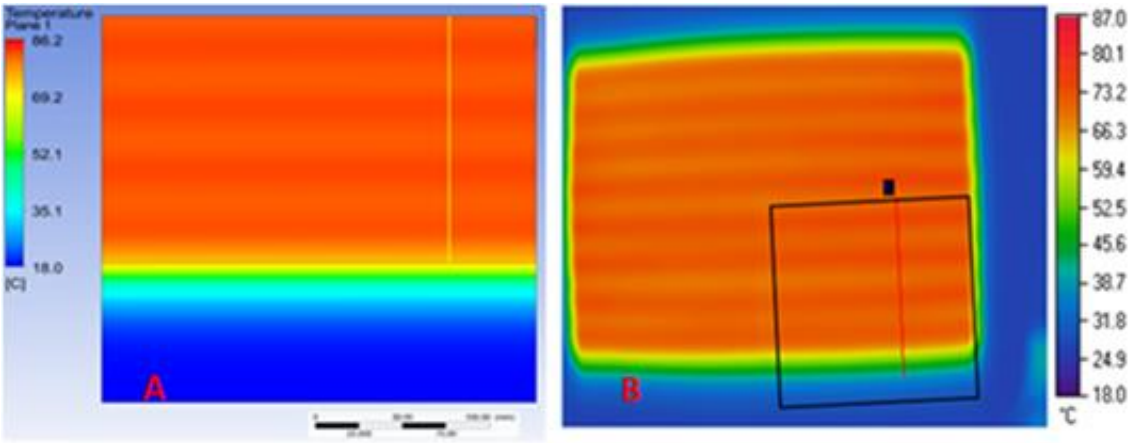

Figure 5-41 Numerical and experimental thermal images of the tool surface at the corresponding heating times. **A**: quarter of the tool model surface, numerically. **B**: total tool surface, experimentally by thermal camera.

- The experimental and numerical isotherm profiles, along a half width of the tool surface (lines showed in Figure 5-41), are presented together in Figure 5-42.

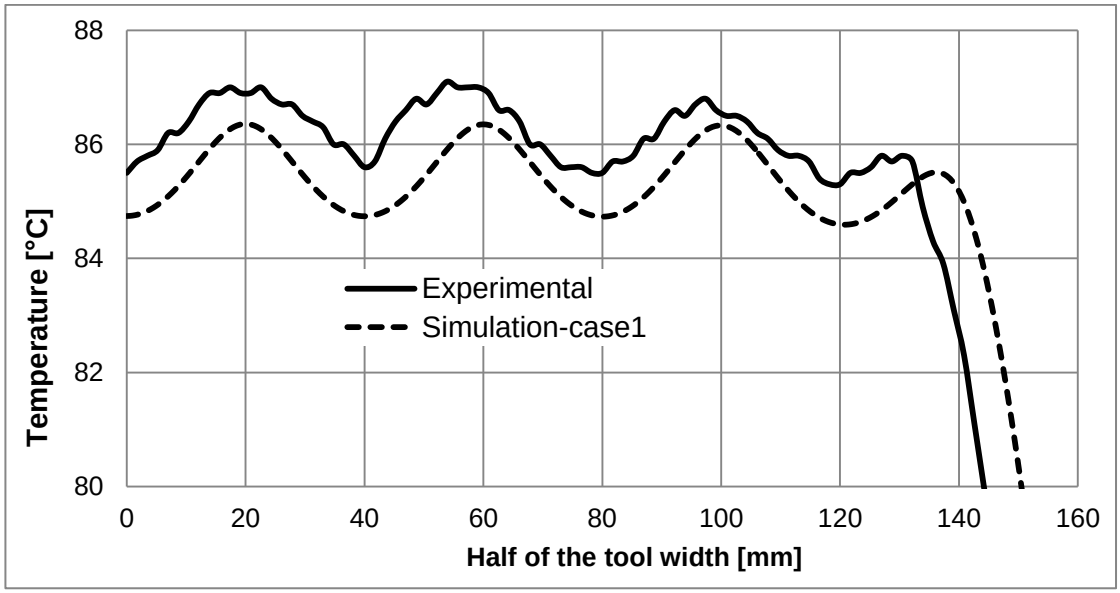

Figure 5-42 Experimental and numerical temperature distribution along a half width of tool face, at the corresponding H_t.

The maximum difference between the numerical and practical temperatures over the tool face varies between 0.3°C and 1°C, which shows a good agreement between the two results. The temperature decrease at the edge is similar for both, although the width of the experimental profile is larger by 6 mm.

- The numerical and experimental transient temperature curves of the slowest corner of the tool face are plotted in Figures 5-43. They show that the experimental heating time is higher due to the delay in the hot water in reaching the desired maximum temperature of 90°C (Section 5.7.2). The thermocouple measurements did not match those of the thermal camera due to the systematic error estimation, but it is acceptable because it falls within the specified tolerance (Section 5.5.2).

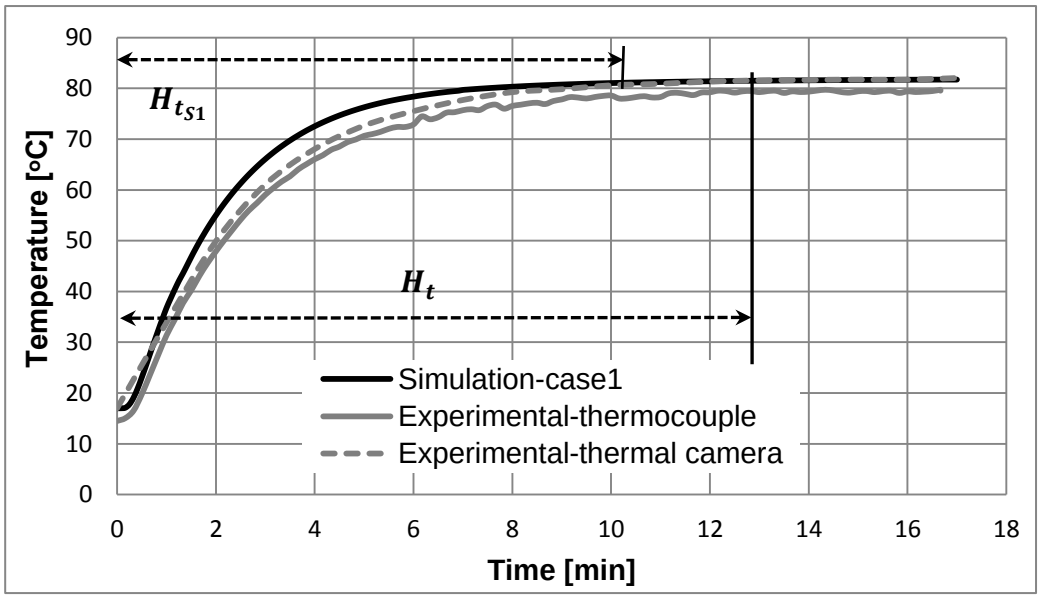

Figure 5-43 Experimental and analytical heating curve of a point at the slowest tool corner.

The various thermal results are summarised in Table 5-15 for comparison and further validation. The table also includes the predicted values of the two optimal designs and their limits that are illustrated in Section 4.8.3.

Table 5-15 Numerical and experimental analysis results of the tool testing, in addition to the predicted optimal values, tool mass is 6.3 kg and target temperature is 81ºC.

Factors of comparison	Units	Simulation (case 1)	Experimental	Predicted Optimal values with limits
Heating time	min	10.3	10	-
Heating time per unit mass	min/kg	1.6	1.59	1.4±0.77 (For the $\mathbf{A_3B_3C_2}$ optimal design)
Area average temperature	ºC	84.6	84.9	
Temperature variation over the tool face	ºC	3.6	3.9	4.7±0.4 (For the $\mathbf{A_3B_3C_1}$ optimal design)
Width of temperature decreasing zone (from the edges)	mm	12	17	-
Temperature decrease at the tool edge	ºC	11	16	-
Temperature difference between the outer and the inner channels	ºC	1	1.3	-
Temperature difference between the points over the inner channels (except the outer) and their between	ºC	1.6	1.6	-

The good agreement between experimental and numerical results confirms that the numerical analysis is successful in defining the heating performance of composite tooling and also that appropriate boundary conditions and material properties were used for simulation. The experimental results also confirm that the predicted optimal design of heating time per unit mass ($A_3B_3C_2$), illustrated in Chapter 4, falls within the predicted limits set by the confidence interval in Section 4.8.3.

the experimental heating time per unit mass is slightly higher than the predicted basic value (without limits) of the optimal design ($A_3B_3C_2$) as will the experimental heating time of the tool (with the amended design) is slightly larger than the theoretical value, while heating time is inversely proportional to surface average area temperature (T_{ave}), as concluded previously (Figure 4-16). Accordingly T_{ave} over the face of the tool will be lower than the optimal design

as will the temperature variation (difference between T_{ave} and target temperature of 81°C). This explains why the temperature variation over the experimental tool is lower than that predicted for the second optimal design of $A_3B_3C_1$ (parallel layout, rectangular profile and 50mm separation of the channel).

The channel distance and low thermal conductivity of the existing materials are the main causes of temperature variation perpendicular to the channel alignment, because the heat requires more time (higher than the target heating time) to spread uniformly through the tool material.

5.8 Improved tool design (case 2)

In order to define effects of the tool face side extensions and flow rate difference between the channels on the heating performance of the tool, a new case (case 2) of the tool model (Figure 5-44) without the extended sides and even flow rate was modelled in ANSYS workbench. Equal flow rate of 1.96 l/min is assumed in the parallel channels with the corresponding heat transfer coefficient of 5127 W/m^2.K.

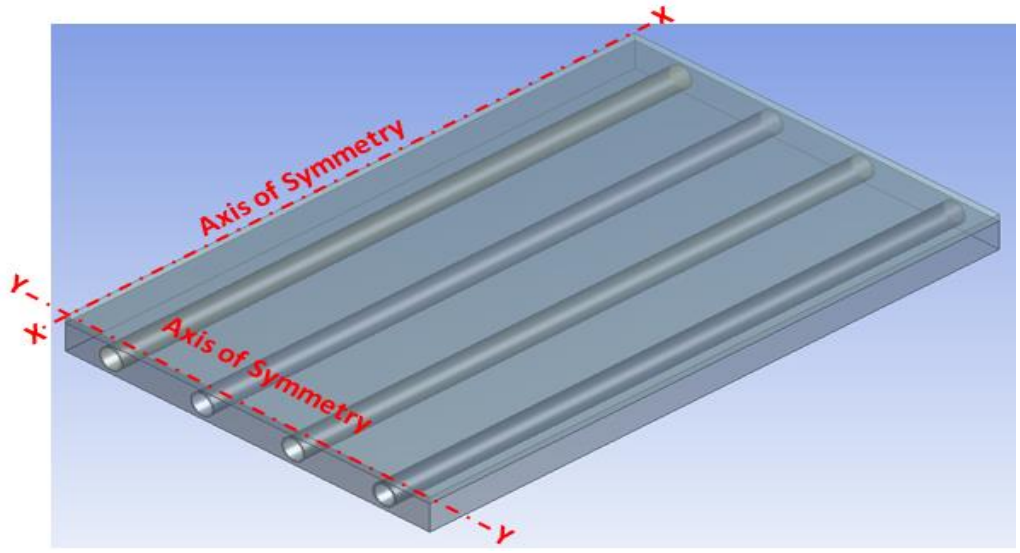

Figure 5-44 Geometry of the improved tool design

5.8.1 Simulation results (case 2)

The transient heating curve of points at the centre and the slowest corner at the model surface (case2) is presented in Figure 5-45. It illustrates that the both points are heat up simultaneously and the slowest corner reaches the target temperature of 81°C after 6.3min.

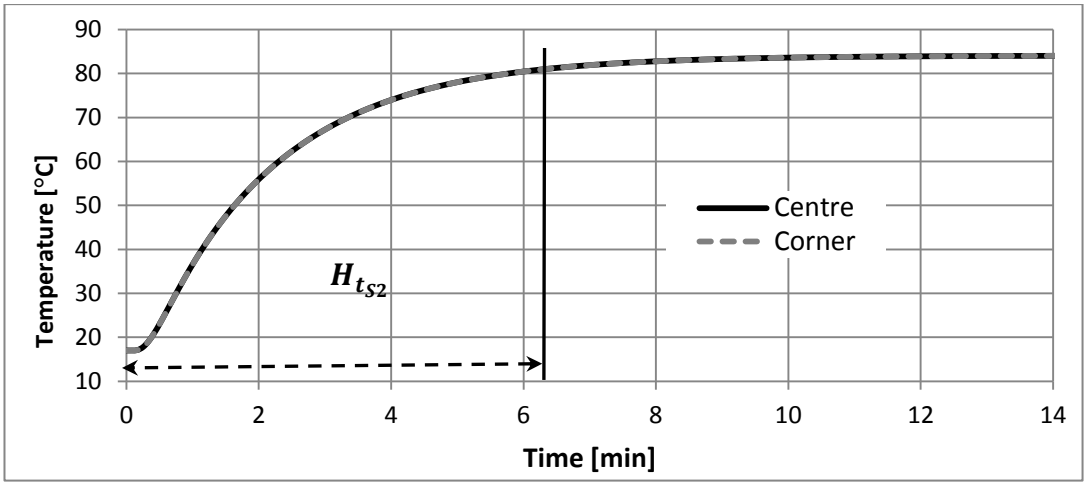

Figure 5-45 Heating curves of points at the centre and corner of the surface of the improved design model (case 2).

Distribution of temperature along the width of the tool face, at the heating time of 6.3 min, is shown in Figure 5-46 and average area temperature is 82.3°C.

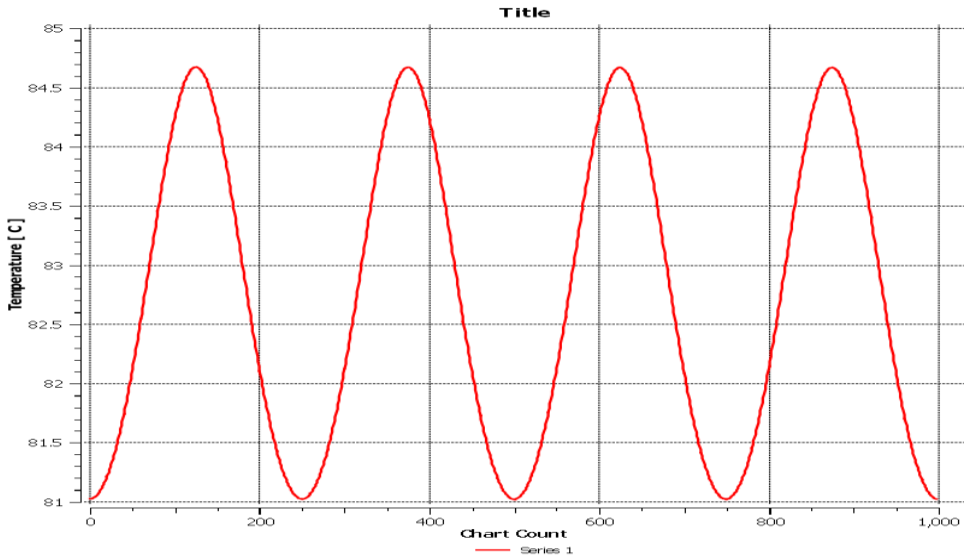

Figure 5-46 Temperature distribution along a half width of the improved tool model surface (case 2), after 6.3 min of heating

However case 2 does not have the problems of thermal decrease near the tool edge and temperature difference between the outer channel and the others, the temperature difference between the points over the channel and those in the middle is very high (4.6°C), compared to case 1 with the basic design (Section 5. 6. 2). Therefore another isotherm, along the face width of the improved tool design model (case 2), is defined at the heating time of 10.3 min to compare with that obtained in Case1 and shown in Figure 5-47 which illustrates that the temperature difference between the points over the channel and those in the middle is reduced to about 1.6°C.

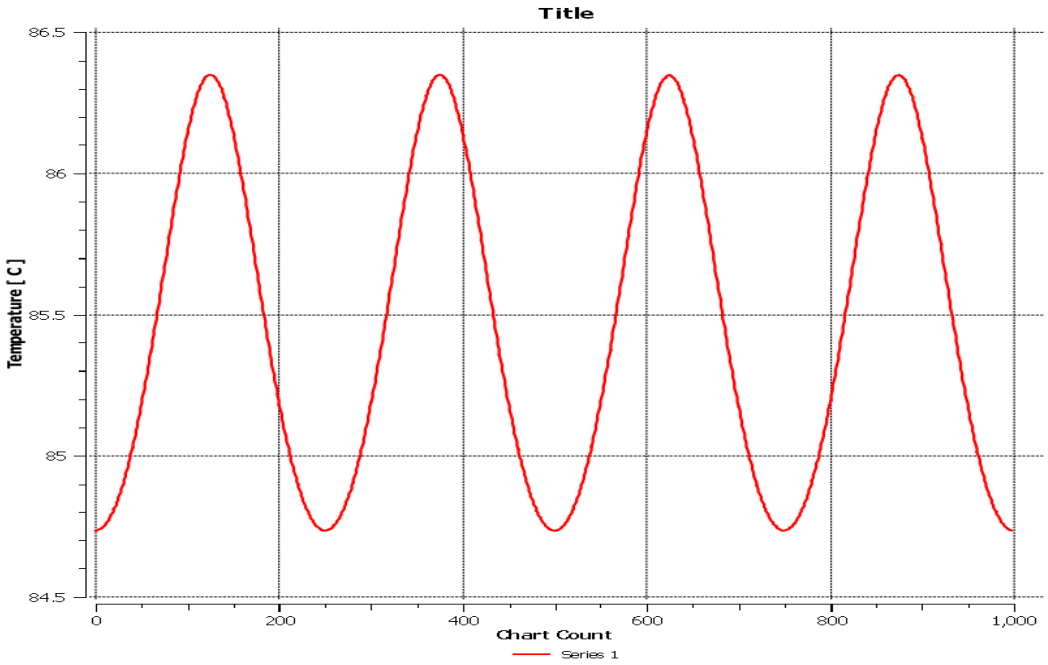

Figure 5-47 Temperature distribution along a half width of the improved tool design model surface (case 2), H_t = 10.3 min

5.8.2 Discussion

In order to compare the both test, the isothermal profiles (along the width of their heated zone surfaces) are plotted together in Figure 5-48, while the transient heating curves of their centre and slowest corner points are presented in Figure 5-49.

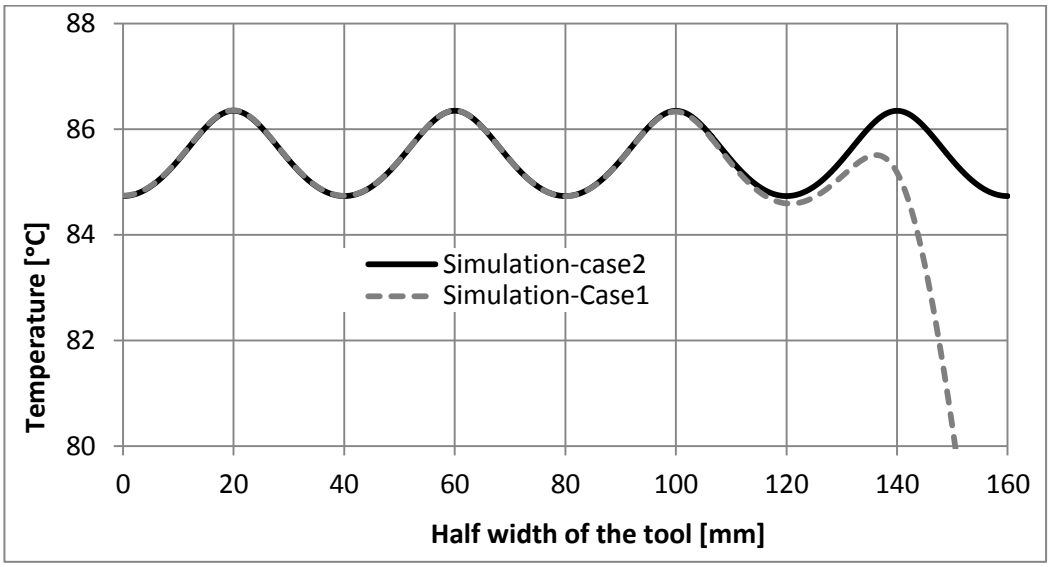

Figure 5-48 Temperature distribution along a half width of the basic and improved tool model surfaces, H_t = 10.3 min

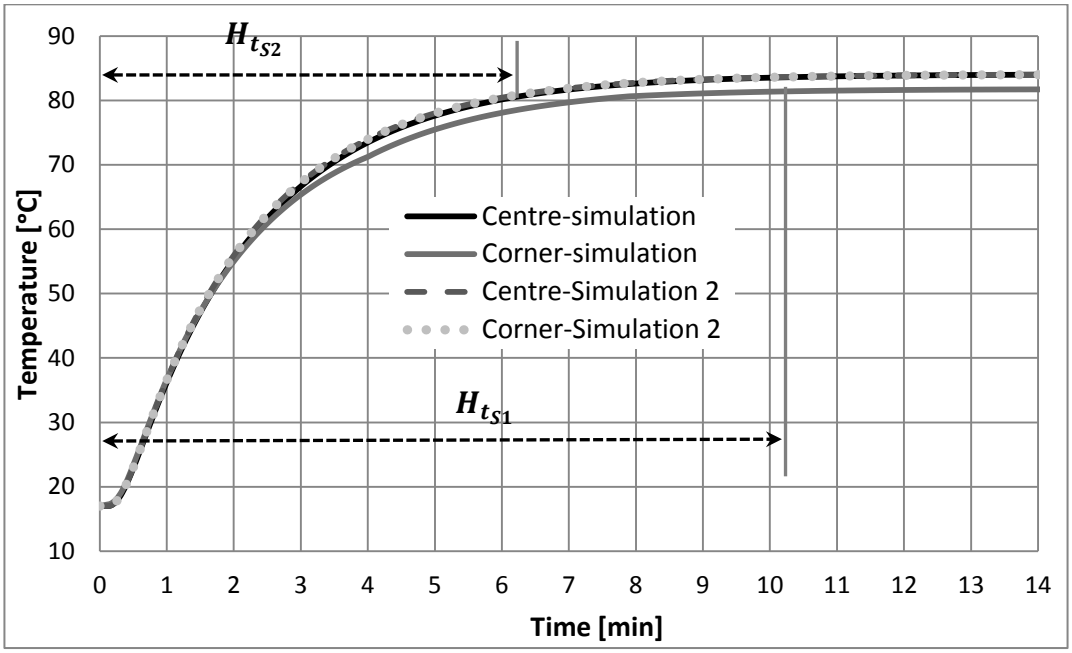

Figure 5-49 Heating curves of points at the centre and the slowest corner of the tool heated zone surface.

Results show that a tool with uniform flow rate and without extended sides can perform heating more efficiently with uniform surface temperature without temperature decreasing near the edges, because the extended edges of the tool face (made of CFRP), in case 1, act as fin in the cooling systems;

especially through the in-plane direction, which possess a relatively high thermal conductivity, compared to the out-plane.

5.9 Conclusion

An experimental tool was manufactured according to the optimal design of $A_3B_3C_2$, which was predicted theoretically, with some amendments to facilitate the production and monitoring of heating performances. The thermal properties of constituent tool materials and boundary conditions were measured experimentally, to set during simulation. A model of the experimental tool is analysed numerically for use in a numerical simulation. The experimental tool is tested practically to verify the predicted optimal design by numerical results. An improved design is proposed to investigate, numerically, the effect of even flow rate in the channels and the extensions of the tool surface on the tool heating performances.

Good agreement between the experimental and numerical results was found, which confirms the suitability of simulation in optimising heating performance and also in appropriate use of the boundary conditions and material properties. Experimental results also confirmed that the optimal design of the integrally water-heated tool falls within the predicted limits set by the confidence interval in section 4.8.3. The improved design shows that both the equal flow rate and the tool face without extension provide higher temperature uniformity and eliminate the temperature decrease zone (near the tool edges) over the tool surface.

Chapter 6
Thermomechanical Analysis of the experimental tool

6.1 Introduction

As the mission of integrally-heated tools are to heat and provide the required curing temperature for processing of composites, they are certainly subjected to various types of thermal loads and deformation, arising from the temperature variation and CTE mismatch between the tool parts. Thermal loads may cause failure the tool and affect its performance, if the tool does not possess adequate strength to resist the generated thermal effects. Therefore a factor of safety (FoS) is applied to provide a design margin over the theoretical design capacity and allow for uncertainty in the design process, which is defined as follows (Paik & Thayamballi, 2003).

$$FOS = \text{tool strength} / \text{thermal load} > 1 \qquad (6\text{-}1)$$

Construction of the heated tool involves different bonded materials (composites and metals) with different CTEs and performs heating up to 90ºC suitable for curing LMT prepreg (Chapters 4 and 5). The tool structure is simulated in ANSYS software to define the behaviour and distribution of the static thermal stresses, strains and deformations caused by temperature variation through the tool geometry. Two models of a bimetallic strip and hollow cylinder are proposed and analysed analytically and numerically to validate the correct assignment of material properties and boundary conditions during the numerical analysis. The linear mechanical properties and CTEs of the tool materials as well as the heating history (transient heating curve) of each tool part (tool surface, Mould and channel) are characterised experimentally and set during the tool modelling. Finally the numerical results of tool thermomechanical behaviour are compared with the measured mechanical properties of the tool material, through the calculation of FoS, to predict the safety and durability of the tool structure during heating.

6.2 Thermomechanical analysis of the heated-tool

6.2.1 Overview of the experimental heated-tool

The experimental water-heated tool involves different parts, i.e. tool surface, mould and channel that are made of CFRP, Alepoxy and copper, respectively (Chapter 5). The materials possess dissimilar thermal properties of conductivity, diffusivity and specific heat, which result in different heating rates for each material. The tool is suitable for moulding a variety of composites with low temperature (90^{o}C) moulding (LTM) liquid resin or prepregs (Chapter 4).

6.2.2 Tool modelling

A quarter of the experimental tool, as shown in Figure 6-1, is modelled in ANSYS workbench using symmetry. Various meshing methods, e.g. edge sizing, sweep and mapped face, are applied to provide lower mesh density (fewer nodes) and better grid connection at the interfaces between the tool parts (Figure 6-2).

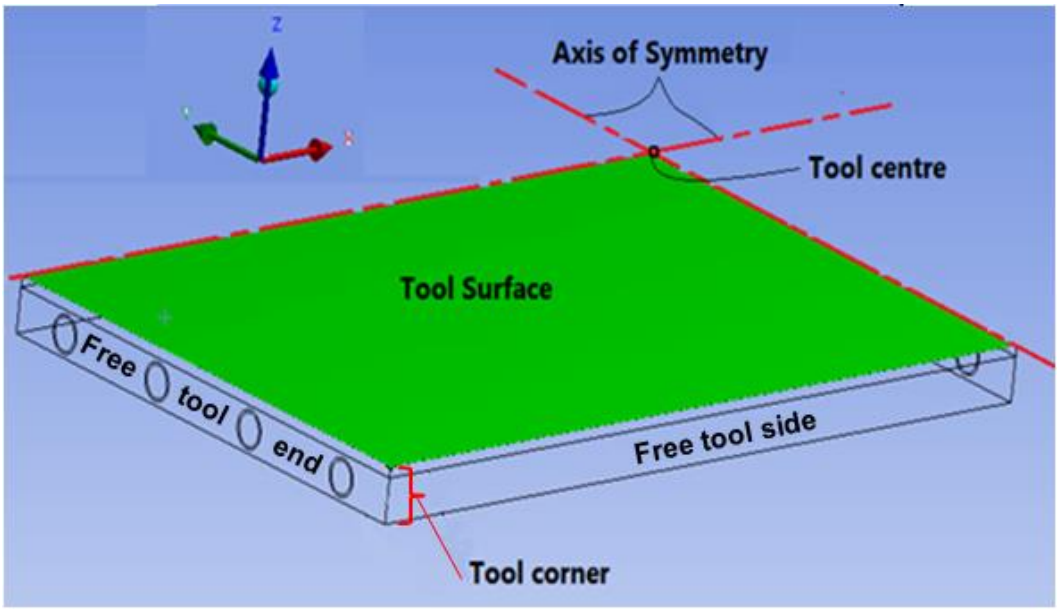

Figure 6-1 The model of a quarter of the experimental tool

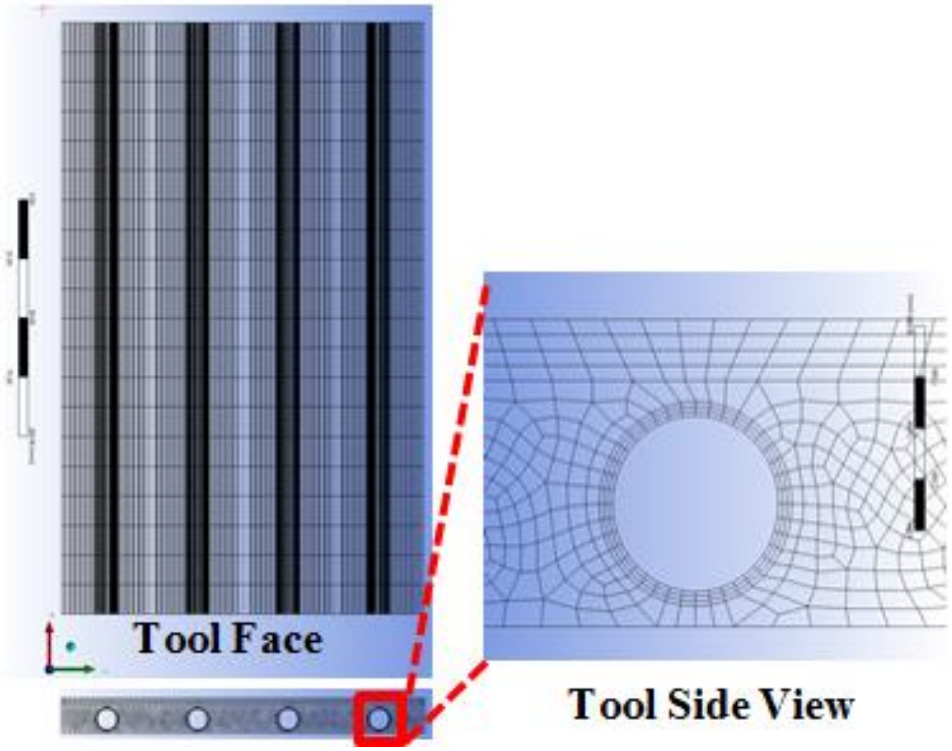

Figure 6-2 Meshing of the experimental tool model.

The mesh quality, as illustrated in Section 3.5.2, is evaluated through the available mesh metric function of the software. The mesh refinement, according to the convergence of a critical result of normal stress at a specified point (see Figure 6-49) over the tool surface, is also performed (Figure 6-3). Accordingly 47,160 elements are preferred because it provides accurate results with lower running time and PC memory required.

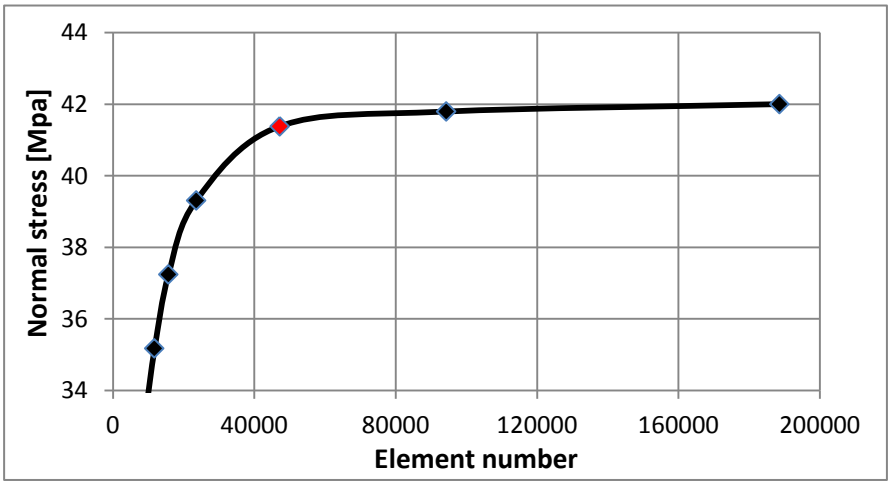

Figure 6-3 Evaluation of the mesh quality by mesh refinement.

The symmetry face (A), as shown in Figure 6-4, is selected as frictionless support face, while the back face (B) of the model is selected to constrain the model displacement in z-direction and prevent rigid body motion during analysis.

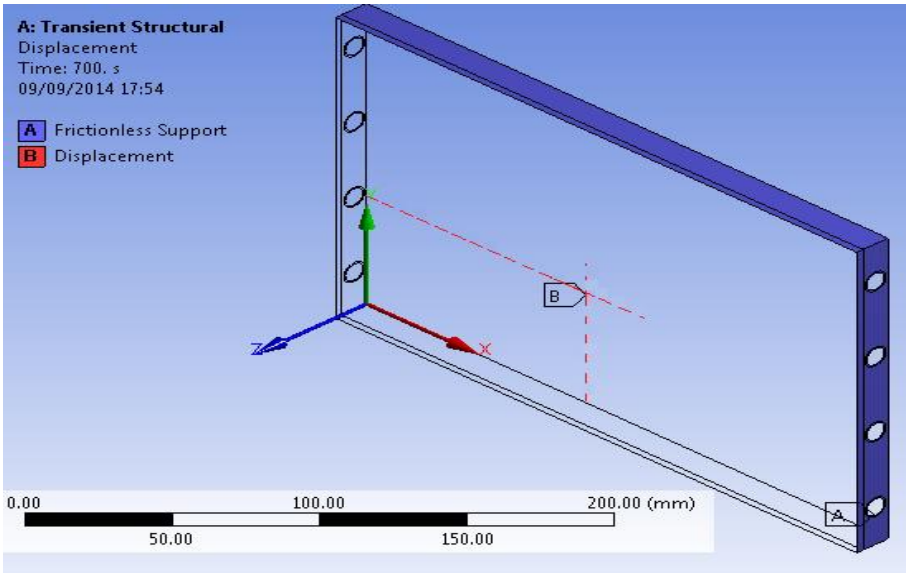

Figure 6-4 The tool model setting for analysis.

6.2.3 Material properties

Analysis of the thermomechanical behaviour of the experimental tool under the effective thermal loads requires the actual mechanical properties and CTEs of the tool materials. Linear mechanical properties and CTE of the tool materials are assumed because of their relatively small variation with temperature and the small heating range of the tool.

6.2.3.1 Mechanical properties

Mechanical properties of pure copper are obtained from that presented in literature by Davis (2001), while the macro-mechanical properties of the lumped composites (CFRP and Alepoxy) are calculated from that of the constituents according to micromechanical rules of mixture (ROM). Alepoxy is a particulate

composite with 0.48 fibre volume fraction (Section 5.3.3), therefore its isotropic (Section 5.4.2) mechanical properties, as listed in Table 6-1, are defined from that of the constituents obtained from literature by the transverse rule of mixture as follows (Richardson, 2012):

$$P_{co} = \frac{P_f P_m}{P_m V_f + P_f(1-V_f)} \qquad (6\text{- }2)$$

Table 6-1 Isotropic mechanical properties of Copper, Alepoxy and its components, (V_f = 0.48).

Mechanical Properties	**Symbol**	**Unit**	**Copper[1]**	**Al[2]** (particle)	**Matrix[2]** (SR8500)	**Alepoxy**
Poisson's ratio	ν	-	0.34	0.345	0.336	0.34
Modulus of Elasticity	E	MPa	$11x10^4$	$71x10^3$	3350	6170
Shear Modulus	G		$41x10^3$	$26x10^3$	2402	2300
Ultimate tensile strength	σ_{uT}		430	310	80	124
Ultimate Compressive strength	σ_{uC}		- 430	607	120	195
Shear strength	τ		172	207	108	140
Tensile yield strength	σ_{yT}		280	280	70	110
Compressive yield strength	σ_{yC}		-280			

1.(Davis, 2001) 2.(East Coast, 2013; Sicomin-Composites, 2013)

The CFRP laminate is an orthotropic composite and mechanical properties of the constituents (carbon non-crimp triaxial fibre and SR8100 epoxy) are defined in Autodesk (2013) software, according to the following plan, as illustrated in Figure 6-5.

- The flexural modulus of the tool face (CFRP laminate) is measured practically, using three-point bending test in accordance with ASTM D790-07 at a span to depth ratio of 32 (Petrescu, Mohora & Ispas, 2013). The flexural test is performed on an Instron 3367 machine, after preparing the uniform rectangular specimens following the proper methodology as defined by Dowling *et al.* (2013), Philpot (2011) and (1998). A flexural modulus of 44.28 GPa is obtained for the CFRP laminate.

- Different CFRP laminas with the actual volume fraction of 0.53 are designed by the available matrices and carbon fibres in the Autodesk software, Figure L-1 (Appendix L).

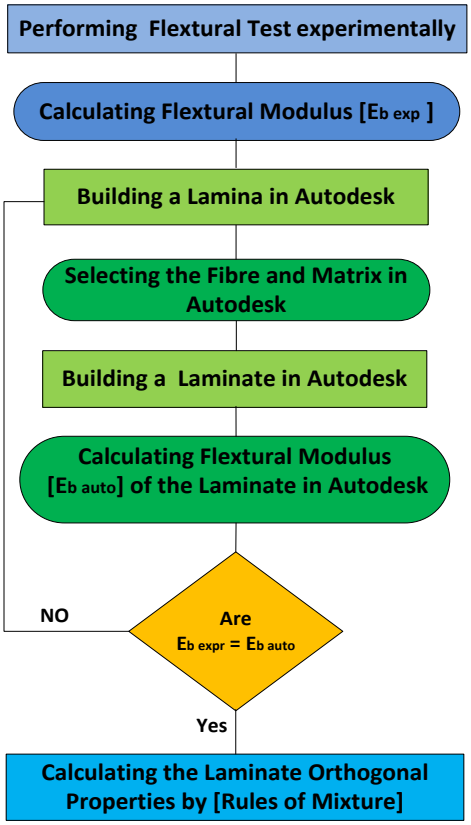

Figure 6-5 Plan of calculating the mechanical properties of CFRP laminate.

- Autodesk defines properties of each lamina formed (Figure L-2).
- Different CFRP laminates, with a fibre orientation of $[45, 0, -45, -45, 90, 45]_S$ and a ply thickness of 0.26 mm, are built in Autodesk by each of the aforementioned laminas (Figure L-3).
- Autodesk also defines the properties of each laminate constructed including flexural modulus as shown in Figure L-4.
- The calculated flexural modulus of each laminate, constructed in Autodesk, is compared with that calculated experimentally to find the one most similar and its mechanical properties are considered as those of the real CFRP laminate.

Figure L-4 illustrates the orthotropic properties of the selected (the one most similar) laminate, which has a closest flexural modulus of 44.05 GPa. Its constituents are (T300 Carbon) and (MY750-Epoxy) with the mechanical properties indicated in Figure L-5. Accordingly the desired orthotropic mechanical properties of the actual CFRP laminate are defined (Table 6-2).

Table 6-2 Orthotropic mechanical properties of the CFRP laminate, $V_f = 0.53$

Properties	**Symbol**	**Units**	**Fibre**	**Matrix**	**CFRP Laminate**	
					In-plane	Out-plane
Poisson's ratio	υ	-	From Autodesk		0.451	0.219
Modulus of elasticity	E	MPa			35700	8100
Shear modulus	G				21500	2830
Tensile strength	σ_T		3530	80	739	164
Compressive strength	σ_C		- 2181	-120	- 490	- 240
Shear Strength	τ		21.94	113	53	50

6.2.3.2 Coefficient of thermal expansion (CTE)

The electrical resistance strain gauge is the most common technique for measuring coefficient of thermal expansion (CTE) in accordance with the ASTM D5335-14 standard test method (NEN, 2014). The method determines the test material CTE by comparing with that of a reference material with a known expansion characteristic (IPC, 2000; Joven *et al.*, 2012; Scalea, 1998). In this PhD study, a copper plate is selected as a reference material, which is analysed by X-ray Fluorescence (XRF) method to define the composition as listed in Table 6-3. The analysis is achieved in the School of Geography, Earth and Environmental Sciences laboratories at Plymouth University.

Table 6-3 The reference material (copper) composition, XRF method.

Composition	**Cu**	**Pb**	**Ba**	**Cr**	**Ag**	**Sn**	**Fe**	**V**
%	99.8036	0.1152	0.0303	0.0062	0.0042	0.0113	0.0256	0.0037

Consequently the desired CTE of the reference copper plate is defined as that of C18700 type copper from literature and equals $17.7x10^{-6^{o}}C^{-1}$ (Davis, 2001). The applied gauges, in the current test, are linear SGD-10 type and have 1000Ω resistance, 2.13 gauge factor and ± 0.235% tolerance. The thermal expansion tests are achieved as follows.

- A flat square specimen of 50 mm length and 3 mm thickness is prepared for each of the reference (copper), CFRP and Alepoxy materials.
- Two gauges, as shown in Figure 6-6A, are attached to the Alepoxy specimen in the directions of x and y, to capture the expected in-plane expansion characteristic of the isotropic Alepoxy, while three gauges (Figure 6-6B) are mounted on each of the reference and the CFRP samples in the directions of x, y and there between at 45° because of the orthotropic behaviour of CFRP material (Micro-Measurements, 2010; Scalea, 1998).

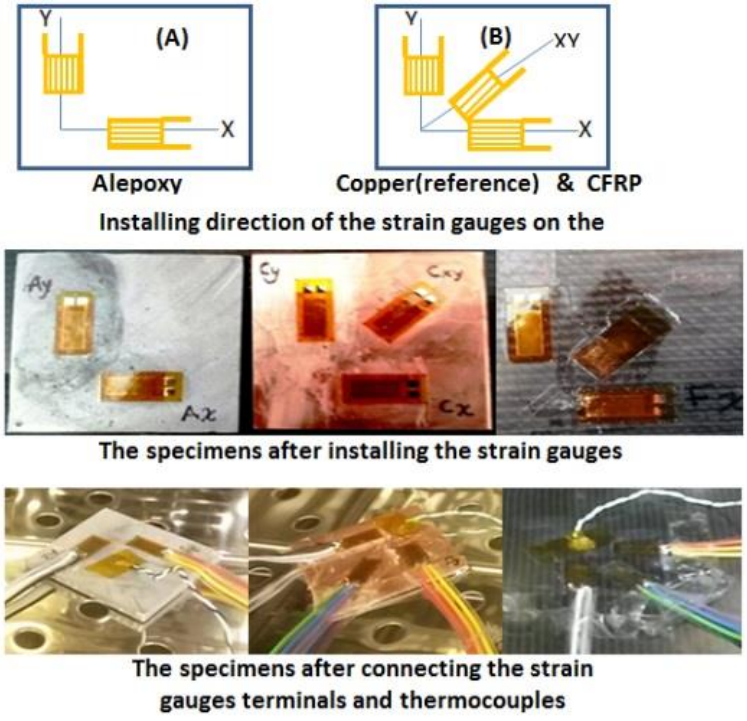

Figure 6-6 CTE test specimens.

- A K-type thermocouple (Section 5.5.2) is mounted on each specimen, in adjacent to the strain gauges within 6mm, which are connected to a USB-TC data acquisition DAQ to indicate the specimen and the gauge temperature during heating.
- The strain gauges are also connected separately to a strain indicator and recorder device using quarter-bridge circuits as shown in Figure 6-7.

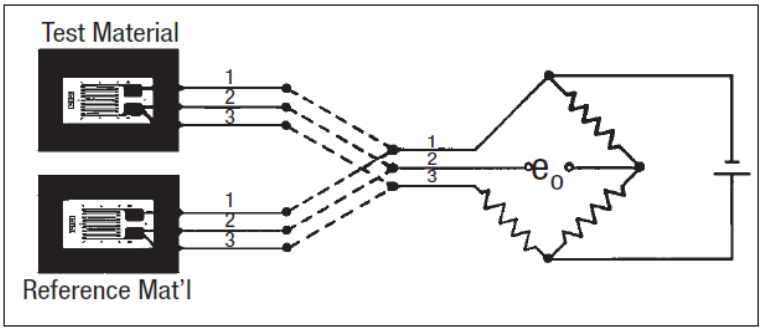

Figure 6-7 Separate quarter bridge circuit method for connecting the strain gauges (Micro-Measurements, 2010).

The strain indicator device of Micro-Measurement, MM type and P3-A105 model (± 0.1% reading accuracy of ± 3 count) is produced by Vishay precision group to record and save the output data (thermal apparent strain) of the strain gauges (Micro-Measurements, 2011). Figure 6-8 illustrates the connection mode of strain gauge terminals to the channels of the strain indicator.

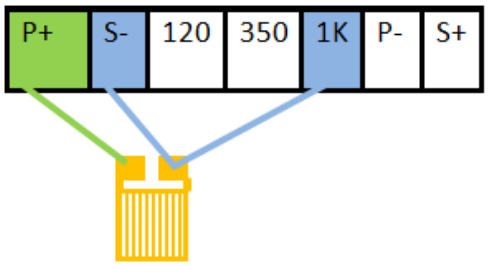

Figure 6-8 Connection of strain gauge terminals to the channels of the strain indicator device.

- The specimens are placed in an oven (Heraeus type 6420), while they are connected to the measuring devices outside the oven.
- The temperature controller of the oven is set according to a heating curve between 30ºC and 90ºC, as illustrated in Figure 6-9, with a ramp rate of 2°C/min and two dwells of 1.30 h and 1h, respectively.

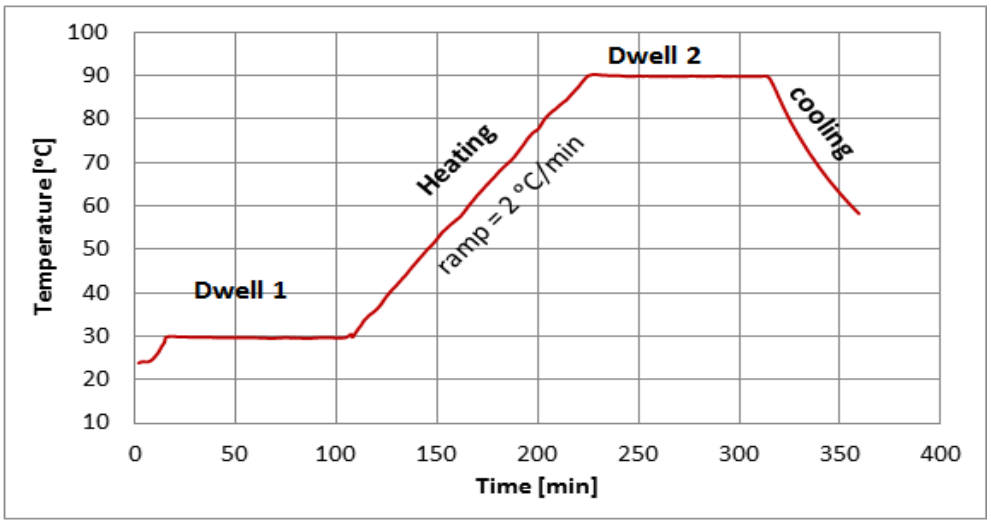

Figure 6-9 The heating curve of the specimens during the CTE test

- The outputs (apparent thermal strain) of the adjacent strain gauges are plotted versus the recorded heating temperature. Figure 6-10 shows results of the x-axis test.

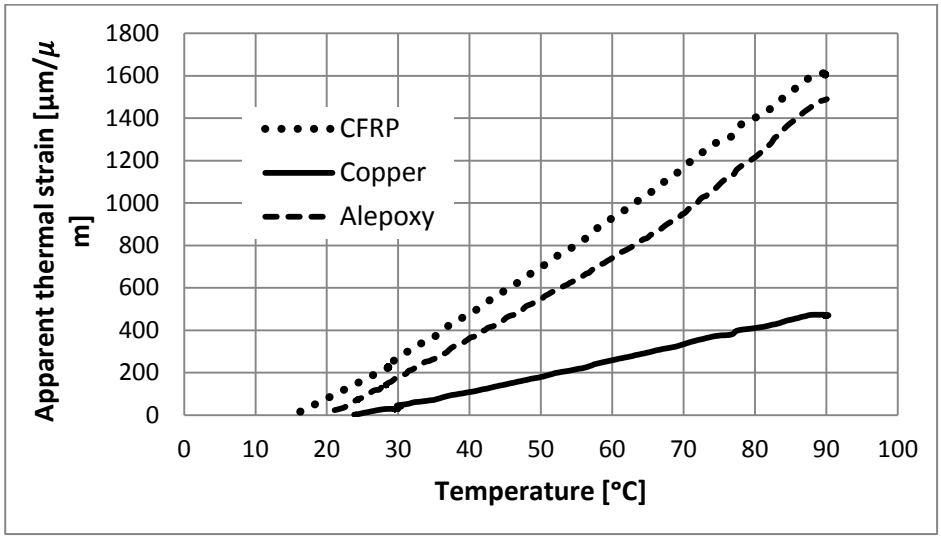

Figure 6-10 X-axis thermal strains of the specimens.

- Consequently the CTE values of the test materials, as listed in Table 6-4, are calculated by the following expressions (IPC, 2000).

$$\alpha_m = \alpha_r + \frac{\Delta\varepsilon_m - \Delta\varepsilon_r}{\Delta T} \qquad (6\text{- }3)$$

Where $\Delta T = T_{max} - T_{min}$, $\Delta\varepsilon_m = \varepsilon_{m_{max}} - \varepsilon_{m_{min}}$ and $\Delta\varepsilon_r = \varepsilon_{r_{max}} - \varepsilon_{r_{min}}$

Table 6-4 The tool materials CTE test results.

Direction		Δ **ε** (between 30 °C to 90 °C) m/m			**CTE** 10^{-6} m/m °C^{-1}		
		Cu	Alepoxy	CFRP	Cu	Alepoxy	CFRP
in-plane	X	-4.4 x 10^{-4}	1.28 x10^{-3}	-1.38 x 10^{-3}	17.7	32	1.9
	Y	-4.6 x 10^{-4}	1.33 x10^{-3}	-1.41 x 10^{-3}		32	1.8
	XY	-3.4 x 10^{-4}	-	-1.27 x 10^{-3}		-	2.1
	Average XY	measured				32	1.9
out-plane Z		calculated				32	2.26

The CTE test results show that the in-plane (longitudinal and traverse) CTEs of Alepoxy are quite similar, but a difference of about ± 0.1 x 10^{-6} °C^{-1} exists for the CFRP, therefore an average of 1.9 x 10^{-6} °C^{-1} is used. The through-thickness CTE of Alepoxy is assumed to be equal to its in-plane due to its isotropic behaviour (Section 5.4.2), but the out-plane CTE of CFRP laminate differs from that of the in-plane because of the orthotropic behaviour. The out-of-plane CTE of the CFRP cannot be measured experimentally because its thickness is too small, therefore the through-thickness CTE of the CFRP laminate is calculated by the ROM according to the in-plane CTE of the laminate and that of the fibre equals 1.2 x 10^{-6} °C^{-1} (Figure L-5).

6.2.4 Transient heating boundary of the tool parts

With a number of K-type thermocouples distributed at the tool interfaces between the mould tool face and the channel as well as at the tool back face, as illustrated in Section 5.7, the instantaneous temperature change of each tool

part was measured (Section 5.7.2) at various points and their average is defined as the heating curve of the part, as plotted in Figure 6-11.

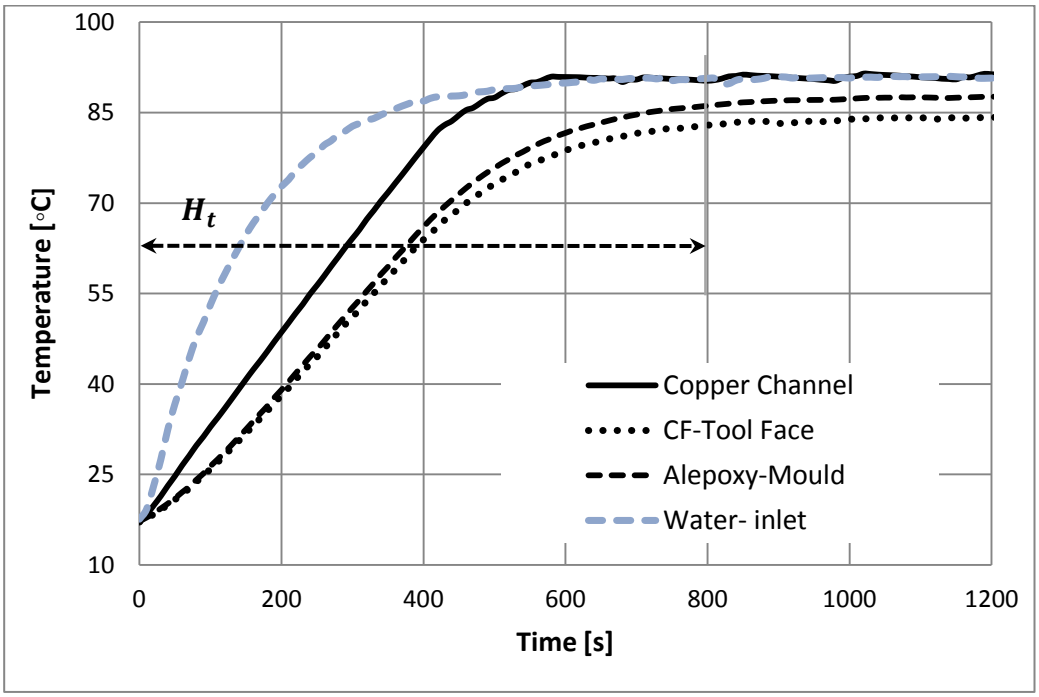

Figure 6-11 Heating curves of the tool parts.

Accordingly the fastest and the slowest heated parts, the channel (copper) and the tool face (CFRP), respectively, are defined. The maximum temperature variation between them is 15.6°C and occurs after about 400s then reduces to 6.8°C (steady state) at about 800s. Consequently the heating period of 700s is selected for defining and setting the transient heating boundaries of each tool part during simulation.

6.2.5 Verification

Two simple analytical models, a bimaterial strip and a hollow cylinder, are proposed in this PhD study to validate the correct assigning of boundary conditions and material properties during simulating the experimental tool structure under the effective thermal loads.

6.2.5.1 Bi-metallic strip model

The proposed model, as defined by Eischen et al. (1990), is a bimetallic strip of aluminium (at the bottom) and molybdenum (at the top), Figure 2-9, that works under an assumed temperature change of 240°C. Dimensions and properties of the strip are listed in Table 6-5 and total length of the strip is 50.8 mm.

Table 6-5 Dimensions and properties of the bimetallic strip (Eischen, Chung & Kim, 1990).

Details	Symbol	Units	Al -Strip	Mo - Strip	Bi-metallic Strip
			High dilatable	Low dilatable	
Height	h	mm	2.5	2.5	5
Half length	L	mm	25.4	25.4	25.4
Width	w	mm	1	1	1
Modulus of elasticity	E	GPa	71	325	-
CTE	α	10^{-6}°C^{-1}	23.6	4.90	-
Poisson's ratio	υ	-	0.345	0.293	-

The materials of the bimetallic strip model are defined as low (Mo) and high (Al) dilatable or expandable according to their thermal expansion. The deflection and the normal stress extremes (maximum and minimum) are calculated analytically, using Timoshenko's (1925) model for the bimetallic strip that requires calculation of curvature radius, generated axial forces, initially, and bending moments, as illustrated in Appendix A (Timoshenko, 1925; Timoshenko & Goodier, 1951).

Half of the bimetallic strip is modelled in ANSYS workbench using symmetry, and a frictionless support is imposed at the symmetry plane (A), as illustrated in Figure 6-12. Four vortices on the corners of the symmetry plane are selected to constrain the motion of model in the z-direction only. The model is meshed by a sizing method that enables smooth meshing at the interface and its surrounding. Accordingly the model is split into 14.7×10^3 elements (Figure6-13).

The mesh quality, as illustrated in Section 3.5.2, is also checked through the available mesh metric function of the software.

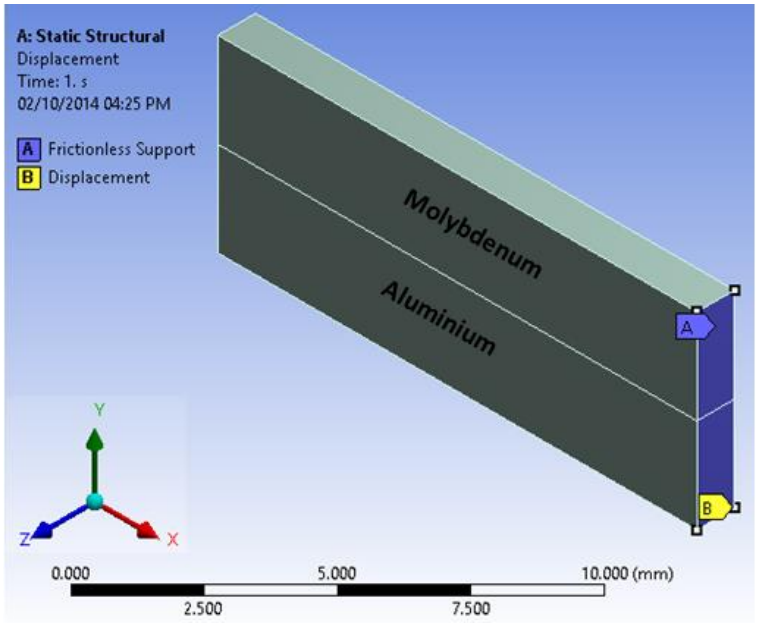

Figure 6-12 Symmetry and displacement surfaces of the bimetallic strip model in ANSYS workbench

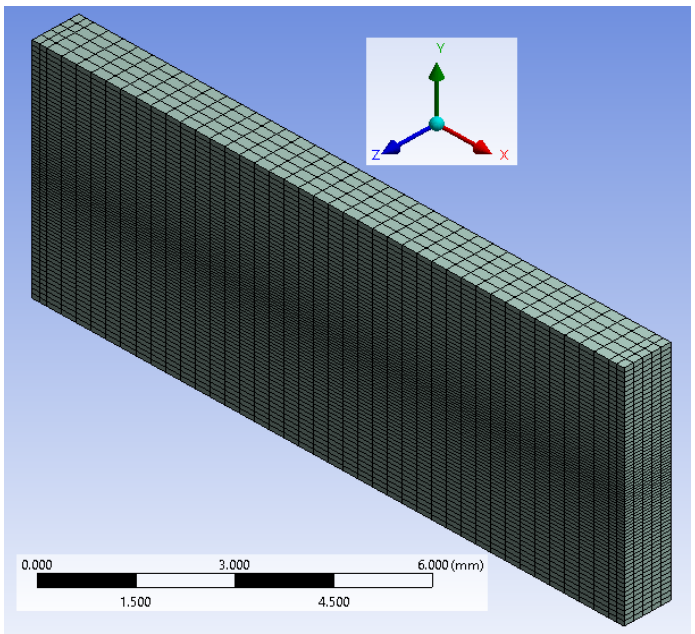

Figure 6-13 Meshing of the bimetallic model, using sizing method

Distribution of the longitudinal (x-axis) normal stress and directional (y-axis) deformation in the bimetallic strip, according to the numerical results, are illustrated in Figures 6-14 and 6-15, respectively. Accordingly the maximum and minimum amounts are defined and listed with the analytical results in Table 6-6,

and absolute difference is calculated between the both values of each characteristic.

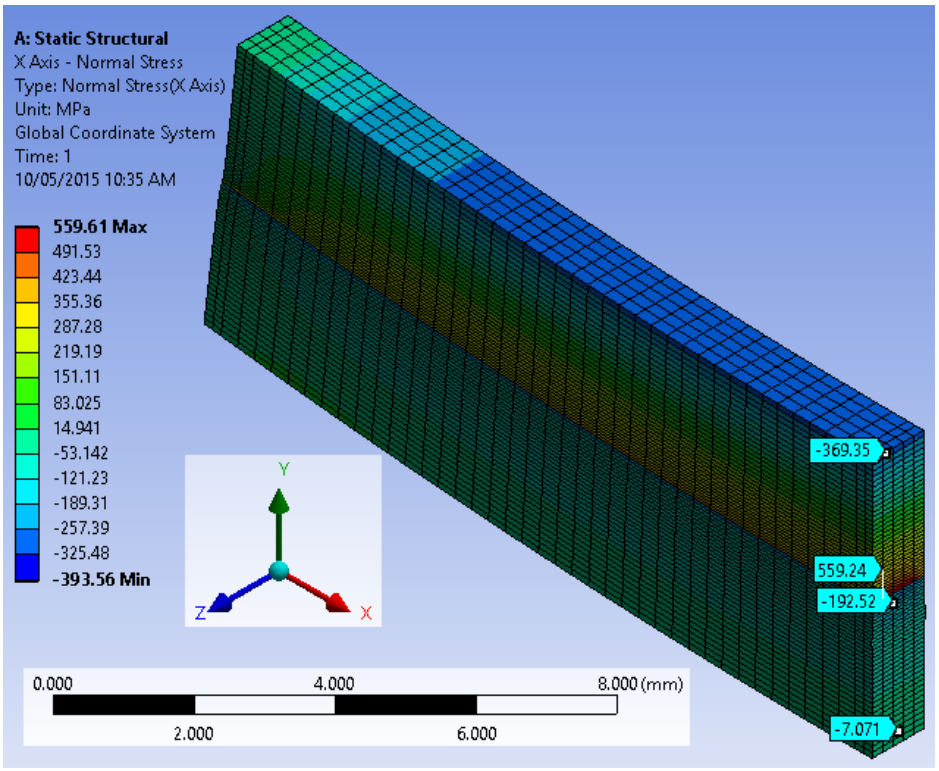

Figure 6-14 Longitudinal (x-axis) normal stresses in the bimetallic strip.

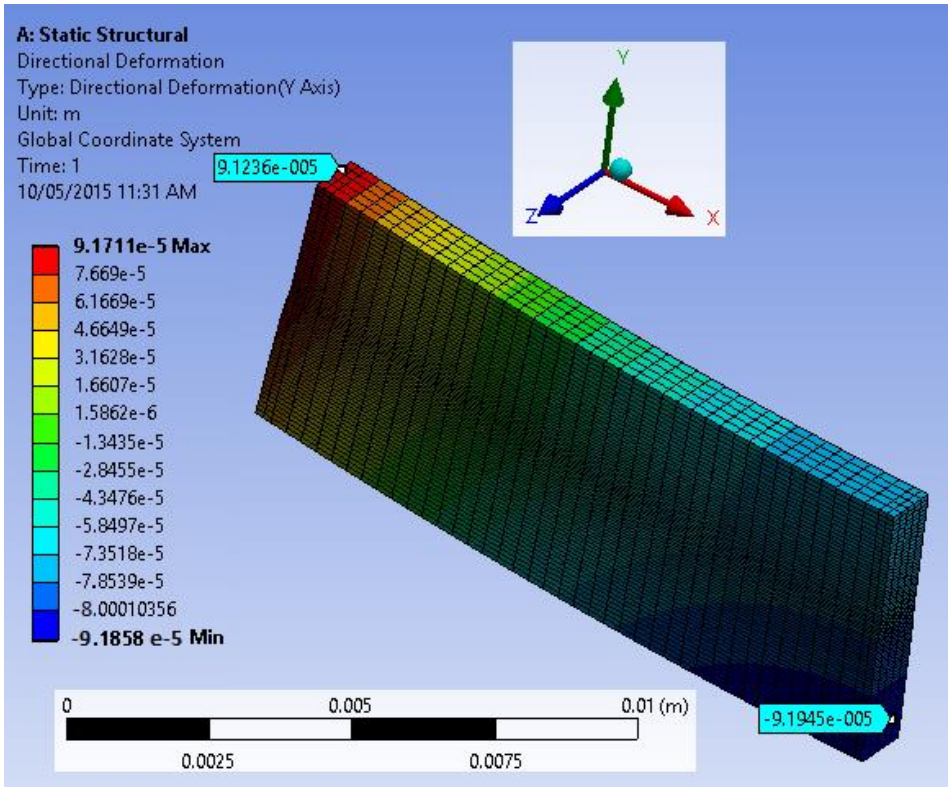

Figure 6-15 Longitudinal (x-axis) deformation in the bimetallic strip.

Table 6-6 Numerical and analytical results of of the bimetallic strip analysis

Analysis methods	δ	$\sigma_{H_{max}}$	$\sigma_{H_{min}}$	$\sigma_{L_{max}}$	$\sigma_{L_{min}}$
	mm	MPa			
Analytic	9.23×10^{-2}	-6.6	-192.6	559	-369
Numerical	9.17×10^{-2}	-7.1	-192.53	559.2	-369.4
Absolute difference percentage	0.7%	0.1%	0.03%	0.03%	0.11%

Three paths, as shown in Figure 6-16, are selected on the strip geometry to illustrate the generated thermal stresses, strains and deformations along them. The arrows show directions of the characteristic measurements.

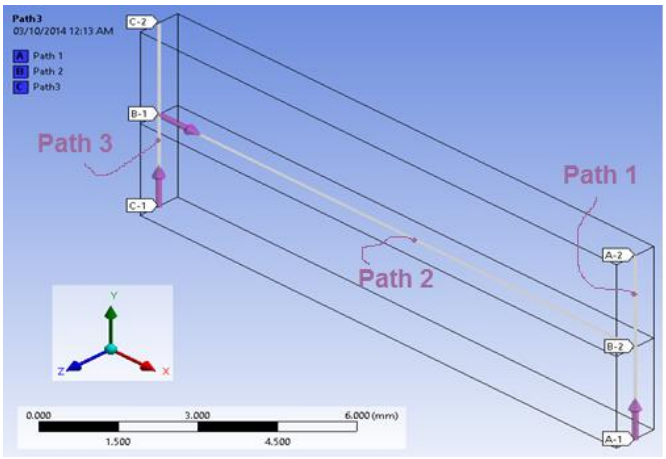

Figure 6-16 The selected paths in the bimetallic strip

Variation of the longitudinal (x-axis) normal stress, along the paths 1 and 2, is illustrated in Figures 6-17 and 6-18, respectively. Out-plane (y-axis) deformation of the bimetallic strip, along paths 3, are shown in Figures 6-19.

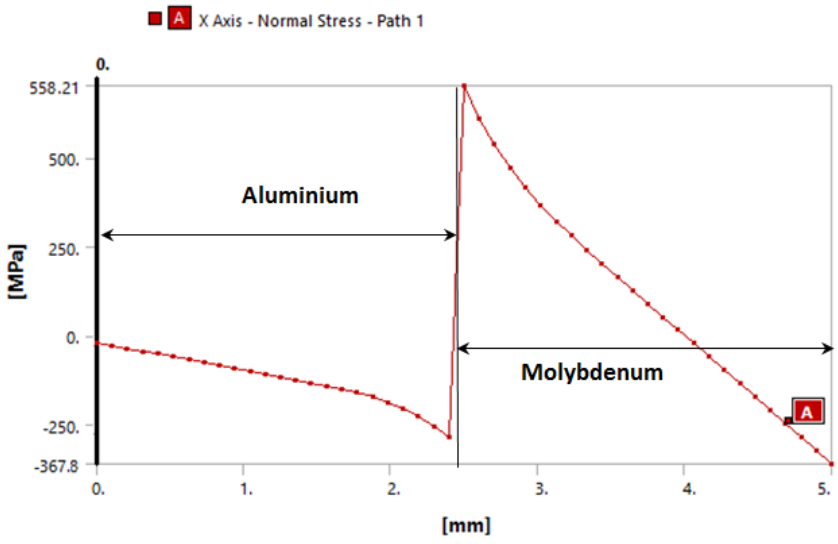

Figure 6-17 Longitudinal (x-axis) normal stress in the bimetallic strip, along path1.

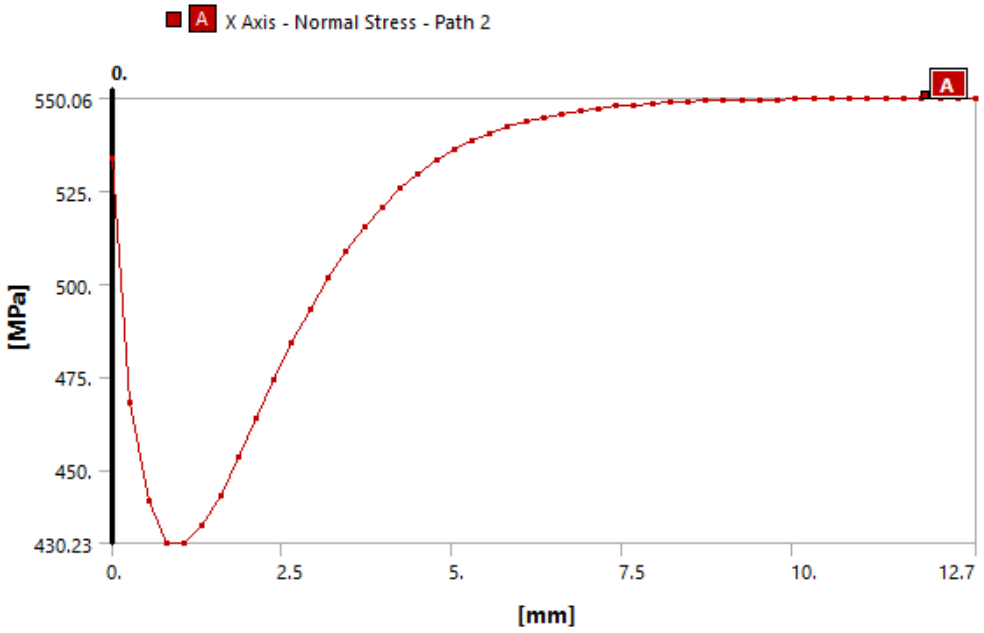

Figure 6-18 Longitudinal (x-axis) normal stresses in the bimetallic strip, along path 2.

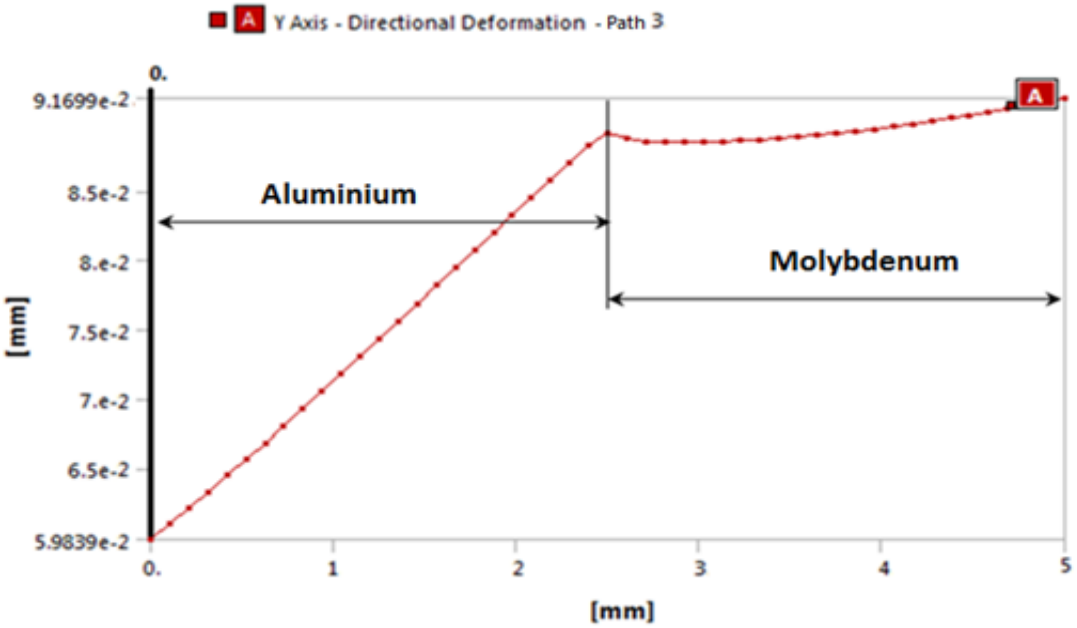

Figure 6-19 Out-plane (y-axis) deformation in the bimetallic strip, along path 3.

Very low differences are obtained between the numerical and analytical results of deflection and normal stress extremes (Table 6-6). Numerical results show that the strip bends towards the molybdenum because it has lower CTE. The maximum normal stress occurs at the strip interface (Figure 6-17), but decreases in a complex manner near the free edges (Figure 6-18), at a distance

of about a quarter of the strip length, due to overlapping the bending moments generated at the free edges, as shown in Figure 2-9. Also Figure 6-19 illustrates that the maximum deformation occurs at the top (concave) and bottom (convex) faces of the strip.

6.2.5.2 Cylindrical Model

The tool channel has a cylindrical profile and transfers hot water (at 90ºC) to heat the tool from ambient temperature (17ºC), so it is subjected to thermal stresses and deformation. Therefore a copper tube of 60 mm length, 5 mm external diameter and 0.7 mm wall thickness, is proposed as a validation with a temperature variation of 73ºC through the wall thickness. The copper properties are listed in Table 6-1. The mathematical model of Timoshenko (1956) for thin wall hollow cylinders (Appendix B) is applied to calculate the bending moment over the free ends of the model and consequently the maximum amounts of thermal-related deformation, strain and stress (longitudinal and tangential) in the tube. Then a half-length of the tube (Figure 6-20), due to symmetry, is designed in ANSYS workbench with normal meshing that split the model into 8,436 elements. The model is initially simulated in ANSYS steady-state thermal, as shown in Figure 6-21, to define the effective thermal load (temperature variation). Then the model structure is analysed numerically, in the ANSYS static structural code, under the effective thermal load imported from previous thermal analysis. Although the model is axisymmetric, its 3D geometry is analysed to offer the best understanding of the structural behaviour of the model and half of the model is simulated due to symmetry.

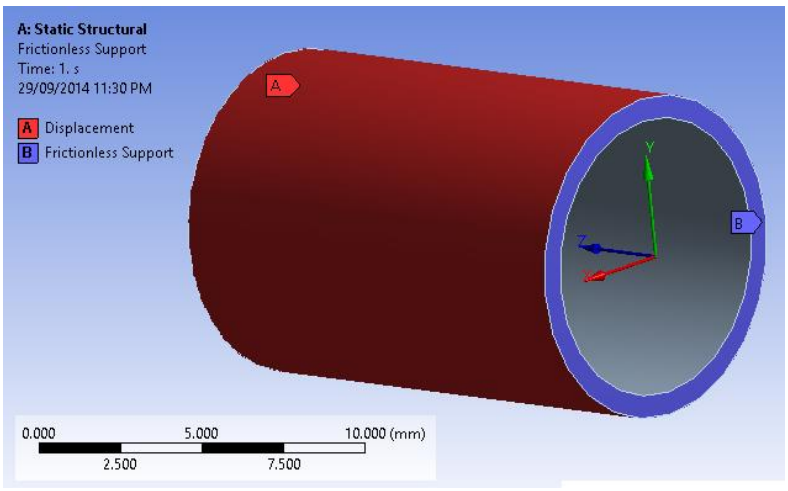

Figure 6-20 Modelling of the tube in ANSYS workbench

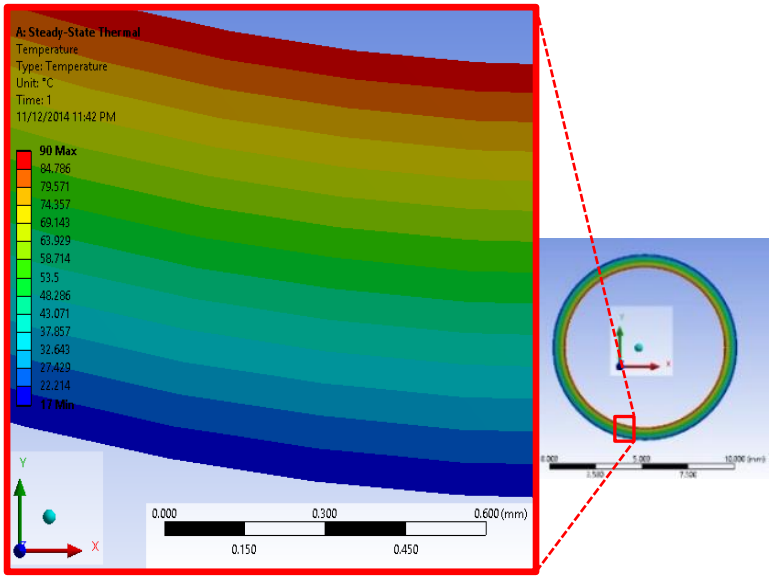

Figure 6-21 Temperature distribution throughout the tube thickness, defined numerically

The model side face (B), as shown in Figure 6-20, is selected as a frictional support and the outer face of the tube is selected to constrain the model displacement in z-direction. The governing equations for the thermal stress are as follows (Akbarimoosavi & Yaghoubi, 2014).

$$\sigma_\theta = \frac{E\alpha}{(1-\upsilon)}\frac{1}{r^2}\left[\frac{r^2-r_i^2}{r_o^2-r_i^2}\int_{r_i}^{r_o} T.rdr + \int_{r_i}^{r} T.rdr - T.r^2\right] \quad (6\text{- }4)$$

$$\sigma_r = \frac{E\alpha}{(1-\upsilon)}\frac{1}{r^2}\left[\frac{r^2-r_i^2}{r_o^2-r_i^2}\int_{r_i}^{r_o} T.rdr - \int_{r_i}^{r} T.rdr\right] \quad (6\text{- }5)$$

$$\sigma_z = \frac{E\alpha}{(1-\upsilon)}\left[\frac{2}{r_o^2-r_i^2}\int_{r_i}^{r_o} T.rdr - T\right] \quad (6\text{- }6)$$

Three paths (Figure 6-22) are created on the model, through the length and wall thickness, to illustrate distribution of thermal stress, deflection and elastic strain along them. The arrows show the direction of the characteristic measurement.

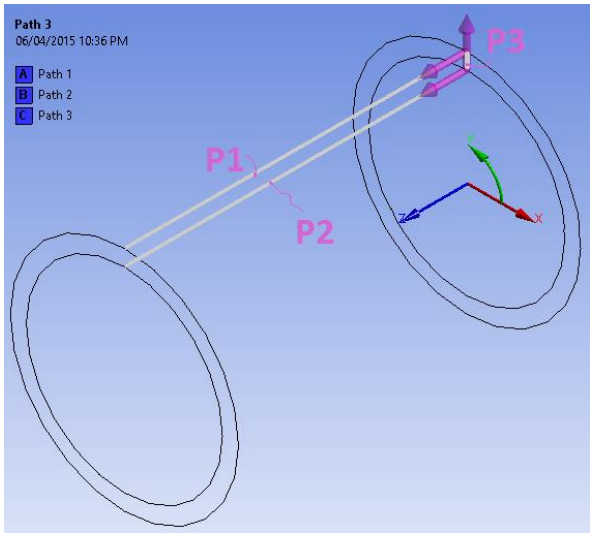

Figure 6-22 The longitudinal and radial paths in the tube model

The distribution of numerical tangential normal stresses, radial deformation and tangential normal elastic strain are illustrated in Figures 6-23, 6-24 and 6-25, respectively.

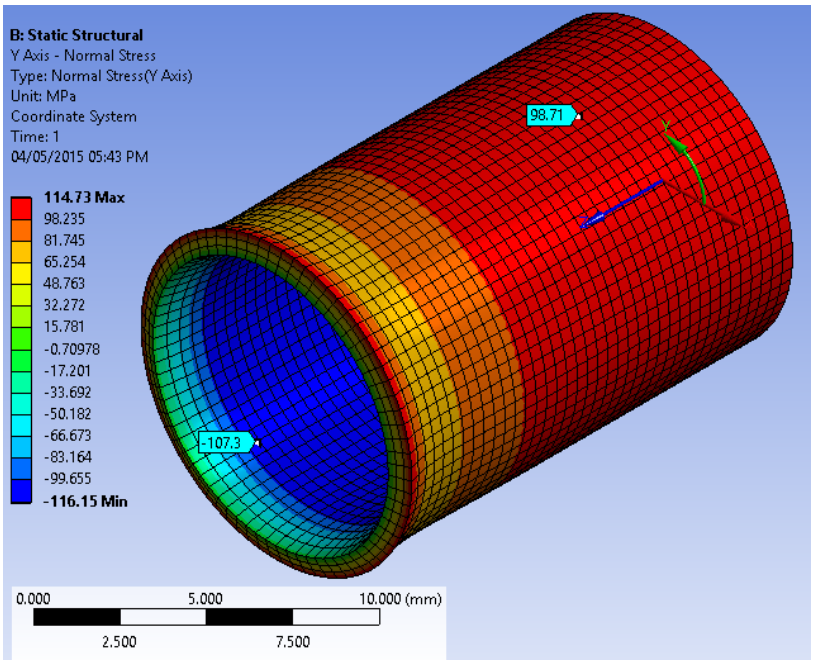

Figure 6-23 Tangential normal stress in the cylindrical model.

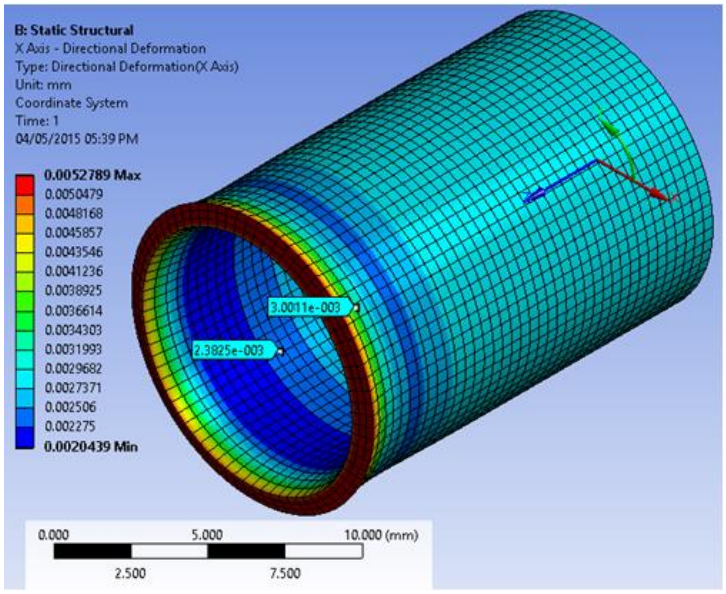

Figure 6-24 Radial deformation in the cylindrical model.

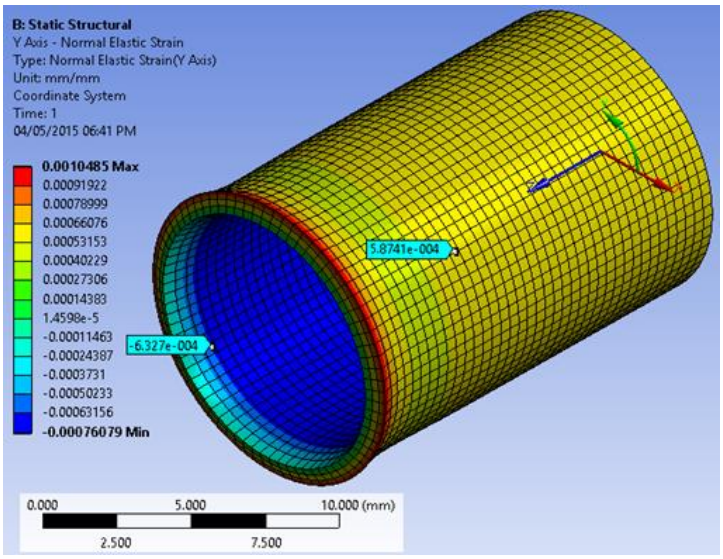

Figure 6-25 Tangential normal elastic strain in the cylindrical model.

Accordingly amounts of maximum deformation, strain and stress ranges in the rest of the tube body (except the free edges) are defined (labelled in the previous figures) and listed in Table 6-7 with that of the analytical results.

Table 6-7 The analytic and numerical analysis results of the cylindrical model

Analysis Method	δ_{max}	ε_{max}	$\sigma_z = \sigma_\theta$
	mm	mm/mm	MPa
Analytic	2.96 x 10^{-3}	5.82x 10^{-4}	-109.03 to 97.8
Numerical	3 x 10^{-3}	5.9 x 10^{-4}	-107.85 to 98.7
Absolute difference	1.3%	1.4%	1.3%

The tangential normal stress in the tube, along paths 1 and 2, is illustrated in Figures 6-26 and shows complex changes near the free edges, along a distance of about one twelfth of the total tube length. Also Figure 6-27 shows a high tangential stress gradient (-107.85 MPa to 98.64MPa) across the tube wall thickness (on path 3).

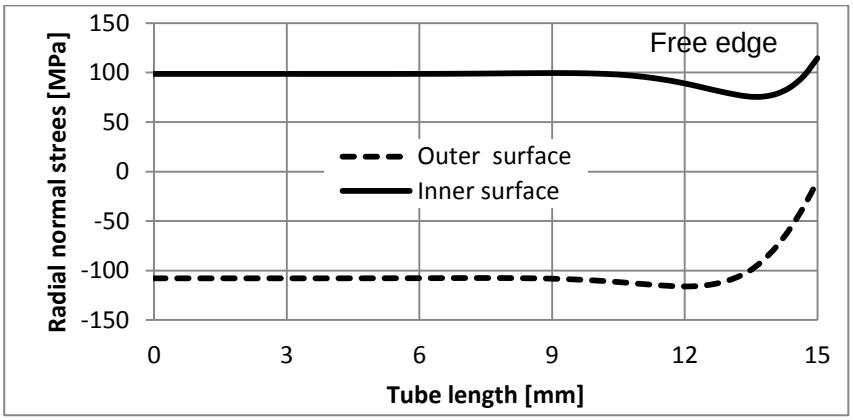

Figure 6-26 Tangential normal stress along the tube length (paths 1 and 2).

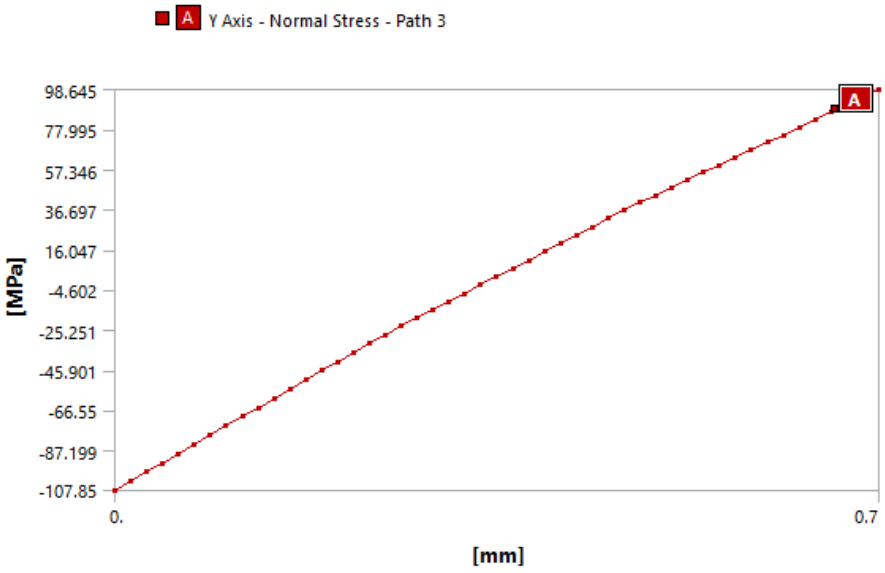

Figure 6-27 Tangential normal stress along the tube wall thickness (path 3).

The axial and radial deformations on the outer and inner surfaces of the tube, along paths 1 and 2, are illustrated in Figures 6-28 and 6-29, respectively, and explain that the higher deformation occurs at the free edges of the tube. Figure 6-30 presents the increment of radial deformation across the tube thickness (path 3) ranging between 2.5 x 10^{-3} to 3 x 10^{-3} mm.

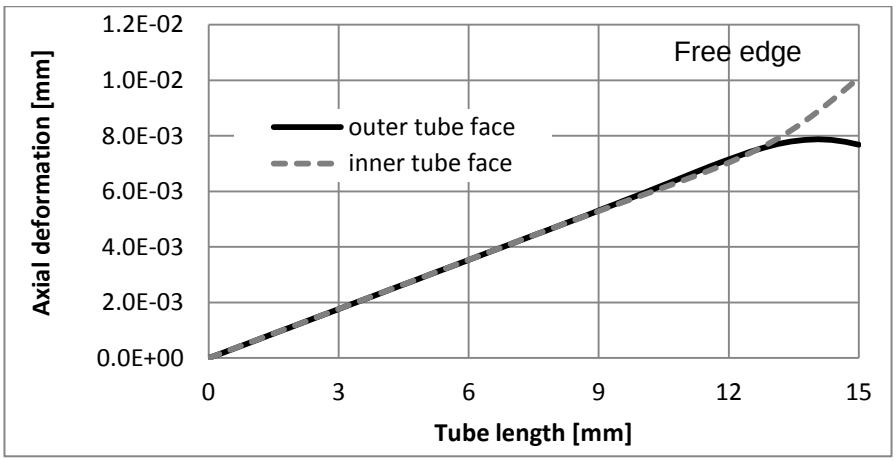

Figure 6-28 Axial deformation on the tube surfaces, along paths 1 and 2.

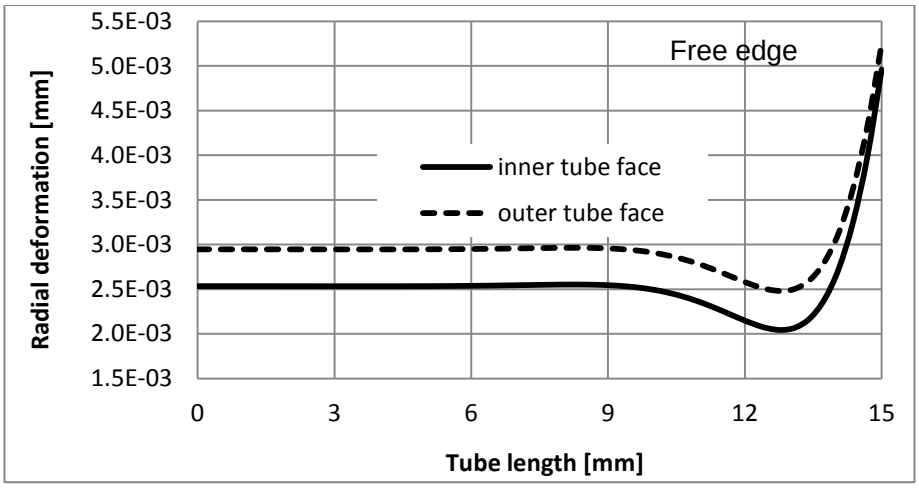

Figure 6-29 Radial deformation on the tube surfaces, along paths 1 and 2.

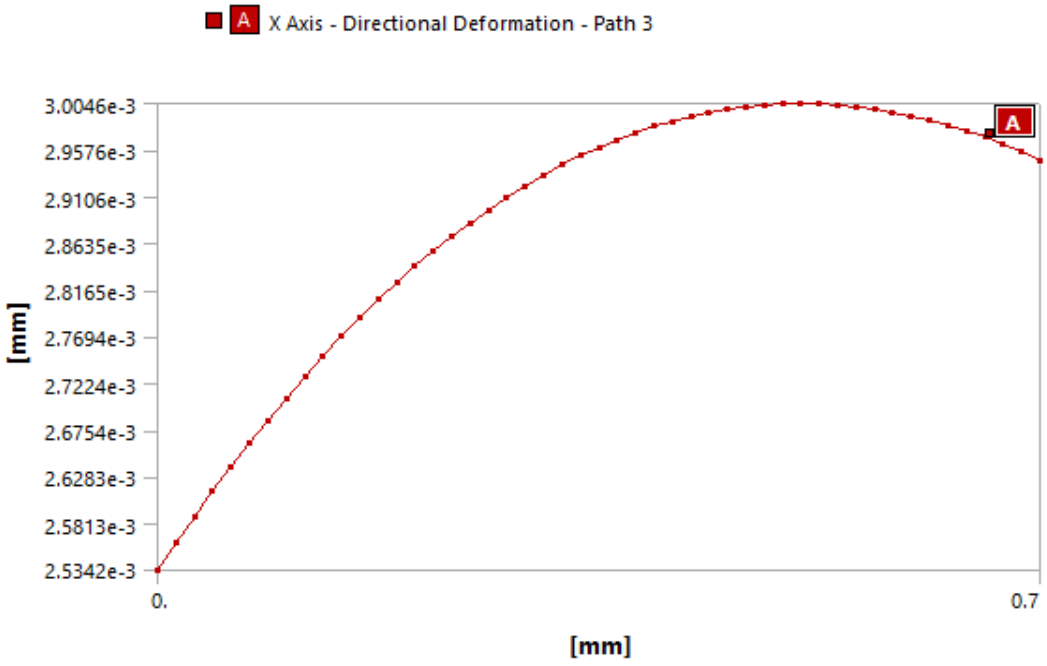

Figure 6-30 Radial deformation along the tube wall thickness (path 3)

The radial elastic strain on the tube inner and outer surfaces, along paths 1 and 2, is shown in Figure 6-31, while Figure 6-32 illustrates the strain gradient between - 6.44×10^{-4} and 5.9×10^{-4} across the tube thickness (path 3).

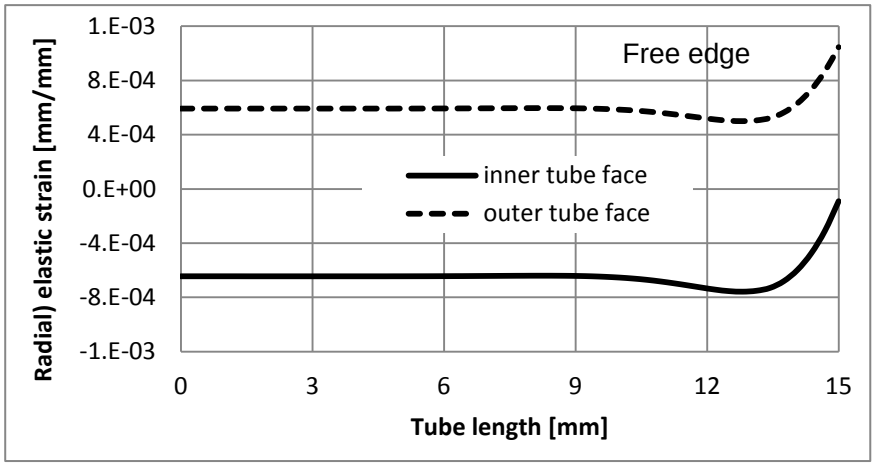

Figure 6-31 Radial elastic strain on the tube surfaces along paths 1 and 2

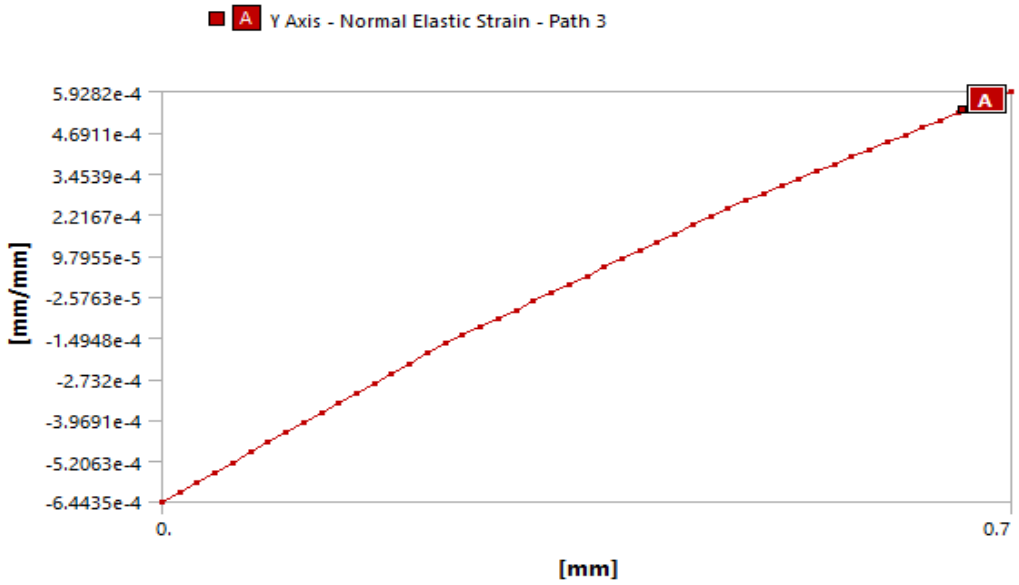

Figure 6-32 Radial elastic strain along the tube wall thickness (path 3)

Very small absolute differences, as listed in Table 6-7, are found between the amounts of maximum analytical and numerical deformations, stresses and strains of the model. Also results indicated complex change of the thermomechanical characteristics (deflection, stress and strain) near the tube free edges.

6.2.5.3 Verification conclusion

The small absolute difference between the analytical and numerical results of both the cylinderical and bimetallic strip models, confirms that boundary conditions and material properties have been assumed correctly during the numerical analysis of the experimental tool structure, using ANSYS software.

6.3 Tool simulation results

Several paths (P1 to P8), as shown in Figure 6-33, are selected along the tool longitudinal (x-axis), traverse (y-axis) and through thickness (z-axis) directions for defining the tool simulation results of deformations, stresses (normal and shear) and strains. The paths are near or pass through the zones of maximum deformation (e.g. tool corner and free side edges). The arrow on each path refers to the measurement direction of the required characteristic. The free outside faces of the tool, according to the tool corner and centre, are named “free side” and “free edge” during discussion.

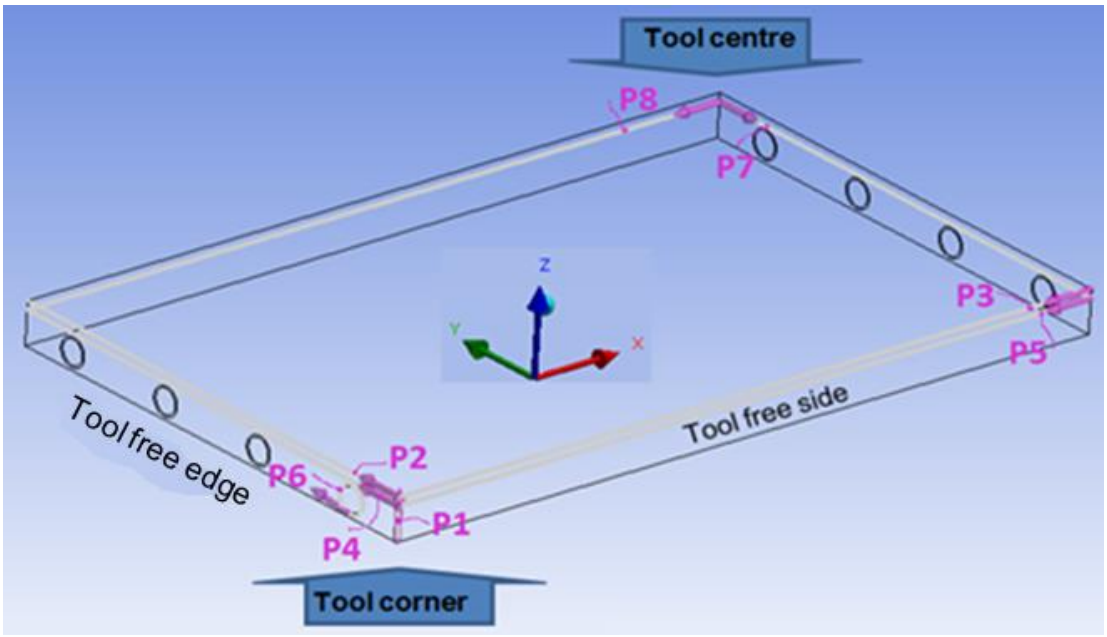

Figure 6-33 selected paths on the tool model geometry.

6.3.1 Total deformations

The transient total deformation in all the tool is plotted in Figure 6-34, which increases almost linearly until about 400s, then gradually (with slow rate) until reaches steady state at about 700s. This behaviour of tool deformation is due to the temperature difference behaviour that increases during the initial heating period of 400s (Section 6.7.2).

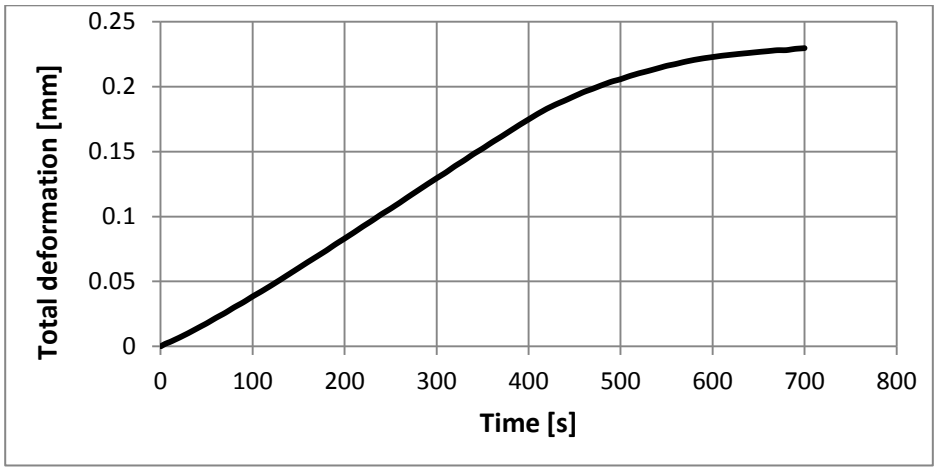

Figure 6-34 Transient total deformation in the tool.

Maximum total deformation of the tool is 0.23 mm, occurring at the free ends, especially around the tool corners, as shown Figure 6-35, which also explains the tool bending towards the tool surface near the free edges, sides and especially the corners due to the lower CTE of CFRP compared to Alepoxy. Figure 6-36 illustrates that the total deformation at the transverse symmetry face of the tool (opposite to the tool free edge) is lower and does not exceed 0.107 mm. The high deformation of the tool near the free edges is due to the high deformation of free ends of the copper channels reaches 0.23 mm, as illustrated in Figure 6-37, while it does not exceed 0.18 mm in the rest of the channel.

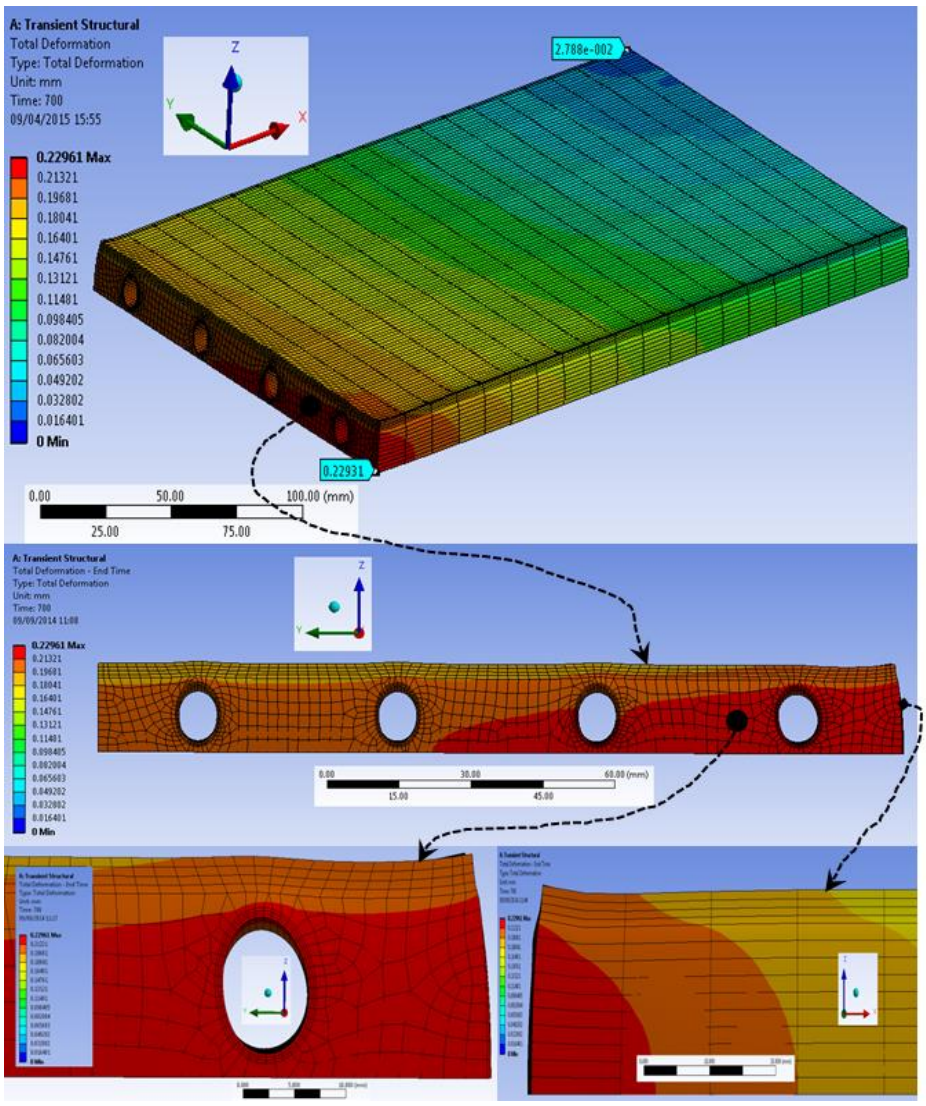

Figure 6-35 Total deformation in the tool model and its free edges, H_t = 700s

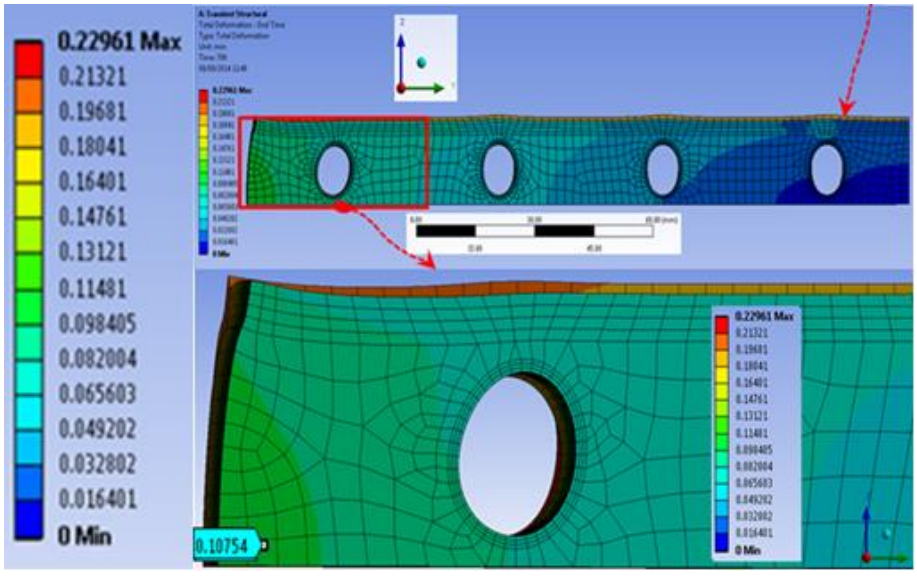

Figure 6-36 Total deformation in the tool and its transverse symmetry side (opposite to the free edge), H_t = 700s

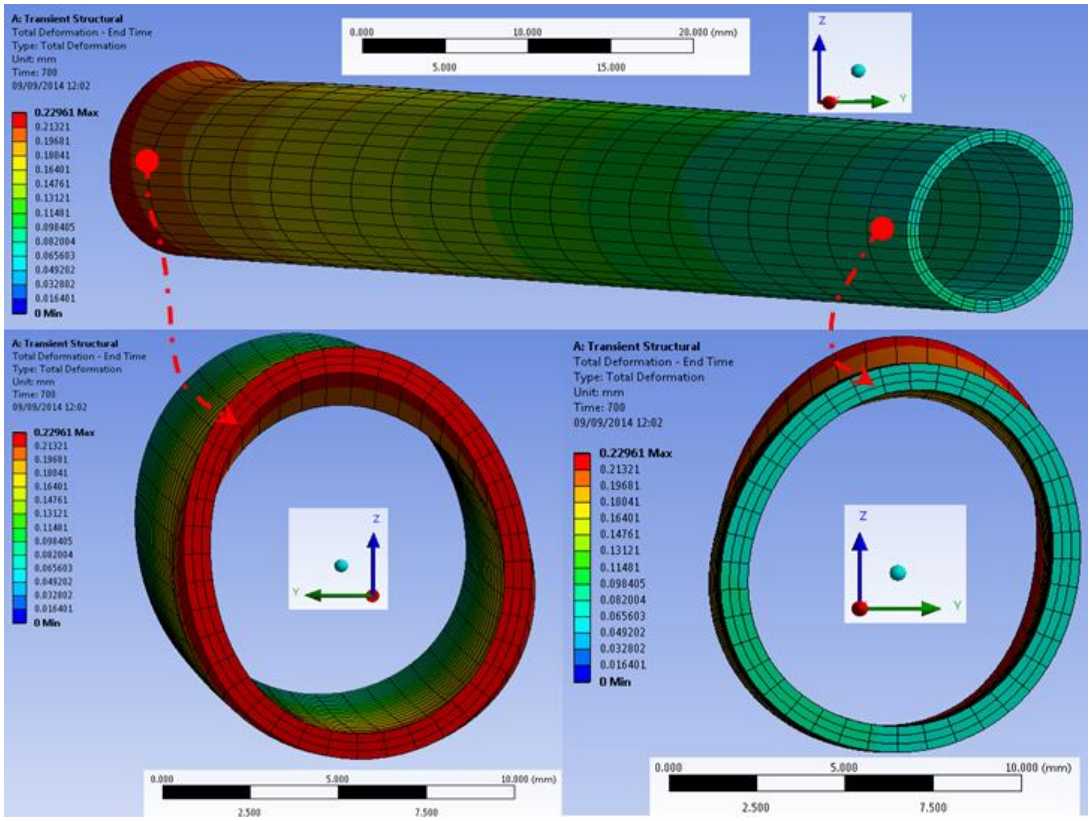

Figure 6-37 Total deformation in a channel, H_t = 700s

6.3.2 Directional deformation

The tool directional deformations, along each path (of P1, P4, P5 and P6) are plotted together in Figures 6-38 to 6-41, which illustrate that the maximum deformation occurs in the longitudinal (x) direction along all the paths and reaches about 0.21 mm.

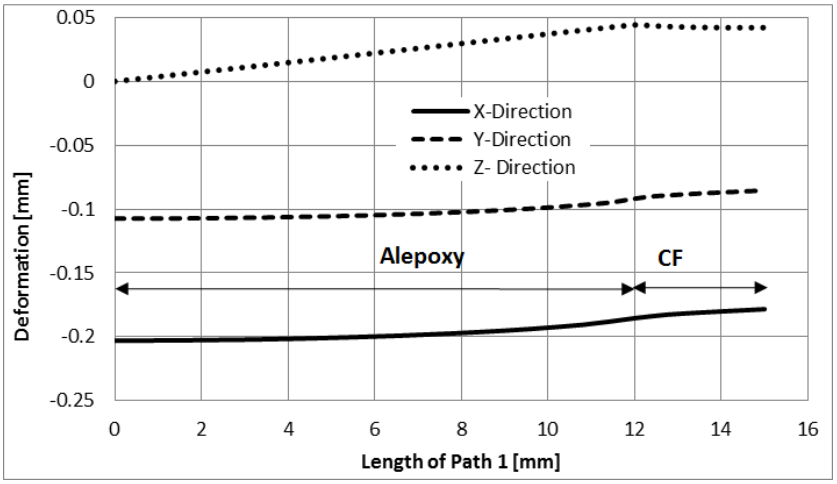

Figure 6-38 Directional deformations along path 1, H_t = 700s

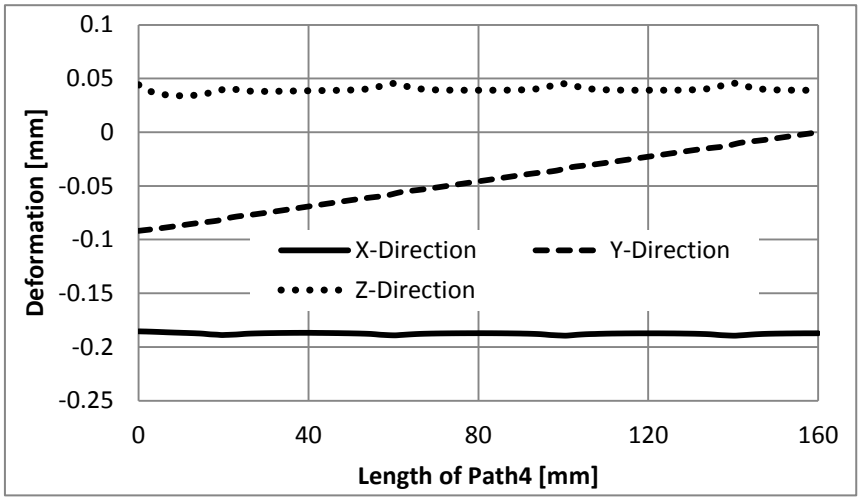

Figure 6-39 Directional deformations along path 4, H_t = 700s

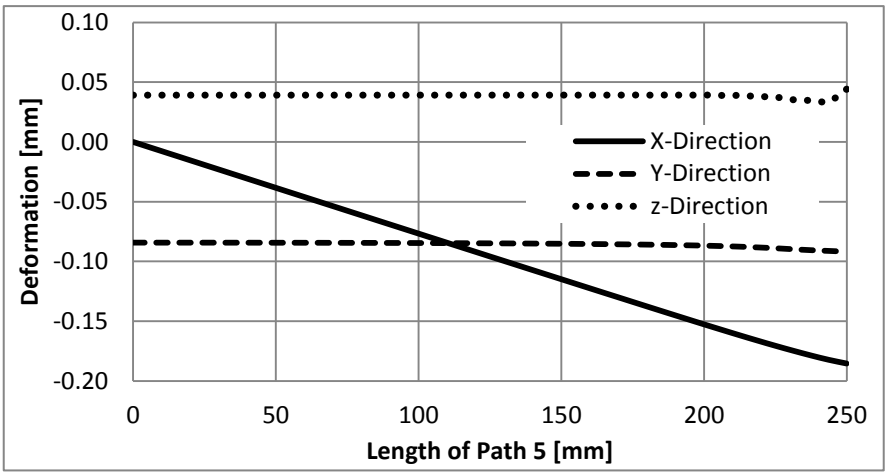

Figure 6-40 Directional deformations along path 5, H_t = 700s

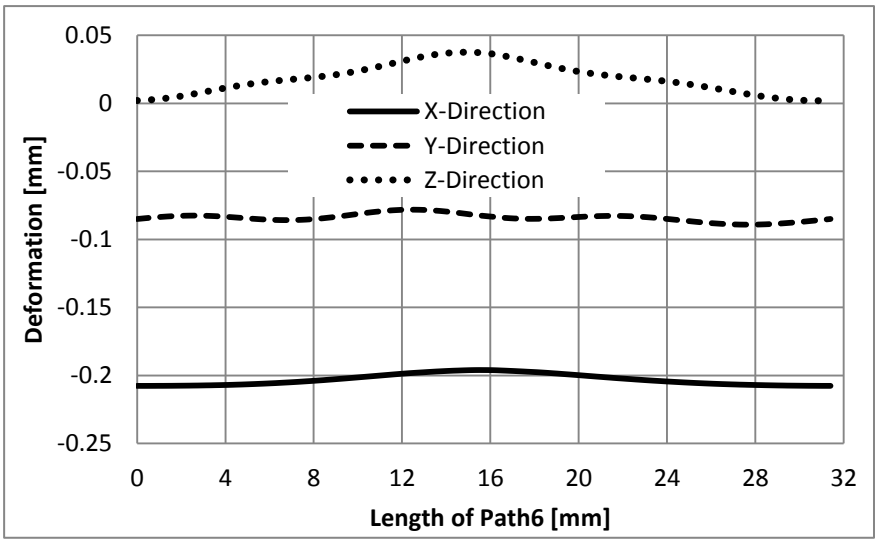

Figure 6-41 Directional deformations along path 6, H_t = 700s

6.3.3 Normal (tensile and compressive) elastic strain

Figures 6-42 to 6-44 illustrate that the highest longitudinal (x-axis) normal elastic strain of -1.2 x 10^{-3} occurs only near the free edges of the tool interface between Alepoxy and CFRP, while it does not exceed -7.8 x 10^{-4} mm/mm in the rest of the tool body. The tool surface (CFRP) is in tension, while the other parts are under compression due to the difference between their thermal expansions.

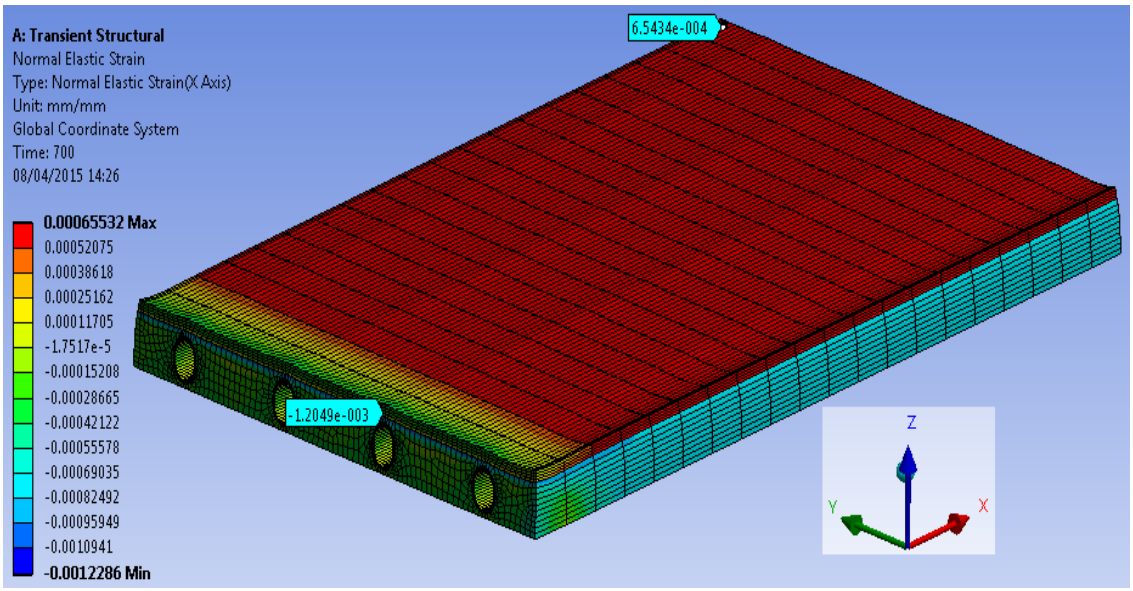

Figure 6-42 Longitudinal (x-axis) normal elastic strain in the tool, H_t = 700s

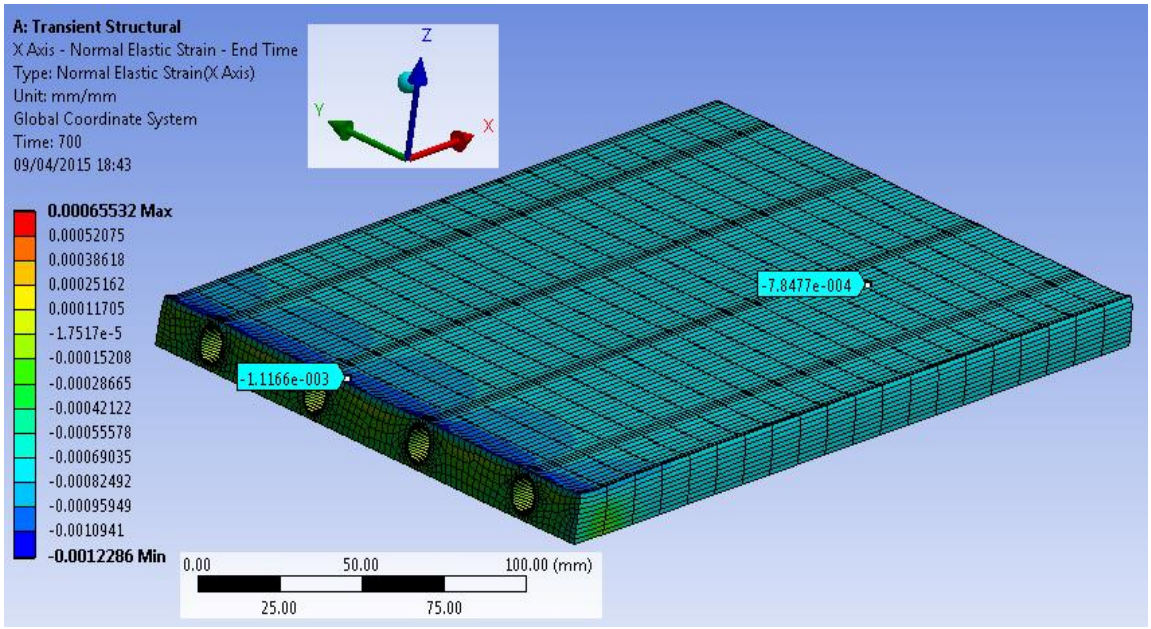

Figure 6-43 Longitudinal (x-axis) normal elastic strain in the mould, H_t = 700s

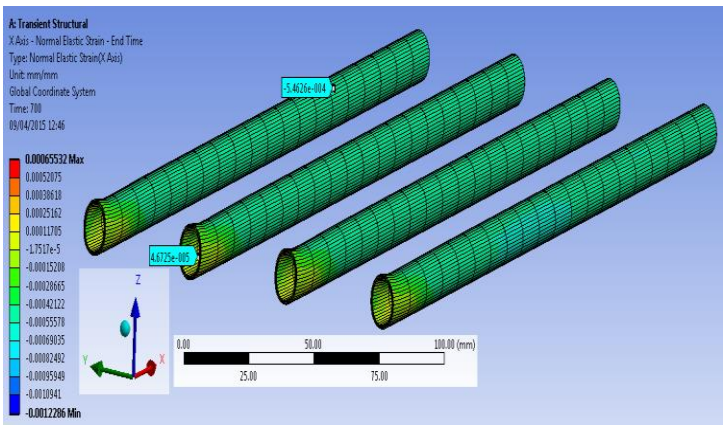

Figure 6-44 Longitudinal (x-axis) normal elastic strain in the channels, H_t = 700s

The maximum elastic strain along the tool corners (path 1), as illustrated in Figure 6-45, is - 8.3 x 10^{-4} and occurs at the interface between the Alepoxy and CFRP, while it is 6.5 x 10^{-4} through the rest of the interface and reduces near the tool free edges and sides as shown in Figures 6-46 and 6-47, respectively.

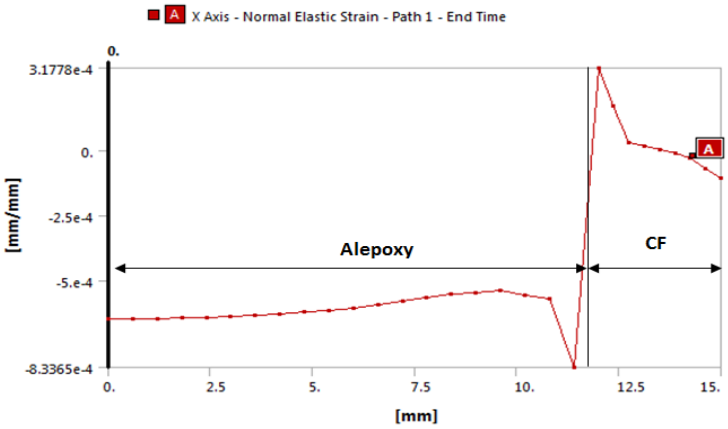

Figure 6-45 Longitudinal (x-axis) normal elastic strain along path 1, H_t = 700s

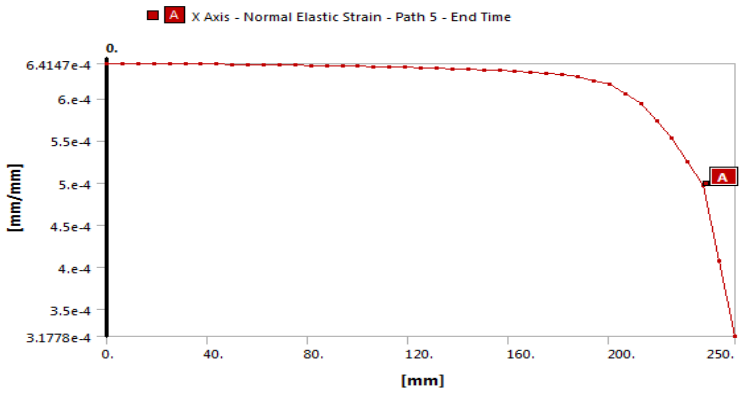

Figure 6-46 Longitudinal (x-axis) normal elastic strain along path 5, H_t = 700s

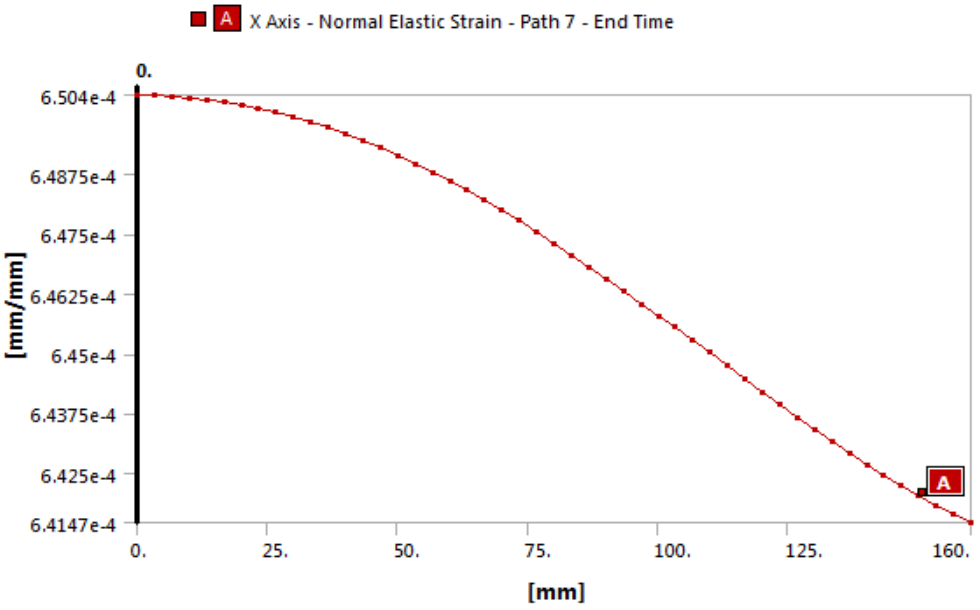

Figure 6-47 Longitudinal (x-axis) normal elastic strain along path 7, H_t = 700s

6.3.4 Normal (tensile and compressive) stresses

The transient longitudinal thermal stresses (tension and compression) are plotted in Figure 6-48, which illustrates an almost linear increase of the stress until about 400s then the increasing rate slows down until it reaches the steady state after about 700s of heating.

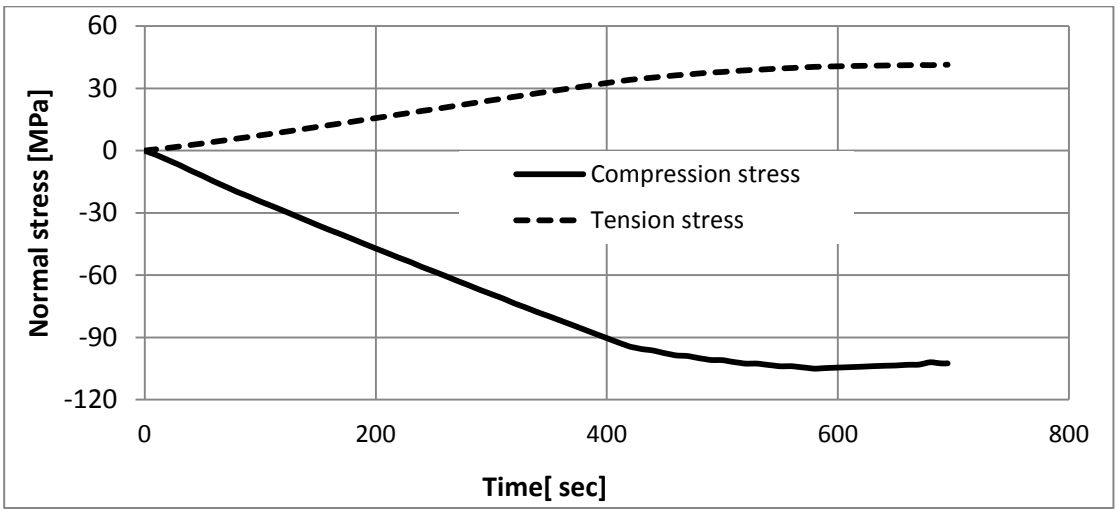

Figure 6-48 Longitudinal (x-axis) normal stresses in the tool model

Figure 6-49 illustrates that the maximum tension stress of 41.4 MPa occurs in the CFRP (tool face) due to its low CTE, while the maximum compressive stress of -102.4 MPa occurs at the internal face of the high dilatable channels, as shown in Figure 6-50, and both reduce near the free edges, corners and sides.

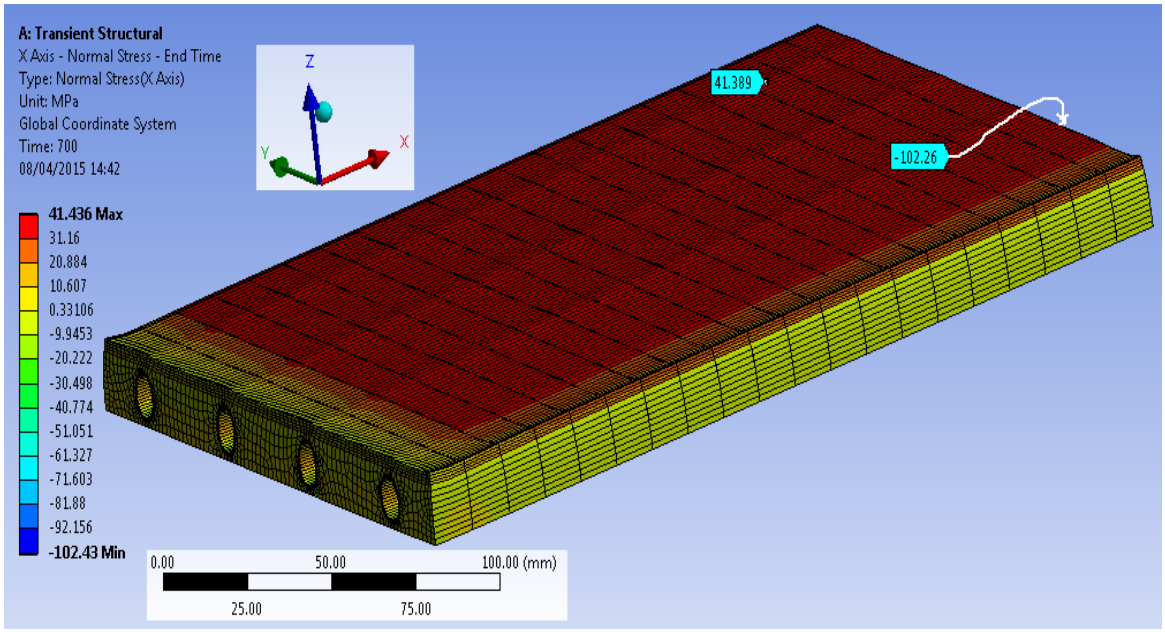

Figure 6-49 Longitudinal (x-axis) normal stresses in the tool, H_t = 700s

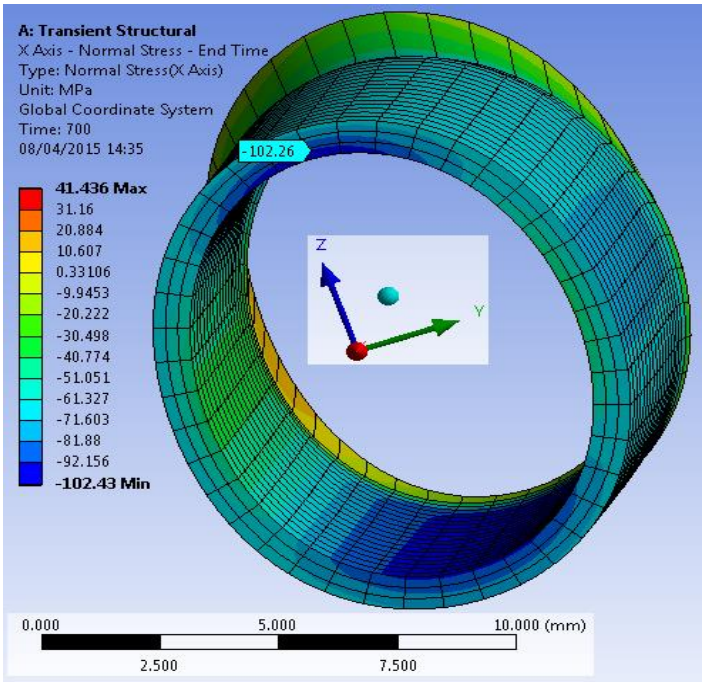

Figure 6-50 Longitudinal (x-axis) normal stress in a channel, H_t = 700s

Figures 6-51 to 6-54 illustrate the normal stress along the P1, P6, P7 and P8 paths, respectively. The normal stress along the tool corners (P1), as shown in Figure 6-51, changes intricately at the interface between the CFRP and Alepoxy reaching the maximum value of about 15 MPa in the x-direction. Complex change also occurs to the normal stress along the channel free edges (P6), as shown in Figure 6-52, and its maximum value of 15 MPa occurs in the radial direction. The complex changes of normal stress, along some paths, is due the overlapping of the bending moments generated at the free edges of the bonded materials (Alepoxy, CFRP and copper) as a result of the expansion restriction between them.

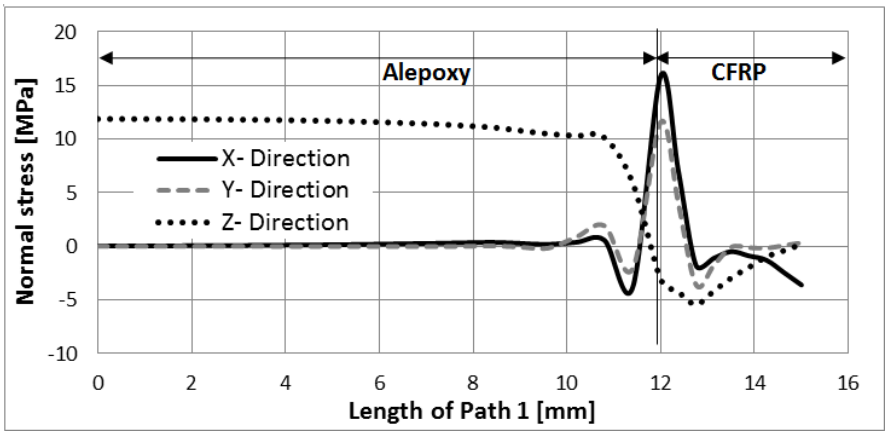

Figure 6-51 Normal stress along path 1, H_t = 700s

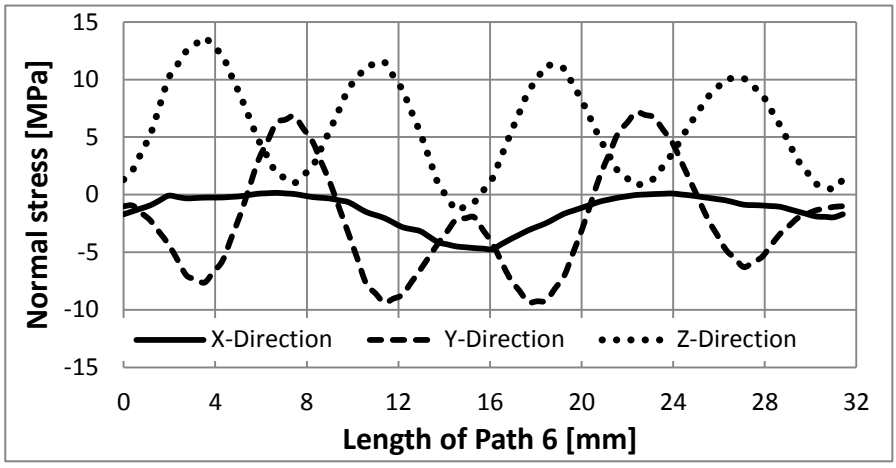

Figure 6-52 Normal stress along path 6, H_t = 700s.

Also the maximum normal stress, along the transverse and longitudinal symmetry sides of the tool interface between CFRP and Alepoxy (P7) (Figures 6-53), is 38.8 MPa and occurs in the longitudinal (x-direction), especially over the channels.

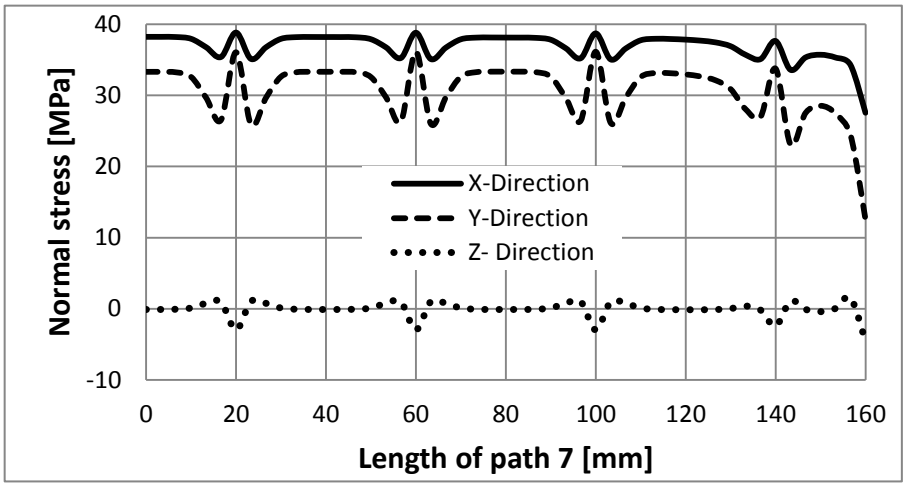

Figure 6-53 Normal stresses along path 7, H_t = 700s.

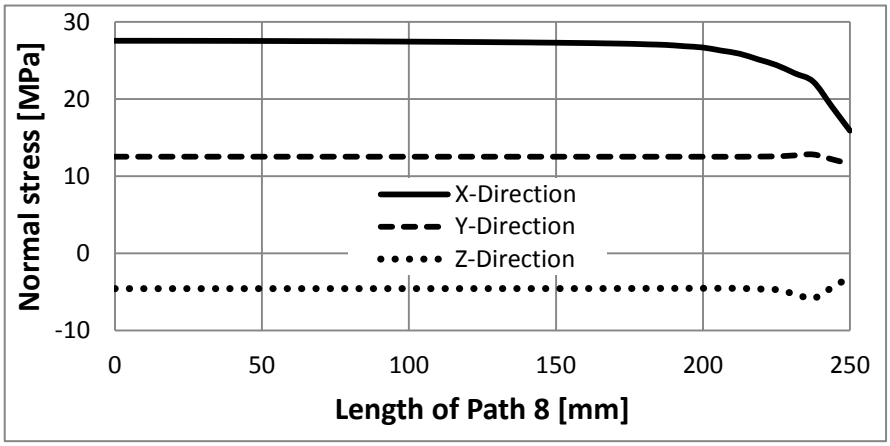

Figure 6-54 Normal stresses along path 8, H_t = 700s.

6.3.5 Plane shear stress

Figure 6-55 shows that the total xy-plane shear stress (at the interfaces between the tool face, mould and channels) generally does not exceed 0.1MPa, but reaches ± 24 MPa occurs just near the free ends of channel, as shown in Figure 6-56.

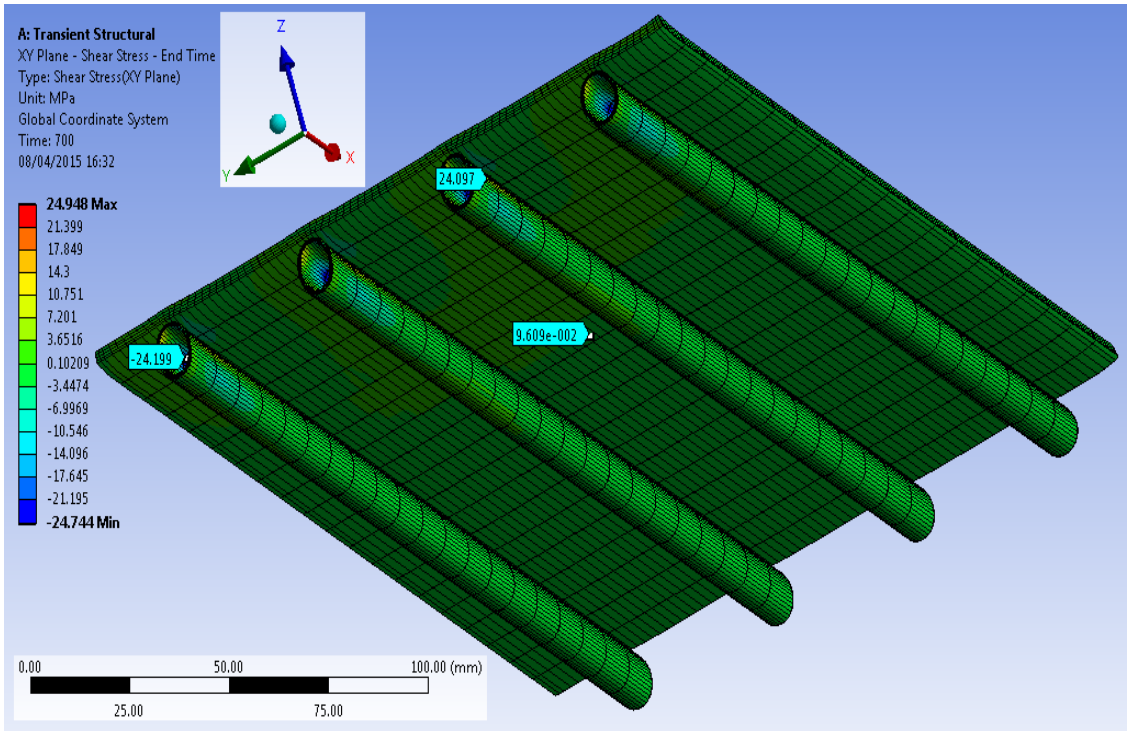

Figure 6-55 XY-plane shear stresses in the tool face and channel

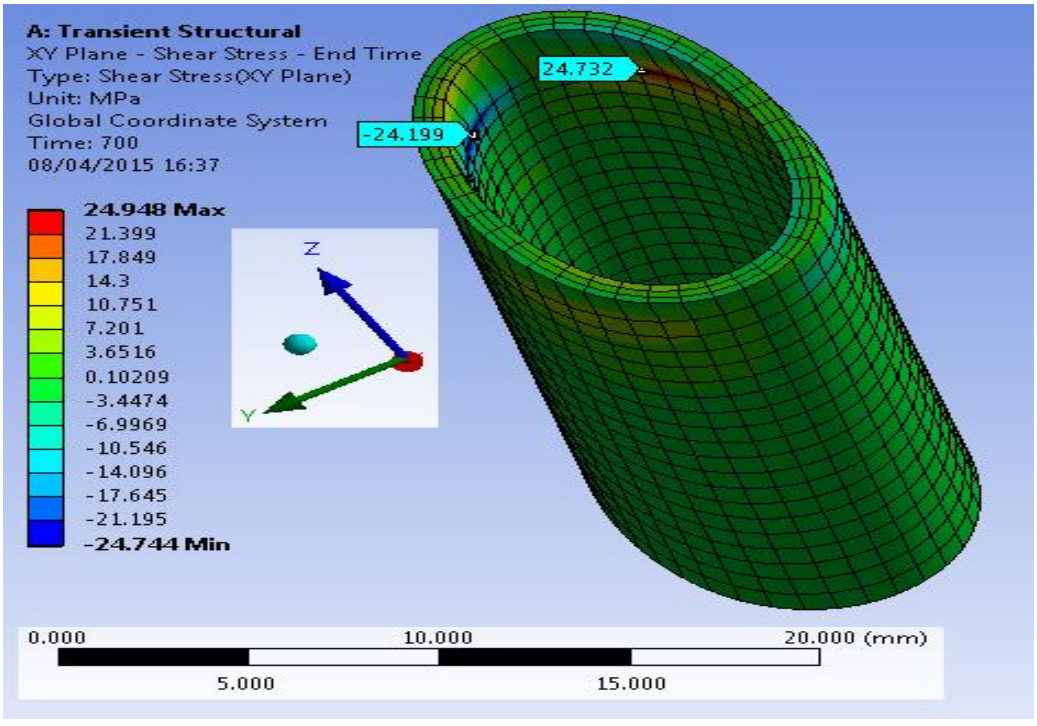

Figure 6-56 XY-plane shear stresses in the channel

The maximum in-plane shear along the transverse free edges (P4) of the interface between the Alepoxy and CFRP, as illustrated in Figures 6-57, is 8.6 MPa in the XZ-plane, particularly over the channels. This is due to the intricate

change of shear stress along the free edges of the interface between the channel and Alepoxy (P6), as shown in Figure 6-58, which reaches the maximum value of 7.8 MPa in YZ-plane.

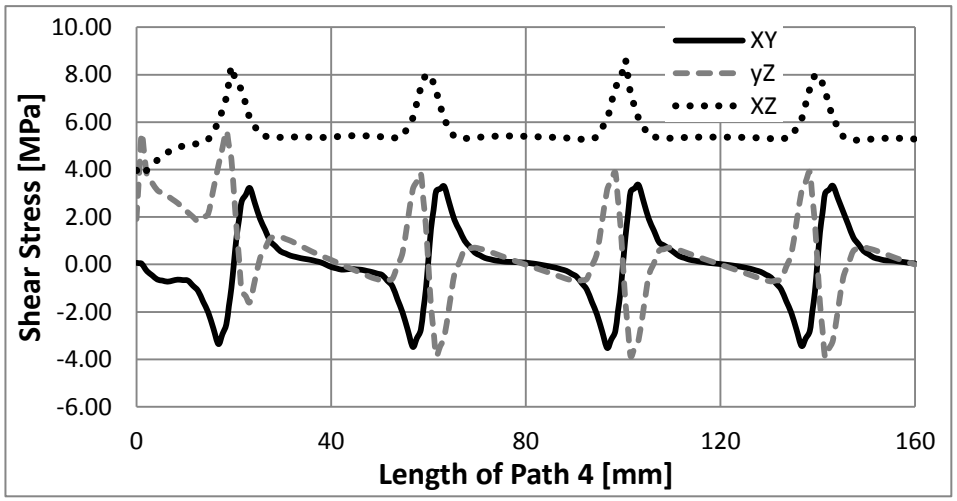

Figure 6-57 In-plane shear stresses along path 5.

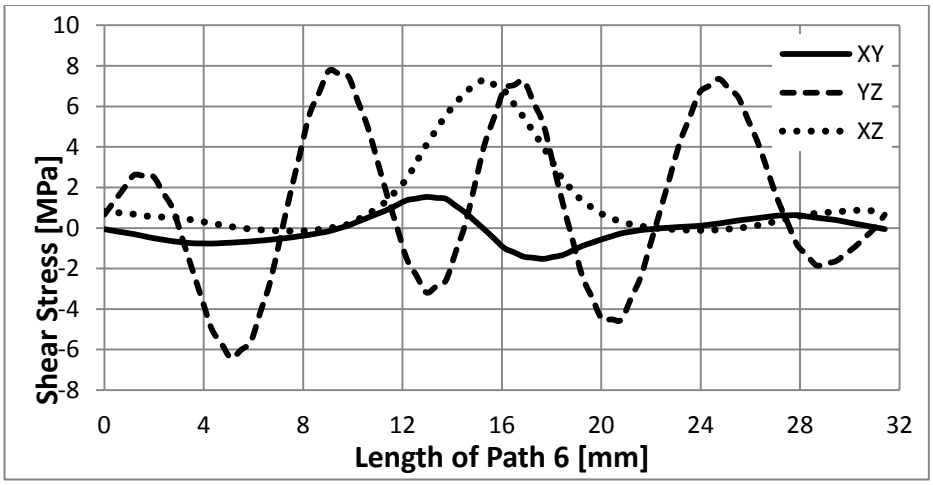

Figure 6-58 In-plane shear stresses along path 6 (the mould channel interface).

6.4 Conclusion

Correct assignment of the boundary condition and material properties during the tool simulation is confirmed by proposing two simple analytic models of a bimetallic strip and a hollow cylinder. Numerical results of the tool analysis show that

- The thermal deformation and normal (tension and compression) stresses, in the heated tool, have the same trend as temperature variation between the tool parts, which increases linearly at the beginning of heating until about 400s, then the increasing rate slows down until steady state at about 700s.
- The highest thermal stresses occur in the tool body due to the expansion restriction between the bonded parts, while the highest deformation occurs near the free edges, corners and sides of the tool due to the local irregularities and overlapping the bending moments as a result of thermal loading.
- The maximum values of normal stresses, plane shear, normal elastic strain and deformation occur on the internal face of the high dilatable copper channel, the free edges of the tool and its parts that reach about -102 MPa, 24 MPa, -1.2 $x10^{-3}$mm/mm and 0.23 mm, respectively.
- Amounts of the static thermomechanical characteristics (normal stresses, plane shear, normal elastic strain and deformation) anywhere in the tool body, except the locations illustrated previously, does not exceed 41.4 MPa, 0.1 MPa, 7.8 x 10^{-4} mm/mm and 0.18 mm, respectively.
- As a consequence of these results and depending on the ultimate strengths of the tool materials (Table 6-1 and 6-2), the lowest FoS value of each thermal effect (normal stresses, plane shear, and normal elastic strain) as determined by Equation 6-1 equals 4, 7, and 2, respectively. This show that the allowable elastic limits of the tool materials are not exceeded and the experimental tool statically remains safe (no failures) during heating.

- The weakest part of the tool is the mould that gives lower FoS of 2 against generated maximum normal strain, which made of a particulate composite of Alepoxy and its strength generally depends on the weak matrix material. So the tool failure is expected to start in this part when the tool is used repeatedly.

Results of this PhD study showed the static behaviour of the experimental tool and its durability during heating, but further investigation is required to define the tool lifecycle (thermal fatigue life) under repeated cycles of heating. Numerical prediction of the tool fatigue life under reversible thermal loads requires actual fatigue life data (S-N curve) of the tool materials. Fatigue behaviour under reversal thermal loads differs from that under mechanical (under reversal mechanical loads) because the temperature variation that produce thermal loads also affects the material properties (i.e. strength modulus, CTE, volume and Tg). Therefore fatigue life data of the tool materials must be obtained under the effect of actual thermal loads with monitoring the initiation of cracks and delaminations during the repeated cycle that require long term experiments.

Chapter 7

General discussion, conclusion and recommendations

7.1 General discussion

Although Integrally-heated tools have the potential to overcome the problems of autoclave processing and produce complex and large components in one piece, still they have problems of heating and component quality. On this basis, this PhD research has been carried out to improve the heating performance of integrally water-heated composite tooling, suitable for processing a variety of low temperature liquid or prepreg composites with acceptable quality. The heating performance of integrally fluid-heated tools depends basically on the thermal properties of the tool materials, heating medium (fluid) type, tool geometry and the three parameters of channel alignment, channel profile and channel separation.

Although composites have lower thermal conductivity compared to metallic materials, the tool architecture is made of composite because of its low density and low CTE that reduces the mismatch between the tool and the composite components. Water is selected as the heating medium because, compared to other fluids, it is suitable for clean room processing and superior in achieving the desired temperature uniformly over the mould face with the lowest cost, time and consumed energy. Water can provide temperature up to 90ºC, but it will be suitable for manufacturing LTM prepregs that are widely used in various sectors of industry. Although embedding copper channels may be expensive, adds weight to the tool and presenting a challenge in repair, it is used in this PhD study because it can provide better heat transfer with lower heat loss.

Three parameters which have not been previously studied are chosen as design factors due to the expectation of their significance in optimising the

design of a tool that can achieve the most uniform temperature at the minimum heating time. The first parameter of channel profile is considered with a fixed cross section area for the three forms of circular, square and rectangular, which provide dissimilar hydraulic diameters and convection surface area. The levels of this parameter are selected because they significantly affect the pressure drop, mass flow rate, flow regime and hence heat transfer coefficient of the fluid as well as the amount of heat that enters the mould. Three economic and easy to manufacture layouts (levels) of zigzag, helical and parallel were chosen for the second parameter with the aim of reducing heat loss from the mould and the path of heat conduction. The effect of channel separation has been studied by Guilong et al. (2010) and Wang et al. (2011b), but this was for metallic tool in the fields of plastic injection manufacturing, which differs from that for composite tooling as illustrated in the conclusion. The parameter of channel separation is selected to assist in defining the conformal distance that can achieve a reasonable heating performance for a composite tool. Accordingly nine test case designs are proposed for the heated tool, using Taghuchi's OA that provides minimum number of experiments necessary to study the influence of the desired factors in an economical way.

Compared to the experimental tests, simulation can be achieved faster and cheaper and facilitates analysis, prediction and innovation in the design and behaviour of the proposed models. Therefore the proposed designed cases of the heated tool was analysed numerically using the powerful ANSYS simulation software (CFX and Static Structural codes). The simulation method solves the complex governing equations that describe the system by iteration and provides approximate results; therefore prior to each simulation process the selected codes were verified analytically to validate the suitability of the numerical

approach in assigning correctly the material properties and boundary conditions. Two different analytical models that calculate the one dimensional (1D) transient heat transfer between water and the proposed model surface are applied for further assurance. In order to perform the simulations with lower running time and PC memory size the following facilities are selected:

- The maximum mesh size (element number) with acceptable mesh quality and time step size that gives accurate results.
- Two dimensional (2D) simulation, rather than to three dimensional (3D).
- Using an average value for the nonlinear properties of water.

The proposed nine designs of the tool test cases are simulated with the following conditions:

- Thicknesses of the tool parts, in all proposed tool models (test cases) were kept constant.
- The in-plane dimensions of the tool were considered according to the amounts of channel separation to maintain constant volume or mass contribution of each tool part (tool face, channel, mould, insulation and back face) in all the cases.
- A high flow rate that heats the tool faster was considered to ensure turbulent flow, with Re $>10^4$, in the channels.
- The tool surface is considered without any curing laminate because this PhD research aims to investigate the thermal response (temperature distribution across the tool face and heating time) of the tool at different points on the tool surface. As mentioned by Ding et al. (2001), cure of the composite parts occurs by a complex heat transfer that involves

conduction, convection by resin flow, exothermic heat of cure reaction as well as phase change due to resin polymerisation.

- Free air convection is considered over the tool face to represent the worst case heat loss (Petrykowski, 2012).
- Perfect contact is assumed between the adjacent solid materials, therefore no heat transfer resistance is assumed at the tool interfaces.
- The water temperature is considered to be at 90°C (during the 2D simulation of test cases as illustrated in Chapter 3) because the cold water (through the channel), as it was concluded from the numerical tests, reaches its bulk temperature in a very short time of approximately 30s (6% of the total tool heating time), and also this boundary condition could be achieved practically in industry with established commonly-available resources, as noted by Ding et al. (2001).

In order to facilitate comparison between the heating performances of the proposed test case designs, according to their numerical results, the following strategies are defined:

- A target temperature of 81°C has been used to avoid uncertainties as the operating temperature is approached asymptotically.
- Two response variables of heating time per unit mass and surface temperature variation across the tool face are defined instead of heating time and tool face temperature, respectively, because the latter could not provide valid response characteristics, while the volume and mass of the test models are different.

The statistical approach of S/N ratio has been applied to control the numerical response variables (heating time per unit mass and temperature variation), while ANOVA is applied to determine the effect of each design parameter on

the response strategies with regard to optimisation within the range of variables considered.

An experimental tool was built according to the predicted optimal design, after amending the optimal amount of channel separation and the number of the parallel channels. The amendments were performed to facilitate the tool manufacturing, increase its surface area and also facilitate temperature observation across the tool surface with special sensors. Alepoxy and CFRP composites were used to construct the mould and the tool face, respectively. Although they were selected according to availability and cost, the CFRP also provides high strength/density ratio, high wear resistance and low thermal inertia and CTE, while Alepoxy mixture can facilitate embedding the channel, provide a coherent joint with the tool face laminate and attain a strong mould with an expected through-thickness thermal conductivity higher than CFRP.

The tool was manufactured with an integrated method that can be performed successfully, provide good contact between the tool parts and eliminate the problems of production e.g. void contents, resin rich, residual strain and low volume fraction as much as possible. Different samples of the materials used were tested to calculate the actual thermal properties of diffusivity, conductivity and thermal expansion to set during simulation with the actual boundary conditions. Then an experimental tool model was simulated in ANSYS software to define the tool heating performances of the amended optimal design, as explained in Section 5.2, (heating time and surface temperature uniformity). The experimental tool was also tested practically, within a test rig, to define its heating ability, verify the simulation results and prove the suitability of numerical modelling in optimising heating performance of the integrally heated tools. The

utilised test devices (thermocouples, thermal camera and flowmeter), during the experimental tests, are calibrated to ensure the most actual measurements.

Since the experimental tool, in this PhD research, comprises different materials (composites and metals) with different CTEs and is exposed to thermal loading during use, the thermomechanical behaviour of the tool is analysed numerically, using ANSYS transient structural, to predict the static thermomechanical behaviours of the tool structure during heating. Initially the linear mechanical properties and CTEs of the constituent materials (the macro-properties of the lumped composites are considered) and their processing heating history (transient heating curve) are defined experimentally to set during simulation. Finally the tool durability, during heating, is defined by calculating lowest FoS value of each thermal effect (normal stresses, plane shear, and normal elastic strain) according to the corresponding maximum numerical results and actual properties of the tool materials.

7.2 Research implementation

This PhD study has developed an easy to build integrally-heated tool that can reduce curing time and energy consumption, and provides acceptable heating performance with lower cost, which should make the tool attractive to composite manufacturers in many industry sectors (e.g.; construction automotive and rail, pipes and tanks, wind energy, aerospace, consumer goods, sports and marine) that are using the LTM prepregs and liquid epoxies in manufacturing their products.

7.3 General conclusion

It was concluded during this PhD study that:

- Circular channel cross-section remains the most appropriate and economical profile due to its availability and ease of application.
- Parallel layout is the most crucial parameter in achieving the optimal characteristics of temperature uniformity and heating time over the surface of the desired tool.
- Low thermal conductivity of the composite materials leads to different conclusions regarding optimal channel spacing.
- Experimental results also confirmed the suitability of simulation in optimising heating performance and also the validity of the boundary conditions and material properties.
- Experimental results also confirmed that the optimal design of the integrally water-heated tool falls within the predicted limits set by the confidence interval.
- The thermal deformation and normal (tension and compression) stresses, in the heated tool, have the same trend as temperature variation between the tool parts, which increases linearly at the beginning of heating until about 400s, and then the increasing rate slows down until steady state at about 700s.
- The highest normal stress, plane shear, normal elastic strain and deformation occur on the free edges of the tool.
- The experimental tool statically remains safe (no failures) during heating.

7.4 Recommendations for future work

Various case studies (in the design, strength, durability, etc. of the tool that can improve the performance, productivity, lifetime of the tool with reducing its production cost) are left for future work due to the time limitation of this PhD study. Further investigations will be required to:

- Adapt the results of this PhD research to the geometric complexities of production tooling. That is because this PhD work only considered the heating performance across the surface of a flat tool; the most critical point in composite industry is producing components with complex shape that requires tools or moulds to have surfaces with the same form and the temperature distribution across complex tool surfaces also depends on the tool geometry and the heat transfer coefficient depends on the surface inclination and orientation (Athanasopoulos *et al.*, 2013).
- Evaluate the curing ability of the produced experimental tool because the efficiency of composite processing depends on performing the cure cycles with considerations illustrated in section 2.5.
- Improve the thermal properties of the experimental tool, especially in the out-plane direction, through the development of material properties or application of techniques to increase thermal conductivity. That is because Improvement of thermal conductivity of the composites produces improvement in the tool heating performance.
- Determining the long-term performance of the produced integrally heated tool, in terms of differential expansion and contraction under repeated thermal cycles. That is because heating changes the tool material properties and possibility of delamination at interfaces between the linked

materials due the weak matrix that may affect the tool heating performance before fatigue failure.

- Improve the tool design and obtaining lower CTE tool materials that increase the tool resistance to the effective thermal loads, because this will be helpful in increasing the tool working lifetime and its productivity.

Appendices

Appendix A: Timoshenko model for bi- metallic strips

- The total moment and the moment at each strip are defined as follows

$$F \cdot \frac{h_i}{2} = M_L + M_H \qquad \text{(A-1)}$$

When $M_H = \frac{E_H I_H}{\mathcal{R}}$, $M_L = \frac{E_L I_L}{\mathcal{R}}$, $I_H = \frac{w_H h_H^3}{12}$ and $I_L = \frac{w_L h_L^3}{12}$

Each suffix of L and H refers to the strip that has lower and higher CTE, respectively.

- The Interfacial force (Load)

$$F = \frac{2(E_H I_H + E_L I_L)}{h_i \mathcal{R}} \qquad \text{(A-2)}$$

$$F_H = F_L = F \qquad \text{(A-3)}$$

- Radius of curvature

While $\varepsilon_{L_{thermal}} + \varepsilon_{L_{elastic}} + \varepsilon_{L_{plastic}} = \varepsilon_{H_{thermal}} - \varepsilon_{H_{elastic}} - \varepsilon_{H_{plastic}}$

Accordingly $\alpha_L \Delta T + \frac{F_L}{E_L A_L} + \frac{h_L}{2\mathcal{R}} = \alpha_H \Delta T - \frac{F_H}{E_H A_H} - \frac{h_H}{2\mathcal{R}}$

So the radius of curvature at the interface of both metals

$$\mathcal{R} = \frac{h_i^2 + 4(E_H I_H + E_L I_L)\left(\frac{1}{E_H A_H} + \frac{1}{E_L A_L}\right)}{2h_i(\alpha_H - \alpha_L)\Delta T} \qquad \text{(A-4)}$$

- Deflection

$$\delta = \frac{1}{\mathcal{R}} . \frac{\mathrm{L}^2}{8} \qquad \text{(A-5)}$$

- Thermal internal stresses

When $y_H = \frac{-h_H}{2}$, $y_L = \frac{h_L}{2}$, $A_H = h_H w_H$ *and* $A_L = h_L w_L$

Maximum normal stress at the top surface (concave) of strip H (under compression)

$$\sigma_{H_{max}} = \frac{-F}{A_H} + \frac{E_H y_H}{\mathcal{R}} \qquad \text{(A-6)}$$

Minimum normal stress at interface of strip H (under compression)

$$\sigma_{H_{min}} = \frac{-F}{A_H} - \frac{E_H y_H}{\mathcal{R}} \qquad \text{(A-7)}$$

Maximum normal stress at interface of strip L (under tension)

$$\sigma_{L_{max}} = \frac{F}{A_L} + \frac{E_L y_L}{\mathcal{R}} \qquad \text{(A-8)}$$

Minimum normal stress at the bottom surface (convex) of strip L (under tension)

$$\sigma_{L_{min}} = \frac{F}{A_L} - \frac{E_L y_L}{\mathcal{R}} \qquad \text{(A-9)}$$

Appendix B: Timoshenko model for single tube

- Temperature distribution along the tube wall thickness.

$$T = \left(\frac{\Delta T}{\log(r_o/r_i)}\log(r_o/r)\right) + T_o \qquad \text{(B-1)}$$

When $\Delta T = T_i - T_o$

- The axial and tangential thermal stresses for small thickness tubes in comparison with the outer radius.

$$(\sigma_\theta)_{r=r_i} = (\sigma_z)_{r=r_i} = -\frac{E\alpha\Delta T}{2(1-v)}\left[1 + \frac{m}{2}\right] \qquad \text{(B-2)}$$

$$(\sigma_\theta)_{r=r_i} = (\sigma_z)_{r=r_i} = \frac{E\alpha\Delta T}{2(1-v)}\left[1 - \frac{m}{2}\right] \qquad \text{(B-3)}$$

When $m = \frac{r_o}{r_i} - 1$

- Bending moment per unit length along the tube edges of the cylinder.

$$M_o = \frac{E\alpha\Delta T}{2(1-v)}\frac{h^2}{6} \quad [N] \qquad \text{(B-5)}$$

- Deflection along z-axis.

$$\delta = \frac{M_o e^{-\beta z}}{2\beta^2 D}(\cos\beta z - \sin\beta z) \qquad [mm] \qquad \text{(B-6)}$$

Or

$$\delta = \frac{\alpha c\Delta T\sqrt{1-v^2}}{2\sqrt{3}\,(1-v)} e^{-\beta z}(\cos\beta z - \sin\beta z) \qquad [mm] \qquad \text{(B-7)}$$

When $c = \frac{r_i + r_o}{2}$

The maximum deflection is evidently at the end $z = 0$

$$(\delta_{max})_{z=0} = \frac{M_o}{2\beta^2 D} = \frac{\alpha c \Delta T \sqrt{1-v^2}}{\sqrt{3}\,(1-v)} \qquad \text{(B-8)}$$

When $D = \frac{Eh^3}{12(1-v^2)}$ $[N.m]$, $\beta = \sqrt[4]{\frac{3(1-v^2)}{c^2 h^2}}$ $[\frac{1}{mm}]$ and $c = \frac{(r_o + r_i)}{2}$

- Strain in the tangential direction

$$\varepsilon_\theta = \frac{\delta_{max}}{c} = \frac{\alpha \Delta T \sqrt{1-v^2}}{2\sqrt{3}\,(1-v)} \quad [mm/mm] \qquad \text{(B-9)}$$

Appendix C: Equations of free air convection

- for vertical plane or cylinder (Holman, 2002)

$$h = 1.42\left(\frac{\Delta T}{L_s}\right)^{1/4} \quad \text{When} \quad 10^4 \le Ra_L \le 10^9$$

$$h_s = 1.31(\Delta T)^{1/3} \quad \text{When} \quad Ra_L \ge 10^9$$

When $L_s = height\ of\ the\ vertical\ plane$

- for horizontal cylinder

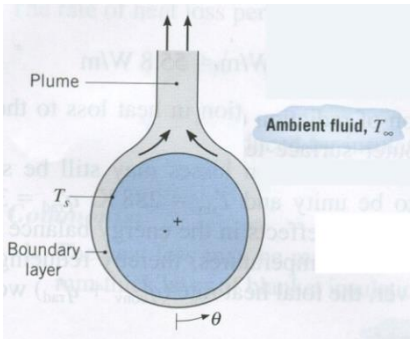

$$h_c = 1.32\left(\frac{\Delta T}{D}\right)^{1/4} \quad \text{When} \quad 10^4 \le Ra_L \le 10^9$$

$$h_c = 1.24(\Delta T)^{1/3} \quad \text{When} \quad Ra_L \ge 10^9$$

- for horizontal plane

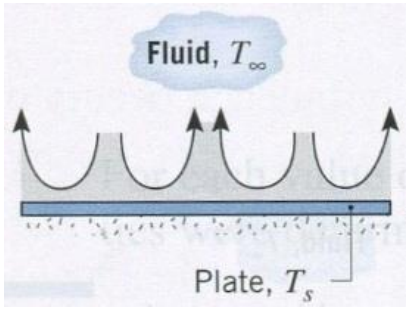

- Facing upward:

$$h_t = 1.32\left(\frac{\Delta T}{L}\right)^{1/4} \quad \text{When} \quad 10^4 \le Ra_L \le 10^9$$

$$h_t = 1.52(\Delta T)^{1/3} \quad \text{When} \quad Ra_L \ge 10^9$$

- Facing downward:

$$h_b = 0.59\left(\frac{\Delta T}{L}\right)^{1/4} \quad \text{When} \quad 10^4 \le Ra_L \le 10^9$$

$$L_o = \frac{A_s}{P}$$

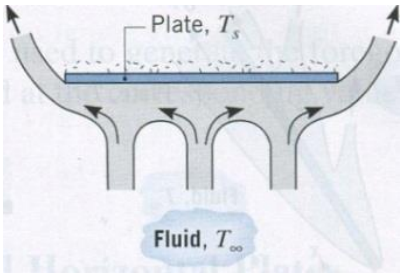

Appendix D: Thermal properties of water

Transient thermal properties of water, while u=1m/s (Holman, 2002)

Reference Temperature	Density	Dynamic Viscosity	Specific Heat	Conductivity	Reynolds No.	Prandtl No.	Thermal convection
	ρ	μ	c_p	k	Re_D	Pr	h
°C	Kg/m^3	$Kg/m.s$	$J/kg.K$	-	-	-	$W/m.K$
0	999.8	1.8×10^{-3}	4225	0.57	4468.4	13.4	3818.7
4.44	999.8	1.6×10^{-3}	4208	0.58	5160.3	11.3	4077.0
10	999.2	1.3×10^{-3}	4195	0.59	6102.0	9.4	4398.6
15.56	998.6	1.1×10^{-3}	4186	0.60	7132.9	7.9	4724.6
21.11	997.4	9.8×10^{-4}	4179	0.60	8142.0	6.8	5020.7
26.67	995.8	8.6×10^{-4}	4175	0.61	9263.3	5.8	5333.5
32.22	994.9	7.7×10^{-4}	4173	0.62	10404.2	5.1	5633.0
37.78	993	6.8×10^{-4}	4172	0.63	11648.1	4.5	5927.9
43.33	990.6	6.2×10^{-4}	4172	0.64	12864.9	4.0	6203.2
48.89	988.8	5.6×10^{-4}	4173	0.64	14075.4	3.6	6468.6
54.44	985.7	5.1×10^{-4}	4175	0.65	15371.5	3.3	6724.6
57.5	984.5	4.9×10^{-4}	4177	0.65	16008.1	3.2	6848.4
60	983.3	4.7×10^{-4}	4179	0.65	16701.5	3.0	6979.5
65.55	980.3	4.3×10^{-4}	4183	0.66	18238.1	2.7	7256.6
71.11	977.3	4.0×10^{-4}	4186	0.67	19497.3	2.5	7486.6
76.67	973.7	3.7×10^{-4}	4191	0.67	20939.8	2.3	7716.6
82.22	970.2	3.5×10^{-4}	4195	0.67	22367.7	2.2	7950.0
87.78	966.7	3.3×10^{-4}	4199	0.68	23650.2	2.0	8135.1
90	964.95	3.2×10^{-4}	4202	0.68	24390.5	2.0	8243.0
93.33	963.2	3.1×10^{-4}	4204	0.68	25181.7	1.9	8356.0
104.4	955.1	2.7×10^{-4}	4216	0.68	28617.2	1.6	8821.4

Appendix E: First analytical model

(Note: volumes and areas are defined for a unit length)

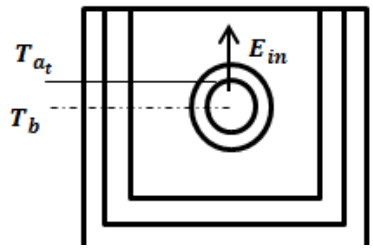

$$\mathrm{E_{in}} = \mathrm{U}\left(\mathrm{T_b} - \mathrm{T_{a_t}}\right) \qquad \text{(E- 1)}$$

$$U = hA_s \qquad \text{(E- 2)}$$

$$A_s = \pi D_h L_c \qquad \text{(E- 3)}$$

$$E_{out} = U_1\left(T_{m_t} - T_\infty\right) + U_2\left(T_{w_t} - T_\infty\right)$$

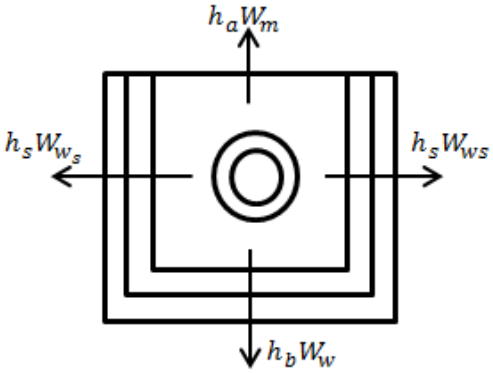

$$E_{out} = U_1 T_{m_t} + U_2 T_{w_t} - (U_1 + U_2)T_\infty \qquad \text{(E- 4)}$$

$$U_1 = h_t A_1 \qquad \text{(E- 5)}$$

$$A_1 = W_m L_c \qquad \text{(E- 6)}$$

$$U_2 = (h_b A_2 + 2h_s A_3) \qquad \text{(E- 7)}$$

$$A_2 = W_w L_c \qquad \text{(E- 8)}$$

$$\mathrm{A_3} = \mathrm{W_{ws}L_c} \qquad \text{(E- 9)}$$

$$E_{ST} = M_t \frac{dT_m}{dt} \qquad \text{(E- 10)}$$

$$\mathrm{M_t} = \rho_\mathrm{t} \mathrm{V_t} \mathrm{c_{p_t}} = \rho_\mathrm{c} \mathrm{V_c} \mathrm{c_{p_c}} + \rho_\mathrm{m} \mathrm{V_m} \mathrm{c_{p_m}} \qquad \text{(E- 11)}$$

$$\mathrm{V_c} = \frac{\pi\left(\mathrm{D_o^2} - \mathrm{D_i^2}\right)}{4} \mathrm{L_c} \qquad \text{(E- 12)}$$

$$\mathrm{V_m} = \left[\mathrm{W_m^2} - \left(\frac{\pi \mathrm{D_o^2}}{4}\right)\right] \mathrm{L_c} \qquad \text{(E- 13)}$$

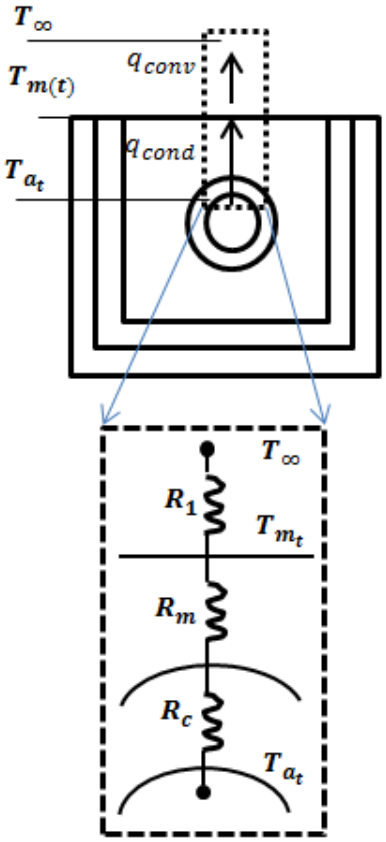

By assuming steady state condition at the moulding surface of the square model and applying the surface energy balance:

$$E_{out} = q_{conv} = q_{cond}$$

$$U_1(T_{m_t} - T_\infty) = \frac{(T_{a_t} - T_{m_t})}{R_1}$$

$$\mathrm{R_1 = 4(R_c + R_m)} \qquad \text{(E- 14)}$$

The conduction resistance of the mould and the channel are found according to shape factor relations in Appendix (F):

$$R_c = \frac{\ln(D_o/D_i)}{2\pi L_c k_c} \qquad \text{(E- 15)}$$

$$R_m = \frac{\ln(1.08W_m/D_o)}{2\pi L_c k_m} \qquad \text{(E- 16)}$$

$$T_{a_t} = (1 + U_1R_1)T_{m_t} - U_1R_1T_\infty \qquad \text{(E- 17)}$$

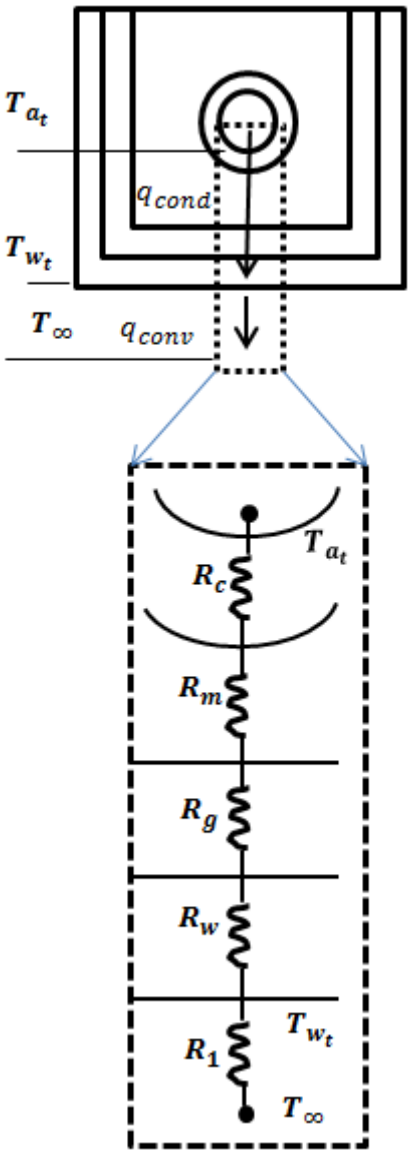

After assuming the steady state condition and applying energy balance at the external side and bottom faces.

$$E_{out} = q_{conv} = q_{cond}$$

$$U_2(T_{w_t} - T_\infty) = \frac{(T_{a_t} - T_{w_t})}{R_2}$$

$$T_{w_t} = \frac{T_{a_t} + U_2R_2T_\infty}{1 + U_2R_2} \qquad \text{(E- 18)}$$

$$R_2 = \frac{4}{3}(R_c + R_m + R_g + R_w) \qquad \text{(E- 19)}$$

$$R_g = \frac{0.785\,ln(W_g/W_m)}{2\pi L_c k_g} \qquad \text{(E- 20)}$$

$$R_w = \frac{0.785\ln(W_w/W_g)}{2\pi L_c k_w} \qquad \text{(E- 21)}$$

Substituting Equation E-17 in Equation E-18:

$$T_{w_t} = \frac{\left[(1 + U_1R_1)T_{m_t} - U_1R_1T_\infty\right] + U_2R_2T_\infty}{(1 + U_2R_2)}$$

$$T_{w_t} = \frac{1 + U_1R_1}{(1 + U_2R_2)}T_{m_t} + \frac{U_2R_2 - U_1R_1}{(1 + U_2R_2)}T_\infty$$

$$M = \frac{(1+U_1R_1)}{(1+U_2R_2)} \qquad \text{(E- 22)}$$

$$M_1 = \frac{(U_2R_2-U_1R_1)}{(1+U_2R_2)} \qquad \text{(E- 23)}$$

$$T_{w_t} = MT_{m_t} + M_1T_\infty \qquad \text{(E- 24)}$$

Applying Energy conservation equation:

$$E_{in} - E_{out} = E_{st} \qquad \text{(E- 25)}$$

Substituting Equations E-1, E-4 and E-10 in Equation E-25:

$$U\left(T_b - T_{a_t}\right) - U_1T_{m_t} - U_2T_{w_t} + (U_1 + U_2)T_\infty = M_t\frac{dT_m}{dt} \qquad \text{(E- 26)}$$

Substituting Equations E-11, E-17 and E-11 in Equation F-26:

$$UT_b - U\left[(1 + U_1R_1)T_{m_t} - U_1R_1T_\infty\right] - U_1T_{m_t} + (U_1 + U_2)T_\infty - U_2\left[MT_{m_t} + M_1T_\infty\right]$$
$$= \rho_tV_tc_{p_t}\frac{dT_m}{dt}$$

$$UT_b - (UU_1R_3 + U_1 + U_2 - U_2M_1)T_\infty - [U(1 + U_1R_1) + U_1 + U_2M]T_{m_t}$$
$$= \rho_tV_tc_t\frac{dT_m}{dt}$$

$$g_1 = \rho_tV_tc_{p_t} = \rho_cV_cc_{p_c} + \rho_mV_mc_{p_m} \qquad \text{(E- 27)}$$

$$g_2 = U(1 + U_1R_1) + U_1 + U_2M \qquad \text{(E- 28)}$$

$$g_3 = UT_b - (UU_1R_1 + U_1+U_2 - U_2M_1)T_\infty \qquad \text{(E- 29)}$$

$$\therefore g_3 - g_2T_{m_t} = g_1\frac{dT_m}{dt} \qquad \text{(E- 30)}$$

After dividing both sides of Equation E-30 by g_1:

$$\frac{dT_{m_t}}{dt} + \frac{g_2}{g_1} T_{m_t} = \frac{g_3}{g_1}$$

$$T_{m_t} = \frac{\int e^{\int \frac{g_2}{g_1} dt} . \frac{g_3}{g_1} dt + C}{e^{\int \frac{g_2}{g_1} dt}}$$

$$T_{m_t} = e^{-\frac{g_2}{g_1} t} \left[\int e^{\frac{g_2}{g_1} t} . \frac{g_3}{g_1} dt + C \right]$$

$$T_{m_t} = e^{-\frac{g_2}{g_1} t} \left[\int \frac{g_3}{g_1} . \left(\frac{g_2/g_1}{g_2/g_1} \right) . e^{\frac{g_2}{g_1} t} dt + C \right]$$

$$T_{m_t} = e^{-\frac{g_2}{g_1} t} \left[\frac{g_3}{g_2} \int e^{\frac{g_2}{g_1} t} . \frac{g_2}{g_1} dt + C \right]$$

$$T_{m_t} = e^{-\frac{g_2}{g_1} t} \left[\frac{g_3}{g_2} e^{\frac{g_2}{g_1} t} + C \right]$$

$$T_{m_t} = \frac{g_3}{g_2} e^{-\frac{g_2}{g_1} t + \frac{g_2}{g_1} t} + C e^{-\frac{g_2}{g_1} t}$$

$$T_{m_t} = \frac{g_3}{g_2} + C e^{-\frac{g_2}{g_1} t} \qquad \text{(E- 31)}$$

When $t = 0$ Equation E-31 becomes:

$$T_{m_0} = \frac{g_3}{g_2} + C e^{-\frac{g_2}{g_1}(0)}$$

$$\therefore C = T_{m_0} - \frac{g_3}{g_2} \qquad \text{(E- 32)}$$

Substituting Equation E-32 in Equation E-31:

$$\boldsymbol{T_{m_t} = \frac{g_3}{g_2} + \left(T_{m_0} - \frac{g_3}{g_2} \right) e^{-\frac{g_2}{g_1} t}} \qquad \text{(E- 33)}$$

Appendix F: Conduction shape factors

Conduction shape factors and dimensionless conduction heat rates for selected systems (Incropera & DeWitt, 1996).

(a) Shape factors [$q = Sk(T_1 - T_2)$]

System	Schematic	Restrictions	Shape Factor
Case 1 Isothermal sphere buried in a semi-infinite medium	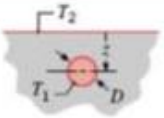	$z > D/2$	$\frac{2\pi D}{1 - D/4z}$
Case 2 Horizontal isothermal cylinder of length L buried in a semi-infinite medium	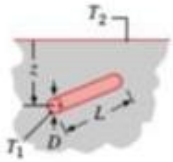	$L \gg D$ $L \gg D$ $z > 3D/2$	$\frac{2\pi L}{\cosh^{-1}(2z/D)}$ $\frac{2\pi L}{\ln(4z/D)}$
Case 3 Vertical cylinder in a semi-infinite medium	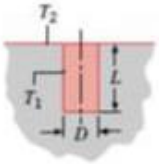	$L \gg D$	$\frac{2\pi L}{\ln(4L/D)}$
Case 4 Conduction between two cylinders of length L in infinite medium	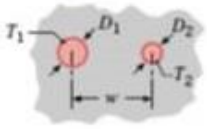	$L \gg D_1, D_2$ $L \gg w$	$\frac{2\pi L}{\cosh^{-1}\left(\frac{4w^2 - D_1^2 - D_2^2}{2D_1D_2}\right)}$
Case 5 Horizontal circular cylinder of length L midway between parallel planes of equal length and infinite width	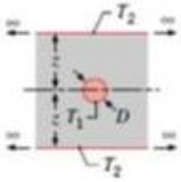	$z \gg D/2$ $L \gg z$	$\frac{2\pi L}{\ln(8z/\pi D)}$
Case 6 Circular cylinder of length L centered in a square solid of equal length	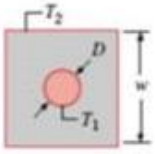	$w > D$ $L \gg w$	$\frac{2\pi L}{\ln(1.08\,w/D)}$
Case 7 Eccentric circular cylinder of length L in a cylinder of equal length	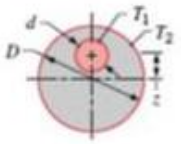	$D > d$ $L \gg D$	$\frac{2\pi L}{\cosh^{-1}\left(\frac{D^2 + d^2 - 4z^2}{2Dd}\right)}$

System	Schematic	Restrictions	Shape Factor
Case 8 Conduction through the edge of adjoining walls	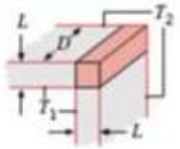	$D > 5L$	$0.54D$
Case 9 Conduction through corner of three walls with a temperature difference ΔT_{1-2} across the walls		$L \ll$ length and width of wall	$0.15L$
Case 10 Disk of diameter D and temperature T_1 on a semi-infinite medium of thermal conductivity k and temperature T_2	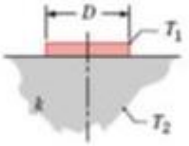	None	$2D$
Case 11 Square channel of length L	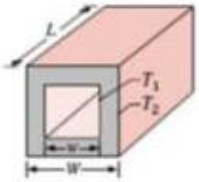	$\frac{W}{w} < 1.4$ $\frac{W}{w} > 1.4$ $L \gg W$	$\frac{2\pi L}{0.785 \ln (W/w)}$ $\frac{2\pi L}{0.930 \ln (W/w) - 0.050}$

(*b*) **Dimensionless conduction heat rates** [$q = q''_w k A_s (T_1 - T_2)/L_c$; $L_c = (A_s/4\pi)^{1/2}$]

Appendix G: Calculation of tool geometry

The tool geometry is calculated according to the channel separation

- Channel length

Fixed channel length and tool surface area are assumed in the test cases depending on the channel separation as:

$$L_c = L_{hel} = \left(9.5 + \frac{3\pi}{2}\right) W_m \qquad \text{(G- 1)}$$

$$\text{Tool surface area} = A_t^2 = 16W_m^2 \qquad \text{(G- 2)}$$

- Ratio of channel length to the tool surface area

$$R_j = \frac{L_c}{A_t^2} = \frac{\left(9.5+\frac{3\pi}{2}\right)}{16W_m} = \frac{19+3\pi}{32W_m} \qquad \text{(G- 3)}$$

- Other tool dimensions

Tool dimensions, Figure 4-7a, are determined according to the values of W_m as follows:

$$L_{zig} = \left(10 + \frac{3\pi}{2}\right) W_m \qquad \text{(G- 4)}$$

$$L_{par} = 14W_m \qquad \text{(G- 5)}$$

$$A_t = 4W_m \qquad \text{(G- 6)}$$

$$B_t = 3W_m \qquad \text{(G- 7)}$$

$$C_t = 2W_m - \left(\frac{L_{zig}-L_c}{4}\right) \qquad \text{(G- 8)}$$

$$D_t = 3.5W_m + \left(\frac{L_c-L_{par}}{4}\right) \qquad \text{(G- 9)}$$

$$r_b = W_m/2 \qquad \text{(G- 10)}$$

Appendix H: Flow in the parallel channels

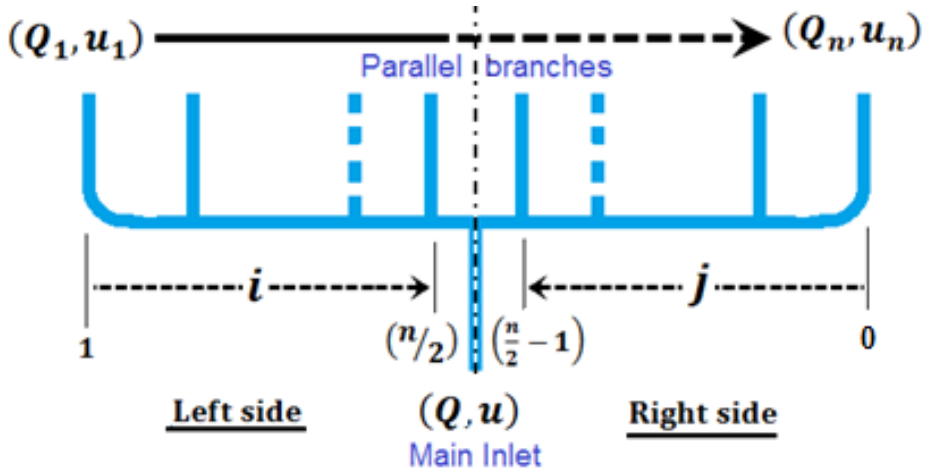

Calculation is achieved with the following considerations (Daugherty, Franzini & Finnemore, 1989; Douglas, Gasiorek & Swaffield, 1995; Munson, 2010).

- Pressure drop of the main inlet and all the parallel branches are equal, Equation (4-11).
- Volumetric flow rate of the main inlet equal the sum of the parallel branches, Equation (4-12).
- Internal diameter of the main inlet and all branches are equal.
- The number of the branches (n) is even and the branches on the left and right are symmetric.

$$\because \quad \Delta p_i = \frac{8 f L_i Q_i^2}{\pi^2 D_h^5} \qquad \text{For} \qquad i = (1\ to\ n) \qquad \text{(H- 1)}$$

Substituting in Equation (4-11)

$$L_1 Q_1^2 = L_i Q_i^2 \qquad \text{For} \qquad i = (1\ to\ n) \qquad \text{(H- 2)}$$

$$\because Q = A_c u \qquad \text{(H- 3)}$$

Substituting Equation (H-3) in (H-2)

$$L_1 u_1^2 = L_i u_i^2 \qquad \text{For} \qquad i = (1\ to\ n) \qquad \text{(H- 4)}$$

Accordingly

$$u_i = \sqrt{\frac{L_1}{L_i}}\ \ u_1 \qquad \text{For} \qquad i = (1\ to\ n) \qquad \text{(H- 5)}$$

Due to symmetry

$$\sum_{i=1}^{n/2} Q_i = \sum_{j=0}^{\left(\frac{n}{2}-1\right)} Q_{(n-j)} \qquad \text{(H- 6)}$$

Accordingly Equation (4-12) can be written as follows

$$Q = 2\left(\sum_{i=1}^{n/2} Q_i\right) \qquad \text{(H- 7)}$$

Substituting Equations H-3 and H-5 in H-7

$$u = 2u_1 \left(\sum_{i=1}^{n/2} \sqrt{\frac{L_1}{L_i}}\right) \qquad \text{(H- 8)}$$

$$\therefore \quad u_1 = \frac{u}{2\left(\sum_{i=1}^{n/2} \sqrt{\frac{L_1}{L_i}}\right)} \qquad \text{(H- 9)}$$

Length of the symmetric channels can be calculated as follows:

$$L_i = L_{(n-j)} = L_t + (n - 2i + 1)W_m \qquad \text{(H- 10)}$$

Where $i = [1\ to\ \left(\frac{n}{2}\right)]$ and $j = [0\ to\ \left(\frac{n}{2} - 1\right)]$

After calculating each of u_1 (Equation H-9) and channel lengths (Equation H-10), the fluid velocity in each branch can be calculated by Equation H-5

Appendix I: ANOVA equations

- **Average performance**

Initial sum of the test results contain each parameter at each given level:

$$S_{P_j} = \sum_{i=1}^{z} \left(y_{P_j}\right)_i \qquad \text{(I- 1)}$$

The average performance is a simple mean of the test result values. So, for each parameter at each given level:

$$f_{P_j} = \frac{S_{P_j}}{N} \qquad \text{(I- 2)}$$

- **Sum of Squares**

The deviation of a factor from the overall mean gives the relative significance of that factor. So the total sum of squared deviation is (Kamaruddin, Khan & Wan, 2004):

$$SS_T = (\sum_{i=1}^{n} y_i^2) - \frac{1}{n}(\sum_{i=1}^{n} y_i)^2 \qquad \text{(I- 3)}$$

The sum of squared deviation of each parameter is:

$$SS_P = \frac{1}{N}\left(\sum_{j=1}^{N_P} f_{P_j}^2\right) - \frac{1}{n}(\sum_{i=1}^{n} y_i)^2 \qquad \text{(I- 4)}$$

Then the sum of squared deviations of the error term is defined by:

$$SS_e = SS_T - (SS_A + SS_B + SS_C) \qquad \text{(I- 5)}$$

Finally, the percentage contribution of each factor in the total sum of squared deviations is:

$$P_P = \frac{SS_P}{SS_T} \quad \text{(I- 6)}$$

- **Degrees of freedom**

Degrees of freedom for each parameter and the error term are calculated as (Kamaruddin, et al., 2004; Roy, 2001):

$$f_T = n - 1 \quad \text{(I- 7)}$$

$$f_P = N_P - 1 \quad \text{(I- 8)}$$

$$f_e = f_T + (f_A + f_B + f_C) \quad \text{(I- 9)}$$

- **Variance and Variance ratio**

The variance or the mean square of each factor is:

$$V_P = \frac{SS_P}{f_P} \quad \text{(I- 10)}$$

The statistical tool F-test, named after Fisher (Roy, 1990), identifies which design parameters have a significant effect on the quality characteristic. Generally, F<1 indicates negligible significance of the parameter. The value of variance ratio of each parameter is determined by:

$$F_P = \frac{V_P}{V_e} \quad \text{(I- 11)}$$

$$V_e = \frac{SS_e}{f_e} \quad \text{(I- 12)}$$

- **Pooling**

A test of significance determines whether the factor effect should be pooled or not. This test is achieved after selecting a confidence level between 90% and

99% providing that its F-Table is available (Roy, 2001). Then the F ratio is determined from the F-Table, depending on the values of f_P and f_e. Finally, $F_P > F$ -ratio for any factor means that it has a significant effect on the performance. The opposite applies if the parameter is of low significance and it is pooled. Then the error term variance ratio is defined as:

$$\bar{V}_e = \frac{SS_B}{\bar{f}_e} = \frac{SS_B}{f_T - (f_A + f_C)} \qquad \text{(I- 13)}$$

- Expected result at optimum condition

The expected result at the combination the optimal design parameters can be predicted by:

$$y_{opt} = \mathrm{f}_{\mathrm{A}_{\mathrm{opt}}} + \mathrm{f}_{\mathrm{C}_{\mathrm{opt}}} - \frac{1}{n}\sum_{i=1}^{n} y_i \qquad \text{(I- 14)}$$

While the value of $\mathrm{y}_{\mathrm{opt}}$ is in the logarithmic format as the S/N ratios, its equivalent value could be calculated as follows:

$$x_{opt} = \sqrt{10^{-(y_{opt})/10}} \qquad \text{(I- 15)}$$

- **Confidence intervals**

A range of values for the expected optimal result can be defined by the confidence interval. It depends on the error variance and degrees of freedom, which are defined in Tables 4-9 and 4-10.

$$C.I. = \pm\sqrt{\left(F\left(1, \bar{f}_e\right) \times \bar{V}_e / M\right)} \qquad \text{(I- 16)}$$

After assuming a confidence level between 90% and 99%, value of $F\left(1, \bar{f}_e\right)$ is determined from the F-Table according to DOFs of 1 and $\bar{f}_e$ (Roy, 2001). In this PhD research M value that equals 2.25 was calculated as follows:

$$M = \frac{n}{f_{mean}\ (which\ equals\ 1\ always) + (f_A + f_C)} \qquad \text{(I- 17)}$$

$$M = \frac{9}{1 + (2 + 1)} = 2.25$$

Appendix J: Manufacturing of the CFRP laminate

- **Calculation**

  - A thickness of 4 mm and the maximum applicable volume fraction 0.6, which can provide sufficient strength and lower heat transfer resistance as illustrated in Chapter 4, are assumed initially for the required CFRP laminate.
  - the desired number of 4 layers are calculated by the following expression (Tian, 2011).

$$n_l = \frac{V_f \rho_f t_l}{A_f} \qquad \text{(J- 1)}$$

  - The required resin weight is calculated by multiplying the total of its volumes in the laminate, the flow medium and the pipe by its density with a little extra for the bottom of the feed cup.

- **Processing**

  - Double square layers of 52 cm length are cut from each fabric type (Section 5.3.2) to achieve the four desired layers.
  - The layers are stacked, Figure 5-3, over a flat steel tool surface according to the stacking sequence of $[(0, \pm 45)/(90, \pm 45)]_s$.
  - Vacuum bagging arrangement, as shown in Figure 5-4, is performed to hold the laminate plies together until the resin cures.
  - The laminate is post-cured in an oven for 16 hours at 60^{o}C with a ramp rate of 3°C/min.

Appendix K: Density, weight and volume fractions of Alepoxy mixture

- **Calculation requires the following data, initially:**
  - Proposed fibre volume fraction.
  - Desired volume of the mixture.
  - Defined densities, by the producer, of each constituent.
  - Defined volume and mixing ratios, by the producer, of the matrix (resin and hardener).
- **Calculation of the fibre contribution weight**.

$$\bar{W}_f = \rho_f \bar{V}_f \qquad \text{(K- 1)}$$

$$\because\ V_f = \frac{\bar{V}_f}{\bar{V}_{co}}$$

$$\therefore\ \bar{V}_f\ =\ V_f\ \bar{V}_{co} \qquad \text{(K- 2)}$$

Substitution of Equation K-2 in K-1

$$\bar{W}_f = \rho_f V_f \bar{V}_{co} \qquad \text{(K- 3)}$$

- **Calculation of the matrix (resin and hardener) contribution weight**.

$$\because\ \bar{V}_{co} = \bar{V}_f + \bar{V}_{ma} \qquad \text{(K- 4)}$$

$$\bar{V}_{ma} =\ \bar{V}_{co} - \bar{V}_f \qquad \text{(K- 5)}$$

Substituting Equation K-2 in K-5

$$\bar{V}_{ma} =\ \bar{V}_{co}\left(1 - V_f\right) \qquad \text{(K- 6)}$$

Also $\bar{V}_{ma} = \bar{V}_r + \bar{V}_h$ (K- 7)

$$\therefore\ \bar{V}_{co}\left(1 - V_f\right) = \bar{V}_r + \bar{V}_h \qquad \text{(K- 8)}$$

According to the Sicomin-Composites specification, the volume mixing ratio between the applied resin (SR8500) and hardener (SD8601) is as follows.

$$\frac{\bar{V}_r}{\bar{V}_h} = \frac{100}{42.5}$$

$$\therefore\ \bar{V}_h = 0.425\ \bar{V}_r \qquad \text{(K- 9)}$$

Substituting Equation K-9 in K-8

$$\bar{V}_{co}\left(1 - V_f\right) = \bar{V}_r + 0.425\ \bar{V}_r \qquad \text{(K- 10)}$$

Accordingly

$$\bar{V}_r = \bar{V}_{co}\frac{\left(1-V_f\right)}{1.425} \qquad \text{(K- 11)}$$

Then

$$\bar{W}_r = \rho_r \bar{V}_r = \rho_r\ \bar{V}_{co}\frac{\left(1-V_f\right)}{1.425} \qquad \text{(K- 12)}$$

So, the hardener weight can be calculated From Equations K-9 and K-11, as follows

$$\bar{W}_h = \rho_h \bar{V}_h = 0.425\ \bar{V}_{co}\frac{\left(1-V_f\right)}{1.425}\rho_h\rho_r \qquad \text{(K- 13)}$$

Also it can be calculated from the weight mixing ratio of the applied resin (SR8500) and hardener (SD8601), defined by the Sicomin-Composites specification, as follows.

$$\frac{\bar{W}_r}{\bar{W}_h} = \frac{100}{35}$$

$$\therefore \bar{W}_h = 0.35\ \bar{W}_r \qquad \text{(K- 14)}$$

- **Calculation volume fractions of the resin and hardener according to the volume of the produced composite mixture**.

Dividing both sides of Equation K-11 by $\bar{V}_{co}$

$$V_r = \frac{\left(1-V_f\right)}{1.425} \qquad \text{(K- 15)}$$

Dividing both sides of Equation K-9 by $\bar{V}_{co}$ and then substituting Equation K-13

$$V_h = 0.425\ \frac{\left(1-V_f\right)}{1.425} \qquad \text{(K- 16)}$$

- **Calculation density of the produced composite mixture**.

$$\because \ \bar{W}_{co} = \bar{W}_f + \bar{W}_{ma}$$

$$\because \ \bar{W}_{ma} = \bar{W}_r + \bar{W}_h$$

$$\therefore \ \bar{W}_{co} = \bar{W}_f + \bar{W}_r + \bar{W}_h$$

Accordingly

$$\rho_{co}\bar{V}_{co} = \rho_f\bar{V}_f + \rho_r\bar{V}_r + \rho_h\bar{V}_h \qquad \text{(K- 17)}$$

Dividing both sides by $\bar{V}_{co}$

$$\rho_{co} = \rho_f V_f + \rho_r V_r + \rho_h V_h$$

Accordingly

$$\rho_{co} = \rho_f V_f + \rho_{ma} V_{ma} \qquad \text{(K- 18)}$$

Substituting Equations K-15 and K-16 in Equation K-18

$$\rho_{co} = \rho_f V_f + \left(\rho_r + 0.425\rho_h\right)\frac{(1-V_f)}{1.425} \qquad \text{(K- 19)}$$

Or

$$\rho_{co} = \rho_f V_f + \rho_{ma}\left(1 - V_f\right)$$

Appendix L: Autodesk results

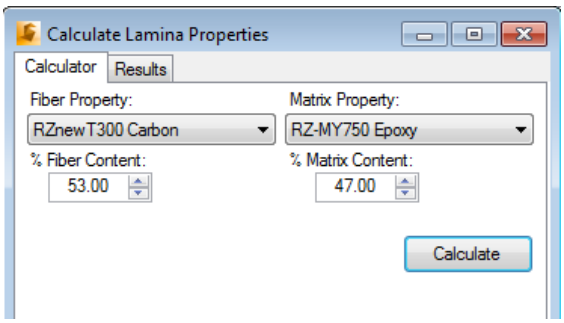

Figure L-1 Design of a CFRP lamina in the Autodesk

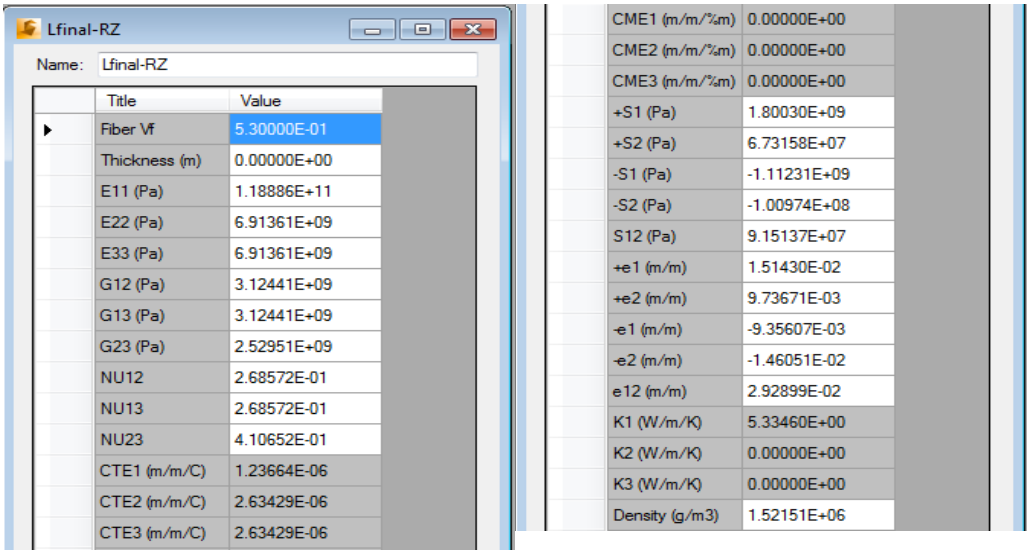

Figure L- 1 The orthotropic properties of the most proper CFRP lamina.

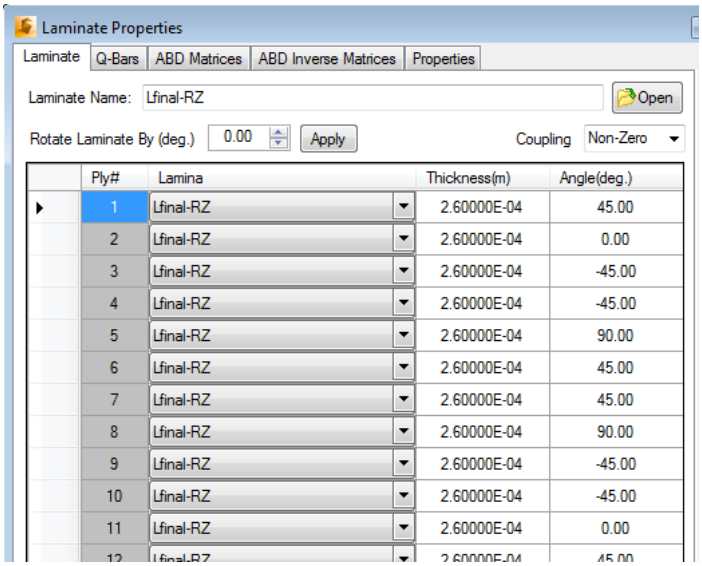

Figure L-2 Design of a CFRP laminates in Autodesk software.

Laminate | Q-Bars | ABD Matrices | ABD Inverse Matrices | Properties

2D

Title	Value
Ex (Pa)	3.56956E+10
Ey (Pa)	3.56956E+10
Gxy (Pa)	2.14748E+10
NUxy	4.51085E-01
NUyx	4.51085E-01
Exb (Pa)	4.40584E+10
Eyb (Pa)	2.24668E+10
Gxyb (Pa)	2.12096E+10
NUxyb	-6.74390E-01
NUyxb	-3.43894E-01
CTEx (m/m/C)	1.33129E-06
CTEy (m/m/C)	1.33129E-06
CTExy (m/m/C)	2.20677E-23
CTExk (1/m/C)	4.52346E-20
CTEyk (1/m/C)	-2.21722E-20
CTExyk (1/m/C)	4.52346E-20
CMEx (m/m/%m)	0.00000E+00
CMEy (m/m/%m)	0.00000E+00
CMExy (m/m/%m)	0.00000E+00
CMExk (1/m/C)	0.00000E+00
CMEyk (1/m/C)	0.00000E+00
CMEyk (1/m/C)	0.00000E+00
Density (g/m3)	1.52151E+06
Thickness (m)	3.12000E-03

3D

Title	Value
Ex (Pa)	3.56975E+10
Ey (Pa)	3.56975E+10
Ez (Pa)	8.06955E+09
Gxy (Pa)	2.14767E+10
Gxz (Pa)	2.82696E+09
Gyz (Pa)	2.82696E+09
NUxy	4.51055E-01
NUyx	4.51055E-01
NUxz	2.18769E-01
NUzx	4.94534E-02
NUyz	2.18769E-01
NUzy	4.94534E-02
CTEx (m/m/C)	1.33129E-06
CTEy (m/m/C)	1.33129E-06
CTEz (m/m/C)	3.14110E-06
CTEyz (m/m/C)	0.00000E+00
CTEzx (m/m/C)	0.00000E+00
CTExy (m/m/C)	5.95000E-24
CMEx (m/m/%m)	0.00000E+00
CMEy (m/m/%m)	0.00000E+00
CMEz (m/m/%m)	0.00000E+00
CMEyz (m/m/%m)	0.00000E+00
CMEzx (m/m/%m)	0.00000E+00
CMExy (m/m/%m)	0.00000E+00
Kx (W/m/K)	2.66730E+00
Ky (W/m/K)	2.66730E+00
Kz (W/m/K)	0.00000E+00
Kxy (W/m/K)	5.55112E-17
Density (g/m3)	1.52151E+06
Thickness (m)	3.12000E-03

Figure L-3 The orthotropic properties of the most appropriate designed laminate.

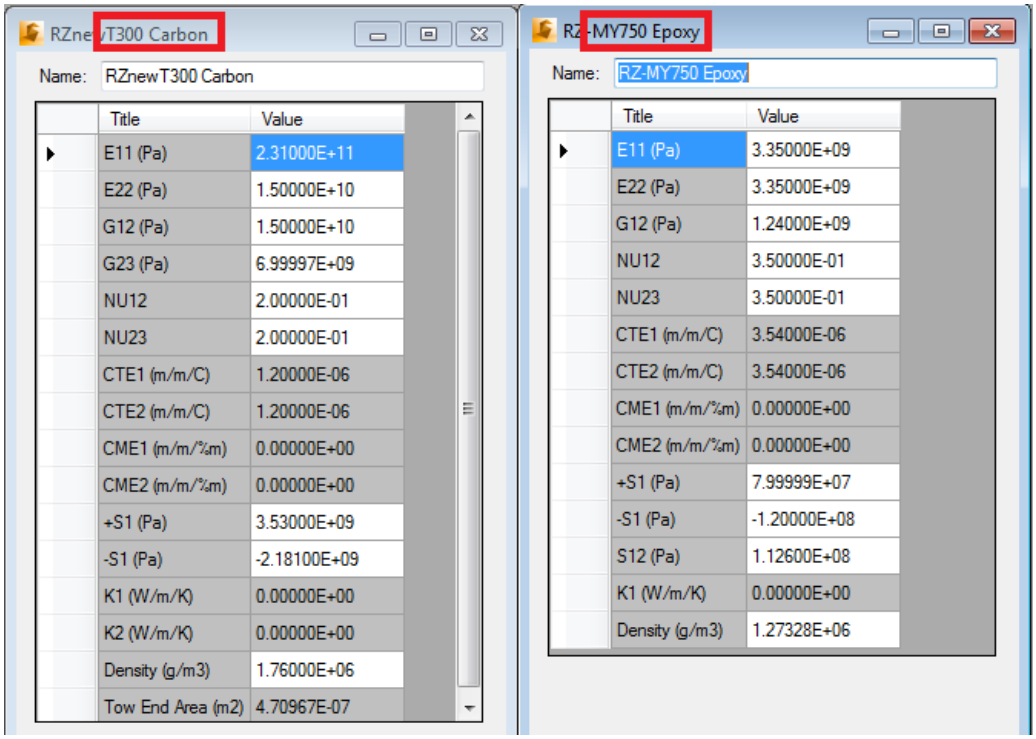

Figure L-4 Properties of the contributed fibre (T300 Carbon) and matrix (MY750 Epoxy).

References

References

Abawi, A. T. (2004) *The Bending of Bonded Layers Due to Thermal Stress.* Available at: http://hlsresearch.com/personnel/abawi/papers/bend.pdf (Accessed: 12/10/2014).

Abdullah, A. H., Alias, S. K., Jenal, N., Abdan, K. & Ali, A. (2012) 'Fatigue Behavior of Kenaf Fibre Reinforced Epoxy Composites'. *Engineering Journal*, 16 (5).

ACG-Staff (2007) 'Prepreg selection guide'. *High-Performance Composites*, [Online]. Available at: http://www.compositesworld.com/products/prepreg-selection-guide---912007 (Accessed: 13/11/2013).

ACG-Staff (2014) 'Tooling'. *Composites World*, [Online]. Available at: http://www.compositesworld.com/articles/tooling.

ACG-Staff (2015) 'Tooling '. *High-Performance Composites*, [Online]. Available at: http://www.compositesworld.com/articles/tooling-2015 (Accessed: 23/07/2015).

Adams, D. S., Bowles, D. E. & Herakovich, C. T. (1986) 'Thermally induced transverse cracking in graphite-epoxy cross-ply laminates'. *Journal of reinforced Plastics and composites*, 5 (3). pp 152-169.

Akatsuka, M. & Takezawa, Y. (2003) 'Study of high thermal conductive epoxy resins containing controlled high-order structures'. *Journal of Applied Polymer Science*, 89 (9). pp 2464-2467.

Akbarimoosavi, S. M. & Yaghoubi, M. (2014) '3D Thermal-structural Analysis of an Absorber Tube of a Parabolic Trough Collector and the Effect of Tube Deflection on Optical Efficiency'. *Energy Procedia*, 49 (0). pp 2433-2443.

Almeida, d., Neto, S. F. M. & Nogueira, Z. d. S. (1994) 'Effect of void content on the strength of composite laminates'. *Composite Structures*, 28 (2). pp 139-148.

ANSYS (2009) *ANSYS-CFX-Pre User's Guide, version 12.0, .* Available at: http://www1.ansys.com/customer/content/documentation/120/cfx/xtutr.pdf (Accessed: 06/02/2013).

Archambeault, B. & Connor, S. (2008) 'Proper model validation is important for all EMI/EMC applications', *Proc. IEEE International Symposium on Electromagnetic Compatibility EMC 2008*. pp. 1-8.

Arney, M. W., Grove, S. M., Progoulakis, I., Searle, T. J., Short, D., Spooner, J. & Summerscales, J. (2004) 'Integrally-heated tooling for the manufacture of fibre-reinforced composites', *Proceedings of Composites Processing, CPA, April 2004*. Bromsgrove.

Arnold, D. N. (2015) *Stability, consistency, and convergence of numerical discretizations.* Encyclopedia of Applied and Computational Mathematics, B. Engquist, ed., Springer. Available at: http://www.ima.umn.edu/stability~arnold//papers/.pdf (Accessed: 22/03/2015).

Ashby, M. F. (2011) *Materials Selection in Mechanical Design*. 4th edn. Butterworth-Heinemann Ltd.

Askeland, D. R., Fulay, P. P., Wright, W. J. & Bhattacharya, D. K. (2011) *The Science and Engineering of Materials* 6th edn. Stamford, Conn. : Cengage Learning.

ASTM D792-13 (2013) 'Standard Test Methods for Density and Specific Gravity (Relative Density) of Plastics by Displacement'.[in *ASTM International, West Conshohocken, Book of Standards*. 8.1. (Accessed:ASTM D792-13

ASTM E1461-11 (2013) 'Standard Test Method for Thermal Diffusivity by the Flash Method'.[in *ASTM International, West Conshohocken, Book of Standards*. 14.05, ( ). (Accessed:ASTM E1461-11

Astrom, B. T. (1997) *Manufacturing of polymer composites.* London: Chapman & Hall.

Athanasopoulos, N., Koutsoukis, G., Vlachos, D. & Kostopoulos, V. (2013) 'Temperature uniformity analysis and development of open lightweight composite molds using carbon fibers as heating elements'. *Composites Part B: Engineering*, 50 (0). pp 279-289.

Autodesk (2013) 'Simulation Composite Design User's Guide'.

Baker, R. C. (2000) *Flow Measurement Handbook: Industrial Designs, Operating Principles, Performance and Applications.* Cambridge: Cambridge University Press.

Bandyopadhyay, A. & Odegard, G. (2012) 'Molecular modeling of crosslink distribution in epoxy polymers'. *Modelling and Simulation in Materials Science and Engineering*, 20 (4). pp 18.

Baril-Gosselin, S. (2013) *Improving Integrally Heated Composite Tooling Through Cold Sprayed Copper Coatings and Heat Transfer Simulations*. Master Thesis. University of Ottawa, Canada.

Bashford, D. (2007) *Prepreg Technology for Out of Autoclave (OOA) Cure Processing Presented* ACG-umeco composites. Available at: http://compositesgateway.org/presentation/ACG_OOA.pdf (Accessed: 04/01/2015).

Bell, J. & Mueller, A. (1984) *Wolverine Engineering Data Book II*. Wolverine tube Inc. . [Online]. Available at: http://www.wlv.com/products/databook/databook.pdf (Accessed: 27/02/2012).

Bishop, W. (1992) 'Co-cured integral tool-face stiffening- a new design concept for advanced composite prepreg tooling'. *Conference of Composites Tooling (II)*. Amsterdam, The Netherlands.

Black, S. (2010a) 'SQRTM enables net-shape parts'. *High Performance Composites*, [Online]. Available at: http://www.compositesworld.com/articles/sqrtm-enables-net-shape-parts (Accessed: 07/06/2012).

Black, S. (2010b) 'Mold heating study proves pressurized water system'. *High-Performance Composites*, [Online]. Available at: http://www.compositesworld.com/articles/mold-heating-study-proves-pressurized-water-system (Accessed: 05/01/2015).

Black, S. (2011) 'Tooling for Composites: Evolutionary Trajectory'. *High Performance Composites*, (July), [Online]. Available at: http://www.compositesworld.com/articles/tooling-for-composites-evolutionary-trajectory (Accessed: 06/06/2012).

Bokstein, B. S., Mendelev, M. I. & Srolovitz, D. J. (2014) *Thermodynamics and Kinetics in Materials Science.* USA: Oxford University

Bond, D., Nesbitt, A., Coinen, V. & Brosius, D. (2005) 'The evaluation and development of the Quickstep Out-of-Autoclave composites processing method', *Proceedings of the UK Composites Processing Association*. Stoke, UK.

Boyce, D. & Prybyla, S. (2010) 'Tailorable Heating System for Out-Of-Autoclave Tooling and Heated Composite Applications'. *1st SAMPE's Spring Conference and Exhibition* Seattle, WA.USA: 17-20 May SAMPE, pp 9. Available at: https://getinfo.de/app/Tailorable-Heating-System-for-Out-Of-Autoclave/id/BLCP%3ACN077354424 (Accessed: 08/06/2012).

Brandes, J. (2008) 'Mould heating technology'. *Reinforced Plastics*, 52 (5). pp 22.

Bromley, H. S. (2015) *Investigation of integrally-heated tooling and thermal modeling methodologies for the rapid cure of aerospace composites*. Master Thesis. Massachusetts Institute of Technology.

Brown, M. E. (2011) *Introduction to Thermal Analysis: Techniques and Applications.* Netherlands: Springer.

Bruno, A. B. & Weiner, J. H. (2011) *Theory of Thermal Stresses* USA: Dover Publications Inc.

BS 7658 (1995) 'Carbon fibre -Detemunation of size content'. *Part 3*, British Standards Institution, pp 12.

Burton, T., Jenkins, N., Sharpe, D. & Bossanyi, E. (2011) 'Blade Manufacturing Processes'. *Wind Energy Handbook.* 2nd edn. UK: Wiley, pp 780

Callister, W. D. (2002) *Materials science and engineering : an introduction.* 6th edn. UK: Wiley

Campbell, F. C. (2004) *Manfacturing processes for advanced composites* New York: Elsevier

Carden, A. E. (1963) *Thermal Fatigue- an Analysis of the Experimental Method.* USA: Oak Ridge National Laboratory-U.S. Atomic Energy Commision. Available at: http://web.ornl.gov/info/reports/1963/3445605489316.pdf (Accessed: 12/10/2014).

Carlson, R. & Kardomateas, G. A. (1996) *An introduction to fatigue in metals and composites.* 1st edn. Chapman & Hall.

Carson, J. S. (2005) 'Introduction to modeling and simulation', *Proceedings of the 2005 Winter Simulation Conference*. IEEE, pp. 8

Cassel, B., Salamon, A., Sahle-Demessie, E., Zhao, A. & Gagliardi, N. (2012) 'Improved Hyper DSC Method to Determine Specific Heat Capacity of Nanocomposites and Probe for High-Temperature Devitrification'. [Online]. Available at: http://www.perkinelmer.co.uk/PDFs/Downloads/APP_NanocompositesHyperDSC.pdf.

Cengel, A. & Boles, A. (2002) *Thermodynamics: An engineering approach.* 3rd edn. New York: McGraw-Hill.

Chen, S. C., Peng, H. S., Chang, J. A. & Jong, W. R. (2005) 'Rapid mold surface heating/cooling using electromagnetic induction technology', *Mechatronics, 2005. ICM '05. IEEE International Conference on*. 10-12 July 2005. pp. 771-776.

Chen, W. & Nelson, C. (1979) 'Thermal stress in bonded joints'. *IBM Journal of Research and Development*, 23 (2). pp 179-188.

Chen, Y. H., Tam, S. C., Chen, W. L. & Zheng, H. Y. (1996) 'Application of the Taguchi method in the optimization of laser micro-engraving of photomasks'. *International Journal of Materials and Product Technology*, 11 (3-4). pp 333-344.

Ciriscioli, P. R. & Springer, G. S. (1990) *Smart autoclave cure of composites.* Lancaster, US: Technomic Publishing Company Inc.

Coenen, V., Hatrick, M., Law, H., Brosius, D., Nesbitt, A. & Bond, D. (2005) 'A feasibility study of Quickstep processing of an aerospace composite Material'. *Proceedings of 26th SAMPE Europe International Conference and Forums. Paris. 2005.*,

Cohen, D., Hyer, M. W. & Tompkins, S. S. (1984) 'The effects of thermal cycling on matrix cracking and stiffness changes in composite tubes'. *16th SAMPE Technical Conference* Albuquerque, New Mexico: October 9-11, 1984, pp 577-588. Available at: http://ntrs.nasa.gov/search.jsp?print=yes&R=19850055248 (Accessed: 01/02/2013).

CPA (2006) *Introduction to Composites* Composite Processing Association.

Cripps, D. (1998) *Composite Materials Handbook*. SP Systems. [Online]. Available at: http://www.bolton.ac.uk/CODATE/SPHandbook.pdf (Accessed: 25/02/2015).

Cripps, D., Searle, T. & Summerscales, J. (2000) 'Open mould techniques for thermoset composites'. *Comprehensive composite materials encyclopædia*, 2 pp 737-761.

Crompton, T. R. (2013) *Thermal Methods of Polymer Analysis* Rapra Technology Ltd.

Cunningham, J. E., Monaghan, P. F., Brogan, M. T. & Cassidy, S. F. (1997) 'Modelling of pre-heating of flat panels prior to press forming'. *Composites Part A: Applied Science and Manufacturing*, 28 (1). pp 17-24.

Cytec (2014) *Tooling Solutions-A unique approach to composite tooling.* Cytec Industries Inc. Available at: https://www.cytec.com/sites/default/files/files/IM-3006-EN-Tooling_A4-SINGLE.pdf (Accessed: 05/01/2015).

Dang, C., Bernetich, K., Butler, G. & Carter, E. (2011) 'Mechanical Comparison of Out-of-Autoclave Prepreg Part to Conventional Autoclave Prepreg Part'. *American Helicopter Society 67th Annual Forum*. Virginia Beach, VA: May 3-5, 2011.

Daniel, I. M. & Ishai, O. (2006) *Engineering mechanics of composite materials.* 2nd edn. New York, USA: Oxford University Press.

Daugherty, R. L., Franzini, J. B. & Finnemore, E. J. (1989) *Fluid mechanics with engineering applications.* SI metric edn. McGraw Hill

Davies, L., Day, R., Bond, D., Nesbitt, A., Ellis, J. & Gardon, E. (2007) 'Effect of cure cycle heat transfer rates on the physical and mechanical properties of an epoxy matrix composite'. *Composites Science and Technology*, 67 (9). pp 1892-1899.

Davis, E. A. (2008) *A Study of a Combined 2D Axisymmetric and 3D Cyclically Symmetric Finite Element Model of a Turbine Disk*. Master Thesis. Rensselaer Polytechnic Institute.

Davis, J. R. (2001) *Copper and copper alloys.* Materials Park, OH : ASM International

Derringh, E., Halliday, D. & Resnick, R. (1988) *Fundamentals of physics.* 3rd edn. Wiley.

Dimla, D. E., Camilotto, M. & Miani, F. (2005) 'Design and optimisation of conformal cooling channels in injection moulding tools'. *Journal of Materials Processing Technology*, 164-165 (0). pp 1294-1300.

Ding, Y., Chiu, W. K. & Liu, X. L. (1999) 'Numerical investigation on thermal response of oil-heated tool for manufacture of composite products'. *Composite Structures*, 47 (1-4). pp 491-495.

Ding, Y., Chiu, W. K., Liu, X. L. & Whittingham, B. (2001) 'Modelling of thermal response of oil-heated tools due to different flow rates for the manufacture of composite structures'. *Composite Structures*, 54 (4). pp 477-488.

Douglas, J. F., Gasiorek, J. M. & Swaffield, J. A. (1995) *Fluid mechanics.* 3rd edn. Longman Scientific & Technical.

Dowling, N. E., Prasad, K. S. & Narayanasamy, R. (2013) *Mechanical behavior of materials: engineering methods for deformation, fracture, and fatigue.* Harlow : Pearson Education

East Coast (2013) *Aluminium powder-250 mesh.* Available at: http://www.ecfibreglasssupplies.co.uk/p-817-aluminium-powder-250-mesh.aspx (Accessed: 06/02/2014).

Eischen, J. W., Chung, C. & Kim, J. H. (1990) 'Realistic Modeling of Edge Effect Stresses in Bimaterial Elements'. *Journal of Electronic Packaging*, 112 (1). pp 16-23.

Eselun, S., Wolfe, E. & Neubert, H. (1979) 'Microcracking effects on dimensional stability'. *The enigma of the eighties: Environment, economics, energy*, pp 1290-1309.

Exstar (1981) *Specific heat capacity measurements using DSC 1*. Tokyo, Japan: SII Nanotechnology. Available at: http://www.thass.org/DOWN/applications/App_SIINT/TA011.pdf (Accessed: 06/02/2014).

Fallah, N., Bailey, C., Cross, M. & Taylor, G. (2000) 'Comparison of finite element and finite volume methods application in geometrically nonlinear stress analysis'. *Applied Mathematical Modelling*, 24 (7). pp 439-455.

Figiel, T. & Kamiński, M. (2003) 'Mechanical and thermal fatigue delamination of curved layered composites'. *Computers & Structures*, 81 (18–19). pp 1865-1873.

Fo-van, C. (1983) 'Thermal contact stresses of bi-metal strip thermostat'. *Applied Mathematics and Mechanics*, 4 (3). pp 363-376.

Fraley, S., Oom, M., Terrien, B. & Date, J. Z. (2006) *Design of experiments via Taguchi methods: orthogonal arrays*. Michigan Chemical Process Dynamics and Controls Open Text book, USA 2.3 (2006): 4. [Online]. Available at: http://www.scribd.com/doc/187982142/Design-of-Experiments-via-Taguchi-Methods-Orthogonal-Arrays#scribd (Accessed: 03/08/2013).

France, L. B. d. L. & Alanta, G. (2009) 'Induction Tooling Technology'. *Composites Technology*, [Online]. Available at: http://www.compositesworld.com/products/induction-tooling-technology (Accessed: 23/5/2015).

FrontlineSolvers (2014) *Simulation.* Developers of the Excel Solver. Available at: http://www.solver.com/simulation-tutorial (Accessed: 06/01/2015).

Gallagher, D. P. (2012) *Through-Thickness Thermal Conductivity Improvement Of Carbon Fiber Reinforced Composites By Using A Heterogeneously Structured Resin Matrix* Master Thesis. The Florida State University.

Gardiner, G. (2008) 'Automating and optimizing autoclave cure'. *High-Performance Composites*, [Online]. Available at: http://www.compositesworld.com/articles/automating-and-optimizing-autoclave-cure (Accessed: 26/02/2015).

Gardiner, G. (2011) 'Out-of-autoclave prepregs: Hype or revolution?'. *High-Performance Composites*, (January), [Online]. Available at: http://www.compositesworld.com/articles/out-of-autoclave-prepregs-hype-or-revolution (Accessed: 07/06/2014).

Gardiner, G. (2015) 'Heated composites'. *Composites World*, [Online]. Available at: http://www.compositesworld.com/blog/post/heated-composites (Accessed: 02/05/2015).

Garschke, C., Weimer, C., Parlevliet, P. P. & Fox, B. L. (2012) 'Out-of-autoclave cure cycle study of a resin film infusion process using in situ process monitoring'. *Composites Part A: Applied Science and Manufacturing*, 43 (6). pp 935-944.

Gebhart, B. (1971) *Heat Transfer*. Second edn. New York McGraw-Hill.

Gerasimov, A. (2006) *Modelling Turbulent Flows with FLUENT*. [Computer Program]. ANSYS, Inc.: Available at: http://www.ae.metu.edu.tr/seminar/Turbulence_Seminar/Modelling_turbulent_flows_with_FLUENT.pdf

Gibbons, G. J., Hansell, R., Thacker, G. & Arnett, G. (2009) 'State of the art in low-cost, rapid composite forming tooling technologies'. *Journal of advanced materials*, 41 (2). pp 5-19.

Goertzen, W. K. & Kessler, M. R. (2006) 'Creep behavior of carbon fiber/epoxy matrix composites'. *Materials Science and Engineering: A*, 421 (1–2). pp 217-225.

Goldstein, R., Sparrow, E. & Jones, D. (1973) 'Natural convection mass transfer adjacent to horizontal plates'. *International Journal of Heat and Mass Transfer*, 16 (5). pp 1025-1035.

Gopalsamy, B. M., Mondal, B. & Ghosh, S. (2009) 'Taguchi method and ANOVA: An approach for process parameters optimization of hard machining while machining hardened steel'. *Journal of scientific & industrial Research*, 68, pp 686-695.

Graham, N. (2000) *Method of manufacturing composites*. Google Patents. Available at: http://www.google.com/patents/US6149844 (Accessed: 04/01/2015).

Griepink, B. & Tolg, G. (1989) 'Sample Digestion for the Determination of Elemental Traces in Matrices of Environmental Concern'. *Pure & Appl. Chem.*, 61 (6). pp 1139-1146.

Griffiths, B. & Noble, N. (2004) 'Process and tooling for Low Cost, Rapid Curing of Composites Structures '. *SAMPE Journal*, 40 (1). pp 41-46.

Grossmann, C., Roos, H.-G. & Stynes, M. (2007) *Numerical Treatment of Partial Differential Equations*. 3rd edn. Springer.

Grove, S. (2014) *Rules of mixture for elastic properties*. University of Plymouth. Available at: http://www.tech.plym.ac.uk/sme/mats333/rules%20of%20mixture.pdf (Accessed: 17/06/2014).

Grove, S., Progoulakis, I., Seale, T. & Summerscales, J. (2005) 'Heated Tooling for Aerospace Composites Manufacture'. *SAMPE Journal*, 41 (7). pp 36-45.

Grove, S. M., Popham, E. & Miles, M. E. (2006) 'An investigation of the skin/core bond in honeycomb sandwich structures using statistical experimentation techniques'. *Composites Part A: Applied Science and Manufacturing*, 37 (5). pp 804-812.

Guilong, W., Guoqun, Z., Huiping, L. & Yanjin, G. (2010) 'Analysis of thermal cycling efficiency and optimal design of heating/cooling systems for rapid heat cycle injection molding process'. *Materials & Design*, 31 (7). pp 3426-3441.

Hagstrand, P., Bonjour, F. and Manson, A. (2005) 'The influence of void content on the structural flexural performance of unidirectional glass fibre reinforced polypropylene composites'. *Composites A*, 36, pp 705-714.

Han, S. & Chung, D. (2011) 'Increasing the through-thickness thermal conductivity of carbon fiber polymer–matrix composite by curing pressure increase and filler incorporation'. *Composites Science and Technology*, 71 (16). pp 1944-1952.

Han, S., Lin, J. T., Yamada, Y. & Chung, D. (2008) 'Enhancing the thermal conductivity and compressive modulus of carbon fiber polymer–matrix composites in the through-thickness direction by nanostructuring the interlaminar interface with carbon black'. *Carbon*, 46 (7). pp 1060-1071.

Han, Y. M. & Hahn, H. T. (1989) 'Ply cracking and property degradations of symmetric balanced laminates under general in-plane loading'. *Composites Science and Technology*, 35 (4). pp 377-397.

Hancox, N. L. (1998) 'Thermal effects on polymer matrix composites: Part 1. Thermal cycling'. *Materials & Design*, 19 (3). pp 85-91.

Harris, B. (2003) *Fatigue in composites : science and technology of the fatigue response of fibre-reinforced plastics.* UK: Cambridge : Woodhead

Harris, C., Starnes, JH and Shuart, MJ (2001) *An Assessment of the State-of-the-Art in the Design and Manufacturing of Large Composite Structures for Aerospace Vehicles.* USA.NASA/TM-2001-210844: NASA Langley Research Centre. Available at: http://www.abbottaerospace.com/download/reference_data/composites/faa_nasa_composite_papers/NASA-TM-210844.pdf (Accessed: 22/04/2014).

Hayes, B. S., Gilbert, E. N. & Seferis, J. C. (2000) 'Scaling complications of dual temperature cure resin prepreg systems in airplane part manufacture'. *Composites Part A: Applied Science and Manufacturing*, 31 (7). pp 717-725.

Hayes, S. A., Wilson, P. R., Lafferty, A. D., Altinkurt, G., Collinson, M. & Lin, K.-J. (2014) 'Direct electrical cure of carbon fibre composites'. *ECCM16*. Seville,Spain,22-26 June 2014.

Herakovich, C. T. & Hyer, M. W. (1986) 'Damage-induced property changes in composites subjected to cyclic thermal loading'. *Engineering Fracture Mechanics*, 25 (5–6). pp 779-791.

Herring, M. L. & Fox, B. L. (2011) 'The effect of a rapid curing process on the surface finish of a carbon fibre epoxy composite'. *Composites Part B: Engineering*, 42 (5). pp 1035-1043.

Hexcel (1998) *3501-6 Epoxy Matrix.* Available at: http://www.hexcel.com/Resources/DataSheets/Prepreg-Data-Sheets/3501-6_eu.pdf (Accessed: 04/01/2015).

Hind, S. & Robitaille, F. (2010) 'Measurement, modeling, and variability of thermal conductivity for structural polymer composites'. *Polymer Composites*, 31 (5). pp 847-857.

Holman, J. P. (2002) *Heat Transfer*. 9th edn. New York: McGaw-Hill.

Hou, T. & Jensen, B. (2004) 'Evaluation of Double-Vacuum-Bag Process for Composite Fabrication', *Proceedings of 49 th SAMPE International Symposium & Exhibition*. Long Beach, CA.

Hsiao, K. (2013) *Gas transport and water vaporization in out-of-autoclave prepreg laminates* Master Thesis. The University of British Columbia.

Huber, R. (2013) 'Temperature Measurement with Thermocouples: Application Note'. *OSRAM Opto Semiconductors*, pp 1-13.

Iaccarino, G. (2009) *Numerical Methods for Fluid Mechanics.* Stanford University, Mechanical Engineering: . Available at: http://web.stanford.edu/class/me469a/handouts/handout2.pdf (Accessed: 22/03/2015).

Incropera, F. & DeWitt, D. (1996) *Fundamentals of heat and mass transfer* Chichester : Wiley, 1996.

Incropera, F. P., Dewitt, D. P., Bergman, T. L. & Lavin, A. s. (2013) *Principles of Heat and Mass Transfer*. 7th edn. Singapore: John Wily & Sons Pte. Ltd.

Instruction LTI/CHEM/037 (2003) 'Composite Fibre/Resin/Void Content Using Matrix Digestion Method'. *Issue 1, GKN Aerospace Services, Cowes, UK*,

IPC (2000) *IPC-TM-650 Test Methods Manual.* Association Connecting Electronics Industries. Available at: http://www.ipc.org/test-methods.aspx or http://www.ipc.org/TM/2.4.41.2A.pdf (Accessed: 03/02/2013).

Irfan, M. A. & Chapman, W. (2009) 'Thermal stresses in radiant tubes due to axial, circumferential and radial temperature distributions'. *Applied Thermal Engineering*, 29 (10). pp 1913-1920.

ISO 14125 (1998) *Fibre-reinforced plastic composites-determination of flexural properties.* European Committee for Standardization. Available at: http://www.iso.org/iso/catalogue_detail.htm?csnumber=23637 (Accessed: 05/05/2015).

Janna, W. S. (2000) *Engineering heat transfer* 2nd ed. edn. Boca Raton, Fla : CRC Press.

Jauregui, R. & Silva, F. (2011) 'Numerical validation methods'. *Numerical Analysis—Theory and Application*, pp 155-174.

JCFA (2014) *Type of Carbon Fiber Products and their Special Features.* Japan Carbon Fibre Manufacture's Association Available at: http://www.carbonfiber.gr.jp/english/material/type.html (Accessed: 24/02/2015).

Ji, Q. L., Zhang, M. Q., Rong, M. Z., Wetzel, B. & Friedrich, K. (2005) 'Friction and Wear of Epoxy Composites Containing Surface Modified SiC Nanoparticles'. *Tribology Letters*, 20 (2). pp 115-123.

Jiang, S., Zhang, C. & Wang, B. (2002) 'Optimum arrangement of gate and vent locations for RTM process design using a mesh distance-based approach'. *Composites Part A: Applied Science and Manufacturing*, 33 (4). pp 471-481.

Johnston, A. A. (1997) *An integrated model of the development of process-induced deformation in autoclave processing of composite structures*. PhD Thesis. University of British Columbia.

Jones, J. C. (2000) *The Principles of Thermal Sciences and Their Application to Engineering.* Whittles Publishing.

Joven, R., Das, R., Ahmed, A., Roozbehjavan, P. & Minaie, B. (2012) 'Thermal properties of carbon fiber/epoxy composites with different fabric weaves'. *SAMPE International Symposium Proceedings*, . Charleston, SC. Available at: https://www.researchgate.net/publication/262007032_Thermal_properties_of_carbon_fiberepoxy_composites_with_different_fabric_weaves.

Kaden, M. (2015) Efficient and Flexible Induction-Based Heating Technology for FRP Repair. *JEC composites Magazine*, (97) 71-72.

Kaiser, G., Shmolzer, S., Knappe, S., Rapp, D., Meyer, M. & Lindemann, A. (2014) 'Characterizing High-Tech Composites by Means of Thermal Analysis'. *SAMPE Journal*, 50 (1). pp 7-12.

Kamaruddin, S., Khan, Z. A. & Wan, K. S. (2004) 'The use of the Taguchi Method in Determining the Optimum Plastic Injection Moulding Parameters for the Production of a Consumer Product'. *Jurnal Mekanikal*, Bil.18, pp 98 – 110.

Kamiya, N. (1979) 'Bimodulus Thermoelasticity Considering Temperature-Dependent Material Properties'. *Mechanics of Bimodulus Materials*, 33, pp 29-37.

Kawai, M., Yajima, S., Hachinohe, A. & Kawase, Y. (2001) 'High-temperature off-axis fatigue behaviour of unidirectional carbon-fibre-reinforced composites with different resin matrices'. *Composites Science and Technology*, 61 (9). pp 1285-1302.

Kays, W. M. & Crawford, M. E. (1993) *Convective Heat and Mass Transfer*. 3rd edn. McGraw-Hill.

Khairul, A. M. & Anghelescu, M. S. (2009) ' Analysis of Deformation and Residual Stress in Composites Processed on a Carbon foam Tooling'. *Composite Materials*, 43 (19). pp 2057-2069.

Kochetov, R., Andritsch, T., Lafont, U., Morshuis, P., Picken, S. & Smit, J. (2009) 'Thermal behaviour of epoxy resin filled with high thermal conductivity nanopowders', *Electrical Insulation Conference (EIC)* IEEE, pp. 524-528.

Konzelmann, S., Hoffmann, C., Merte, R. & Peier, D. (2008) 'Thermal and electrical properties of aluminum nitride filled epoxy-resin compound'. *Dielectrics and Electrical Insulation, IEEE Transactions on*, 15 (2). pp 327-333.

Kopeliovich, D. (2012) *Structure of composites.* Substances Technologies. Available at: http://www.substech.com/dokuwiki/doku.php?id=structure_of_composites (Accessed: 20/04/2015).

Kosar, V., Gomzi, Z. & Antunović, S. (2005) 'Cure of polyester resin in a cylindrical mould heated by air'. *Thermochimica Acta*, 433 (1–2). pp 134-141.

Kreith, F. & Black, W. Z. (1980) *Basic heat transfer.* New York: Harper and Row.

Kruckenberg, T. M. & Paton, R. (1998) *Resin transfer moulding for aerospace structures.* Dordrecht, the Netherlands: Kluwer Academic Publishers.

Kwak, M., Robinson, P., Bismarck, A. & Wise, R. (2015) 'Microwave curing of carbon–epoxy composites: Penetration depth and material characterisation'. *Composites Part A: Applied Science and Manufacturing*, 75 pp 18-27.

Lacovara, B. (1995) 'Considering Resin Transfer Molding'. *Composites Fabrication Association*, [Online]. Available at: http://www-old.me.gatech.edu/jonathan.colton/me4793/rtmpaper.pdf (Accessed: 18/09/2013).

Lafarie-Frenot, M. C. & Ho, N. Q. (2006) 'Influence of free edge interlaminar stresses on damage process in CFRP laminates under thermal cycling conditions'. *Composites Science and Technology*, 66 (10). pp 1354-1365.

Law, A. M. (2003) 'How to Conduct a Successful Simulation Study', *Proceedings of the 35th conference on winter simulation- 07-10 Dec, 2003*. New Orleans, LA, USA Winter Simulation Conference, pp. 66-70.

Lawrence, J. M., Simacek, P., Laurenzi, S. & Advani, S. G. (2006) 'Flow Modeling of the Compression Resin Transfer Molding Process'. *the 8th international conference on flow process in composite materials (FPCM80)*. Douai, France. Available at: http://www.tech.plym.ac.uk/sme/FPCM/FPCM08/FPCM8/papers/FPCM8_31.pdf (Accessed: 18/09/2013).

Lawrence, K. L. (2011) *ANSYS Workbench Tutorial Release 13.* UoT, Alington,USA: Sharof Development Corporation (SDC) Publication.

LeggeroForte (2014) *Composite tooling design.* Available at: http://www.leggero-forte.com/#toggle-id-4 (Accessed: 04/01/2015).

Li, J., Zhang, C., Liang, R. & Wang, B. (2008) 'Robust design of composites manufacturing processes with process simulation and optimisation methods'. *International Journal of production Research*, 46 (8). pp 2087-2104.

Li, T.-Q., Seymour, J. D., Powell, R. L., McCarthy, K. L., Ödberg, L. & McCarthy, M. J. (1994) 'Turbulent pipe flow studied by time-averaged NMR imaging: Measurements of velocity profile and turbulent intensity'. *Magnetic Resonance Imaging*, 12 (6). pp 923-934.

Li, X. & Strieder, W. (2009) 'Emissivity of High-Temperature Fiber Composites'. *Industrial & Engineering Chemistry Research*, 48 (4). pp 2236-2244.

Loos, A. C. & Springer, G. S. (1983) 'Curing of Epoxy Matrix Composites'. *Journal of Composite Materials*, 17 (2). pp 135-169.

Lorincz, J. (2009) *Tooling to Match Composite Production.* 51-56 pp. Available at: http://www.sme.org/MEMagazine/Article.aspx?id=19355&taxid=1461 (Accessed: 10/12/2014).

Lucas, R. & Danford, H. (2009) 'Case studies: low cost, high-strength, large carbon foam tooling'. *SAMPE Journal*, 45 (1). pp 20-28.

Lynn, C., Hind, S., Li, C. & Raizenne, D. (2010) 'Conductive Heat Transfer and Real-Time Cure Control for Bonding Full Scale Composite Structures', *Proceedings of the International SAMPE Technical Conference 2010*. Salt Lake City, USA, pp. 1–12.

Madenci, E. & Guven, I. (2015) *The Finite Element Method and Applications in Engineering Using ANSYS.* Springer.

Mahrenholtz, O. & Johnson, W. (1962) 'On Bi-metal Thermostats'. *International Journal of Mechanical Sciences*, 4 (1). pp 35-52.

Mansfield, R. G. (2015) *Basic commodity-type man-made fibers can be modified to produce specialty fibers.* Hong Kong: Center Of The Fiber Industry. Available at: http://www.textileworld.com/Issues/2003/February/Fiber_World/Engineered_Performance (Accessed: 24/02/2015).

Maria, A. (1997) 'Introduction to Modeling and Simulation'. *Proceedings of the 29th conference on Winter simulation*. Atlanta, Georgia, USA: IEEE Computer Society, pp 7-13. Available at: http://dl.acm.org/citation.cfm?id=268440 (Accessed: 06/01/2015).

Marriott, M. J. & Jayaratne, R. (2010) 'Hydraulic roughness–links between Manning's coefficient, Nikuradse's equivalent sand roughness and bed grain size', *Proceedings of Advances in Computing and Technology, 5th Annual Conference*. University of East London, pp. 27-32.

Marsh, G. (2003) 'Mould tool heating – the oven-free alternative'. *Reinforced Plastics*, 47 (11). pp 38-41.

Martinez, I. (2014) *Thermal Effects on Materials.* Available at: http://webserver.dmt.upm.es/~isidoro/ot1/Thermal%20effects%20on%20materials.pdf (Accessed: 12/10/2014).

Mason, K. (2006) 'Autoclave Quality outside the autoclave'. *High-Performance Composites*, (March), [Online]. Available at: http://www.compositesworld.com/articles/autoclave-quality-outside-the-autoclave (Accessed: 06/06/2012).

MatWeb (2014) 'Foam Core Material '. in DataSheet *DIAB Divinycell H 160 Sandwich Core Material* MatWeb: DIAB, Inc. Available at: http://www.matweb.com/search/DataSheet.aspx?MatGUID=da57c5a813ce43b3a81d82e3600e40a4 (Accessed: 10/02/2013).

Maxim-Integrated (2007) 'Implementing Cold-Junction Compensation in Thermocouple Applications', [Online]. Available at: http://pdfserv.maximintegrated.com/en/an/AN4026.pdf (Accessed: 09/02/2014).

Mazumdar, S. K. (2001) *Composites manufacturing : materials, product, and process engineering*. USA: CRC Press

McGee, S. H. (1982) 'Curing characteristics of particulate-filled thermosets'. *Polymer Engineering & Science*, 22 (8). pp 484-491.

Menter, F., Ferreira, J. C., Esch, T., Konno, B. & Germany, A. C. F. X. (2003) 'The SST Turbulence Model with Improved Wall Treatment for Heat Transfer Predictions in Gas Turbines', *Proceedings of the International Gas Turbine Congress-IGTC2003-TS-059*.

Micro-Measurements (2010) *Strain Gauges and Instruments: Measurement of thermal expansion coefficient using strain gauges*. Micro-Measurements. Available at: http://www.vishaypg.com/docs/11063/tn5131tn.pdf (Accessed: 01/02/2013).

Micro-Measurements (2011) *Strain Indicator and Recorder*. Available at: http://www.vishaypg.com/docs/11102/p3.pdf (Accessed: 06/02/2014).

Milella, E., Spena, P., Giusto, G. & Thomas, J. (2014) 'The Influence of Several Fillers on the Thermochemical and Mechanical Properties of High Performance Thermoplastic Polymers'. *ECCM16*. Seville-Spain: 22-26 June 2014.

MITRE (2014) 'Verification and Validation of Simulation Models'. *Winter Simulation Conference (WSC)*. Savannah, GA, USA: December 7-10, 2014. Available at: http://www.mitre.org/publications/systems-engineering-guide/se-lifecycle-building-blocks/other-se-lifecycle-building-blocks-articles/verification-and-validation-of-simulation-models (Accessed: 06/01/2015).

Monaghan, P., Brogan, M. & Oosthuizen, P. (1991) 'Heat transfer in an autoclave for processing thermoplastic composites'. *Composites Manufacturing*, 2 (3-4). pp 233-242.

Montoya, A. (2003) 'Effect of Cure Process on Glass Transition Temperature'. *Materials Engineering Branch*, 89, p. 3 [Online]. Available at: https://code541.gsfc.nasa.gov/Uploads_materials_tips_PDFs/TIP%20089R.pdf. (Accessed: 20/05/2015).

Morena, J. J. (1990) *Mould fabrications* in International Encyclopedia of composites. vol. 3. New York: VCH Publishers.

Morena, J. J. (2007) *Advanced composite mold making*. Kriger Publishing Company, Malabar, Fl, USA.

Morey, B. (2010) 'Tooling it up for composites'. *Manufacturing Engineering*, pp 57–63.

Morgan, R. (2014) *Metal Faced Composite Tooling*. morganic metal solutions. nanocrystalline metals Available at: http://morganicmetalsolutions.com/pdf/metal_faced_composite_tooling.pdf (Accessed: 23/03/2015).

Morton, K. W. (1996) *Numerical Solution of Convection-Deffusion Problems.* London: Chapman & Hall.

Müller, G. (2002) *Engineering Applications of ANSYS Inside Siemens AG.* Siemens AG, Erlangen, Germany: ANSYS Incorporated. Available at: http://www.ansys.com//staticassets/ANSYS/staticassets/resourcelibrary/whitepaper/siemens-wp8.pdf (Accessed: 23/01/2015).

Munson, B. R. (2010) *Fundamentals of fluid mechanics.* 6th edn. USA: Hoboken N.J. Wiley.

Murisic, N., Pausader, B., Peschka, D. & Bertozzi, A. L. (2013) 'Dynamics of particle settling and resuspension in viscous liquid films'. *Journal of Fluid Mechanics*, 717, pp 203-231.

Murphy, J. (1994) 'Moulds and Mould Design'. *Chapter 3 in Reinforced Plastic Handbook.* Oxford: Elsiver Advanced Technology pp 226-231.

Nagai, Y. & Lai, G. C. (1997) 'Thermal conductivity of epoxy resin filled with particulate aluminum nitride powder'. *Journal of the Ceramic Society of Japan*, 105 (3). pp 197-200.

Nair, C. P. R., Mathew, D. & Ninan, K. N. (2001) 'Cyanate Ester Resins, Recent Developments'. *Chapter 1 in New Polymerization Techniques and Synthetic Methodologies.* Berlin Heidelberg: Springer pp 1-99.

Naphon, P. & Wongwises, S. (2006) 'A review of flow and heat transfer characteristics in curved tubes'. *Renewable and sustainable energy reviews*, 10 (5). pp 463-490.

NEN (2014) *Standard Test Method for Linear Coefficient of Thermal Expansion of Rock Using Bonded Electric Resistance Strain Gauges.* Nederlands. 7 pp. Available at: https://www.nen.nl/NEN-Shop-2/Standard/ASTM-D533514.htm (Accessed: 03/05/2015).

Neuer, G. (1992) 'Emissivity measurments on graphite and composite materials in the visible and infrared spectral range'. *Quantitative infrared thermography (QIRT)-Eurotherm Series*, 92 (27). pp 359-364.

NI (2011) *Temperature Measurements with Thermocouples: How-To Guide.* Available at: http://www.technologyreview.com/sites/default/files/legacy/temperature_measurements_with_thermocouples.pdf (Accessed: 15/3/2013).

Nikishkov, G. P. (2004) *Introduction to the finite element method*. [Online]. Available at: http://nliebeaux.free.fr/ressources/introfem.pdf (Accessed: 17/06/2015).

Noda, I. & Rubingh, D. (1992) 'The influence of the fiber/matrix interface on local glass transition temperature', *Polymer solutions, blends, and interfaces: proceedings of the Procter and Gamble UERP symposium*. Elsevier Science Ltd, pp. 339.

Nunes dos Santos, W., Mummery, P. & Wallwork, A. (2005) 'Thermal diffusivity of polymers by the laser flash technique'. *Polymer Testing*, 24 (5). pp 628-634.

O'neili, M. J. (1966) 'Measurement of Specific Heat Functions by Differential Scanning Calorimetry'. *The Perkin-Elmer Corp., Norwalk, Conn.*, 38 (10). pp 1331-1336.

Ó Brádaigh, M., C., Adrian, D., Derrick, D. & P.J., F. (2011) 'Electrically-Heated Ceramic Composite Tooling for Out-of-Autoclave Manufacturing of Large Composite Structures ', *Proceedings of SAMPE 2011 Conference* Long Beach, California, USA May 23-26, 2011. pp. 14.

Oberkampf, W. L., Trucano, T. G. & Hirsch, C. (2004) 'Verification, validation, and predictive capability in computational engineering and physics'. *Applied Mechanics Reviews*, 57 (5). pp 345-384.

Orlove, G. (2012) *Thermographic Measurement Techniques - Measuring Emissivity.* world class infrared training for thermography professionals. Available at: http://irinformir.blogspot.co.uk/2012/02/thermographic-measurement-techniques.html (Accessed: 12/12/2013).

Pace, D. K. (2004) 'Modeling and simulation verification and validation challenges'. *Johns Hopkins APL Technical Digest*, 25 (2). pp 163-172.

Paik, J. K. & Thayamballi, A. K. (2003) *Ultimate limit state design of steel-plated structures.* John Wiley & Sons.

Papanicolaou, G., Xepapadaki, A. & Angelakopoulos, G. (2012) 'Modeling the mechanical properties of notched aluminum—epoxy particulate composites'. *Journal of Applied Polymer Science*, 126 (2). pp 559-568.

Park, C. H. & McManus, H. L. (1996) 'Thermally induced damage in composite laminates: Predictive methodology and experimental investigation'. *Composites Science and Technology*, 56 (10). pp 1209-1219.

Parker, S., Chandra, M., Yates, B., Dootson, M. & Walters, B. (1981) 'The influence of distribution between fibre orientations upon the thermal expansion characteristics of carbon fibre-reinforced plastics'. *Composites*, 12 (4). pp 281-287.

Payette, S., Smith, A. W., Hubert, P., Goyette, K. & Kazanas, C. (2015) 'Out-of-Autoclave Manufacturing: Benchmarking of an Integrally Heated Tool-Plate'. *SAMPE Journal*, 51 (1). pp 27-35.

Peir´o, J. & Sherwin, S. (2005) 'Finite Difference, Finite Element and Finite Volume Methods for Partial Differential Equations'. *Handbook of Materials Modeling.* S. Yip edn.: Springer, pp 1-32.

Performance Composites Ltd 'Mechanical Properties of Carbon Fibre Composite Materials, Fibre / Epoxy resin (120°C Cure)'. Available at: http://www.performance-composites.com/carbonfibre/mechanicalproperties_2.asp (Accessed: 15/02/2015).

Petrescu, I., Mohora, C. & Ispas, C. (2013) 'The Determination of Young Modulus For CFRP Using Three Point Bending Test at Different Span Lengths'. *Journal Scientific Bulletin Series D*, 75 (1). pp 121-128.

Petrykowski, K. (2012) *Temperature Control Methods for Out-of-Autoclave Composite Molding.* SME Composites. 26 pp. Available at: http://www.single-temp.co.uk/fileadmin/downloads/PDF_Composites/Temperature_Control_Methods_for_Out-of-Autoclave_Composite_Molding.pdf (Accessed: 19/12/2014).

Petrykowski, K. & Fischer, J. (2012) 'A study comparing electric, oil and pressurised water heating for composite moulding'. *JEC composites Magazine,* August/September (75). pp 42-47.

Phatak, O. (2012) 'Weighted Average Calculation'. Buzzel. [Online]. Available at: http://www.buzzle.com/articles/weighted-average-calculation.html (Accessed: 20/09/2013).

Philpot, T. A. (2011) *Mechanics of materials : an integrated learning system.* 2nd edn. Hoboken, NJ : John Wiley.

Pigford, R. L., Ashraf, M. & Miron, Y. D. (1983) 'Flow distribution in piping manifolds'. *Industrial & Engineering Chemistry Fundamentals*, 22 (4). pp 463-471.

Plesu, V., Granger, R., Bouzon, J. & Vergnaud, J. M. (1994) 'Deconvolution of the thermal effects of the heat of conduction and heat of cure reaction for an unsaturated polyester'. *Thermochimica Acta*, 241 (0). pp 67-85.

PMC *Mold Temperature Control Effectiveness Electric Heat vs. Pressurised Water.* PMC smart solutions. Available at: http://www.single-temp.co.uk/fileadmin/downloads/PDF_Composites/PMC_Test_electric_heat_vs_water.pdf (Accessed: 05/01/2015).

Potter, K. (1997) *Resin transfer moulding.* London, UK: Chapman & Hall.

PPM Solution Ltd. (2014) *Electrical Engineers.* 18 Staclers Road, Newport, Isle of Wight PO30 2BZ: . Available at: www.ppmsolutios.co.uk and http://www.britaine.co.uk/ppm-solutions-ltd-F120FC40713D744 (Accessed: 20/09/2014).

Progoulakis, I. (2004) *Heated tooling for aerospace composites manufacture*. Master Thesis. University of Plymouth.

Prusa, J. & Yao, L. (1982) 'Numerical solution for fully developed flow in heated curved tubes'. *Journal of Fluid Mechanics*, 123 pp 503-522.

Raizenne, D., Hind, S. & Li, C. (2005) 'Integral heating and real time process control for resin infusion applications', *Proceedings of the 37th ISTC SAMPE Fall Technical Conference*. Seattle, WA, USA, pp. 1–11.

Raizenne, D., Hind, S. & Poupore, J. (2006) 'Integral Heating For Composite Tooling', Lo, J., Nishino, T., Hoa, S.V., Hamada, H., Nakai, A. and Poon, C. eds.). *Design, Manufacturing and Applications of Composites: Proceedings of the Sixth Joint Canada-Japan Workshop on Composites*. Toronto, Canada, Augest 2006 DES tech Publications, Inc., pp. 133-140.

Ramanujam, N., Vaddadi, P., Nakamura, T. & Singh, R. P. (2008) 'Interlaminar fatigue crack growth of cross-ply composites under thermal cycles'. *Composite Structures*, 85 (2). pp 175-187.

Rao, N. (1991) *Design formulas for plastics Engineers.* 2nd edn. Hanser.

Rao, S. R. & Padmanabhan, G. (2012) 'Application of Taguchi methods and ANOVA in optimization of process parameters for metal removal rate in electrochemical machining of Al/5%SiC composites'. *International Journal of Engineering Research and Applications (IJERA)*, 2 (3). pp 192-197.

Reddy, J. N. (2005) *An introduction to the finite element method.* 3rd edn. vol. 2. McGraw-Hill New York.

Repecka, L. & Boyd, J. (2002) 'Vacuum-bag-only-curable prepregs that produce void-free parts'. *47th International SAMPE Symposium and Exhibition MAY 12-16, 2002*. Long Beach, CA, pp 1862-1874. Available at: <Go to ISI>://WOS:000177401800166 (Accessed: 20/12/2014).

Richardson, D. (2012) *The fundamental principles of composite material stiffness predictions.* Bristol: University of West England (UWE). Available at: http://compositesgateway.org/presentation/Property-Prediction.pdf (Accessed: 12/03/2014).

Ridgard, C. (2009) 'Out of autoclave composite technology for aerospace, defense and space structures', *Proceedings of SAMPE 2009, Baltimore, MD, May 18-21*.

Roark, R. J. & Raymond, J. R. (1989) *Roark's formulas for stress and strain.* 6th edn. McGraw-Hill.

Roberts, G. D., Pereira, J. M., Revilock, D., Binienda, W. K., Xie, M. & Braley, M. (2003) 'Ballistic impact of composite plates and half-rings with soft projectiles', *Proc., 44th AIAA/ASME/ASCE/AHS Structures, Structural Dynamics, and Materials Conf*. pp. 2461-2482.

Rogin, M. (2010) *The Basics of Pipe Thermal Expansion.* Pumps & Systems. Available at: http://www.pumpsandsystems.com/topics/piping/basics-pipe-thermal-expansion (Accessed: 12/10/2014).

Roover, C., Bertrand, V. (2011) 'Highly integrated structure manufactured in one-shot with prepreg UD tape'. *JEC Composites*, 62, pp 40-42.

Rosato, D. V. (2004) *Reinforced plastics handbook.* 3rd edn. New York : Elsevier

Ross, P. J. (1989) *Taguchi Techiques for Quality Engineering.* New York: McGraw-Hill.

Roy, R. K. (1990) *A primer on the Taguchi method.* Dearborn, Mich Society of Manufacturing Engineers

Roy, R. K. (2001) *Design of experiments using the taguchi approach.* New York: Wiley.

Rudd, C. D., Long, A. C., Kendall, K. N. & Mangin, C. (1997) *Liquid moulding technologies: resin transfer moulding, structural reation injection moulding and related composites processing techniques* 1st edn. Cambridge : Woodhead.

Sargent, R. G. (2013) 'Verification and validation of simulation models'. *Journal of Simulation*, 7 (1). pp 12-24.

Satterfield, Z. (2013) 'Reading Centrifugal Pump Curves'. *Tech Brief*, 12 (1). pp 1-5.

Scalea, F. L. d. (1998) 'Measurement of thermal expansion coefficients of composites using strain gages'. *Experimental mechanics*, 38 (4). pp 233-241.

Schuster, J., Heider, D., Sharp, K. & Glowania, M. (2008) 'Thermal conductivities of three-dimensionally woven fabric composites'. *Composites Science and Technology*, 68 (9). pp 2085–2091.

Schuster, J., Heider, D., Sharp, K. & Glowania, M. (2009) 'Measuring and modeling the thermal conductivities of three-dimensionally woven fabric composites'. *Mechanics of Composite Materials*, 45 (2). pp 165-174.

Schwarz, G., Krahn, F. & Hartwig, G. (1991) 'Thermal expansion of carbon fibre composites with thermoplastic matrices'. *Cryogenics*, 31 (4). pp 244-247.

Scott Bader Company (2005) *Performance Resins in Composites.* Scott Bader Company Ltd: Wollaston, Wellingborough, Northamptonshire NN29 7RL.

Senthilkumar, N., Kalaichelvan, K. & Elangovan, K. (2012) 'Mechanical Behaviour of Aluminum particulate epoxy composite–Experimental study and Numerical simulation'. *International Journal of Mechanical and Materials Engineering, 7 (3),* pp 214-221.

Shahidi, E. (2000) 'Composite tooling solutions for new manufacturing', *Proceedings of the 1st Stade Composite Colloquium Techniques*. Stade, Germany, pp. 145-158.

Sherwin, G. R. (1999) 'Non-autoclave processing of advanced composite repairs'. *International Journal of Adhesion and Adhesives*, 19 (2–3). pp 155-159.

Shigue, C. Y., dos Santos, R. G. S., Baldan, C. A. & Ruppert-Filho, E. (2004) 'Monitoring the epoxy curing by the dielectric thermal analysis method'. *Applied Superconductivity, IEEE Transactions on*, 14 (2). pp 1173-1176.

Sicomin-Composites (2013) *Epoxy resin systems Multi purpose for composites applications.* Available at: http://www.matrix-composites.co.uk/prod-data-sheet/old/sr-8500-860x-uk.pdf (Accessed: 06/02/2014).

Sigmatex (2014) *Global Carbon Composite Solutions.* UK: Sigmatex UK Limited. Available at: http://www.sigmatex.com/technical/technical-specifications/ (Accessed: 17/06/2015).

Singh, N., Sarita, R. & Sonal, A. (2014) 'Polymer Nanocomposites and Cr(VI) Removal from Water'. *Nanoscience & Technology*, 1 (1).

Skordos, A. A., Maistros, G. M., Turmel, D. J. & Partridge, I. K. (1997) 'Modelling Heat Generation and Transfer during Cure of Thermoset Composites Processed by Resin Transfer Moulding (RTM)', *5th International Conference on Automated Composites September 4-5, 1997, Glasgow, UK*.

Skordos, A. A. & Partridge, I. K. (1999) 'Monitoring and Heat Transfer Modelling of the Cure of Thermoset Composites Processed by Resin Transfer Moulding'. *Polymer Composites '99, October 6-8*. Quebec, Canada. Available at: https://dspace.lib.cranfield.ac.uk/handle/1826/1880 (Accessed: 11/02/2015).

Slesinger N., S. T., Arafath A. R. A., and Poursartip A., (2009) 'Heat Transfer Coefficient Distribution'. *17th ICCM* Edinburgh: 27 Jul - 31 Jul, pp 1–10.

Sloan, J. (2011) 'Microwave: An alternative to the autoclave?'. *High-Performance Composites*, [Online]. Available at: http://www.compositesworld.com/articles/microwave-an-alternative-to-the-autoclave.

Sloan, J. (2013) 'Pressurized Water-based mold temperature control comes to composites '. *High-Performance Composites magazine*, (January), [Online]. Available at: http://www.compositesworld.com/articles/pressurized-water-based-mold-temperature-control-comes-to-composites (Accessed: 04/04/2015).

Sloan, J. (2014) 'Roctool Announces New High-volume Molding Process'. *Composites World*, [Online]. Available at: http://www.compositesworld.com/blog/post/roctool-announces-new-high-volume-molding-process (Accessed: 25/04/2015).

SP Systems (2001) *Guide to Composites*. Engineering Materials, UK. Available at: http://www.composites.ugent.be/home_made_composites/documentation/SP_Composites_Guide.pdf (Accessed: 21/04/2015).

Speyer, R. F. (1994) *Thermal Analysis of Materials.* CRC Press Inc.

Stadtländer, C. (2007) 'Scanning electron microscopy and transmission electron microscopy of mollicutes: challenges and opportunities'. *Modern research and educational topics in microscopy*, 1, pp 122-131.

Stolarski, T., Nakasone, Y. & Yoshimoto, S. (2006) *Engineering analysis with ANSYS software*. Elsevier Butterworth-Heineman.

Stone, H. J. (2014) *Course D: Mechanical Behaviour of Materials.* University of Cambridge. Available at: http://www.msm.cam.ac.uk/teaching/partIA/courseD/IA_Course_D_Practical_Booklet.pdf (Accessed: 12/10/2014).

Stringer, L. G. (1989) 'Optimization of the wet lay-up/vacuum bag process for the fabrication of carbon fibre epoxy composites with high fibre fraction and low void content'. *Composites*, 20 (5). pp 441-452.

Strong, A. (2008) *Fundamentals of composites manufacturing: materials, methods and applications.* Dearborn, Mich.: Society of Manufacturing Engineers.

Suhir, E. (1989) 'Interfacial stresses in bimetal thermostats'. *Journal of Applied mechanics*, 56 (3). pp 595-600.

Surface Generation (2011) *Production of Functional Specifications.* Available at: http://www.surface-generation.com./ (Accessed: 14/04/2015).

T&PI (2014) *How to Determine Emissivity Values.* Technical Information Data Bulletin, USA: Temperature & Process Instruments Inc. Available at: http://www.tnp-instruments.com/sitebuildercontent/sitebuilderfiles/Infrared%20Thermometer%20and%20Emissivity.pdf (Accessed: 12/08/2013).

Tanigawa, Y., Ootao, Y. & Kawamura, R. (1991) 'Thermal bending of laminated composite rectangular plates and nonhomogenneous plates due to partial heating'. *Jornal of Thermal Stresses*, 14 (3). pp 285-308.

Tavman, I., Aydogdu, Y., Kök, M., Turgut, A. & Ezan, A. (2011) 'Measurement of heat capacity and thermal conductivity of HDPE/expanded graphite nanocomposites by differential scanning calorimetry'. *Archives of Material Science and Engineering*, 50 (1). pp 56-60.

TenCate (2013) *Application of Out of Autoclave (OOA) Composite Prepregs.* AZO Materials. Available at: http://www.azom.com/article.aspx?ArticleID=7970 (Accessed: 20/12/2014).

Thomas, G. P. (2013) *Composite Prepregs – Manufacturing, Benefits and Applications.* Available at: http://www.azom.com/article.aspx?ArticleID=8353#3 (Accessed: 10/08/2014).

Thuis, H. G. S. J. (1999) 'Development of a composite cargo door for an aircraft'. *Composite Structures*, 47 (1–4). pp 813-819.

Tian, T. (2011) *Anisotropic Thermal Property Measurement of Carbon-fiber/Epoxy Composite Materials*. PhD Thesis. University of Nebraska - Lincoln.

Tiberghien, G. (2015) Power transfer in complex shape heated moulds or functional composites. *JEC composites Magazine*, (99) 48-51.

Timoshenko, S. (1925) 'Analysis of Bi-metal Thermostats'. *Journal of the Optical Society of America*, 11 (3). pp 233-255.

Timoshenko, S. (1956) *Strength of Materials.* 3rd edn. New Jersey: D.Van Nostrand Company,Inc.

Timoshenko, S. & Goodier, J. N. (1951) *Theory of Elasticity.* 2nd edn. McGraw-Hill

Tomlinson, W. J. & Stapley, D. (1977) 'Thermal conductivity of epoxy resin-aluminium'. *Journal of Materials Science*, 12 (8). pp 1689-1690.

Tompkins, S. & Williams, S. L. (1984) 'Effects of thermal cycling on mechanical properties of graphite polyimide'. *Journal of Spacecraft and Rockets*, 21 (3). pp 274-280.

Tong, R., Hoa, S. V. & Chen, M. (2011) 'Cost Analysis on L-shape Composite Component Manufacturing'. *18th International Conference on Composite Materials*. Jeju Island, South Korea: 21-26 Aug Jeju International Convention Center. Available at: http://www.iccm-central.org/Proceedings/ICCM18proceedings/data/2.%20Oral%20Presentation/Aug23(Tuesday)/T34%20Processing%20of%20Out-of-autoclave%20Prepregs/T34-5-IF1958.pdf (Accessed: 24/03/2015).

Transcat (2014) *How to Determine the "EMISSIVITY" of an object.* Newsletter: RAYTEK - Infrared Temperature Measurement Solutions. Available at: http://www.transcat.com/technical-reference/newsletters/Det_Emissivity_Raytek.htm (Accessed: 4/6/2013).

Versteeg, H. K. & Malalasekera, W. (2007) *A Introduction to Computational Fluid Dynamics The Finite Volume Method.* 2nd edn. London: Pearson Educational Limited.

Vesilind, P. A., Perirce, J. J. & Weiner, R. F. (1994) *Enviromental Engineering.* 3rd edn. Butterworth Heinemann.

Vries, H. P. J. d. (2002) 'Development of generic composite box structures with prepreg preforms and RTM', *Society for the Advancement of Material and Process Engineering. International SAMPE Europe conference*. pp. 725-736.

Walczyk, D. & Kuppers, J. (2012) 'Thermal press curing of advanced thermoset composite laminate parts'. *Composites Part A: Applied Science and Manufacturing*, 43 (4). pp 635-646.

Walczyk, D. F. & Yoo, S. (2009) 'Design and fabrication of a laminated thermoforming tool with enhanced features'. *Journal of Manufacturing Processes*, 11 (1). pp 8-18.

Wang, G., Zhao, G. & Guan, Y. (2011) 'Research on optimum heating system design for rapid thermal response mold with electric heating based on response surface methodology and particle swarm optimization'. *Journal of Applied Polymer Science*, 119 (2). pp 902-921.

Wang, G., Zhao, G., Li, H. & Guan, Y. (2010) 'Research of thermal response simulation and mold structure optimization for rapid heat cycle molding processes, respectively, with steam heating and electric heating'. *Materials & Design*, 31 (1). pp 382-395.

Wang, G., Zhao, G., Li, H. & Guan, Y. (2011a) 'Multi-objective optimization design of the heating/cooling channels of the steam-heating rapid thermal response mold using particle swarm optimization'. *International Journal of Thermal Sciences*, 50 (5). pp 790-802.

Wang, G., Zhao, G., Li, H. & Guan, Y. (2011b) 'Research on optimization design of the heating/cooling channels for rapid heat cycle molding based on response surface methodology and constrained particle swarm optimization'. *Expert Systems with Applications*, 38 (6). pp 6705-6719.

Wang, Y. Y., Yu, K.-M., Wang, C. C. L. & Zhang, Y. (2011c) 'Automatic design of conformal cooling circuits for rapid tooling'. *Computer-Aided Design*, 43 (8). pp 1001-1010.

Witik, R. A., Gaille, F., Teuscher, R., Ringwald, H., Michaud, V. & Månson, J.-A. (2011) 'Assessing the Economic and Environmental Potential of Out of Autoclave Processing'. *18th International Conference on Composite Materials* Jeju Island, South Korea: 21-26 Aug Jeju International Convention Center. Available at: http://www.iccm-central.org/Proceedings/ICCM18proceedings/data/2.%20Oral%20Presentation/Aug23(Tuesday)/T34%20Processing%20of%20Out-of-autoclave%20Prepregs/T34-2-AF1510.pdf (Accessed: 15/02/2014).

Xu, X., Sachs, E. & Allen, S. (2001) 'The design of conformal cooling channels in injection molding tooling'. *Polymer Engineering & Science*, 41 (7). pp 1265-1279.

Xu, Y. & Chung, D. (2000) 'Increasing the thermal conductivity of boron nitride and aluminum nitride particle epoxy-matrix composites by particle surface treatments'. *Composite Interfaces*, 7 (4). pp 243-256.

Yan, X. (2007) 'Finite element modeling of curing of epoxy matrix composites'. *Journal of Applied Polymer Science*, 103 (4). pp 2310-2319.

Yao, D., Chen, S.-C. & Kim, B. H. (2008) 'Rapid thermal cycling of injection molds: An overview on technical approaches and applications'. *Advances in Polymer Technology*, 27 (4). pp 233-255.

Yoo, S. (2008) 'Design of Conformal Cooling/ Heating Channels for Layered Tooling'. *International Conference on Smart Manufacturing Application*. KINTEX,Gyeonggi-do, Korea: April. 9-11, . Available at: http://ieeexplore.ieee.org/stamp/stamp.jsp?tp=&arnumber=4505626 (Accessed: 28/08/2012).

Yoo, S. & Walczyk, D. F. (2007) 'A Preliminary Study of Sealing and Heat Transfer Performance of Conformal Channels and Cooling Fins in Laminated Tooling '. *Journal of Manufacturing Science and Engineering-transactions of The Asme*, 129 (2). pp 388-399.

Young, J. & Whitaker, T. (1973) 'Specific heat of peanuts by differential scanning calorimetry'. *Transactions of the ASAE*, 16 (3). pp 522-524.

Zhang, C., Binienda, W. K., Morscher, G., Martin, R. E. & Kohlman, L. W. (2012) 'Finite Element Modeling of Thermal Cycling Induced Microcracking in Carbon/Epoxy Triaxial Braided Composites'. *Earth and Space 2012 Conference, 15-18 Apr*. Pasadena, CA; United States. Available at: http://ntrs.nasa.gov/search.jsp?R=20120012918 (Accessed: 17/06/2014).

Zhang, C., Binienda, W. K., Morscher, G. N., Martin, R. E. & Kohlman, L. W. (2013) 'Experimental and FEM study of thermal cycling induced microcracking in carbon/epoxy triaxial braided composites'. *Composites Part A: Applied Science and Manufacturing*, 46 (0). pp 34-44.

Zhang, J., Guo, Q. & Fox, B. L. (2009) 'Study on thermoplastic-modified multifunctional epoxies: Influence of heating rate on cure behaviour and phase separation'. *Composites Science and Technology*, 69 (7–8). pp 1172-1179.

Zhou, W. & Yu, D. (2010) 'Thermal and dielectric properties of the aluminum particle/epoxy resin composites'. *Journal of Applied Polymer Science*, 118 (6). pp 3156-3166.

Zhu, B. L., Wang, J., Ma, J., Wu, J., Yung, K. C. & Xie, C. S. (2013) 'Preparation and properties of aluminum nitride-filled epoxy composites: Effect of filler characteristics and composite processing conditions'. *Journal of Applied Polymer Science*, 127 (5). pp 3456-3466.

Zimmer, M., Fan, X., Bao, J., Liang, R., Wang, B., Zhang, C. & Brooks, J. (2012) 'Through-Thickness Thermal Conductivity Prediction Study on Nanocomposites and Multiscale Composites'. *Material Science and Applications*, 3 pp 131-138.

Zung-fang, B. D.-x., Wang (1986) 'Thermal bending of thick rectangular plates of bimodulus composite materials'. *Applied Mathmatics and Mechanics*, 7 (8). pp 795-801.